Nancy-Université

INPL

AVERTISSEMENT

Ce document est le fruit d'un long travail approuvé par le jury de soutenance et mis à disposition de l'ensemble de la communauté universitaire élargie.
Il est soumis à la propriété intellectuelle de l'auteur au même titre que sa version papier. Ceci implique une obligation de citation et de référencement lors de l'utilisation de ce document.
D'autre part, toute contrefaçon, plagiat, reproduction illicite entraîne une poursuite pénale.

Contact SCD INPL: mailto:scdinpl@inpl-nancy.fr

LIENS

Code de la propriété intellectuelle. Articles L 122.4
Code de la propriété intellectuelle. Articles L 335.2 – L 335.10
http://www.cfcopies.com/V2/leg/leg_droi.php
http://www.culture.gouv.fr/culture/infos-pratiques/droits/protection.htm

Nancy-Université INPL

INSTITUT NATONAL POLYTECHNIQUE DE LORRAINE
ECOLE DOCTORALE RP2E
Laboratoire des Sciences du Génie Chimique

THESE

Présentée et soutenue publiquement le 17 décembre 2009
pour l'obtention du grade de Docteur de l'INPL

par

Van Viet NGO

Modélisation du transport de l'eau et des Hydrocarbures Aromatiques Polycycliques (HAP) dans les sols de friches industrielles

Directeur de thèse :	Marie-Odile SIMONNOT	Professeur, INPL (EEIGM) Nancy
Co-directeur de thèse :	Abderazzak LATIFI	Professeur, INPL (ENSIC), Nancy

Composition du jury

Président du jury :	Michel SARDIN	Professeur, INPL (ENSIC), Nancy
Rapporteurs :	Jean-Paul GAUDET	Ingénieur de Recherche, LTHE, Grenoble
	Michel LEGRET	Directeur de Recherche, LCPC, Nantes
Examinateurs :	Abderazzak LATIFI	Professeur, INPL (ENSIC), Nancy
	Marie-Odile SIMONNOT	Professeur, INPL (EEIGM) Nancy
Membres invités :	Stéphanie OUVRARD	Chargée de Recherche, INRA, Nancy

Remerciements

J'aimerais tout d'abord remercier la directrice et le co-directeur de cette thèse, Mme Marie-Odile SIMONNOT et M. Abderrazak LATIFI, Professeurs à l'Institut National Polytechnique de Lorraine pour m'avoir guidé, encouragé, conseillé et fait confiance pendant trois ans de thèse en me laissant une grande liberté. Chacun avec sa propre manière, avec ses dynamiques et ses compétences scientifiques m'a permis de mener à bien et de faire aboutir ce travail. Je les remercie de tout mon cœur.

Mes remerciements vont ensuite à M. Michel SARDIN, Professeur à l'Institut National Polytechnique de Lorraine, Directeur du Laboratoire des Sciences du Génie Chimique, pour la gentillesse et la patience qu'il a manifestées à mon égard durant cette thèse, pour tous les conseils qu'il a bien voulu me donner et aussi pour m'avoir fait l'honneur de présider le jury de soutenance.

Mes sincères remerciements vont à M. Jean-Paul GAUDET, Ingénieur de Recherche au Laboratoire d'étude des Transferts en Hydrologie et Environnement, CNRS, Grenoble et à M. Michel LEGRET, Directeur de Recherche au Laboratoire Central des Ponts et Chaussées, Bouguenais, qui m'ont fait l'honneur d'être les rapporteurs de cette thèse, à Mlle Stéphanie OUVRARD, chargée de recherche INRA qui a accepté d'être examinateur.

Ce travail n'aurait pu être mené à bien sans l'aide du GISFI, Groupement d'Intérêt Scientifique sur les Friches Industrielles, au travers de son soutien scientifique et matériel. Je remercie très chaleureusement M. Jean-Louis MOREL, Professeur à l'Institut National Polytechnique de Lorraine, Président du GISFI pour son soutien pendant trois ans de thèse. Une grande partie de ce travail n'aurait pu être réalisé sans le transfert de données effectué par Noële RAOULT, directrice du GISFI, Je lui adresse donc mes sincères remerciements. Je profite de ces quelques lignes pour remercier aussi tous les membres du GISFI.

Je tiens à remercier aussi Lise LUCAS, Maître de Conférences, dont la participation, la contribution, les conseils m'ont permis de mieux réaliser ce travail de thèse.

Merci beaucoup à mon collaborateur et ami, Julien MICHEL, pour ses aides et ses conseils toujours très pertinents. Je tiens à remercier les amis qui m'ont aidé à améliorer mon français, résoudre les problèmes de logistique au cours des années de thèse, et passé ensemble de bons moments de loisir: Romain BARBAROUX, Valérie GUJISAITE, Julien LEMAIRE, Paula Tereza DE SOUZA E SILVA. J'aimerais remercier très sincèrement Michelle et Jean-François CAMUS pour ses aides, ses souvenirs, ses encouragements pendant mon séjour à Nancy. Je voudrais remercier aussi mes amis vietnamiens de la classe K45A: Tuan, Loan, Hung, Hinh, Phuong, Ha pour leurs encouragements.

Je n'oublierai pas les aides permanentes reçues de la part du personnel technique et administratif du Laboratoire des Sciences du Génie Chimique: Fabrice BENARD, Corinne DE CRUZ, Bruno DELFOLIE, Annie FREY, Muriel HAUDOT, Nelly LOZINGUEZ, Josiane MORAS, Claudine PASQUIER.

Je remercie tout particulièrement ma chère épouse, mon amie, mon amour, Định, pour ton soutien quotidien indéfectible, tes encouragements pour passer les moments difficiles, ton enthousiasme contagieux à l'égard de mes travaux comme de la vie en général. Et alors ma petite chérie, Lily Quỳnh Trang, toi, tu ne comprends pas encore le travail de papa, et pourquoi papa va à Massy seulement deux fois par mois pour te voir, rentre très tardivement et ne passe pas beaucoup de temps pour jouer avec toi (lors de la période de la fin de thèse quand toi et ta maman retournent à Nancy pour me soutenir)… Mais c'est toi, ma petite chérie, qui a été vraiment ma source d'énergie, ma force pour bien avancer ce travail de thèse… Oh, how I love you, my babies!

Enfin, je remercie nos familles, mes parents, ma belle-mère, mon beau-père, mes sœurs, mes frères pours leur aide et surtout leurs encouragements pendant mon séjour à l'étranger.

Sommaire

Introduction générale *17*

Chapitre I : Théorie et état de l'art de la modélisation de l'écoulement d'eau et du transport de soluté en milieu poreux *20*

1. Introduction **21**

2. Notions fondamentales concernant le milieu poreux **21**

2.1. Présentation du sol 21
2.2. Porosité 22
2.3. Masse volumique 23
2.4. Teneur en eau volumique 23
2.5. Potentiel de pression 24
2.6. Loi de Darcy 24
2.7. Conductivité hydraulique 25
2.8. Relations θ(h) et K(h) 25
2.8.1. Relation teneur en eau - potentiel de pression θ(h) 25
2.8.2. Relation conductivité hydraulique - potentiel de pression K(h) 26

3. Ecoulement d'eau en milieu poreux à saturation variable **27**

3.1. Modèle d'écoulement d'eau uniforme 27
3.2. Ecoulement préférentiel 28
3.2.1. Modèle à double porosité (Dual-Porosity Model) 29
3.2.2. Modèle à double perméabilité (Dual-Permeability Model) 29
3.2.3. Transfert d'eau entre régions 30

4. Transport d'un soluté en milieu poreux **30**

4.1. Processus de transport de soluté 30
4.1.1. Diffusion moléculaire 30
4.1.2. Dispersion 31
4.1.3. Convection 31
4.2. Modèle de convection-dispersion 32
4.2.1. Les équations de transport 32
4.2.2. La sorption linéaire et non linéaire 32
4.3. Transport hors équilibre 34
4.3.1. Transport hors équilibre physique 34
a. Modèle à double porosité et modèle d'eau mobile-immobile *34*
b. Modèle à double perméabilité *36*
4.3.2. Transport hors équilibre chimique 36
a. Modèle à un site cinétique de sorption (One-Site Sorption Model) *36*
b. Modèle à deux sites de sorption (Two-Site Model) *37*

4.3.3. Transport facilité par les colloïdes 38

5. Codes de calcul 40

5.1. Modèles analytiques 40
5.2. Modèles numériques 40

6. Optimisation des paramètres 43

6.1. Méthodes inverses 44
6.2. Solution de la méthode inverse 45

7. Analyse de sensibilité et d'estimabilité 46

8. Conclusion et objectifs de la thèse 48

Chapitre II : Modélisation de l'écoulement d'eau dans les parcelles 50

1. Introduction 51

2. Matériels et méthodes 51

2.1. Description des parcelles 51
2.2. Ecoulement d'eau dans les parcelles 52
2.2.1. Equations décrivant l'écoulement d'eau 52
2.2.2. Propriétés hydrauliques du sol non saturé 52
2.2.3. Conditions initiale et aux limites 53
2.3. Calcul du bilan d'eau dans les parcelles 53
2.4. Données d'entrée 53
2.4.1. Précipitation quotidienne 53
2.4.2. Evapotranspiration et interception quotidienne 53
2.4.3. Distribution des racines 55
2.4.4. Paramètres hydrodynamiques 55

3. Résultats et discussions 56

3.1. Hauteur d'eau dans les bacs de rétention 56
3.2. Comparaison des hauteurs d'eau mesurées et calculées dans les bacs de rétention 57

4. Conclusions et perspectives 59

Chapitre III : Analyse d'estimabilité des paramètres du modèle d'écoulement uniforme 60

1. Introduction 62

2. Material and methods 63

2.1. Experimental system 63
2.2. Model description 63

2.3. Model parameters –initial and boundary conditions 64
2.4. Sensitivity analysis 65
2.5. Estimability analysis 65
2.6. Optimization 65
2.7. Model performance analysis 66

3. Result and discussions 67

3.1. Background data 67
3.2. Sensitivity and estimability analysis based on hourly data 67
3.3. Sensitivity and estimability analysis based on daily output predictions 70
3.4. Optimization result 72
3.5. Influence of soil heterogeneity on calibration results 77
3.6. Model Estimation 79

4. Conclusions 80

Chapitre IV : Analyse d'estimabilité des paramètres du modèle à double porosité 82

1. Introduction 83

2. Material and methods 84

2.1. Experimental description 84
2.2. Model description 86
2.3. Parameter estimation and initial condition, boundary condition 87
2.4. Sensitivity analysis 88
2.5. Estimability analysis 89
2.6. Optimization 91
2.7. Model performance analysis 92

3. Result and discussions 93

3.1. Sensitivity analysis 93
3.2. Estimability analysis 94
3.3. Optimization results 97

4. Conclusions 104

Chapitre V : Simulation du transport de traceur (bromure) dans un lysimètre de terrain 106

1. Introduction 107

2. Materials and methods 109

2.1. System description 109

2.2. Model description ... 109
2.2.1. Single-porosity model ... 109
2.2.2. Dual-porosity model ... 110
2.2.3. Initial condition and boundary conditions ... 111
2.3. Data used ... 112
2.4. Sensitivity analysis ... 112
2.5. Estimability analysis ... 114
2.6. Temporal moments of the residence time distribution ... 116

3. Results and discussion ... 117
3.1. Sensitivity analysis ... 117
3.2. Parameter estimability ... 121
3.3. Comparison of the SPM and DPM ... 124

4. Conclusions ... 127

Chapitre VI : Simulation du transport des HAP dans les colonnes de sol 128

1. Introduction ... 130

2. Material and methods ... 131
2.1. Experimental description ... 131
2.2. Model description ... 132
2.3. Estimability analysis ... 133
2.4. Initial input parameters and parameter optimization ... 135

3. Results and discussion ... 136
3.1. Parameter estimability ... 136
3.1.1. Saturated column ... 136
3.1.2. Nonsaturated column ... 139
3.2. Parameter optimization ... 141
3.2.1. Saturated column ... 141
3.2.2. Nonsaturated column ... 143

4. Conclusions ... 147

Conclusion générale ... 149

Références ... 153

Annexes ... 160

Liste des figures

Chapitre 1

Figure I-1. Triangle des textures du sol permettant de classer les sols selon leur granulométrie (Crevoisier, 2005)..... 22

Figure I-2. Schéma illustrant la porosité du sol..... 23

Figure I-3. Exemples de courbes de rétention d'eau (Gujisaite, 2008)..... 26

Figure I-4. Illustration de l'écoulement préférentiel par le traceur coloré (Sander and Gerke, 2007) . 28

Figure I-5. Concepts des modèles hors équilibre physique pour le transport d'eau et de soluté : θ est la teneur en eau volumique, θ_{mo} et θ_{im} sont respectivement les teneurs en eau volumique dans les phases mobile et immobile, θ_M et θ_F sont respectivement les teneurs en eau volumique des macropores et micropores, c est la concentration de soluté avec les indices qui ont les mêmes sens que pour la teneur en eau volumique, C est la concentration totale de soluté dans la phase liquide (d'après (Simunek and van Genuchten, 2008)..... 34

Figure I-6. Concepts des modèles hors équilibre physique pour le transport d'eau et de soluté (d'après (Simunek and van Genuchten, 2008). 35

Figure I-7. Schémas conceptuels des modèles hors équilibre chimique pour le transport de soluté réactif : θ est la teneur en eau volumique, c est la concentration de soluté, s^e est la concentration adsorbée qui est à équilibre avec la concentration de soluté dans la phase liquide, s^k est la concentration adsorbée correspondant avec la fraction de sorption cinétique (d'après Simunek and van Genuchten, 2008). 37

Figure I-8. Le transport de HAP à l'échelle d'une parcelle sous conditions climatiques naturelles.... 39

Figure I-9. Schéma du plan et des objectifs de la thèse..... 49

Chapitre 2

Figure II-1. Schéma des parcelles à la station expérimentale du GISFI, Homécourt, Lorraine..... 52

Figure II-2. Représentation schématique des flux d'eau dans les parcelles..... 52

Figure II-3. Courbe de rétention d'eau pour la terre polluée de Homécourt (Michel, 2009b)..... 56

Figure II-4. Hauteurs d'eau mesurées dans les bacs de rétention correspondent respectivement aux parcelles de terre nue, avec végétation spontanée et avec luzerne 57

Figure II-5. Comparaison des hauteurs d'eau mesurées et simulées dans les bacs de rétentions pour les parcelles de terre nue 58

Figure II-6. Comparaison des hauteurs d'eau mesurées et simulées dans les bacs de rétention pour les parcelles de (a) végétation spontanée (b) luzerne 58

Chapitre 3

Figure III-2. Daily data and simulated values when daily pressure heads and water contents were simultaneously included in the objective function (SPM1): (a) pressure heads at 100 cm depth, (b) pressure heads at 150 cm depth, (c) water contents at 50 cm depth and (d) water content at 100 cm depth. 73

Figure III-3. Daily data and simulated values for 3 scenarios: (a) SPM2 using the data as in SPM1 plus the last value of cumulative bottom flux and evaporation, (b) SPM3 using the data as in SPM1 plus 10 water retention values and their weights were supposed to be 0.001 and (c) SPM4 using the data as in SPM3, the weight of 10 water retention values were supposed to be 0.1. 76

Figure III-4. Daily data and simulated values when lysimeter system was divided into 4 layers (SPM-4la): (a) pressure heads at 100 cm depth, (b) pressure heads at 150 cm depth, (c) water contents at 50 cm depth and (d) water content at 100 cm depth. 78

Figure III-5. Comparison of daily data and predicted values for two scenarios SPM_2la and SPM_4la: (a) pressure heads at 100 cm depth, (b) pressure heads at 150 cm depth, (c) water contents at 50 cm depth, (d) water content at 100 cm depth and (e) water contents at 150 cm depth. 79

Chapitre 4

Figure V-1. Sensitivity of Br^- BTCs to (a) the hydraulic property shape factor n, (b) the saturated water content θ_s, (c) the saturated hydraulic conductivity Ks and (d) the dispersivity λ for the SPM. 119

Figure V-2. Sensitivity of Br^- BTCs to (a) the saturated water content in the mobile region $\theta_{s,mo}$, (b) the saturated water content in the immobile region $\theta_{s,im}$, (c) the dispersivity λ and (d) the first-order rate solute transfer coefficient ω_s for the DPM. 120

Figure V-3. Illustration of the effects of the first-order rate solute transfer coefficient ω_s and the first-order rate water transfer coefficient ω_w on the Br^- BTCs for the DPM: (a) SPM and reference case of the DPM, (b) ω_s is decreased 10 and 100 times and ω_w is fixed, (c) ω_w is decreased 10 and 100 times and ω_s is fixed. 126

Chapitre 5

Figure V-1. Sensitivity of Br^- BTCs to (a) the hydraulic property shape factor n, (b) the saturated water content θ_s, (c) the saturated hydraulic conductivity Ks and (d) the dispersivity λ for the SPM. 119

Figure V-2. Sensitivity of Br^- BTCs to (a) the saturated water content in the mobile region $\theta_{s,mo}$, (b) the saturated water content in the immobile region $\theta_{s,im}$, (c) the dispersivity λ and (d) the first-order rate solute transfer coefficient ω_s for the DPM. 120

Figure V-3. Illustration of the effects of the first-order rate solute transfer coefficient ω_s and the first-order rate water transfer coefficient ω_w on the Br^- BTCs for the DPM: (a) SPM and reference case of the DPM, (b) ω_s is decreased 10 and 100 times and ω_w is fixed, (c) ω_w is decreased 10 and 100 times and ω_s is fixed. 126

Chapitre 6

Figure VI-1. Experimental set up 131

Figure VI-2. Comparison of the measured and simulated ACE concentrations in the leaching solution of the saturated column: (a) when parameters f and $\underline{\omega}$ were simultaneously optimized, (b) when parameters K_d and $\underline{\omega}$ were simultaneously optimized 142

Figure VI-3. Comparison of the measured and simulated FLA and PYR concentrations in the leaching solution of the saturated column: (a) when parameter f optimized based on the observed FLA concentrations, (b) when parameter f optimized based on the observed PYR concentrations 143

Figure VI-4. Comparison of the measured and simulated ACE concentrations in the leaching solution of the nonsaturated column: (a) f and $\underline{\omega}$ were simultaneously optimized, (b) K_d and $\underline{\omega}$ were simultaneously optimized, and (c) f, $\underline{\omega}$, λ, and K_d were simultaneously optimized 145

Figure VI-5. Comparison of the measured and simulated FLA and PYR concentrations in the leaching solution of the nonsaturated column: (a) f and λ were simultaneously optimized based on the observed FLA concentrations, (b) K_d and λ were simultaneously optimized based on the observed FLA concentrations, (c) f and λ were simultaneously optimized based on the observed PYR concentrations, and (d) K_d and λ were simultaneously optimized based on the observed PYR concentrations..... 146

Liste des tableaux

Chapitre 1

Tableau I-1. Valeurs représentatives de la conductivité hydraulique à saturation pour les différents types de textures de sol (Clapp and Hornberger, 1978) 25

Tableau I-2. Les différents types d'équations de sorption (d'après Simunek and van Genuchten, 2006) 33

Tableau I-3. Les équations des modèles et les paramètres de l'écoulement d'eau et de transport de soluté 38

Tableau I-4. Caractéristiques de deux logiciels couramment utilisés dans le domaine de sciences du sol (adapté à partir de la revue de (Kohne et al., 2009a) 42

Tableau I-5. Exemples des applications du logiciel HYDRUS-1D ou 2D (adapté à partir de la revue de (Kohne et al., 2009a) 43

Chapitre 2

Tableau II-1. Caractéristiques de la terre de Homécourt (Michel, 2009b) 55

Tableau II-2. Valeurs des paramètres de van Genuchten pour la terre d'Homécourt..... 56

Chapitre 3

Table III-1. Description and initial values of the 5 SPM parameters for soil layer in the lysimeter vessel 64

Table III-2. Sensitivity of the 5 SPM parameters to hourly output predictions 68

Table III-3. Estimability order of the 5 SPM parameters as a function of hourly measurements in the lysimeter: (a) pressure heads at 3 depths, (b) water contents at 3 depths, (c) cumulative bottom flux and (d) cumulative evaporation. 69

Table III-4. Estimability order of the 5 SPM parameters when hourly pressure heads and hourly water contents were combined. 69

Table III-5. Net influence (%) of the more estimable SPM parameter(s) on the remaining one(s) when hourly pressure heads and water contents were combined. 69

Table III-6. Sensitivity of the 5 SPM parameters to daily output predictions..... 71

Table III-7. Estimability order of the 5 SPM parameters as a function of daily measurements in the lysimeter: (a) pressure heads at 3 depths, (b) water contents at 3 depths, (c) cumulative bottom flux and (d) cumulative evaporation. 71

Table III-8. Estimability order of the 5 SPM parameters when daily pressure heads and water contents at 3 depths in the lysimeter were combined 71

Table III-9. Net influence (%) of the more estimable parameters on the remaining ones, daily pressure heads and water contents being combined 72

Table III-10. Soil hydraulic parameters, with corresponding confidence intervals, estimated from daily data using HYDRUS-1D for the 4 scenarios..... 74

Table III-11. Mean absolute error (MAE), root mean square error (RMSE), modified index of agreement (MIA) between observed data and simulated values for 4 scenarios shown in Figures 1 and 2. 75

Table III-12. Soil hydraulic parameters, with corresponding confidence intervals, estimated from daily data using HYDRUS-1D for 3 soil layers 77

Table III-13. Mean absolute error (MAE), root mean square error (RMSE), index of agreement (IA), modified index of agreement (MIA) between observed data and calculated values (figure III-3) 77

Table III-14. Mean absolute error (MAE), root mean square error (RMSE), modified index of agreement (MIA) between the observed data and calculated values (figure III-4) 78

Chapitre 4

Table IV-1. Description and initial value of 8 parameters in dual-porosity model 87

Table IV-2. Sensitivity classes 89

Table IV-3. Sensitivity coefficients of 8 parameters in dual-porosity model to different daily data ... 94

Table IV-4. Estimability order of 8 parameters in dual-porosity model in function of daily measurements in the lysimeter: (a) pressure heads, (b) water contents, (c) cumulative water at lower boundary of the lysimeter, (d) evaporation at upper boundary of the lysimeter 95

Table IV-5. Estimability order of 8 parameters in dual-porosity model daily pressure heads and daily water contents at 3 depths in the lysimeter were investigated at the same time..... 96

Table IV-6. Net influence of the more estimable parameter(s) on the remaining model parameter(s) for the dual-porosity model when daily pressure heads and daily water contents were investigated at the same time..... 97

Table IV-7. Soil hydraulic parameters of dual-porosity model (DPM), with corresponding confidence intervals, estimated from daily data using HYDRUS-1D for different scenarios 98

Table IV-8. Mean absolute error (MAE), Root mean square error (RMSE), Modified of index agreement (MIA) comparing observed data and simulated values shows in figure 2 100

Table IV-9. Soil hydraulic parameter in dual-porosity model (DPM), with corresponding confidence intervals, estimated from daily data using HYDRUS-1D for different scenarios 102

Table IV-10. Mean absolute error (MAE), Root mean square error (RMSE), Modified of index agreement (MIA) comparing the observed data and the simulated values as showed in figures 3 and 4 103

Chapitre 5

Table V-1. Definition and initial values of the SPM and DPM parameters. 113

Table V-2. Sensitivity classes based on vpc and on I_{norm} 114

Table V-3. Results of the SPM and DPM parameter sensitivity analysis. 117

Table V-4. Estimability order of the 7 SPM parameters based on Br^- BTCs 121

Table V-5. Estimability order of the DPM 11 parameters based on Br- BTCs † 122

Table V-6. Correlation classes 122

Table V-7. Net influence of the more estimable parameter(s) on the remaining one(s) for the SPM † 123

Table V-8. Net influence of the more estimable parameter(s) on the remaining one(s) for the DPM † 123

Table V-9. Effect of ω_w and ω_s on the residence time distribution 124

Chapitre 6

Table VI-1. Experimental conditions 132

Table VI-2. Definition and initial values of four solute transport parameters in the two-site sorption model (2SM) 135

Table VI-3. Estimability order of four solute transport parameters based on ACE, FLA, and PYR leaching in the saturated column, respectively 138

Table VI-4. Estimability order and correlations of four solute transport parameters based on ACE, FLA, and PYR leaching in the nonsaturated column, respectively 140

Table VI-5. Solute transport parameters in the two-site sorption model, with the corresponding confidence intervals, estimated from measured ACE concentrations in the leaching solution of the saturated column using HYDRUS-1D and the modified index of agreement (MIA) 141

Table VI-6. Fraction of sites with instantaneous sorption in the two-site sorption model, as well as its confidence interval, estimated from measured FLA and PYR concentrations, respectively, in the leaching solution of the saturated column using HYDRUS-1D and the modified index of agreement (MIA) 142

Table VI-7. Solute transport parameters in the two-site sorption model, with the corresponding confidence intervals, estimated from measured ACE concentrations in the leaching solution of the nonsaturated column using HYDRUS-1D and also the modified index of agreement (MIA)..... 144

Table VI-8. Solute transport parameters in the two-site sorption model, as well as its confidence interval, estimated from measured FLA and PYR concentrations, respectively, in the leaching solution of the nonsaturated column using HYDRUS-1D and also the modified index of agreement (MIA).. 147

Liste des symboles et abréviations utilisés

Symbole	Signification	Unité
C	concentration du soluté dans la phase liquide	$M\ L^{-3}$
c_{im}	concentration du soluté dans l'eau immobile	$M\ L^{-3}$
c_{mo}	concentration du soluté dans l'eau mobile	$M\ L^{-3}$
D	coefficient de dispersion	$L^2\ T^{-1}$
D_e	coefficient de dispersion effectif	$L^2\ T^{-1}$
D_h	coefficient de dispersion hydrodynamique	$L^2\ T^{-1}$
D^w	coefficient de diffusion binaire du soluté dans l'eau	$L^2\ T^{-1}$
D_e	coefficient de diffusion effectif dans la solution de sol	$L^2\ T^{-1}$
f_e	fraction de sites qui est supposée en équilibre avec la phase liquide	-
f_{mo}	fraction de sites de sorption en contact avec l'eau mobile	-
g	accélération de la pesanteur	$L\ T^{-2}$
H	charge hydraulique	L
h	potentiel de pression	L
h_f	potentiel de pression dans les macropores	L
h_m	potentiel de pression dans les matrices du sol	L
I	coefficient de sensibilité -	
I_{nor}	coefficient de sensibilité normalisé -	
K_d	coefficient de distribution du soluté entre phases liquide et solide	$L^3\ M^{-1}$
K_F	coefficient d'isotherme de Freundlich	$M^{-\beta}\ L^{-3\beta}$
K_f	conductivité hydraulique dans les macropores	$L\ T^{-1}$
K(h)	conductivité hydraulique	$L\ T^{-1}$
K_m	conductivité hydraulique dans la matrice du sol	$L\ T^{-1}$
K_s	conductivité hydraulique à saturation	$L\ T^{-1}$
l	coefficient de connexion des pores (modèle de van Genuchten)	-
M_s	masse de la phase solide	M
M_t	masse totale du solide humide	M
n	paramètre empirique dans le modèle de van Genuchten	-
R	facteur de retard	-

s^e	fraction sur laquelle la sorption des solutés est instantanée	-
s^k	fraction sur laquelle la sorption des solutés est limitée par la cinétique	-
s	concentration du soluté dans la phase solide	$M\ M^{-1}$
s_{mo}	concentration du soluté dans la région mobile	$M\ M^{-1}$
S_e	saturation effective	-
q	vitesse de Darcy	$L\ T^{-1}$
t	temps	T
V_e	volume total d'eau dans le milieu poreux	L^3
V_p	volume des pores	L^3
V_t	volume total du système de sol	L^3
V_S	volume de solide sec	L^3
v	vitesse moyenne de l'eau dans les pores	$L\ T^{-1}$
z	coordonnée spatiale	L
Z	matrice de sensibilité	-

Lettres grecques

Symbole	Signification	Unité
α	paramètre empirique du modèle de van Genuchten	L^{-1}
α_k	constante de vitesse du premier ordre dans le modèle à deux sites de sorption	T^{-1}
β	coefficient d'isotherme de Freundlich	-
ξ	facteur de tortuosité	-
Γ_w	vitesse de transfert d'eau entre les deux régions d'eau mobile et immobile	T^{-1}
Γ_S	vitesse de transfert de soluté entre les deux régions d'eau mobile et immobile	$M\ L^3\ T^{-1}$
ε	porosité du sol	$L^3\ L^{-3}$
ρ_h	masse volumique apparente humide	$M\ L^{-3}$
ρ_s	masse volumique apparente sèche	$M\ L^{-3}$
ρ_r	masse volumique réelle du solide	$M\ L^{-3}$
η	coefficient d'isotherme de Langmuir	$L^3\ M^{-1}$

λ	dispersivité	L
θ	teneur en eau volumique	$L^3 L^{-3}$
θ_f	teneur en eau volumique dans les macropores	$L^3 L^{-3}$
θ_m	teneur en eau volumique dans les matrice du sol	$L^3 L^{-3}$
θ_r	teneur en eau volumique résiduelle	$L^3 L^{-3}$
θ_s	teneur en eau volumique à saturation	$L^3 L^{-3}$
ω	rapport du volume de macropores au volume total	-
ω_{mim}	coefficient de transfert du soluté entre deux régions mobile et immobile	T^{-1}
ω_{dp}	coefficient de transfert du soluté entre les macropores et les matrices du sol	T^{-1}
ω_w	coefficient de transfert d'eau du premier ordre	T^{-1}
Φ	terme source et/ou de réaction chimique	$M L^{-3} T^{-1}$
Φ_k	réactions sur les sites de sorption cinétique	$M L^{-3} T^{-1}$
Φ_f	terme source et/ou de réaction chimique dans les macropores	$M L^{-3} T^{-1}$
Φ_m	terme source et/ou de réaction chimique dans la matrice du sol	$M L^{-3} T^{-1}$
Φ_{mo}	terme source et/ou de réaction chimique dans la région mobile	$M L^{-3} T^{-1}$
Φ_{im}	terme source et/ou de réaction chimique dans la région immobile	$M \quad L^{-3} \quad T^{-1}$

Abréviation	**Signification**
CDE	Modèle de convection-dispersion
HAP	Hydrocarbures aromatiques polycycliques
MIM	Modèle d'eau mobile-immobile
DPM	Modèle à double porosité

Introduction générale

Dans le passé, les activités humaines et particulièrement les activités industrielles ont provoqué la dissémination d'un très grand nombre de composés chimiques dans les compartiments de l'environnement, notamment dans les sols. Les cessations d'activité et fermetures d'usines ont donné naissance à d'immenses superficies de friches industrielles. Actuellement, tous les pays industrialisés sont confrontés à la gestion de la dépollution et la reconversion de ces friches. En France, elles sont très nombreuses dans les grandes agglomérations et dans les anciennes régions à tradition industrielle comme l'Ile de France, le Nord et la Lorraine (http://basol.environnement.gouv.fr). En Lorraine, elles représentent plus de 6 000 ha.

Dans les sols de friches industrielles et dans les nappes contaminées, on rencontre une grande variété de polluants présents seuls ou en mélange. Il s'agit d'hydrocarbures (fractions pétrolières, hydrocarbures chlorés, hydrocarbures aromatiques polycycliques *etc*.), de métaux (zinc, plomb, cadmium, mercure, nickel *etc*.) ou autres composés *(e.g.* arsenic, cyanure). La présence de ces polluants représente un danger pour les écosystèmes et la santé humaine, avec un risque de transfert vers l'homme par l'eau et la chaîne alimentaire. Dans cette thèse, nous nous intéresserons particulièrement aux sols pollués des anciennes usines métallurgiques et cokeries, principalement pollués par des hydrocarbures aromatiques polycycliques (HAP) issus du goudron de houille et par des métaux.

Ce travail se situe dans le contexte du GISFI, Groupement d'Intérêt Scientifique sur les Friches Industrielles (http://www.gisfi.fr). Le GISFI rassemble des laboratoires de recherches de différentes disciplines et des partenaires industriels et institutionnels autour des problématiques liées aux sols de friches industrielles. Il s'intéresse aux procédés de dépollution et à l'étude du devenir des polluants et de leur transfert vers des cibles comme l'eau souterraine et les organismes.

Pour cette dernière problématique et dans le cadre de la démarche de diagnostic et d'évaluation détaillée des risques que présentent les sites pollués, la connaissance et la prévision du devenir des polluants dans l'espace et le temps sont extrêmement importantes. Cette connaissance repose sur les résultats d'investigations à un instant donné ou pendant une période donnée, accompagné d'une modélisation des phénomènes de migration des polluants dans les sols et les eaux souterraines. Dans ce but, l'utilisation de codes de calculs analytiques ou numériques est incontournable pour comprendre et quantifier les processus de transport de polluants. Pour prédire les potentialités de transport de polluants dans les sols et les nappes, de nombreux codes, commerciaux ou libres sont disponibles comme par exemple HYDRUS-1D et 2D, MACRO, SWAP, *etc*. Ces codes proposent un couplage entre l'hydrodynamique en zone saturée et non saturée, les processus bio-physico-chimiques et, pour certains, le transport colloïdal. Un certain nombre d'études montre que le transport des polluants dans la zone non saturée est fortement influencé par des processus comme l'écoulement préférentiel, le transport hors équilibre et le transport facilité par les colloïdes, qui ne sont pas pris en compte dans les modèles classiques.

- Les processus gouvernant **le transport préférentiel** d'eau et de polluants sont probablement les plus difficiles à prendre en compte pour une prédiction précise du transport. En effet, l'écoulement préférentiel est dû à la présence des macropores et autres « irrégularités »

structurales. Ces hétérogénéités du profil de sols provoquent le développement d'instabilités de l'écoulement. On observe aussi dans certain cas la canalisation de l'écoulement due à la présence de couches en pente qui réorientent l'écoulement d'eau de haut en bas.

- L'écart à l'équilibre thermodynamique peut être d'origine physique et/ou chimique. Le transport hors équilibre dit physique est dû à des limitations de type diffusionnel, celui dit « chimique », aux cinétiques réactionnelles.
- Le transport « facilité » correspond au transport des polluants liés à des colloïdes minéraux ou organique. Sa modélisation requiert la compréhension du transport colloïdal, comprenant le détachement des colloïdes, leur migration dans le milieu poreux et leur arrêt. Les modèles de transport colloïdal ont principalement été développés pour la zone saturée.

Ainsi, la prise en compte des processus mentionnés ci-dessus devrait améliorer considérablement la représentation et la prédiction du transport de polluants dans les sols. Mais l'accroissement de la complexité des modèles conduit à une augmentation du nombre de paramètres. Or, beaucoup d'entre eux ne sont pas accessibles directement par l'expérience. De plus, les paramètres mesurables sont le plus souvent obtenus après échantillonnage par des mesures à l'échelle du laboratoire. Leurs valeurs ne sont pas forcément celles qui seraient obtenues à l'échelle du terrain.

Par conséquent, les paramètres des modèles sont souvent obtenus par optimisation, en comparant la réponse du système expérimental à la réponse calculée. Cette réponse peut être par exemple la courbe de percée d'un traceur. Mais cette comparaison est-elle toujours suffisante pour valider les paramètres obtenus par optimisation ? On se heurte souvent à des problèmes concernant la non-unicité et l'incertitude des paramètres estimés. Ces problèmes peuvent être liés à la faible sensibilité des paramètres aux données expérimentales utilisées, à l'insuffisance de l'information des données incluses dans la fonction-objectif, au grand nombre de paramètres optimisés simultanément, à l'existence de corrélations entre les paramètres optimisés voire à l'algorithme local d'optimisation. Des données complémentaires sont quelquefois indispensables pour améliorer la qualité des optimisations. Donc, avant d'optimiser les paramètres, on peut se demander si :

(i) les données expérimentales pour une telle étude contiennent suffisamment d'information pour pouvoir estimer ce nombre de paramètres,

(ii) les paramètres sont corrélés entre eux,

(iii) la qualité des données expérimentales est suffisante, et, le cas échéant, s'il est nécessaire de réaliser des mesures complémentaires.

Pour répondre à ces questions, on a besoin d'une méthode qui doit rendre compte de la **sensibilité** et de **l'estimabilité** des paramètres utilisés. Et pour pouvoir valider les résultats « théoriques », l'utilisation des systèmes expérimentaux bien contrôlés des conditions aux limites et des mesures est indispensable. Dans ce travail de thèse, nous avons utilisé des systèmes expérimentaux à différentes échelles, depuis le laboratoire jusqu'à la parcelle et le lysimètre de terrain. Ce travail est divisé en six chapitres :

- Le premier chapitre rappelle les notions fondamentales concernant le milieu poreux et l'état de l'art de la modélisation de l'écoulement d'eau et du transport de soluté en milieu poreux. Il présente également les codes de calculs existant et les principes de la méthode inverse. Ce

chapitre se termine par la présentation de la démarche et les objectifs scientifiques détaillés de la thèse.

- Le second chapitre présente le test du logiciel HYDRUS-1D pour un cas d'étude concret, celui de la modélisation de l'écoulement d'eau dans des dispositifs parcelles de terrain.
- Le troisième chapitre présente les résultats concernant les études de sensibilité et d'estimabilité ainsi que l'optimisation des paramètres hydrodynamiques à partir de différents types de données expérimentales mesurées dans un lysimètre de terrain. Il repose sur le modèle d'écoulement uniforme implanté dans le logiciel HYDRUS-1D.
- Le quatrième chapitre présente les résultats obtenus cette fois-ci dans le cas de l'écoulement préférentiel implanté dans le logiciel HYDRUS-1D. Les corrélations entre les paramètres y sont étudiées en détails.
- Le cinquième chapitre présente les études de sensibilité et d'estimabilité des paramètres affectant le transport de traceur bromure dans le lysimètre de terrain.
- Le sixième chapitre présente les études de sensibilité et d'estimabilité ainsi que l'optimisation des paramètres de transport du modèle de transport hors équilibre chimique en basant sur la lixiviation des hydrocarbures aromatiques polycycliques.

La conclusion générale reprend les points principaux et ouvre des perspectives.

Nous avons choisi de rédiger les chapitres 3 à 6 sous la forme d'articles soumis à des revues internationales. Le contenu du chapitre 3 a été soumis à *J. Hydrol.*, celui du chapitre 5 à *Vadose Zone J.*, ceux des chapitres 4 et 6 sont en cours de soumission.

Chapitre I : Théorie et état de l'art de la modélisation de l'écoulement d'eau et du transport de soluté en milieu poreux

1. Introduction

Dans ce chapitre, après avoir rappelé rapidement les notions fondamentales concernant le milieu poreux, nous allons présenter en détails les modèles qui permettent de décrire l'écoulement d'eau, l'écoulement préférentiel, le transport hors équilibre physique et chimique. Le transport facilité par les colloïdes est aussi abordé. Ensuite, les codes de calculs couramment utilisés dans la littérature sont synthétisés. La théorie et le principe de la méthode inverse sont décrits en bref afin de donner une vision globale pour l'optimisation des paramètres dans ce travail de thèse. Ce chapitre se termine par les conclusions de la synthèse bibliographique et les objectifs scientifiques de la thèse.

2. Notions fondamentales concernant le milieu poreux

2.1. Présentation du sol

Un sol est une pellicule d'altération recouvrant la roche. Il est formé d'une fraction minérale et de matière organique. Un sol prend naissance à partir de la roche-mère puis il évolue sous l'action des facteurs du milieu, essentiellement le climat et la biosphère :

- la désagrégation mécanique des roches qui donne des fragments,
- l'altération chimique des roches qui produit des ions solubles (cations, anions, silicates).

Ce processus d'altération de la roche forme le complexe d'altération qui comprend les argiles et d'autres constituants comme les oxydes et hydroxydes, carbonates, phosphates, sulfates de fer, aluminium, magnésium et silicium. La kaolinite, par exemple, qui est l'argile la plus fréquemment présente dans les sols a comme formule : $Si_4Al_4O_{10}(OH)_8$.nH2O. Les 10 éléments les plus présents dans les sols sont, dans l'ordre décroissant : O, Si, Al, Fe, C, Ca, K, Na, Mg. Environ la moitié à deux tiers du volume d'un sol est constituée de matière solide. Les composés minéraux représentent, plus de 90 % de cette matière solide. Les éléments traces jouent également un rôle important : Mn, Sr, V, Cr *etc.*

La **matière organique** peut être définie comme une matière carbonée provenant d'êtres vivants végétaux et animaux. Elle est composée d'éléments principaux (C, H, O, N) et d'éléments secondaires (S, P, K, Ca, Mg…). Elle se répartit en quatre groupes selon son origine :

- la matière organique vivante, animale et végétale, qui englobe la totalité de la biomasse en activité,
- les débris d'origine végétale (résidus végétaux, exsudats) et animale (déjections, cadavres) regroupés sous le nom de matière organique fraîche,
- des composés organiques intermédiaires, appelés matière organique transitoire, provenant de l'évolution de la matière organique fraîche,
- des composés organiques stabilisés, les matières humiques (acides humiques et acides fulviques), provenant de l'évolution des matières précédentes.

La distinction entre acides humiques et fulviques est faite sur la base de leur acidité, en relation avec leur structure moléculaire. Les acides fulviques sont réputés plus acides, contenant dans leur molécule

un nombre plus important de groupements fonctionnels donneurs de protons. La composition moyenne de ces matières humiques est très complexe, différentes formules moléculaires sont proposées, par exemple : $C_{187}H_{186}O_{89}N_9S$ (acide humique) et $C_{135}H_{182}O_{95}N_5S_2$ (acide fulvique). Les composés humiques s'associent aux ions minéraux et aux minéraux argileux pour former les complexes argilo-humiques. Ces grosses molécules jouent le rôle de ciment et conditionnent la structure du sol.

La composition du sol comprend des constituants minéraux et organiques. Elle est souvent très complexe du fait de l'hétérogénéité de ces constituants en taille et en propriétés physiques et biochimiques. Cependant, la distribution des particules sable, limon, argile et de matières organiques entrant dans la composition du sol permet de définir une classification en différents types de sol (Crevoisier, 2005).

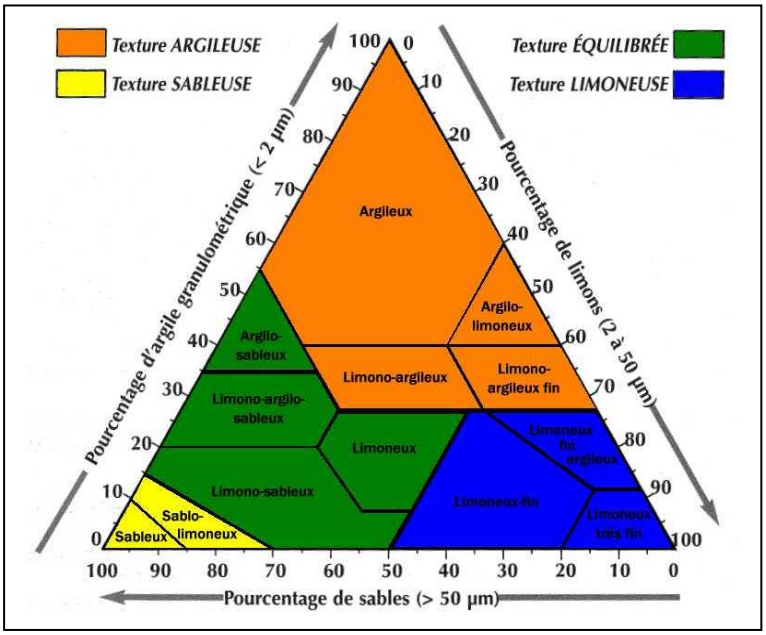

Figure I-1. Triangle des textures du sol permettant de classer les sols selon leur granulométrie (Crevoisier, 2005)

2.2. Porosité

La porosité volumique, ε, d'un sol est définie comme le rapport du volume du vide (également appelé volume des pores V_p [L^3]) au volume total de sol V_t [L^3] :

$$\varepsilon = \frac{V_p}{V_t} \qquad [I.1]$$

On distingue la porosité texturale et la porosité structurale. La **porosité texturale** est liée à l'arrangement des particules entre elles (sable et limons, enrobages ou amas d'argiles). La taille des pores est, dans la matrice argileuse, généralement inférieure à 50 nm. Pour un sable grossier compacté, la taille maximale des pores est de l'ordre de quelques centaines de microns. Cette porosité fine représente un système où prédominent les transferts de types diffusifs ; l'interaction de la phase

liquide avec la matrice y est prépondérante ; les vitesses lentes de transfert ne peuvent concurrencer les cinétiques des réactions physico-chimiques de type sorption qui peuvent s'y produire.

La **porosité structurale** est liée à la constitution du matériau ainsi qu'à son histoire. Les fissures délimitant les agrégats et la porosité tabulaire due aux racines et aux organismes vivants constituent autant d'accidents structuraux qui jouent un rôle préférentiel dans les transferts rapides, le plus souvent verticalement et souvent jusqu'à une grande profondeur.

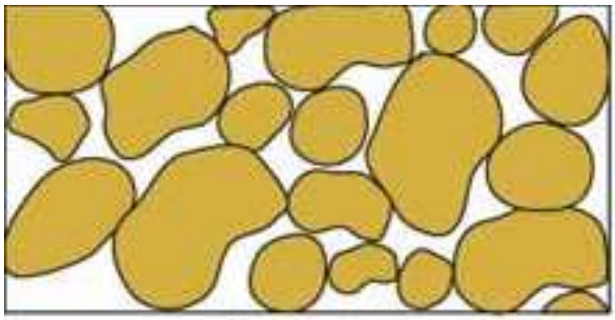

Figure I-2. Schéma illustrant la porosité du sol

Cette distinction détermine l'existence d'un double système de transport : dans les crevasses, les écoulements sont généralement convectifs et dans les massifs délimités par les fissures, les transferts hydriques et de solutés sont de natures diffusives. Ce double déplacement induit l'existence de plusieurs échelles temporelles pour l'écoulement (Jouannin, 2004).

2.3. Masse volumique

La masse volumique apparente humide ou totale d'un milieu poreux, ρ_h [M L^{-3}], est exprimée par :

$$\rho_h = \frac{M_t}{V_t} \qquad [I.2]$$

où M_t est la masse totale du solide humide [M].

La masse volumique apparente sèche, ρ_s [M L^{-3}], est le rapport de la masse du sol sec M_S et du volume total V_t :

$$\rho_s = \frac{M_S}{V_t} \qquad [I.3]$$

La masse volumique réelle du solide, ρ_r [M L^{-3}], est définie par :

$$\rho_r = \frac{M_S}{V_S} \qquad [I.4]$$

où V_S est le volume de solide sec [L^3].

2.4. Teneur en eau volumique

La teneur en eau volumique θ est définie par :

$$\theta = \frac{V_e}{V_t} \qquad [I.5]$$

où V_e est le volume total d'eau dans le milieu poreux [L^3].

Le degré de saturation S représente la fraction du volume des pores V_p occupée par l'eau V_e :

$$S = \frac{V_e}{V_p} = \frac{\theta}{\theta_s} \qquad [I.6]$$

où θ_s est la teneur en eau à saturation [L^3 L^{-3}]. S tend vers 0 dans un sol sec et vers 100% dans un sol totalement saturé.

2.5. Potentiel de pression

Le potentiel de pression est défini comme le travail nécessaire pour déplacer de manière réversible une unité de quantité d'eau de l'état de référence jusqu'à la pression de l'eau dans le volume de sol considéré. Mesurable à l'aide d'un tensiomètre, il est fréquemment aussi nommé potentiel tensiométrique. Dans le milieu poreux, à chaque teneur en eau correspond une répartition des phases air et eau à l'intérieur du volume élémentaire représentatif. La phase d'eau étant continue, les pressions s'y égalisent à une cote donnée z et il en résulte un potentiel de pression, h [L], unique :

$$h = \frac{P_{eau}}{\rho g} \qquad [I.7]$$

où P_{eau} est la pression en eau dans le sol à la cote z [M L^{-1} T^{-2}], ρ est la masse volumique de l'eau [M L^{-3}], g est l'accélération de la pesanteur [L T^{-2}].

Nous pouvons distinguer deux domaines du potentiel de pression. Par définition, la pression relative est nulle au toit de la nappe (surface libre). Par convention, la pression est positive dans la zone saturée et négative dans la zone non saturée.

Le **potentiel total** est décrit par la notion de charge hydraulique, H, et ses composantes sont le potentiel de pression, h [L], et la charge de gravité z [L] :

$$H = h + z \qquad [I.8]$$

Avec l'axe des z dirigé « vers le haut ».

2.6. Loi de Darcy

La loi de Darcy indique que l'écoulement d'un liquide à travers un milieu poreux se fait dans la direction de la force motrice : le gradient de charge hydraulique agissant sur le liquide. Le débit dépend aussi d'une caractéristique fondamentale du sol : la conductivité hydraulique.

A l'échelle macroscopique, la loi de Darcy peut être généralisée aux milieux variablement saturés, en considérant que la conductivité hydraulique est fonction du potentiel de pression :

$$q = -K(h)\frac{\partial H}{\partial z} \qquad [I.9]$$

où q est la vitesse de Darcy [L T^{-1}], $K(h)$ est la conductivité hydraulique [L T^{-1}], H est la charge hydraulique [L].

2.7. Conductivité hydraulique

La conductivité hydraulique, K [L T^{-1}], selon la loi de Darcy, est l'aptitude du milieu poreux à transmettre l'eau qu'il contient pour une teneur en eau donnée. La diminution de la teneur en eau entraîne une diminution rapide de la conductivité hydraulique. En milieu saturé, la conductivité hydraulique est uniforme (dans le cas d'un sol donné et pour une direction d'écoulement donnée) et égale à sa valeur maximale, la conductivité hydraulique à saturation notée K_S.

Tableau I-1. Valeurs représentatives de la conductivité hydraulique à saturation pour les différents types de textures de sol (Clapp and Hornberger, 1978)

Texture	Conductivité hydraulique à saturation Ks (m j^{-1})
Sable	15,21
Sable limoneux	13,51
Limon sableux	2,99
Limon fin	0,62
Limon	0,60
Limon argileux sableux	0,55
Limon argileux fin	0,15
Limon argileux	0,21
Argile sableuse	0,19
Argile fine	0,09
Argile	0,11

2.8. Relations θ(h) et K(h)

Le fonctionnement hydrodynamique d'un sol est contrôlé par deux caractéristiques macroscopiques dépendant à la fois de sa texture et de sa structure :

- La courbe de rétention hydrique, qui relie la teneur en eau volumique, θ, au potentiel de pression, h, et qui exprime la capacité du sol à retenir l'eau à un état énergétique donné.
- La courbe de conductivité hydraulique qui exprime la capacité du sol à transmettre l'eau en fonction de son état de saturation mesuré par h ou θ.

2.8.1. Relation teneur en eau - potentiel de pression θ(h)

Dans la zone non saturée du sol, la teneur en eau et le potentiel de pression varient de manière concomitante. La relation existant entre ces deux paramètres constitue dès lors un élément essentiel de la description de l'état hydrique du milieu poreux non saturé. Cette relation notée θ(h) exprime les

variations d'intensité des forces de capillarité en fonction de la teneur en eau. Graphiquement, elle est représentée par une courbe, dénommée **courbe caractéristique d'humidité du sol** ou **courbe de rétention hydrique** (figure I-3).

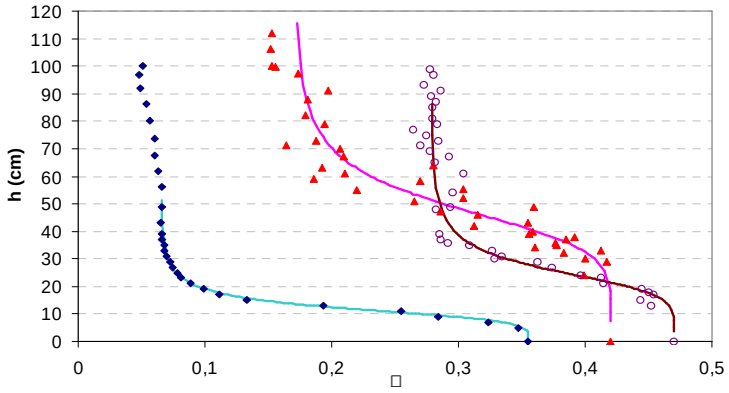

Figure I-3. Exemples de courbes de rétention d'eau (Gujisaite, 2008)

Nous pouvons définir deux types de modèles qui permettent de paramétrer θ(h) : ceux à fondement physique et ceux à fondement mathématique. Les modèles physiques utilisent directement certaines caractéristiques physiques du sol (granulométrie, densité, *etc*.) pour estimer les propriétés hydrodynamiques *(e.g.* Wang et al., 2009 ; Twarakavi et al., 2009. Schaap et al. (2001) ont récemment développé un logiciel nommé ROSETTA pour estimer les paramètres hydrodynamiques du sol à partir des caractéristiques du sol.

Plusieurs auteurs (Brooks and Corey, 1964 ; Campbell, 1974 ; van Genuchten, 1980b) ont proposé des expressions mathématiques de θ(h). Les modèles mathématiques doivent être suffisamment flexibles pour s'adapter à la texture et à la structure des différents types de sols. Nous présentons ici l'expression du modèle de van Genuchten (van Genuchten, 1980b) couramment utilisé dans la littérature:

$$\theta(h)=\begin{cases}\theta_r+(\theta_S-\theta_r)\left(1+|\alpha h|^{1/(1-m)}\right)^{-m} & h<0\\ \theta_S & h\geq 0\end{cases} \qquad \text{[I.10]}$$

où θ_r est la teneur en eau résiduelle [L^3 L^{-3}], θ_s est la teneur en eau à saturation [L^3 L^{-3}], h est le potentiel de pression [L], α est un paramètre empirique [L^{-1}], n est un paramètre empirique (supérieur à 1) [-], m = 1- 1/n, est un paramètre empirique [-].

2.8.2. Relation conductivité hydraulique - potentiel de pression K(h)

La courbe de conductivité hydraulique, K(h), peut se déduire théoriquement – sous certaines hypothèses très restrictives - par celle de Mualem (Mualem, 1976b), modifiée par van Genuchten (van Genuchten, 1980b). Avec le modèle de van Genuchten nous pouvons prédire la conductivité hydraulique connaissant la courbe de rétention hydrique et e la conductivité hydraulique à saturation. Les auteurs obtiennent ainsi une formule continue :

$$K(h)=\begin{cases} K_S.S_e^{l}.\left[1-\left(1-S_e^{1/m}\right)^{m}\right]^{2} & h<0 \\ K_S & h\geq 0 \end{cases} \qquad \text{[I.11]}$$

où K_s est la conductivité à saturation [L T^{-1}], S_e est la saturation effective [-], l est le coefficient de connexion des pores [-]. S_e est le taux de saturation qui s'exprime par :

$$S_e = \frac{\theta-\theta_r}{\theta_S-\theta_r} \qquad \text{[I.12]}$$

où θ_r est la teneur en eau volumique résiduelle [L^3 L^{-3}], θ_S est la teneur en eau volumique à saturation [L^3 L^{-3}].

Le paramètre l est souvent pris égal à 0,5 (Mualem, 1976b).

Ce modèle est très sensible à des petits changements de la courbe θ(h) à proximité de la saturation, surtout quand le paramètre n est proche de 1 (Vogel et al., 2000b). Des petites variations sur la courbe θ(h) peuvent aboutir à des courbes K(h) très différentes quand nous incorporons le paramètre n dans le modèle de (van Genuchten, 1980b).

3. Ecoulement d'eau en milieu poreux à saturation variable

Dans cette section, nous présentons les équations pour l'écoulement d'eau en milieu poreux à saturation variable. Classiquement, la description du transport d'eau dans les sols est basée sur l'équation de Richards qui combine l'équation I-9 de Darcy-Buckingham pour le flux d'eau avec l'équation de conservation de masse. L'équation de Richards prédit un écoulement dans la zone non saturée, même si elle est modifiée en utilisant la variation spatiale des propriétés hydrauliques du sol. En réalité, la zone non saturée peut être extrêmement hétérogène. Certaines de ces hétérogénéités peuvent mener à un processus d'écoulement préférentiel macroscopiquement très difficile à représenter avec l'équation de Richards. Un exemple évident de l'écoulement préférentiel est le mouvement rapide de l'eau et des solutés à travers des macropores, existant entre les agrégats de sol ou créés par des vers de terre ou des canaux de racines *(e.g.* Sander and Gerke, 2007 ; Cey et al., 2009). Dans ce travail, les simulations sont réalisées avec le logiciel HYDRUS-1D, nous allons présenter dans cette partie les équations monodimensionnelles de l'écoulement d'eau ou de transport de soluté.

3.1. Modèle d'écoulement d'eau uniforme

L'écoulement d'eau uniforme est décrit par l'équation de Richards exprimée par:

$$\frac{\partial\theta(h)}{\partial t} = \frac{\partial}{\partial z}\left(K(h)\left(\frac{\partial h}{\partial z}+1\right)\right)-S \qquad \text{[I.13]}$$

où t est le temps [T], z est la coordonnée spatiale [L], S est le volume d'eau pris par unité de temps par les racines [L^3 L^{-3} T^{-1}], θ est la teneur en eau [L^3 L^{-3}], K est la conductivité hydraulique [L T^{-1}] (S peut désigner aussi tout type de source), h est le potentiel de pression [L].

L’équation I.13 est fortement non linéaire, il existe donc relativement peu de cas pour lesquels des solutions analytiques simplifiées peuvent être obtenues. La plupart des applications pratiques de l'équation I.13 exigent une solution numérique, qui peut être obtenue par des méthodes numériques telles que la méthode des différences finies ou la méthode des éléments finis. L’application de ces méthodes pour résoudre les équations de l’écoulement d’eau est décrite en détails dans la référence (Simunek and van Genuchten, 2006).

3.2. Ecoulement préférentiel

De plus en plus d’études montrent que le transport d’eau ne peut pas être décrit correctement par les modèles classiques qui supposent que l’écoulement d’eau est uniforme *(e.g.* Simunek and van Genuchten, 2008). Cela est dû à la présence de macropores ou d'autres canaux par lesquels l'eau et les solutés peuvent se déplacer préférentiellement (figure I-4). Les processus préférentiels de l’écoulement d’eau et de transport des solutés sont probablement les plus difficiles à prendre en compte et rendent difficile la prédiction précise du transport de l’eau et des contaminants dans les sols. Contrairement à l'écoulement uniforme, l’écoulement préférentiel est la conséquence du mouillage irrégulier du profil de sol qui implique que l'eau se déplace plus rapidement dans certaines parties du profil de sol que dans d’autres.

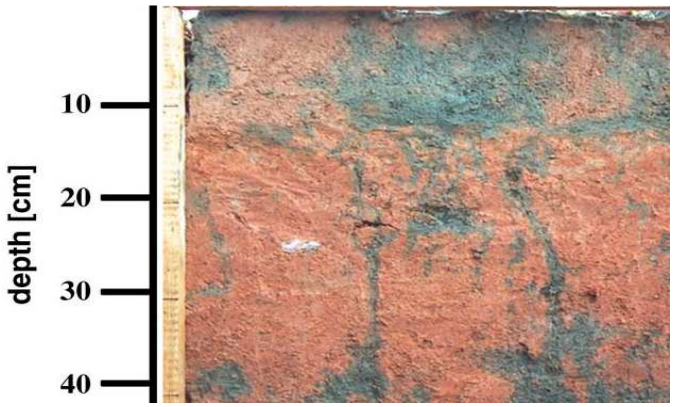

Figure I-4. Illustration de l’écoulement préférentiel par le traceur coloré (Sander and Gerke, 2007)

Hendrickx et Flury (2001) ont défini l’écoulement préférentiel comme l’ensemble des processus par lesquels l'eau et les solutés se déplacent dans certains macropores, canaux ou fissures en évitant toute une fraction de la matrice poreuse. Pour ces raisons, l'eau et les solutés peuvent se propager rapidement à des profondeurs beaucoup plus grandes et beaucoup plus rapidement que prévu par l'équation de Richards. Les raisons majeures de l'écoulement préférentiel sont :

- la présence des macropores et d'autres propriétés structurales,
- le développement d’instabilités d'écoulement provoquées par des hétérogénéités du profil
- et la « canalisation » de l'écoulement dû à la présence des couches en pente qui réorientent l'écoulement d'eau du haut vers le bas.

L'écoulement préférentiel peut être décrit par des modèles comme le modèle à double porosité (dual-porosity model) ou le modèle à double perméabilité (dual-permeability model) *(e.g.* Ventrella et al., 2000 ; Simunek et al., 2001). Ces deux types de modèles supposent que le milieu poreux se compose de deux régions qui sont liées, une associée à la zone entre les agrégats ou macropores, et l'autre comporte les pores internes de l'agrégat ou de la matrice du sol. Le modèle à double porosité suppose que l'eau dans la matrice de sol est stagnante tandis que le modèle à double perméabilité rend compte également d'écoulement d'eau dans la matrice de sol. Les concepts de ces modèles sont illustrés dans les figures I-5 et I-6 (Simunek and van Genuchten, 2008). Leurs avantages et inconvénients sont bien discutés dans l'article de revue (Simunek et al., 2003). Dans cette partie, nous présentons brièvement les équations de ces modèles.

3.2.1. Modèle à double porosité (Dual-Porosity Model)

Le concept du modèle à double porosité suppose que l'écoulement de l'eau est limité aux macropores. L'eau dans la matrice est immobile. La phase liquide est partagée en une région mobile, θ_{mo}, et une région immobile, θ_{im} (van Genuchten and Wierenga, 1976 ; Sardin et al., 1991b ; Simunek et al., 2003 ; Simunek and van Genuchten, 2008) :

$$\theta = \theta_{mo} + \theta_{im} \qquad \text{[I.14]}$$

La formulation de l'écoulement d'eau dans le modèle à double porosité peut être décrite par l'équation de Richards pour la région mobile en combinant avec le terme qui représente la source, Γ_w, afin de prendre en compte l'échange d'eau avec la région immobile *(e.g.* Simunek et al., 2003) :

$$\frac{\partial \theta_{mo}(h_{mo})}{\partial t} = \frac{\partial}{\partial z}\left(K(h_{mo})\frac{\partial h_{mo}}{\partial z} + K(h_{mo}) \right) - \Gamma_w \qquad \text{[I.15a]}$$

$$\frac{\partial \theta_{im}(h_{im})}{\partial t} = \Gamma_w \qquad \text{[I.15b]}$$

où h_{mo} est le potentiel de pression dans la région mobile [L], t est le temps [T], z est la coordonnée spatiale [L], K est la conductivité hydraulique [L T^{-1}].

Le modèle à double porosité a été appliqué dans plusieurs études à l'échelle de colonne de laboratoire ou du terrain *(e.g.* Simunek et al., 2001 ; Kohne et al., 2004a ; Kohne et al., 2006b ; Kodesova et al., 2005b ; Haws et al., 2005).

3.2.2. Modèle à double perméabilité (Dual-Permeability Model)

Différents modèles de double perméabilité peuvent être utilisés pour décrire l'écoulement d'eau et le transport de soluté dans le milieu poreux. Certains modèles utilisent les équations identiques pour le transport d'eau dans la région de macropores et la région de micropores tandis que les autres utilisent différentes formulations pour deux régions. Nous présentons ici l'approche de Gerke et van Genuchten (Gerke and Van Genuchten, 1993b) qui ont utilisé l'équation de Richards pour les deux régions. Les équations de transport d'eau pour la région des macropores (indice f) et pour la région des micropores (indice m) sont les suivantes :

$$\frac{\partial \theta_f(h_f)}{\partial t} = \frac{\partial}{\partial z}\left[K_f(h_f)\left(\frac{\partial h_f}{\partial z} + 1 \right) \right] - S_f(h_f) - \frac{\Gamma_w}{\omega} \qquad \text{[I.16a]}$$

$$\frac{\partial \theta_m(h_m)}{\partial t} = \frac{\partial}{\partial z}\left[K_m(h_m)\left(\frac{\partial h_m}{\partial z}+1\right)\right] - S_m(h_m) + \frac{\Gamma_w}{1-\omega} \qquad \text{[I.16b]}$$

où ω est le rapport du volume de macropores au volume total du système de sol. Cette approche est assez compliquée car elle exige la caractérisation des fonctions de rétention d'eau et de la conductivité hydraulique pour deux régions en même temps. C'est pourquoi l'application du modèle à double perméabilité requiert beaucoup plus de paramètres que celle du modèle à double porosité.

Il a été appliqué dans différentes études comme *(e.g.* Vogel et al., 2000a ; Simunek et al., 2001 ; Kohne et al., 2004). L'écoulement préférentiel est généralement mieux décrit en utilisant le modèle à double perméabilité que le modèle à double porosité mais l'inconvénient du modèle à double perméabilité est d'avoir besoin beaucoup plus de paramètres qui ne sont pas mesurables (Simunek et al., 2003 ; Kohne et al., 2009a).

3.2.3. Transfert d'eau entre régions

Il existe deux approches décrivant la vitesse de transfert d'eau entre deux régions : la première approche est basée sur la différence entre les teneurs en eau effectives des deux régions en utilisant l'équation du premier ordre (Simunek et al., 2001), la seconde approche est basée sur la différence entre les pressions des deux régions (Gerke and Van Genuchten, 1993b). L'avantage de la première est d'avoir besoin de moins de paramètres que la seconde (Simunek et al., 2003). Elle est décrite par l'équation suivante :

$$\Gamma_w = \omega_w\left(S_{e,mo} - S_{e,im}\right) \qquad \text{[I.17]}$$

où ω_w est le coefficient de transfert d'eau du premier ordre [T^{-1}], $S_{e,mo}$ et $S_{e,im}$ sont respectivement les teneurs en eau effectives des régions mobile et immobile.

4. Transport d'un soluté en milieu poreux

4.1. Processus de transport de soluté

Dans la zone non saturée, la majorité des produits chimiques est présente principalement dans les phases liquide et solide, et ils sont transportés pratiquement dans et par l'eau. Les trois processus principaux qui peuvent jouer un rôle important pour le transport des solutés dans la phase liquide sont la diffusion moléculaire, la dispersion hydrodynamique, et la convection. Le flux total d'un soluté dans la phase liquide est la somme des flux dus à ces trois processus :

$$F_T = F_d + F_D + F_C \qquad \text{[I.18]}$$

où F_T représente le flux total du soluté dans la phase liquide [$M\ L^{-2}\ T^{-1}$], F_d, F_D et F_C représentent respectivement les flux transportés par diffusion, dispersion et convection [$M\ L^{-2}\ T^{-1}$].

4.1.1. Diffusion moléculaire

La diffusion moléculaire est un résultat du mouvement aléatoire des molécules chimiques sous l'effet de la température. Elle est définie par rapport aux potentiels chimiques. Ce processus fait déplacer un soluté d'un endroit avec une concentration plus élevée à un autre endroit avec une concentration plus faible. Le transport diffusif peut être décrit par la loi de Fick :

$$F_d = -\theta\xi_1(\theta)D^w \frac{\partial c}{\partial z} = -\theta D^s \frac{\partial c}{\partial z} \qquad [I.19]$$

où D^w est le coefficient de diffusion binaire du soluté dans l'eau [L^2 T^{-1}], D^S est le coefficient de diffusion effective dans la solution de sol [L^2 T^{-1}], c est la concentration du soluté dans la phase liquide [M L^{-3}], ξ_1 est le facteur de tortuosité qui rend compte de l'augmentation des longueurs de trajet et la diminution des sections des solutés de dispersion dans la phase liquide.

Comme la diffusion des solutés dans l'eau de sol est sévèrement entravée par l'air et les particules, le facteur de tortuosité dépend fortement de la teneur en eau. Le modèle pour le facteur de tortuosité couramment utilisé est l'équation de Millington et Quirk (Millington and Quirk, 1961):

$$\xi_1(\theta) = \frac{\theta^{7/3}}{\theta_s^2} \qquad [I.20]$$

où θ_s est la teneur en eau à saturation [L^3 L^{-3}].

4.1.2. Dispersion

Le transport dispersif des solutés résulte de la distribution inégale des vitesses d'écoulement d'eau à l'intérieur et entre les différents pores du sol. La dispersion peut être exprimée à partir de la loi de Newton qui suppose que les vitesses dans un tube capillaire simple suivent une distribution parabolique, avec la plus grande vitesse au niveau de l'axe central et les vitesses nulles aux parois. Donc, les solutés au milieu d'un pore se transportent plus rapidement que les solutés qui sont plus loin du centre. Comme la distribution des solutés ioniques dans un pore dépend de leur charge, quelques types de solutés peuvent se déplacer plus rapidement que d'autres. Les processus précédents de dispersion mènent à un processus hydrodynamique global de dispersion qui peut être décrit mathématiquement en utilisant la loi de Fick comme pour le cas de la diffusion moléculaire :

$$F_D = -\theta D_h \frac{\partial c}{\partial z} = -\theta\lambda v \frac{\partial c}{\partial z} = -\lambda q \frac{\partial c}{\partial z} \qquad [I.21]$$

où D_h est le coefficient de dispersion hydrodynamique [L^2 T^{-1}], v est la vitesse moyenne de l'eau dans les pores [L T^{-1}], λ est la dispersivité [L], q est la densité de flux vertical d'eau [L T^{-1}].

La dispersivité est une propriété importante du transport des solutés, mais il est assez difficile de la mesurer expérimentalement. Elle peut être estimée à partir des courbes de percée des traceurs en utilisant les solutions analytiques de l'équation de convection (*e.g.* Gujisaite, 2008). La dispersivité change souvent avec la distance de déplacement des solutés en milieux hétérogènes. Les valeurs de la dispersivité longitudinale s'étendent typiquement sur environ 1 cm pour les colonnes de laboratoire et sur environ 5-10 cm pour les sols à l'échelle du terrain. Si aucune information n'est disponible, on peut en toute première approximation utiliser une valeur égale à un dixième de la distance de transport pour la dispersivité longitudinale et une valeur d'un centième de la distance de transport pour la dispersivité transversale (*e.g.* Anderson, 1984 ; Simunek and van Genuchten, 2006). Il s'agit toutefois d'une approximation grossière.

4.1.3. Convection

Le transport convectif dans la phase liquide se rapporte au soluté étant transporté avec le fluide mobile. L'équation du transport convectif est décrite par :

$$F_C = qc \qquad [I.22]$$

Le flux total de soluté dans la phase liquide est obtenu par la somme de trois processus : diffusion, dispersion et convection :

$$F_T = qc - \theta D^S \frac{\partial c}{\partial z} - \theta D_h \frac{\partial c}{\partial z} = qc - \theta D_e \frac{\partial c}{\partial z} \qquad [I.23]$$

où D_e est le coefficient de dispersion effective [L^2 T^{-1}] qui prend en compte à la fois la diffusion et la dispersion hydrodynamique.

4.2. Modèle de convection-dispersion

4.2.1. Les équations de transport

Ce modèle est aussi basé sur le principe de conservation de la masse et l'équation monodimensionnelle est la suivante :

$$\frac{\partial(\theta c)}{\partial t} + \rho \frac{\partial s}{\partial t} = \frac{\partial}{\partial z}\left(\theta D_e \frac{\partial c}{\partial z}\right) - \frac{\partial(qc)}{\partial z} - \phi \qquad [I.24]$$

où ρ est la densité du milieu poreux [M L^{-3}], s est la concentration du soluté dans la phase solide [M M^{-1}], D_e est la dispersion effective dans la phase liquide [L^2 T^{-1}], Φ représente le terme source et/ou réaction chimique [M L^{-3} T^{-1}], z est la coordonnée spatiale [L].

On introduit le facteur retard, R [-], dans l'équation précédente, ce qui donne en supposant D_e, q et θ constants :

$$\frac{\partial(\theta c)}{\partial t} + \rho \frac{\partial s}{\partial t} = \frac{\partial(\theta R c)}{\partial t} = \frac{\partial}{\partial z}\left(\theta D_e \frac{\partial c}{\partial z}\right) - \frac{\partial(qc)}{\partial z} - \phi \qquad [I.25]$$

$$R = 1 + \frac{\rho}{\theta}\frac{ds(c)}{dc} \qquad [I.26]$$

Pour le transport des solutés inertes et non adsorbés et sans terme source, nous obtenons la forme simplifiée suivante :

$$\frac{\partial(\theta c)}{\partial t} = \frac{\partial}{\partial z}\left(\theta D_e \frac{\partial c}{\partial z}\right) - \frac{\partial(qc)}{\partial z} \qquad [I.27]$$

Les équations ci-dessus sont habituellement connues « équations de convection-dispersion ». Ce modèle est souvent utilisé pour les études du transport de soluté dans les sols, il peut cependant s'avérer insuffisant dans certains cas, ce qui amène à définir les autres types de modèles.

4.2.2. La sorption linéaire et non linéaire

L'équation de convection-dispersion donnée par l'équation I.25 contient deux concentrations inconnues (celles pour la phase liquide et solide). Pour pouvoir résoudre cette équation, des informations supplémentaires sont nécessaires afin de relier ces deux concentrations. La manière la plus commune est de supposer la sorption instantanée et d'utiliser les isothermes d'adsorption pour

relier ces concentrations. La forme la plus simple de l'isotherme d'adsorption d'un soluté est **l'isotherme linéaire** donnée par l'équation suivante :

$$s = K_d c \qquad \text{[I.28]}$$

où K_d est le coefficient de distribution [$L^3 M^{-1}$].

L'utilisation de l'isotherme linéaire peut simplifier énormément la description mathématique du transport des solutés, mais la sorption et l'échange sont généralement non linéaires et ils dépendent souvent de la présence des autres composés dans la solution de sol. Le facteur retard des solutés pour l'adsorption non linéaire n'est pas constant, contrairement au cas de l'absorption linéaire, il dépend de la concentration. Plusieurs types de modèles ont été proposés dans le passé pour décrire la sorption non linéaire. Les modèles couramment utilisés sont les modèles de Freundlich (Freundlich, 1909) et de Langmuir (Langmuir, 1918) dont les équations sont données ci-dessous :

$$s = K_F c^{\beta} \qquad \text{[I.29]}$$

$$s = \frac{K_d c}{1 + \eta c} \qquad \text{[I.30]}$$

où K_F [$M^{-\beta} L^{-3\beta}$] et β [-] sont les coefficients d'isotherme de Freundlich, η [$L^3 M^{-1}$] est le coefficient d'isotherme de Langmuir. Le tableau I-2 rassemble les différents modèles utilisés dans les études du transport des solutés en milieu poreux (Simunek and van Genuchten, 2006).

Tableau I-2. Les différents types d'équations de sorption (d'après Simunek and van Genuchten, 2006)

Equation	Modèle	Référence
$s = k_1 c$	Linéaire	Lindstrom et al., 1967
$s = K_F c^{\beta}$	Freundlich	Freundlich, 1909
$s = \frac{K_d c}{1 + \eta c}$	Langmuir	Langmuir, 1918
$s = \frac{k_1 c}{1 + k_2 c} + \frac{k_3 c}{1 + k_4 c}$	Double Langmuir	Shapiro and Fried, 1959
$s = k_1 c^{c^{k_2/k_3}}$	Freundlich prolongé	Sibbesen, 1981
$s = \frac{k_1 c}{1 + k_2 c + k_3 \sqrt{c}}$	Gunary	Gunary, 1970
$s = k_1 c^{k_2} - k_3$	Fitter-Sutton	Fitter and Sutton, 1975
$s = \frac{RT}{k_1} \ln(k_2 c)$	Temkin	Bache and Williams, 1971)

4.3. Transport hors équilibre

De plus en plus d'études montrent que l'utilisation du modèle à l'équilibre ne réussit pas toujours à prédire les données expérimentales (*e.g.* (Kohn et al., 2006b ; Boivin et al., 2006). Des expériences au laboratoire et *in situ* ont démontré l'existence d'un écart à l'équilibre (*e.g.* Schwartz et al., 1999 ; Johnson et al., 2003 ; Sander and Gerke, 2007 ; Mahmood-Ul-Hassan et al., 2008). Le transport hors équilibre peut être représenté à l'aide de différents modèles analytiques ou numériques (Toride et al., 1993 ; van Dam et al., 1997 ; Simunek et al., 2005b). Le développement des modèles qui rendent compte de transport hors équilibre comprend deux directions : modèle de transport hors équilibre physique et modèle de transport hors équilibre chimique. Dans la littérature, on trouve aussi la combinaison entre les deux *(e.g.* Pot et al., 2005). L'application du modèle de transport hors équilibre physique ou chimique dépend du système de transport et du type de solutés étudiés. Dans cette section, nous décrivons les concepts et les équations des modèles de transport hors équilibre physique et chimique. Pour plus d'informations concernant ces aspects, on pourra se reporter à la publication (Simunek and van Genuchten, 2008).

4.3.1. Transport hors équilibre physique

a. Modèle à double porosité et modèle d'eau mobile-immobile

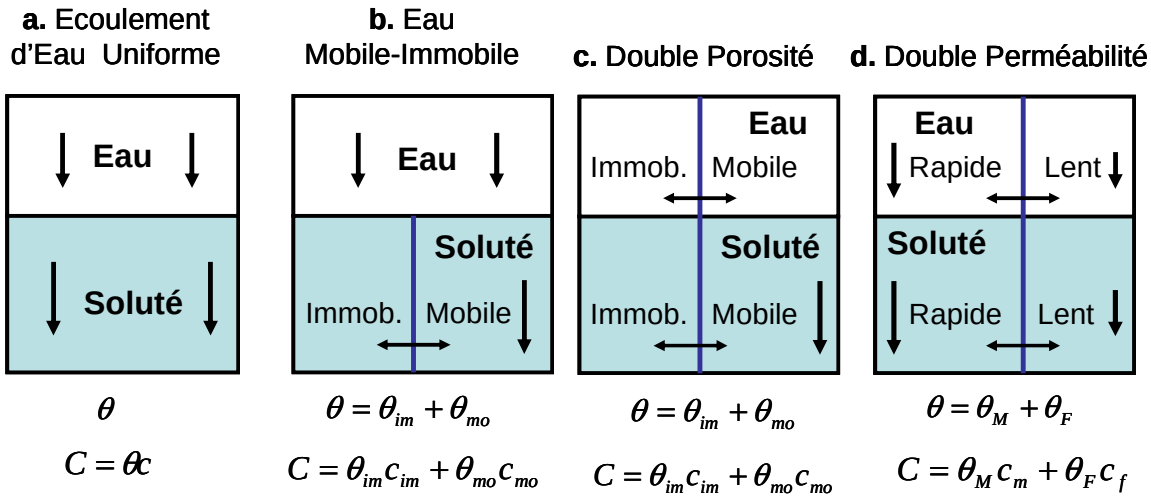

Figure I-5. Concepts des modèles hors équilibre physique pour le transport d'eau et de soluté : θ est la teneur en eau volumique, θ_{mo} et θ_{im} sont respectivement les teneurs en eau volumique dans les phases mobile et immobile, θ_M et θ_F sont respectivement les teneurs en eau volumique des macropores et micropores, c est la concentration de soluté avec les indices qui ont les mêmes sens que pour la teneur en eau volumique, C est la concentration totale de soluté dans la phase liquide (d'après (Simunek and van Genuchten, 2008).

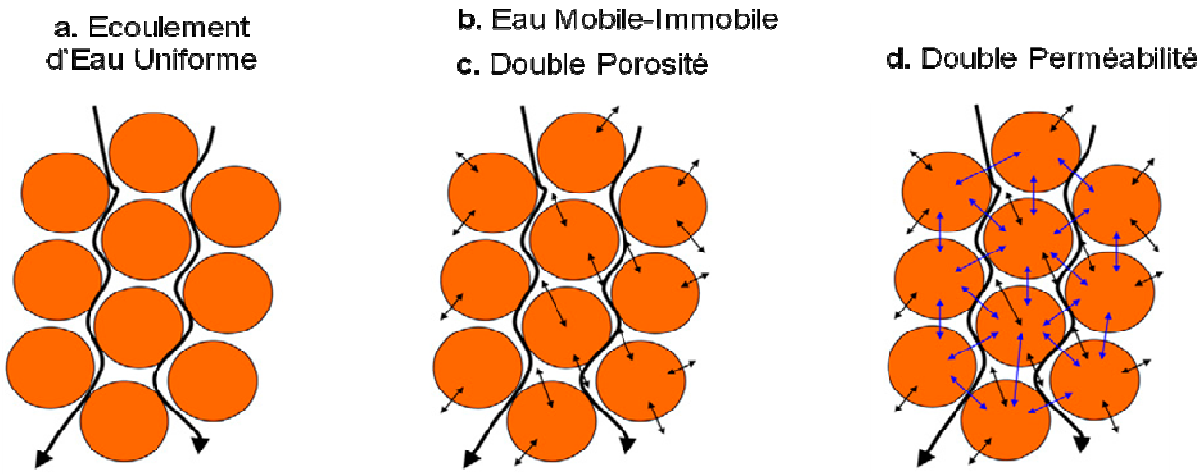

Figure I-6. Concepts des modèles hors équilibre physique pour le transport d'eau et de soluté (d'après (Simunek and van Genuchten, 2008).

Le modèle de transport à deux régions suppose que la phase liquide peut être divisée en deux régions mobile et immobile distinctes, et que l'échange de soluté entre les deux régions peut être représenté par un processus d'échange du premier ordre. Utilisant la même notation qu'avant, l'équation de transport de soluté est décrite respectivement pour la région mobile (indice *mo*) et la région immobile (indice *im*) comme :

$$\frac{\partial_{mo} c_{mo}}{\partial t} + \frac{\partial f_{mo} \rho s_{mo}}{\partial t} = \frac{\partial}{\partial t}\left(\theta_{mo} D_{mo} \frac{\partial c_{mo}}{\partial z}\right) - \frac{\partial q c_{mo}}{\partial z} - \phi_{mo} - \Gamma_S \qquad [I.31a]$$

$$\frac{\partial \theta_{im} c_{im}}{\partial t} + \frac{\partial (1 - f_{mo}) \rho s_{im}}{\partial t} = -\phi_{im} + \Gamma_S \qquad [I.31b]$$

où f_{mo} est la fraction de sites de sorption en contact avec l'eau mobile [-], Φ_{mo} et Φ_{im} sont respectivement les réactions dans la région mobile et la région immobile [M L^3 T^{-1}], Γ_S est la vitesse de transfert de soluté entre deux régions [M L^3 T^{-1}].

La vitesse de transfert du soluté entre deux régions (Γ_S) est définie comme la somme des flux diffusitifs et convectifs:

$$\Gamma_S = \omega_{mim}(c_{mo} - c_{im}) + \Gamma_w c^* \qquad [I.32]$$

où c^* est égale à c_{mo} quand $\Gamma_w > 0$ et à c_{im} quand $\Gamma_w < 0$, et ω_{mim} est le coefficient de transfert du soluté selon la loi du premier ordre [T^{-1}].

Il est important de noter que le terme de convection dans l'équation I.32 est nul pour le modèle d'eau mobile-immobile car avec ce type de modèle la teneur en eau dans la région immobile est supposée constante. On note que les même équations I.31a et I.31b peuvent être utilisées afin de prédire le transport des solutés pour le modèle à double porosité et aussi pour le modèle d'eau mobile-immobile.

b. Modèle à double perméabilité

Il comporte les équations I.16a et I.16b pour l'écoulement d'eau. La formulation du modèle à double perméabilité pour le transport des solutés peut être basée sur l'équation de convection-dispersion pour le transport des solutés dans les macropores et les matrices de sol comme suit (Gerke and Van Genuchten, 1993b) :

$$\frac{\partial \theta_f c_f}{\partial t} + \frac{\partial \rho s_f}{\partial t} = \frac{\partial}{\partial z}\left(\theta_f D_f \frac{\partial c_f}{\partial z} \right) - \frac{\partial q_f c_f}{\partial z} - \phi_f - \frac{\Gamma_S}{w} \qquad \text{[I.33a]}$$

$$\frac{\partial \theta_m c_m}{\partial t} + \frac{\partial \rho s_m}{\partial t} = \frac{\partial}{\partial z}\left(\theta_m D_m \frac{\partial c_m}{\partial z} \right) - \frac{\partial q_m c_m}{\partial z} - \phi_m - \frac{\Gamma_S}{1-w} \qquad \text{[I.33b]}$$

où les indices *f* et *m* représentent respectivement les macropores et la matrice, Φ_f et Φ_m sont respectivement les réactions dans les macropores et la matrice de sol [M L^3 T^{-1}].

La vitesse de transfert du soluté entre les macropores et la matrice est aussi définie comme la somme des flux diffusif et convectif comme suit (Gerke and van Genuchten, 1996) :

$$\Gamma_S = \omega_{dp}(1-w_m)(c_f - c_m) + \Gamma_w c^* \qquad \text{[I.34]}$$

où ω_{dp} est le coefficient de transfert du soluté [T^{-1}] donné par :

$$\omega_{dp} = \frac{\beta}{d^2} D_e \qquad \text{[I.35]}$$

où D_e est le coefficient de diffusion effective [L^2 T^{-1}] qui représente la propriété de diffusion de l'interface entre les macropores et la matrice de sol.

4.3.2. Transport hors équilibre chimique

a. Modèle à un site cinétique de sorption (One-Site Sorption Model)

Quand la sorption dans l'équation de convection-dispersion est cinétique, cette équation doit être complétée avec une équation décrivant la cinétique du processus de sorption. Les équations pour le transport des solutés dans la zone non saturée deviennent :

$$\frac{\partial(\theta c)}{\partial t} + \rho \frac{\partial s}{\partial t} = \frac{\partial}{\partial z}\left(\theta D_e \frac{\partial c}{\partial z} \right) - \frac{\partial(qc)}{\partial z} - \phi \qquad \text{[I.36a]}$$

$$\rho \frac{\partial s^k}{\partial t} = \alpha_k \rho (s_e^k - s^k) - \phi_k \qquad \text{[I.36b]}$$

$$s_e^k = K_d c \qquad \text{[I.36c]}$$

où s_e^k est la concentration adsorbée qui serait atteinte à l'équilibre avec la concentration dans la phase liquide [M M^{-1}], s^k est la concentration adsorbée du site de sorption cinétique [M M^{-1}], α_k est la constante de vitesse du premier ordre qui décrit la cinétique du processus de sorption [T^{-1}], Φ_k représente les réactions sur les sites de sorption cinétique [M L^{-3} T^{-1}].

a. Modèle d'Un Site Cinétique de Sorption

b. Modèle de Deux Sites de Sorption

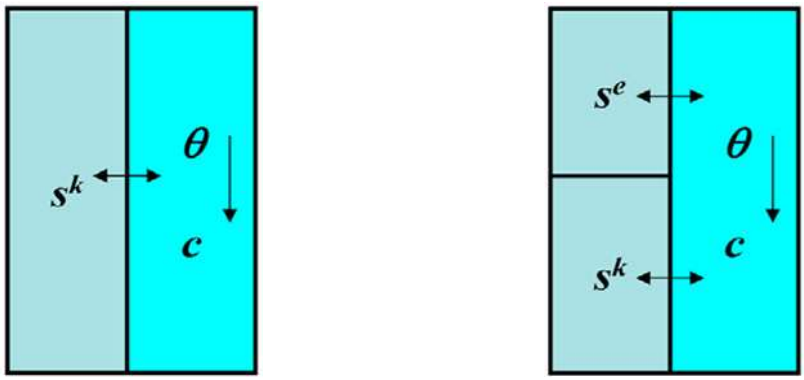

Figure I-7. Schémas conceptuels des modèles hors équilibre chimique pour le transport de soluté réactif : θ est la teneur en eau volumique, c est la concentration de soluté, s^e est la concentration adsorbée qui est à équilibre avec la concentration de soluté dans la phase liquide, s^k est la concentration adsorbée correspondant avec la fraction de sorption cinétique (d'après Simunek and van Genuchten, 2008).

b. Modèle à deux sites de sorption (Two-Site Model)

Le concept de ce modèle (figure I-7) suppose que les sites de sorption sont divisés en deux fractions : la fraction sur laquelle la sorption des solutés est instantanée (s^e, type 1) et la fraction sur laquelle la sorption est limitée par la cinétique (s^k, type 2) :

$$s = s^e + s^k \qquad \text{[I.37]}$$

Les équations décrivent le modèle à deux sites de sorption comme suit :

$$\frac{\partial(\theta c)}{\partial t} + \rho\frac{\partial s^e}{\partial t} + \rho\frac{\partial s^k}{\partial t} = \frac{\partial}{\partial z}\left(\theta D_e \frac{\partial c}{\partial z}\right) - \frac{\partial(qc)}{\partial z} - \phi \qquad \text{[I.38a]}$$

$$s^e = f_e K_d c \qquad \text{[I.38b]}$$

$$\rho\frac{\partial s^k}{\partial t} = \alpha_k \rho\left(s_e^k - s^k\right) - \phi_k \qquad \text{[I.38c]}$$

$$s_e^k = (1 - f_e)K_d c \qquad \text{[I.38d]}$$

où f_e [-] est la fraction de sites qui est supposée en équilibre avec la phase liquide, α_k est la constante de vitesse du premier ordre [T^{-1}], Φ_k représente les réactions sur les sites de sorption cinétique [$M\ L^{-3}\ T^{-1}$].

On note que quand f_e = 0, le modèle à deux sites de sorption redevient le modèle de sorption à un site cinétique car il n'existe que le site de sorption cinétique. Et quand f_e = 1, le modèle à deux sites de sorption redevient le modèle de sorption linéaire.

Tableau I-3. Les équations des modèles et les paramètres de l'écoulement d'eau et de transport de soluté

Modèle	Equation(s) de l'écoulement d'eau	Equations(s) de transport de soluté	Nombre de paramètres	Paramètres
Transport uniforme de l'eau et de soluté	I.13	I.24	7	θ_r, θ_s, α, n, K_s, λ, K_d
Modèle d'eau mobile-immobile	I.13	I.14 I.31a, I.31b I.32	9	θ_r, θ_s, α, n, K_s, λ_{mo}, K_d, f_{mo}, ω_{mim}
Modèle à double porosité	I.14 I.15a I.15b	I.31a I.31b I.32	13	$\theta_{r,im}$, $\theta_{s,im}$, $\theta_{r,mo}$, $\theta_{s,mo}$, α_{mo}, n_{mo}, K_{smo}, λ_{mo}, K_d, f_{mo}, ω_{mim}
Modèle à double perméabilité	I.16a I.16b	I.33a, I.33b I.34 I.35	18	$\theta_{r,m}$, $\theta_{s,m}$, α_m, n_m, $K_{s,m}$, $\theta_{r,f}$, $\theta_{s,f}$, α_f, n_f, $K_{s,f}$, λ_m, λ_f, K_{dm}, K_{df}, ω_{dp}, β, γ, K_{sa}
Modèle à un site cinétique de sorption	I.13	I.36a I.36b I.36c	8	θ_r, θ_s, α, n, K_s, λ, K_d, α_k
Modèle à deux sites de sorption	I.13	I.37 I.38a, I.38b I.38c, I.38d	9	θ_r, θ_s, α, n, K_s, λ, K_d, f_e, α_k

4.3.3. Transport facilité par les colloïdes

Dans un certain nombre de situations, les contaminants fortement adsorbés sur des colloïdes peuvent être transportés plus rapidement que les contaminants dissous dans l'eau. Cette partie ne sera pas à proprement parlée utilisée dans ce travail, mais souhaite quand même en faire une présentation rapide.

Un grand nombre de recherches ont porté sur le transport facilité :

- des métaux lourds (e.g. Grolimund et al., 1996 ; Karathanasis, 1999 ; Sen et al., 2002),
- des radionucléides (e.g. von Gunten et al., 1988 ; Noell et al., 1998),
- des pesticides (e. g. Vinten et al., 1983 ; Kan and Tomson, 1990 ; Lindqvist and Enfield, 1992 ; Sprague et al., 2000),
- de substances pharmaceutiques (e.g. Tolls, 2001 ; Thiele-Bruhn, 2003),
- de HAP (e .g. Totsche et al., 2007) et autres contaminants (e.g. Magee et al., 1991 ; Mansfeldt et al., 2004).

L'augmentation de mobilité des contaminants accroît le risque de contamination des eaux souterraines. La modélisation est très importante pour les études du transport facilité par les colloïdes. Les processus peuvent se dérouler sur une échelle de temps très grande (Contardi et al., 2001 ; Flury and Qiu, 2008). C'est pourquoi on a besoin des modèles pour réaliser des prédictions à long terme. Toutefois, le transport facilité par les colloïdes est un processus complexe qui exige la connaissance de l'écoulement d'eau, du transport des colloïdes (avec la mobilisation des colloïdes, la migration et

l'arrêt), du transport de contaminant dissous, et des interactions entre colloïdes et contaminants *(e.g.* Simunek and van Genuchten, 2006 ; Simunek et al., 2006a ; Flury and Qiu, 2008). Les équations de transport et de bilan de masse doivent être établies pour l'écoulement d'eau, le transport de colloïde, mais également pour décrire les interactions entre contaminants et colloïdes avec leur possibles limitations cinétiques et plus généralement la distribution des contaminants entre les différentes phases (matrice solide, colloïdes, solution) (Simunek and van Genuchten, 2008). C'est pourquoi par rapport aux autres types de modèles, les modèles pour le transport facilité par les colloïdes ont besoin d'un grand nombre de paramètres qui ne sont pas mesurables ni estimables (Pang and Simunek, 2006). La figure I-8 montre que le transport des HAP dans les sols contaminés fait intervenir le transport facilité par les colloïdes.

De plus, la modélisation du transport facilité par les colloïdes est généralement plus complexe pour la zone non saturée que celle pour la zone saturée en raison de la contribution de l'interface air-eau, l'écoulement non uniforme et l'occurrence de l'écoulement transitoire (Simunek et al., 2006a). Il existe un certain nombre d'articles de revue sur le transport colloïdal pour la zone saturée (Ryan and Elimelech, 1996 ; Sen and Khilar, 2006 ; Tufenkji, 2007) et pour la zone non saturée (DeNovio et al., 2004 ; McCarthy and McKay, 2004 ; Flury and Qiu, 2008).

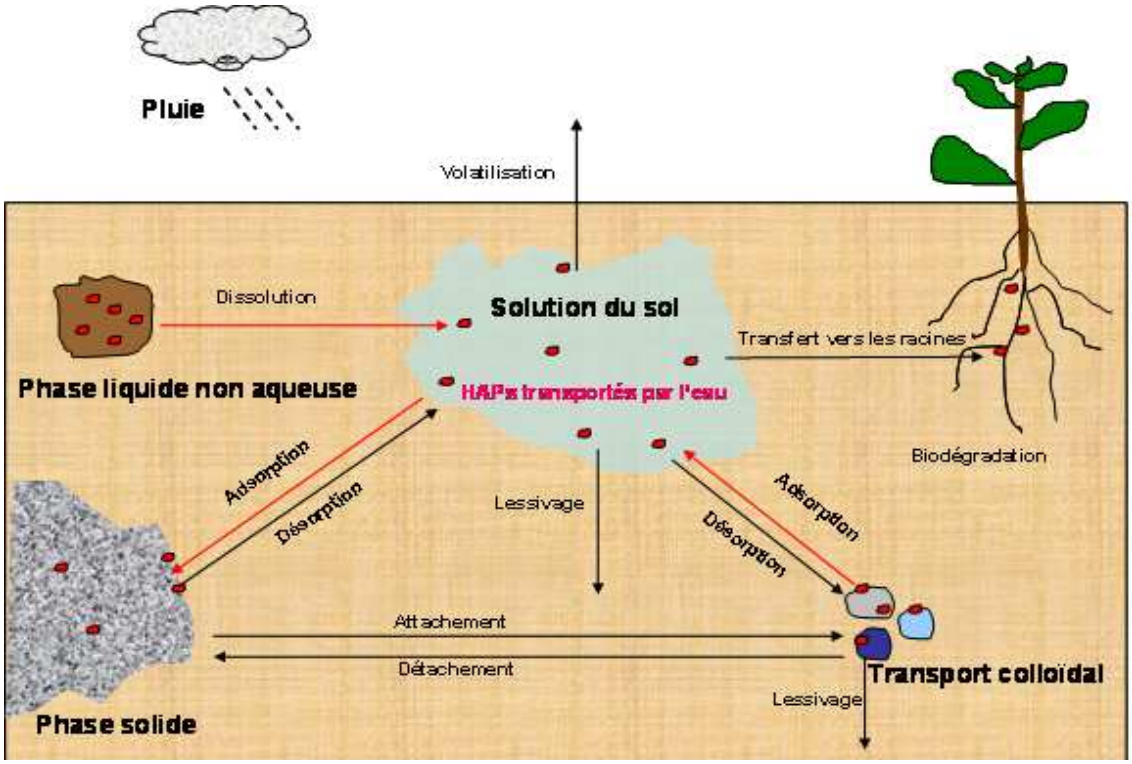

Figure I-8. Le transport de HAP à l'échelle d'une parcelle sous conditions climatiques naturelles

5. Codes de calcul

Dans la littérature, il existe un grand nombre de codes de calcul (modèles) libres ou commerciaux. On présente rapidement dans cette section certains de ces codes.

5.1. Modèles analytiques

Pour certaines conditions (*e.g.* la sorption linéaire avec écoulement d'eau permanent et uniforme) les équations de transport de solutés sont linéaires. Beaucoup de solutions analytiques ont été déterminées dans le passé pour ces types d'équations de transport de solutés, et sont employées couramment pour analyser le transport de solutés pendant l'écoulement à équilibre. Un grand nombre de solutions analytiques existent également pour les équations de l'écoulement d'eau et du transport de solutés dans la zone non saturée, mais elles peuvent être appliquées généralement seulement aux problèmes d'écoulement assez simples *(e.g.* Tilahun et al., 2005 ; Gujisaite, 2008).

Les méthodes analytiques permettent d'obtenir une solution exacte pour un problème particulier. Les modèles analytiques mènent habituellement à une équation explicite pour la concentration de soluté (ou la pression, la teneur en eau, ou la température) à un temps et à un endroit particulier. Les solutions analytiques peuvent être dérivées seulement pour les systèmes de transport simplifiés qui sont présentés par les équations linéaires, sols homogènes, conditions initiales et aux limites constantes ou fortement simplifiées.

Les modèles analytiques monodimensionnels comprennent CFITIM (van Genuchten, 1981), CXTFIT (Parker and van Genuchten, 1984), CXTFIT2 (Toride et al., 1995). CFITM rend compte du transport à équilibre des solutés, tandis que CFITIM rend compte en plus du transport hors équilibre physique et chimique. Le code CXTFIT se situe dans la suite, il a permis d'augmenter les possibilités de CFITIM en prenant en compte plus de types de conditions initiales et aux limites ainsi que les processus de dégradation à premier ordre. CXTFIT2 permet de modéliser les problèmes directs et indirects pour plusieurs types d'équation de transport comme : l'équation de convection-dispersion, les équations de transport hors équilibre physique et chimique. Le code CXTFIT est assez souvent utilisé pour les études de transport de soluté nonréactif ou réactif *(e.g.* (Dong et al., 2002) ; (Jorgensen et al., 2004) ; (Komnitsas et al., 2006) ; (Geyer et al., 2007) ; (Goppert and Goldscheider, 2008).

Il existe aussi des modèles analytiques bi ou tridimensionnels comprenant 3DADE (Leij and Bradford, 1994), N3DADE (Leij and Toride, 1997), STANMOD (Simunek et al., 1999).

5.2. Modèles numériques

Les méthodes numériques permettent aux utilisateurs de concevoir des géométries compliquées qui reflètent les conditions géologiques et hydrologiques complexes, de contrôler les paramètres dans l'espace et le temps, de choisir des conditions initiales et aux limites réalistes et d'étudier les équations de transport non linéaire (Simunek et al., 2005b). Les méthodes numériques subdivisent normalement le temps et les coordonnées spatiales en plus petits « morceaux » (méthode des différences finies, des éléments finis, et des volumes finis) et reformulent la forme continue des équations différentielles partielles en termes de système d'équations algébriques.

Un grand nombre de modèles numériques sont libres pour évaluer l'écoulement d'eau et les processus de transport des solutés dans la zone non saturée comme :

- MACRO (Jarvis, 1994) : http://bgf.mv.slu.se/ShowPage.cfm?OrgenhetSida_ID=5658
- SWAP (van Dam et al., 1997) : http://www.swap.alterra.nl/
- HYDRUS-1D (Simunek et al., 2005b) : http://www.pc-progress.com/

Dans le passé, des modèles numériques ont été développés principalement pour les applications dans le domaine de l'agronomie *(e.g.* Simunek and van Genuchten, 2006). Actuellement, ils sont de plus en plus consacrés à l'étude du devenir des polluants (radionucléides, métaux lourds, pesticides, hydrocarbure aromatiques polycycliques, colloïdes, *etc*.). Certains modèles permettent de prendre en compte des conditions initiales et aux limites complexes et de modéliser en plus le transport de vapeur et de chaleur *(e.g.* Simunek et al., 2005b). Quelques modèles numériques comme DAISY (Hansen et al., 1990), SHAW (Flerchinger et al., 1996), COUP (Jansson and Karlberg, 2001) rendent compte également des processus extrêmement non linéaires liés au cycle de congélation et décongélation. Les récents modèles numériques sont également devenus de plus en plus sophistiqués en termes de type et complexité de processus de transport de solutés qui peuvent être simulés. Enfin, ils ne sont plus limités aux solutés subissant des réactions chimiques relativement simples telles que la sorption linéaire et la dégradation à premier ordre, mais maintenant ils considèrent également une série de la sorption non linéaire, le transport hors équilibre physique et chimique, volatilisation, diffusion de gaz, détachement-attachement colloïdal, et beaucoup d'autres processus. De plus, les modèles numériques permettent aussi de rendre compte d'autres processus comme : l'évapotranspiration, le prélèvement racinaire de soluté, le développement des racines, le transport de la chaleur.

Les développeurs des modèles se concentrent actuellement sur les améliorations des modèles numériques afin de simuler les processus complexes comme le transport hors équilibre physique et chimique, l'écoulement préférentiel, le transport colloïdal *(e.g.* Simunek et al., 2005b ; Simunek and van Genuchten, 2006).

A l'heure actuelle, les logiciels de HYDRUS-1D et 2D sont couramment appliqués pour les études concernant la modélisation de transport d'eau et de solutés dans la zone saturée et non saturée. La version 1D de ce logiciel est gratuite (http://www.pc-progress.com/). Ces deux logiciels utilisent la méthode des éléments finis afin de résoudre l'équation de Richards pour l'écoulement d'eau et l'équation de convection-dispersion pour le transport des solutés. L'équation de Richards utilisée dans ces logiciels est combinée avec le terme source qui représente la prise d'eau par les racines de plantes. Les équations de transport des solutés permettent de décrire également le transport hors équilibre physique et chimique. De plus, le fait de prendre en compte les processus cinétiques d'attachement-détachement avec la phase solide permet aux utilisateurs de simuler le transport des colloïdes.

Dans les logiciels HYDRUS-1D et 2D, les propriétés hydrauliques du sol sont caractérisées en utilisant les différents types de fonctions qui relient la teneur en eau et la conductivité hydraulique (Brooks and Corey, 1964) ; (van Genuchten, 1980b) ; (Kosugi, 1996) ; (Durner, 1994a). De plus, ces logiciels ont implémenté la méthode d'optimisation de Levenberg-Marquardt afin d'estimer les paramètres hydrauliques du sol ainsi que les paramètres de transport de solutés. Les caractéristiques de deux logiciels couramment utilisés sont présentées dans le tableau I-4.

HYDRUS-1D a été récemment couplé avec le logiciel PHREEQC afin de créer un nouveau code nommé HP1 (http://www.sckcen.be/HP1/, (Jacques and Simunek, 2005). Le logiciel HP1 permet aux utilisateurs de simuler le transport multiconstituant et il rend compte de l'interaction entre les composés et des différents processus biochimiques. Dans la littérature, le logiciel HYDRUS est utilisé

pour simuler le transport d'eau ou de solutés réactifs et non réactifs et quelques exemples de son application sont rassemblés dans le tableau I-5.

Tableau I-4. Caractéristiques de deux logiciels couramment utilisés dans le domaine de sciences du sol (adapté à partir de la revue de (Kohne et al., 2009a)

	HYDRUS-1D et 2D	MACRO
Modèles utilisés	[a]SPM, MIM, DPM, DPM-MIM	[a]SPM, DPM
Ecoulement d'eau	Richards	Richards
Transfert d'eau entre deux régions	Premier ordre	Premier ordre
Evapotranspiration potentielle	Penman-Monteith, Hargreaves ou données d'entrée	Penman-Monteith ou données d'entrée
Prévèlement racinaire	Eau, soluté	Eau, soluté
Développement des racines	Oui	Oui
Transport de soluté	Convection-dispersion	
Transfert de soluté entre deux régions	Premier ordre (convection-dispersion)	Premier ordre (convection-dispersion)
Sorption	Linéaire, Freundlich, un site cinétique ou deux sites de sorption	Linéaire, Freundlich, ou deux sites de sorption
Dégradation	Premier ordre	Premier ordre
Volatilisation	Oui	Oui
Méthode inverse	Levenberg-Marquardt	SUFI
Interface graphique utilisateur	Oui	Oui
Forum de discussion	Oui	Non

Tableau I-5. Exemples des applications du logiciel HYDRUS-1D ou 2D (adapté à partir de la revue de (Kohne et al., 2009a)

Echelles	Modèle utilisés	Description des modèles	Auteurs
Colonne	SPM, MIM, DPM (transport d'eau)	1D, équation de Richard, transfert d'eau	(Simunek et al., 2001) ; (Kohne and Mohanty, 2005); (Kohne et al., 2006b)
	SPM, MIM, DPM (soluté non réactif)	1D, équation de convection-dispersion, transfert de soluté	(Zhang et al., 2004) ; (Kohne et al., 2004a)
	SPM, MIM, DPM, DPM-MIM (soluté réactif)	1D, équation de Richards, équation de convection-dispersion, transfert d'eau et de soluté, sorption linéaire ou non linéaire, dégradation	(Pot et al., 2005) ; (Kohne et al., 2006a) ; (Kohne et al., 2006b) ; (Javaux et al., 2006a)
Parcelles	SPM, MIM, DPM (soluté non réactif)	2D, équation de Richards, équation de convection-dispersion, transfert d'eau et de soluté	(Abbasi et al., 2003); (Kohne and Gerke, 2005a)
	SPM, MIM, DPM (soluté réactif)	2D, équation de Richards, équation de convection-dispersion, transfert d'eau et de soluté, sorption linéaire ou non linéaire, dégradation, prélèvement racinaire d'eau	(Kodesova et al., 2005) ; (Gardenas et al., 2006)
Terrain	SPM, MIM, DPM (soluté non réactif)	1D ou 2D, équation de Richards, équation de convection-dispersion, transfert d'eau et de soluté	(Abbasi et al., 2004); (Haws et al., 2005); (Kohne et al., 2006b) ; (Gerke and Kohne, 2004); (Kohne et al., 2006c)

6. Optimisation des paramètres

Comme nous l'avons vu, les logiciels mettent en jeu un nombre de paramètres d'autant plus élevé que les processus considérés sont complexes. Ces paramètres ne sont pas tous accessibles à la mesure directe. Pour les déterminer on a recours à la méthode inverse qui consiste à déduire un jeu de paramètres à partir de données expérimentales accessibles à l'expérience, comme par exemple une courbe de percée mesurée en colonne ou en lysimètre. Nous allons décrire dans un premier temps comment ces paramètres sont obtenus.

6.1. Méthodes inverses

Les méthodes inverses sont basées sur la minimisation d'une fonction objectif qui représente la différence entre les valeurs observées et les valeurs calculées. L'estimation des paramètres est alors itérativement améliorées lors du processus de minimisation jusqu'à ce qu'une précision désirée soit obtenue.

Quand les erreurs de mesure suivent une loi normale avec la moyenne nulle et une matrice de covariance V, la fonction de probabilité peut être écrite comme suit (Bard, 1974) :

$$L(\beta) = (2\pi)^{-n/2} \det^{-1/2} V . \exp\left\{\left(-\tfrac{1}{2}\right)\left[q^* - q(\beta)\right]^T V^{-1}\left[q^* - q(\beta)\right]\right\} \quad \text{[I.39]}$$

où L(β) est la fonction de probabilité, β est le vecteur des paramètres à optimiser *(e.g.* θ_r, θ_s, α, n, K_s, λ), n est le nombre de paramètre à optimiser, q^* = s est le vecteur des mesures *(e.g.* pression, teneur en eau, concentration en soluté), q(β) = {q_1, q_2, …, q_n } est le vecteur des valeurs calculées en fonction des paramètres inconnus.

L'équation I.39 est écrite sous forme logarithmique pour faciliter son utilisation :

$$\ln\left(L(\beta)\right) = -\frac{n}{2}\ln(2\pi) - \frac{1}{2}\ln(\det V) - \frac{1}{2}\left[q^* - q(\beta)\right]^T V^{-1}\left[q^* - q(\beta)\right] \quad \text{[I.40]}$$

Le maximum de la fonction de probabilité doit satisfaire l'équation de probabilité suivante :

$$\frac{\partial \ln(L(\beta))}{\partial \beta} = 0 \quad \text{[I.41]}$$

Si tous les éléments de la matrice de covariance V sont connus, alors la valeur du vecteur des paramètres inconnus, β, qui maximise I.40 doit réduire au minimum l'équation suivante :

$$\phi(\beta) = \left[q^* - q(\beta)\right]^T V^{-1}\left[q^* - q(\beta)\right] \quad \text{[I.42]}$$

Si l'information concernant la distribution des paramètres à optimiser est connue avant l'inversion, cette information peut être ajoutée dans le procédé d'estimation des paramètres en multipliant la fonction de probabilité par la fonction de densité de probabilité précédente, $p_o(\beta)$, qui résume les informations préalables. L'utilisation des informations préalables mène au maximum d'une fonction de densité de probabilité postérieure, $p^*(\beta)$:

$$p^*(\beta) = cL(\beta)p_o(\beta) \quad \text{[I.43]}$$

où c est une constante.

La fonction de densité postérieure est proportionnelle à la fonction de probabilité quand la distribution antérieure est uniforme. L'inclusion des informations préalables mène à la maximisation de l'équation suivante pour Φ :

$$\phi(\beta) = \left[q^* - q(\beta)\right]^T V^{-1}\left[q^* - q(\beta)\right] + \left(\beta - \hat{\beta}\right)^T V_\beta^{-1}\left(\beta - \hat{\beta}\right) \quad \text{[I.44]}$$

où β est le vecteur des paramètres contenant les informations préalables, $\hat{\beta}$ est le vecteur des paramètres associés, V_β est la matrice de covariance pour le vecteur des paramètres β. L'utilisation des informations préalables peut améliorer effectivement la qualité de l'optimisation (Russo et al., 1991b).

Les matrices de covariance V et V_β, appelées quelquefois matrices de poids, fournissent des informations sur l'exactitude des mesures et les corrélations possibles entre les erreurs de mesure et entre les paramètres (Kool et al., 1987). Quand la matrice de covariance V est diagonale et tous les éléments de V_β sont égaux à zéro, c.-à-d., les erreurs de mesure sont non corrélatives et aucune information préalable des paramètres à optimiser n'existe, le critère d'optimisation se réduit au critère :

$$\phi(\beta) = \sum_{i=1}^{n} w_i \left[q_i^* - q_i(\beta)\right]^2 \qquad \text{[I.45]}$$

où w_i est le poids d'un point de mesure i.

6.2. Solution de la méthode inverse

Beaucoup de techniques ont été développées pour résoudre le problème de minimisation non linéaire (*e.g.*, Bard, 1974 ; Kool et al., 1987). Ces méthodes sont itératives en commençant d'abord par l'estimation initiale des paramètres à estimer, β^i, et en étudiant ensuite comment la fonction objectif se comporte à proximité de l'estimation initiale. Sur la base de ce comportement, on choisit un vecteur de direction, v_i, pour avoir les nouvelles valeurs du vecteur des paramètres inconnus :

$$\beta_{i+1} = \beta_i + \rho_i v_i = \beta_i - \rho_i R_i p_i \qquad \text{[I.46]}$$

Ces nouvelles valeurs des paramètres inconnus font diminuer la valeur de la fonction objectif:

$$\phi_{i+1} < \phi_i \qquad \text{[I.47]}$$

où Φ_{i+1} et Φ_i sont respectivement les fonctions objectifs à l'étape d'itération courante et précédente, R_i est une matrice définie positive et ρ_i est une grandeur scalaire qui assure que l'étape d'itération est acceptable.

La méthode inverse est potentiellement très efficace pour estimer les paramètres nécessaires pour caractériser l'écoulement d'eau et le transport des solutés à différentes échelles, notamment quand les techniques de méthode inverse sont incluses dans les modèles numériques. Par exemple, la méthode inverse est utilisée afin d'estimer les paramètres qui caractérisent l'écoulement préférentiel *(e.g.* Simunek et al., 2001; Kohne et al., 2004 ; Kohne et al., 2006b).

Cependant, le problème concernant l'incertitude et la non unicité des paramètres optimisés existe encore (Simunek et al., 2001; Kohne et al., 2004 ; Kohne et al., 2006b). Il se peut que la méthode inverse ne donne pas de bons résultats en raison de l'information insuffisante contenues dans les données expérimentales utilisées dans la fonction objectif, du grand nombre de paramètres optimisés et des corrélations entre les paramètres du modèle qui ont été optimisés simultanément, ou encore à cause de l'algorithme local d' optimisation. Par exemple, deux études (Simunek et al., 2001 ; Kohne et al., 2006b) ont conclu que les seules observations d'écoulement d'eau ne peuvent pas contenir suffisamment l'information pour obtenir l'unicité des paramètres dans le modèle à double perméabilité. En plus, Kohne et al. (Kohne et al., 2004) ont rapporté qu'en raison de la forte corrélation entre les

teneurs en eau à saturation pour deux régions mobile et immobile ($\theta_{s,mo}$ et $\theta_{s,im}$), elles ne sont pas estimables simultanément à partir de l'écoulement d'eau et des transport de traceur à l'échelle de la colonne de laboratoire. D'après Hopmans et Simunek (Hopmans and Simunek, 1999b), l'identifiabilité des paramètres peut être augmentée en réduisant le nombre de paramètres optimisés ou en incluant de l'information expérimentale supplémentaire.

Par conséquent, pour savoir si les données expérimentales d'un système expérimental sont suffisantes pour identifier les paramètres d'un modèle, pour mieux calibrer les paramètres à partir des données expérimentales par la méthode inverse ou pour améliorer la qualité de conception du système expérimental, il est nécessaire d'étudier l'information contenue dans les données expérimentales avant de les utiliser à des fins d'optimisation et d'évaluer des corrélations entre les paramètres du modèle.

7. Analyse de sensibilité et d'estimabilité

Avant d'estimer les paramètres par la solution inverse, il est important de voir la capacité d'estimation de ces paramètres. La capacité d'estimation des paramètre est reliée strictement à l'analyse de sensibilité (Walter, 1982) et dépend de la structure du modèle, de la paramétrisation du modèle et de la conception de l'expérience **(**Yao et al., 2003). Le fait de se concentrer sur les paramètres sensibles nous permet de mieux comprendre et mieux estimer les paramètres et aussi de réduire l'incertitude des estimations (Lenhart et al., 2002).

Mathématiquement, la dépendance d'une variable y en fonction d'un paramètre p est exprimée par la dérivée partielle (Lenhart et al., 2002 ; Yao et al., 2003) :

$$\frac{\partial y(x,t)}{\partial p} \qquad y = 1,\ldots, n \text{ et } p = 1,\ldots, P \qquad [I.48]$$

n est le nombre de variables et P est le nombre de paramètres.

La variation du paramètre p implique le changement de la variable y comme suit :

$$p + \Delta p \rightarrow y^{+} \qquad [I.49]$$

$$p - \Delta p \rightarrow y^{-}$$

On obtiendra le coefficient I à partir de l'approximation de la dérivée partielle :

$$I = \frac{\partial y(x,t)}{\partial p} = \frac{y^{+} - y^{-}}{2\Delta p} \qquad [I.50]$$

Pour que le coefficient ne soit pas dimensionnel, il faut le normaliser :

$$I_{norm} = \frac{p}{y}\left(\frac{y^{+} - y^{-}}{2\Delta p}\right) \qquad [I.51]$$

Le signe du coefficient I_{norm} indique le sens de variation de la variable y quand la valeur du paramètre p est modifiée.

L'estimabilité des paramètres dépend de la structure du modèle, de leur sensibilité et des corrélations entre eux. Elle est évaluée et le sous-ensemble des paramètres estimables est établi suivant la méthode proposée par Yao et al. (2003). Cette méthode permet de quantifier l'effet de chacun des paramètres

sur la variable (notée C ici) et de prendre en compte les corrélations entre paramètres. La matrice de sensibilité des coefficients Z est construite à partir de chaque coefficient individuel (équation I.52) :

$$Z = \begin{bmatrix} \left.\frac{p_1}{C}\frac{\partial C}{\partial p_1}\right|_{t=t_1} & \cdots & \left.\frac{p_m}{C}\frac{\partial C}{\partial p_m}\right|_{t=t_1} \\ \left.\frac{p_1}{C}\frac{\partial C}{\partial p_1}\right|_{t=t_2} & \cdots & \left.\frac{p_m}{C}\frac{\partial C}{\partial p_m}\right|_{t=t_2} \\ \cdots\cdots\cdots\cdots & & \\ \left.\frac{p_1}{C}\frac{\partial C}{\partial p_1}\right|_{t=t_n} & \cdots & \left.\frac{p_m}{C}\frac{\partial C}{\partial p_m}\right|_{t=t_n} \end{bmatrix} \qquad [I.52]$$

Dans la matrice Z, le nombre de colonnes est égal au nombre de paramètres à étudier et chaque rangée correspond à la prédiction à un instant donné. Les éléments de la matrice sont calculés par la méthode des différences finies. Le sous-ensemble des paramètres estimables est calculé selon 8 étapes (Yao et al., 2003) :

1. Calculer la somme des carrés des éléments de chaque colonne,
2. Choisir le paramètre correspondant à la valeur la plus élevée de cette somme comme premier paramètre ; on considère que c'est celui qui a le plus d'influence sur la valeur de prédiction,
3. Désigner par X_L la colonne correspondante (L = 1 pour la 1ère itération),
4. Calculer Z_L, prédiction de la matrice de sensibilité complète de la matrice Z selon :
   $$Z_L = X_L \left(X_L{}^T X_L\right)^{-1} X_L{}^T Z \qquad [I.53]$$
5. Calculer la matrice résiduelle R_L : $R_L = Z - Z_L$ [I.54]
6. Calculer la somme des carrés des résidus pour chaque colonne R_L. La colonne avec la plus grande somme correspond au paramètre le plus estimable qui, parmi ceux qui restent, a le plus grand effet sur les résultats de simulations et qui n'est pas corrélé avec le paramètre déjà sélectionné,
7. Sélectionner la colonne correspondante dans Z et augmenter la matrice X_L en ajoutant la nouvelle colonne. Noter cette nouvelle matrice X_{L+1}.
8. Continuer l'itération et répéter les étapes 4 à 7 jusqu'au dernier paramètre.

On a vu que l'algorithme commençait par le choix du paramètre le plus estimable correspondant à la colonne de Z ayant la plus grande somme quadratique (étapes 1 et 2). Toutefois, ce paramètre risque d'être corrélé avec les paramètres restants. C'est pourquoi il faut orthogonaliser pour classer les influences des paramètres individuels sur la prédiction. Une fois le premier paramètre estimable déterminé, les influences des paramètres restants doivent être ajustées pour toute corrélation qui existe entre la colonne associée au premier paramètre et toute autre colonne de Z afin de pouvoir évaluer l'influence nette de chaque paramètre restant. Cet ajustement est fait par une régression entre toutes les colonnes de la matrice Z initiale et celle associée au paramètre le plus influent. Cette régression aboutit à une matrice de mêmes dimensions que la matrice Z initiale, et la colonne de la matrice résiduelle R_L associée au paramètre le plus influent est une colonne de zéros (étapes 3-5). On poursuit l'orthogonalisation en cherchant la colonne dont la somme quadratique des termes est la plus élevée,

ce qui donne le second paramètre influant sur la prédiction *etc*. L'orthogonalisation est poursuivie jusqu'au dernier paramètre.

8. Conclusion et objectifs de la thèse

Les résultats des travaux synthétisés dans cette revue mettent en évidence les rôles importants de **l'écoulement préférentiel et du transport hors équilibre** sur la modélisation du transport d'eau et de soluté non réactif ou réactif dans le milieu poreux. L'effet de l'écoulement préférentiel et de transport hors équilibre a reçu l'attention de beaucoup d'auteurs, comme l'atteste le très grand nombre de publications sur ce point. Cependant, la caractérisation et la prise en compte de l'écoulement préférentiel et du transport hors équilibre posent encore des difficultés. Ces phénomènes peuvent être décrits en utilisant les concepts de deux régions qui produisent les modèles appelés modèle à double porosité et modèles à double perméabilité. Les applications de ces types de modèles se rencontrent assez souvent dans la littérature mais leurs applications sont encore limitées par rapport à leurs potentialités. En effet, le grand inconvénient de ces modèles est de mettre en jeu plusieurs paramètres qui ne sont pas tous mesurables ou difficiles à mesurer avec certitude. De plus, la modélisation dans la zone non saturée requiert des paramètres mesurés à une échelle convenable ; les mesures effectuées à l'échelle du laboratoire à partir d'échantillons prélevés sur le terrain peuvent être rapides et certaines, mais elles ne sont pas toujours représentatives des processus à l'échelle considérée.

La méthode inverse est donc souvent appliquée afin d'estimer les paramètres à partir de mesures expérimentales. Elle est basée sur la minimisation d'une fonction objectif qui représente la différence entre valeurs observées et valeurs calculées. L'estimation des paramètres est itérativement améliorées lors du procédé de minimisation jusqu'à ce que la précision désirée soit obtenue. La méthode inverse est un moyen potentiellement très efficace pour estimer les paramètres nécessaires pour caractériser l'écoulement d'eau et le transport des solutés à différentes échelles. Cependant, le problème concernant l'incertitude et la non unicité des paramètres optimisés existe encore. Il est dû au fait que (i) les données expérimentales utilisées dans la fonction objectif ne contiennent pas suffisamment d'information, (ii) un grand nombre de paramètres sont optimisés simultanément, (iii) de fortes corrélations peuvent exister entre les paramètres optimisés ou (iv) l'algorithme d'optimisation n'est pas global. Donc, pour bien calibrer les paramètres, il faut améliorer la fiabilité de cette estimation via l'analyse de sensibilité et d'estimabilité ainsi que les études préalables de corrélations existent entre les paramètres à optimiser. L'application de ces méthodes permet d'améliorer la stratégie expérimentale.

Nos objectifs scientifiques principaux sont de :

- Etudier l'écoulement préférentiel et le transport hors équilibre à différentes échelles sous différentes conditions d'écoulement en utilisant les différents types de modèles,
- Etudier la sensibilité et l'estimabilité des paramètres ainsi que leurs corrélations existantes,
- Optimiser les paramètres à partir des différents types de mesures expérimentales

La démarche de la thèse ainsi que les objectifs concrets de chaque chapitre sont présentés sur la figure I-9.

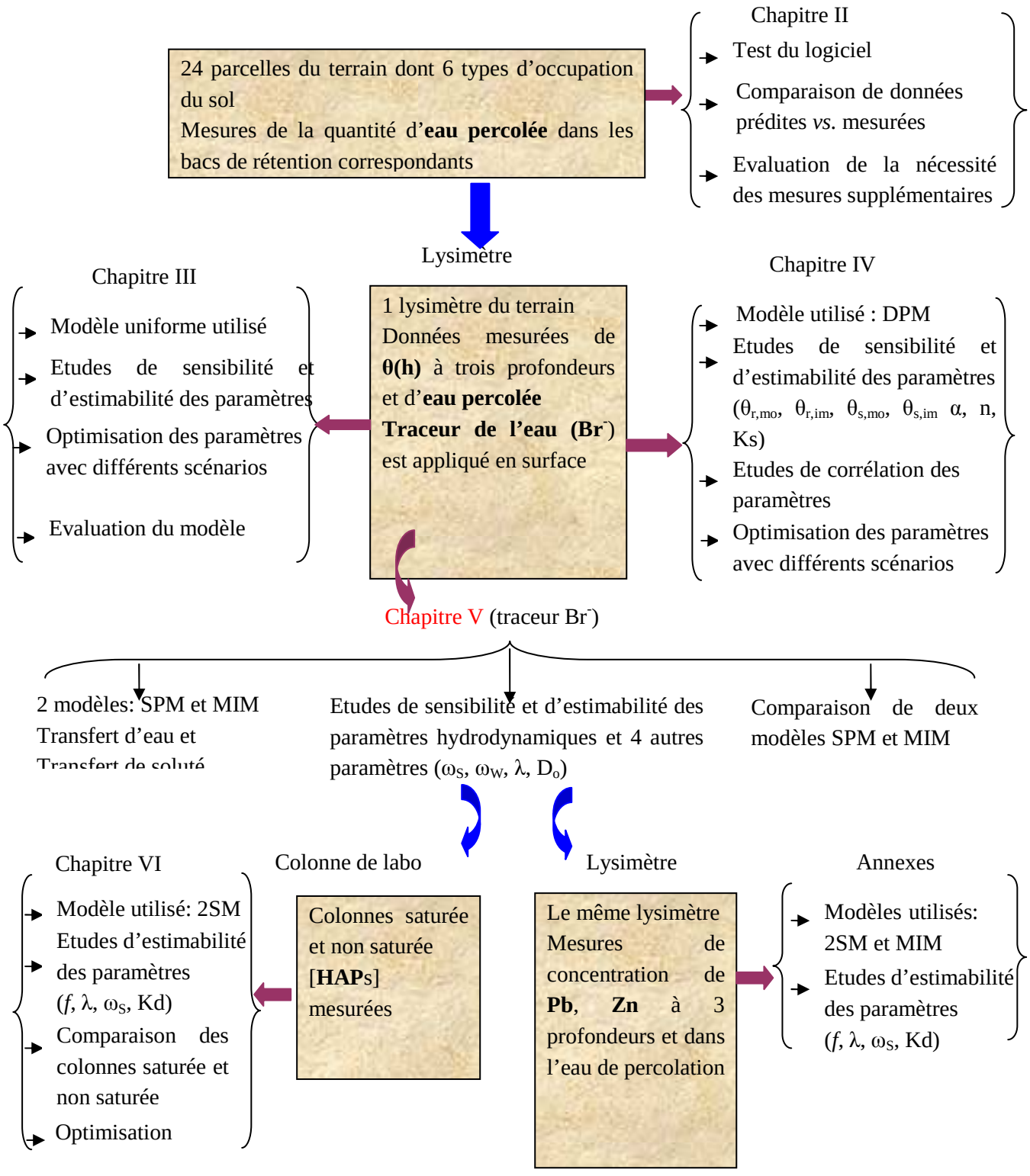

Figure I-9. Schéma du plan et des objectifs de la thèse

Chapitre II : Modélisation de l'écoulement d'eau dans les parcelles

1. Introduction

Dans le cadre de l'étude de la migration des polluants à partir de terres d'anciennes cokeries, le GISFI a mis en place un dispositif expérimental de 24 parcelles (2 m x 3 m x 0,70 m) remplies de différentes terres et soumises à différentes modalités de végétation. Ces parcelles font l'objet d'un certain nombre de travaux portant sur la caractérisation des terres et l'étude de leur possible évolution, la végétation, les microorganismes et la faune du sol. Notre contribution dans ce cadre a porté sur la modélisation du transport de l'eau dans les dispositifs. Nos objectifs pour ce travail sont de (i) voir si le logiciel HYDRUS-1D est valable et utilisable pour les objectifs scientifiques au sein du projet du GISFI, (ii) simuler les hauteurs d'eau percolée dans les bacs de rétention d'eau correspondants à différents types de parcelles et (iii) évaluer la nécessité des mesures supplémentaires sur les parcelles.

2. Matériels et méthodes

2.1. Description des parcelles

La station expérimentale du GISFI possède 24 parcelles qui contenant 6 types d'occupation de sol et 4 répétions (figure II-1) comme terre nue (TN), végétation spontanée (VS), *Thlaspi caerulescens* (TC), luzerne (*medicago sativa*) (MS), luzerne mycorhizée (MSmv) et terre après désorption (TD) sur un ancien site de pollution à Homécourt dans la région de Lorraine (49°14' N, 5°59' E). La taille de la parcelle est 200 x 300 x 70 cm. Les parcelles ont été remplies par 30 cm de gravier au fond suivie d'une fine couche de géotextile et puis 40 cm de terre polluée qui vient du site de Neuves-Maisons (Lorraine) sauf pour les parcelles de TD. Dans chaque parcelle se trouve un drain qui permet de drainer l'eau vers un bac de rétention dont la taille est 45 x 50 x 60 cm. Les bacs sont couverts. La hauteur d'eau de percolation dans les bacs est mesurée de temps en temps et puis ils sont vidés.

Les parcelles sont laissées sous conditions climatiques naturelles. A proximité se trouve une station météorologique qui permet d'enregistrer les données météorologiques horaires comme : la température de l'air, l'humidité de l'air, la vitesse du vent, la direction du vent, la précipitation, le rayonnement solaire, la pression atmosphérique. Au niveau du bilan d'eau dans la parcelle, le flux d'entrée est la pluie et flux de sortie est l'évaporation pour les parcelles de terre nue ou l'évapotranspiration pour les parcelles avec la présence des plantes et l'eau drainée vers le bac de rétention correspondant. Pour les parcelles plantées, ce n'est pas la totalité de la pluie qui arrive à la surface de ces parcelles. Une certaine quantité d'eau de pluie reste sur les feuilles des plantes et puis s'évapore. Ce phénomène est appelé interception. Le bilan d'eau à l'échelle de parcelle est décrit par la figure II-2.

Pour les parcelles de *Thlaspi caerulescens*, ces plantes ne se sont pas développées pendant les périodes de simulations, elles sont donc considérées comme les parcelles de terre nue. La coupure annuelle des luzernes est réalisée au mois de septembre.

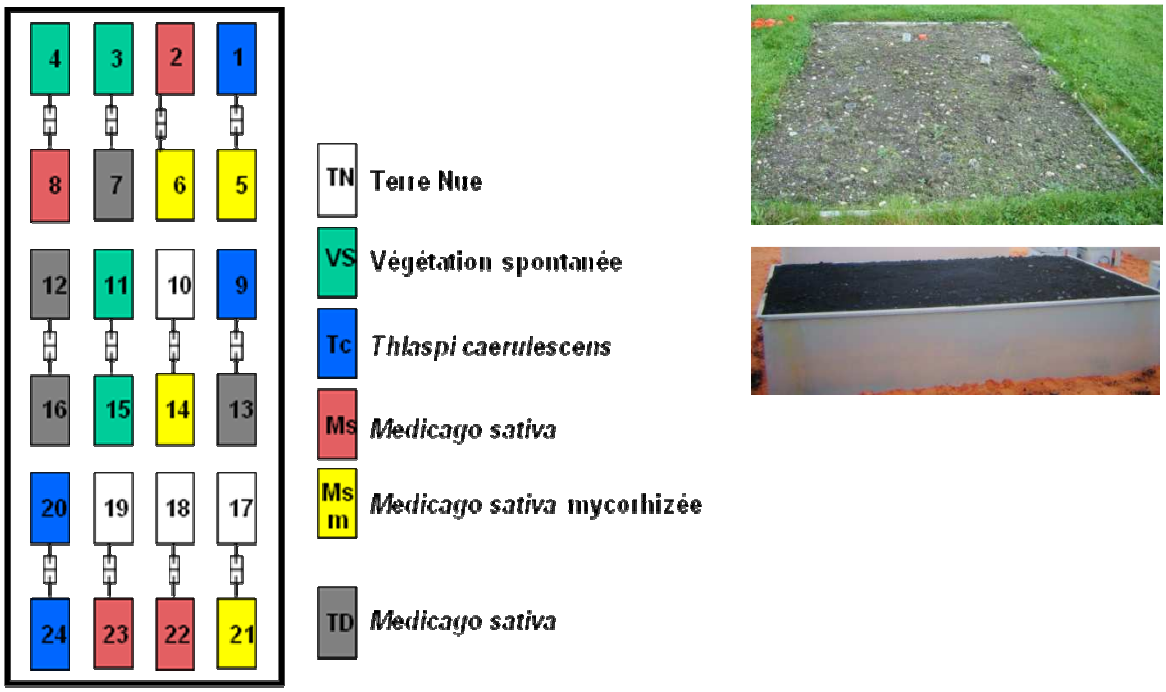

Figure II-1. Schéma des parcelles à la station expérimentale du GISFI, Homécourt, Lorraine

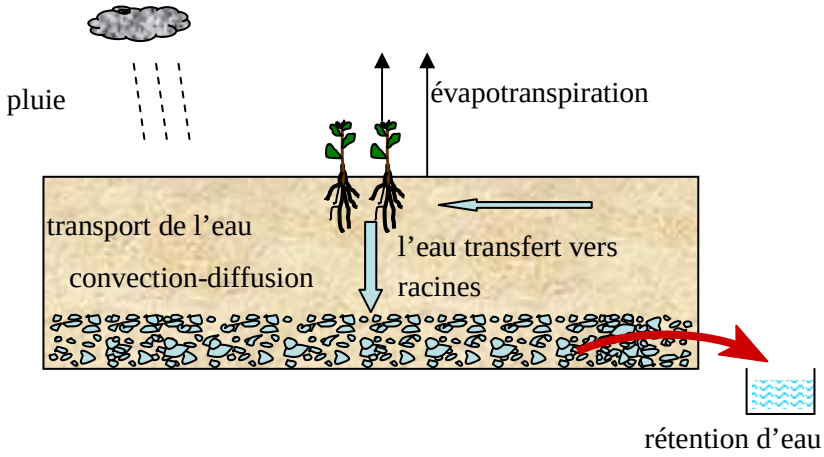

Figure II-2. Représentation schématique des flux d'eau dans les parcelles

2.2. Ecoulement d'eau dans les parcelles

2.2.1. Equations décrivant l'écoulement d'eau

L'équation de transport d'eau est basée sur l'équation de Richards (Eq. I.13).

2.2.2. Propriétés hydrauliques du sol non saturé

Pour résoudre cette équation, il faut connaître les fonctions hydrauliques du sol non saturé. Plusieurs types de modèles sont inclus dans le logiciel de HYDRUS-1D ; on a utilisé le modèle analytique de van Genuchten (van Genuchten, 1980a) (Eq. I.10 et I.11). La fonction hydraulique du sol comporte 5 paramètres inconnus : θ_r, θ_s, α, n et K_s.

2.2.3. Conditions initiale et aux limites

La condition initiale correspond à la teneur en eau du sol dans la parcelle :

$$\theta(z,t) = \theta(z)_{\ t=0} \qquad \text{[II.1]}$$

La condition à la surface de la parcelle (z=0 cm) correspond à : « *Atmospheric Boundary Conditions with Surface Run Off* ». Ce type de condition permet de prendre en compte les flux d'entrée comme la précipitation, l'évaporation, la transpiration en fonction du temps. La condition correspondant au niveau de la couche géotextile de la parcelle est appelée « *seepage face* ».

$$\left| -K\frac{\partial h}{\partial z} - K \right| \le E \quad \text{à z = 0} \qquad \text{[II.2]}$$

et

$$\theta_r \le \theta \le \theta_S \ \text{à z = 0} \qquad \text{[II.3]}$$

où θ_r est la teneur en eau résiduelle [$L^3\ L^{-3}$], θ_s est la teneur en eau à saturation [$L^3\ L^{-3}$], E est l'évapotranspiration quotidienne maximum [$L\ T^{-1}$].

2.3. Calcul du bilan d'eau dans les parcelles

Comme on l'a vu précédemment, la parcelle est partagée en deux couches : la couche de gravier au fond et la couche de sol. Des calculs préliminaires avec HYDRUS-1D ont indiqué que la teneur en eau dans la couche de gravier restait pratiquement constante au cours du temps (en raison de ses caractéristiques hydriques). Donc, pour simplifier les calculs du bilan d'eau, on peut négliger la variation de la teneur en eau dans cette couche. Le bilan sur l'eau s'écrit alors :

$$P^i - ET_c^i = D_e^i - D_e^{i-1} + E_p^i \qquad \text{[II.4]}$$

où P^i est la hauteur de précipitation au jour i [L], ET^i_c est l'évapotranspiration au jour i [L], D^i_e est la quantité d'eau totale dans la parcelle au jour i [L], $D^{i\text{-}1}_e$ est la quantité d'eau totale au jour i-1 [L], E^i_p est le volume d'eau de percolation au jour i [L].

2.4. Données d'entrée

2.4.1. Précipitation quotidienne

La station météorologique fournit les données météorologique horaires suivantes à 2 m de hauteur : la température et l'humidité de l'air, la vitesse et la direction du vent, la précipitation, le rayonnement solaire, la pression atmosphérique. La précipitation quotidienne est calculée en faisant la somme des précipitations horaires pour chaque jour pendant la période de simulation.

2.4.2. Evapotranspiration et interception quotidienne

Plusieurs méthodes permettent de calculer l'évaporation et/ou l'évapotranspiration à partir des données météorologiques comme FAO Penman-Monteith (Allen et al., 1998), Penman-Monteith (Monteith, 1965) , Blaney-Criddle (Blaney and Criddle, 1950) , Penman (Penman, 1948). Parmi ces

méthodes, nous avons choisi celle de Penman-Monteith qui est considérée comme la plus précise (Allen et al., 1998). L'évaporation et l'évapotranspiration quotidienne sont calculées à partir de l'équation :

$$ET_0 = \frac{0.408\Delta(R_n - G) + \gamma \frac{900}{T+273} u_2 (e_s - e_a)}{\Delta + \gamma(1 + 0.34u_2)} \quad [II.5]$$

où ET_o est l'évapotranspiration de référence [L T^{-1}], R_n le rayonnement net à la surface [MJ L^{-2} T^{-1}], G le flux de sol [MJ L^{-2} T^{-1}], T la température de l'air à 2 m de hauteur [^oC], u_2 la vitesse du vent à 2 m de hauteur [L T^{-1}], e_s est la pression de vapeur saturée de l'eau à T [kPa], e_a la pression réelle de vapeur à T [kPa], Δ la pente de la courbe de la pression de vapeur [kPa $^oC^{-1}$], γ la constante psychrométrique [kPa $^oC^{-1}$].

Il est arrivé que la station météorologique ne fonctionne pas bien, ce qui a pu donner lieu à une certaine incertitude sur les valeurs du rayonnement solaire. Nous avons donc cherché des outils permettant d'estimer l'évapotranspiration à partir des données disponibles. Il existe un certain nombre de logiciels libres comme :

DailyET : http://www.cranfield.ac.uk/sas/naturalresources/research/projects/dailyet.jsp
AWSET : https://www.cranfield.ac.uk/sas/naturalresources/research/projects/awset.jsp
REF-ET: http://www.kimberly.uidaho.edu/ref-et/
DYPM : http://biomet.ucdavis.edu/Evapotranspiration/DYPMexe/DYPM.htm

Nous avons choisi DailyET (logiciel libre). Après avoir calculé l'évapotranspiration de référence, on peut calculer l'évapotranspiration pour un type de culture à l'aide de l'équation suivante :

$$ET_c = K_c . ET_0 \quad [II.6]$$

où *Etc* est l'évapotranspiration d'un type de culture [L T^{-1}], K_c le coefficient cultural [-]. Pour ce travail, on suppose que K_c est égal à 1 pour les parcelles de végétation spontanée et de luzernes.

Pour HYDRUS-1D, on a besoin séparément des valeurs de l'évaporation et de la transpiration. On doit tout d'abord estimer l'indice foliaire (LAI) et la fraction de la couverture de surface (FCS) des plantes dans les parcelles. Pour les luzernes et la végétation spontanée, on peut estimer l'indice foliaire et la fraction de couverture de surface à partir de la hauteur (h_c) de ces plantes par les équations suivantes (Evett et al., 1998 ; Nghi et al., 2008) :

$$LAI = 1.5 \ln(h_c) + 5.5 \quad [II.7]$$

$$FCS = 1 - e^{-0.463.LAI} \quad [II.8]$$

L'évaporation, la transpiration et l'interception quotidienne sont calculées respectivement par les équations suivantes :

Transpiration = *Etc*.FCS [II.9a]

Evaporation = *Etc*.(1-FCS) [II.9b]

$$I = a.LAI\left(1 - \frac{1}{1 + \frac{FCS.P}{a.LAI}}\right) \quad [II.9c]$$

Les équations II.9a, II.9b et II.9c indiquent que la hauteur des plantes, h_c, joue un rôle très important sur l'estimation de l'évaporation, de la transpiration et de l'interception quotidienne. Or, cette hauteur n'a pas été mesurée systématiquement pendant la pendant la période choisie pour la simulation, puisque les expérimentateurs ne connaissaient pas l'importance de cette donnée. Nous avons donc estimé les hauteurs, sachant que cela risque d'affecter les résultats.

2.4.3. Distribution des racines

La présence des racines influence fortement les propriétés du sol et l'écoulement de l'eau. La distribution de racines peut augmenter la conductivité hydraulique à saturation de 57 % et la porosité de 1,8% (Rasse et al., 2000). Nous ne disposons pas de mesures de la profondeur et de la distribution des racines dans les parcelles. Pour ce travail, nous avons supposé que la distribution de racines des luzernes était homogène et que la profondeur des racines était de 30 cm.

2.4.4. Paramètres hydrodynamiques

Comme aucune mesure des paramètres hydrodynamiques (également appelés les paramètres de van Genuchten) n'a été faite pour la terre polluée de Neuves Maisons, nous avons utilisé les valeurs de 5 paramètres hydrodynamiques pour la terre polluée de Homécourt (tableau II-1) extraites de la thèse de Gujisaite (Gujisaite, 2008) et de Michel (Michel, 2009b). Ils ont été mesurés selon le protocole présenté ci-dessous.

Une colonne en PVC de 1 m de hauteur et 2,6 cm de diamètre interne a été utilisée (Gujisaite, 2008). Elle était composée de 20 cylindres de 2 cm de hauteur et de 10 éléments de 6 cm de hauteur. La colonne a été remplie de terre de Homécourt. La colonne a d'abord été saturée de bas en haut à l'aide d'une solution de $CaCl_2$ de concentration 2 10^{-3} mol L^{-1} à un débit de 1mL min^{-1}. Puis elle a été drainée par gravité. Enfin, la teneur en eau de chaque élément de la colonne a été déterminée par pesée de la terre avant et après passage à l'étuve à 105 °C jusqu'à ce que la masse soit constante. Une courbe représentant la hauteur (ou la pression) en fonction de la teneur en eau a alors été obtenue. Les valeurs des paramètres hydrodynamiques ont été déterminés par l'optimisation de la courbe $h(\theta)$ en utilisant le logiciel R*ETC* (van Genuchten et al., 1991). Les valeurs de ces paramètres sont présentées dans le tableau II-1.

Tableau II-1. Caractéristiques de la terre de Homécourt (Michel, 2009b)

Granulométrie (g kg^{-1})				Eléments traces totaux (mg kg^{-1})	
Argiles	130	Carbone organique (g kg^{-1})	122	Cr	56,3
Limons fins	119	Azote (g kg^{-1})	2,34	Cu	27,6
Limons grossiers	73	Calcaire total (g kg^{-1})	323	Zn	362
Sables fins	171	pH_{eau}	8,8	Pb	115
Sables grossiers	507	CEC (meq kg^{-1})	112	Cd	5,62

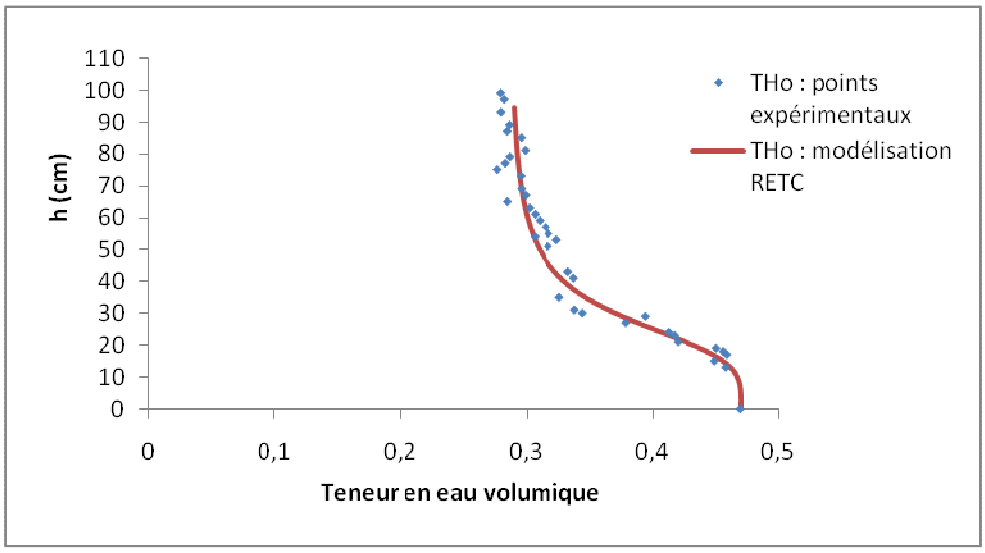

Figure II-3. Courbe de rétention d'eau pour la terre polluée de Homécourt (Michel, 2009b)

Tableau II-2. Valeurs des paramètres de van Genuchten pour la terre d'Homécourt

θ_r	θ_s	α (cm^{-1})	n	K_s ($cm\ j^{-1}$)	l
0,29	0,47	0,039	3,98	5 572,8	0,5

3. Résultats et discussions

3.1. Hauteur d'eau dans les bacs de rétention

La simulation a été réalisée pour la période du 13 mars 2006 au 9 juillet 2007. Pendant cette période, les hauteurs d'eau dans les bacs de rétention ont été mesurées 35 fois mais l'eau avait débordé 26 fois. Il nous reste donc 9 périodes de percolation dont les dates de percolation sont indiquées sur l'axe des abscisses de la figure II-4. Les périodes de percolations en hiver et au printemps ont été représentées en noir sur la figure II-4, elles ne sont pas continues. Nous avons observé que les hauteurs d'eau mesurées étaient presque pareilles pour les parcelles de terre nue et de *Thlaspi caerulescens* car ces plantes ne se sont pas développées pendant la période choisie. De plus, il n'y a eu pas la différence nette entre les hauteurs d'eau mesurées pour les parcelles de *Medicago sativa* (luzerne) et de *Medicago sativa* mycorhizée. Nous allons présenter les résultats concernant trois types de parcelles : terre nue, végétation spontanée et luzerne dont les hauteurs d'eau mesurées dans les bacs de rétention correspondants sont présentées sur la figure II-4.

On observe que pour 5 périodes d'hiver ou de printemps, les hauteurs d'eau mesurées dans les bacs de rétention sont presque les mêmes pour trois types de parcelles. Ceci s'explique par le fait qu'en hiver et au printemps les parcelles avec végétation spontanée et luzerne ne sont pas bien couvertes par les plantes (les luzernes sont coupées en septembre et les herbes sont mortes), l'interception est donc presque nulle. C'est pour cela que la quantité d'eau percolée dans les bacs de rétention n'est pas très différente pour ces types de parcelles. Par contre, pour 4 périodes de percolation en été (légende en rouge sur l'axe des abscisses sur la figure II-4), les hauteurs d'eau mesurées dans les bacs de rétention

pour les parcelles de terre nue sont beaucoup plus élevées que celles pour les parcelles de végétation spontanée et de luzerne, en raison de l'interception, de l'évapotranspiration et de la consommation par les plantes. Pour ces raisons, la quantité réelle de pluie arrivant à la surface du sol est significativement diminuée.

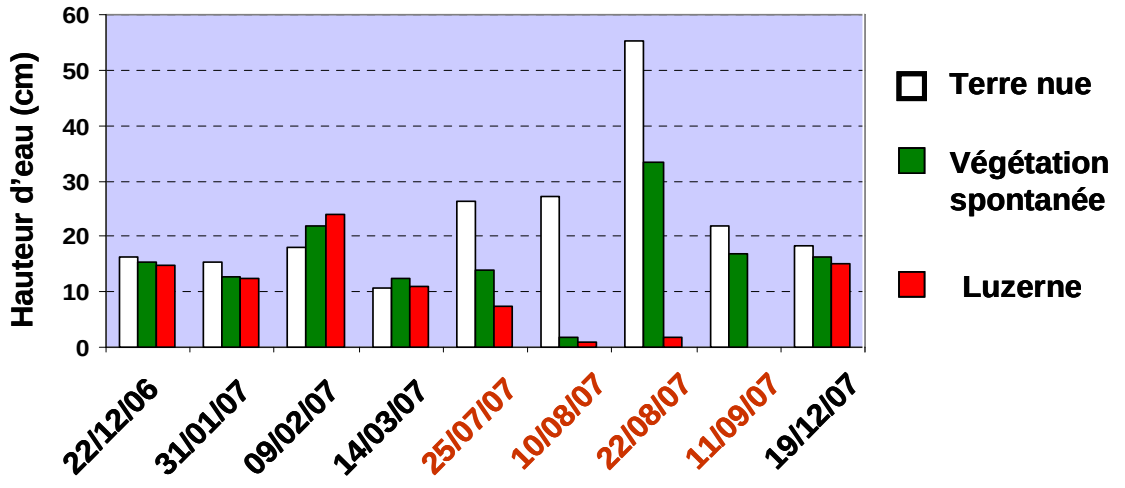

Figure II-4. Hauteurs d'eau mesurées dans les bacs de rétention correspondent respectivement aux parcelles de terre nue, avec végétation spontanée et avec luzerne

3.2. Comparaison des hauteurs d'eau mesurées et calculées dans les bacs de rétention

La figure II-5 présente la comparaison des hauteurs d'eau mesurées et simulées pour les parcelles de terre nue. On trouve un bon accord entre valeurs mesurées et simulées pour les périodes de percolation en hiver et en été. Ainsi, avec le logiciel HYDRUS-1D, on peut prédire assez correctement le bilan d'eau pour les parcelles de terre nue.

La comparaison entre les hauteurs d'eau mesurées et simulées pour les parcelles de végétation spontanée et de luzerne est montrée respectivement sur la figure II-6a et II-6b. Pour ces deux types de parcelles, la prédiction de la quantité d'eau percolée est raisonnable pour les périodes de percolations en hiver et au printemps. Par contre, on observe un grand écart entre les hauteurs mesurée et simulée pour certaines périodes de percolation en été pour ces deux types de parcelles. Par exemple, pour la période de percolation du 10 août 2007 (figure II-6a), la simulation a beaucoup surestimé la hauteur d'eau dans les bacs de rétention : on a trouvé 33 cm par rapport aux 3 cm mesurés pour les parcelles de végétation spontanée et 25 cm par rapport aux 2 cm mesurés pour les parcelles de luzerne. Ces écarts s'expliquent par la surestimation de la quantité de pluie qui atteint effectivement la surface du sol de ces deux types de parcelles. De plus, l'absence de données sur la profondeur et la distribution des racines peut contribuer effectivement à la prédiction erronée des hauteurs d'eau dans les périodes de percolation en été car les plantes sont bien développées lors de cette saison.

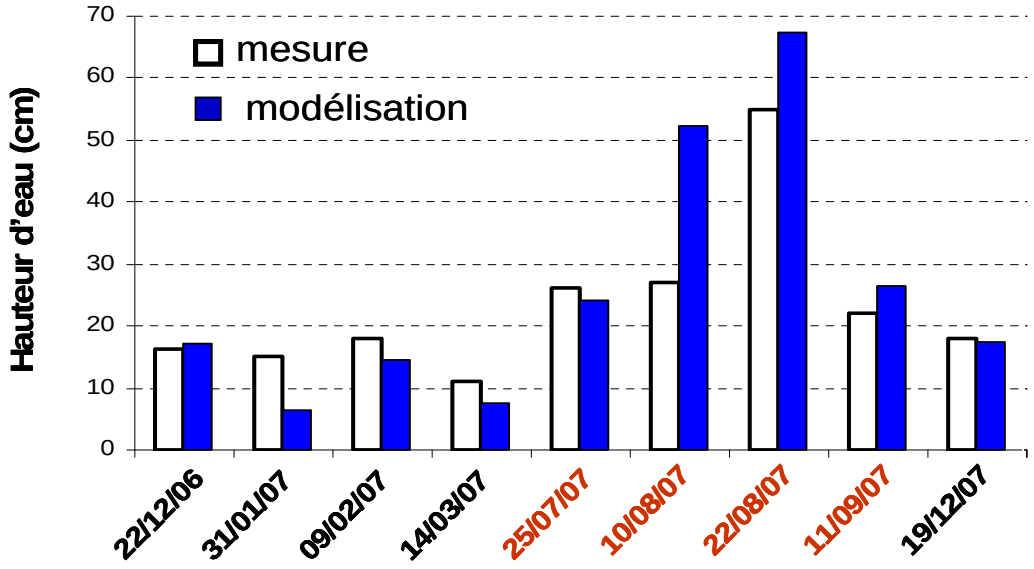

Figure II-5. Comparaison des hauteurs d'eau mesurées et simulées dans les bacs de rétentions pour les parcelles de terre nue

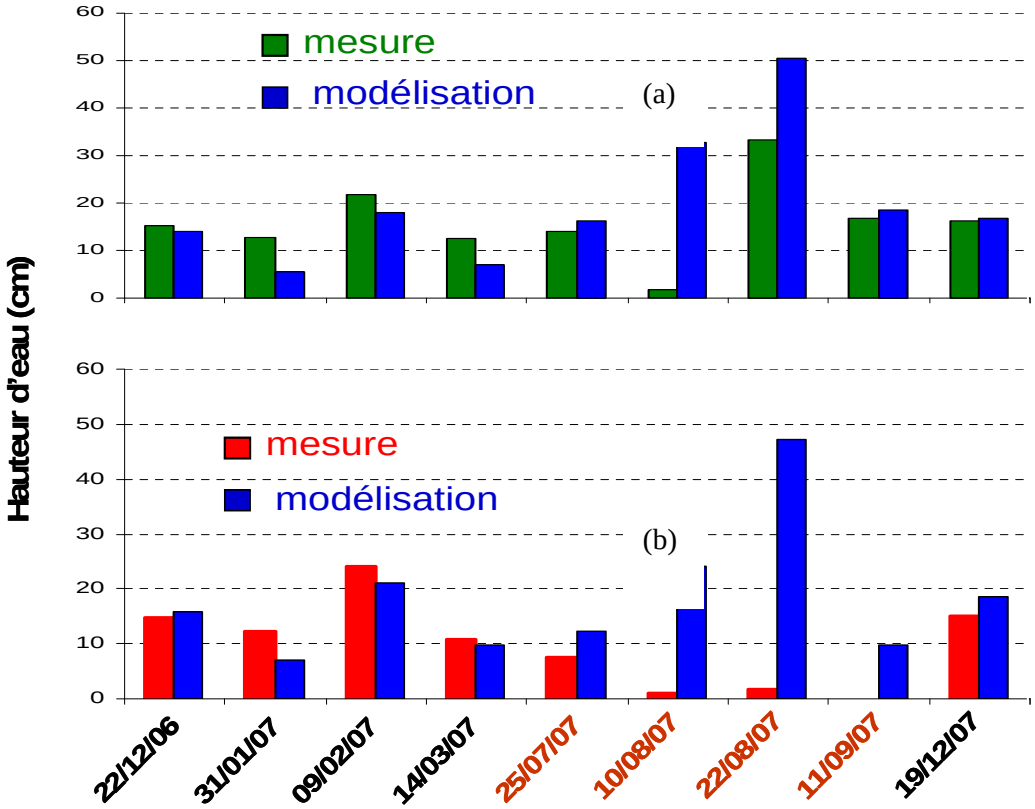

Figure II-6. Comparaison des hauteurs d'eau mesurées et simulées dans les bacs de rétention pour les parcelles de (a) végétation spontanée (b) luzerne

4. Conclusions et perspectives

Pour ce travail, la simulation a été effectuée *a posteriori*, après les mesures sans avoir été prévue en amont. C'est pourquoi certaines données étaient manquantes. Par exemple, la mesure de la hauteur d'eau dans les bacs n'a pas toujours été exploitable, puisque dans certains cas, les bacs avaient débordé. De même les hauteurs de plantes et la distribution et la profondeur des racines n'étaient pas connues.

Pour ces raisons, certains résultats n'ont pas pu être en bon accord avec les valeurs mesurées, en particulier lorsque les plantes avaient une forte influence sur le transport de l'eau, comme en été. Par contre, pour un certain nombre de période, en hiver et au printemps, pour les parcelles de terre nue et de végétation spontanée, les résultats obtenus avec le code HYDRUS-1D étaient en bon accord avec les données expérimentales.

Ainsi, on peut conclure que le bilan hydrique sur le dispositif parcelles peut être correctement établi à l'aide du code HYDRUS dès lors que l'on dispose des données suffisantes.

Si l'on souhaite prédire correctement le transport de l'eau puis des polluants dans les parcelles, il sera nécessaire de collecter des données demandées par le code plus fréquemment et il faudrait également pouvoir instrumenter les parcelles avec des sondes TDR et des tensiomètres afin de mesurer la teneur en eau à différentes hauteurs.

Ce travail montre que la modélisation ne peut être prévue indépendamment de l'expérimentation, mais que modélisation et expérimentation doivent se compléter l'une et l'autre.

Chapitre III : Analyse d'estimabilité des paramètres du modèle d'écoulement uniforme

Estimability analysis of Single-Porosity Model parameters from lysimeter data

Van Viet Ngo [a], M.A. Latifi [a], Marie-Odile Simonnot [a,*]

[a] Laboratoire des Sciences du Génie Chimique, Nancy Université INPL-CNRS,

1, rue Grandville, BP20451, 54001 Nancy Cedex, France

(Article soumis à J. Hydrol.)

Abstract

Lysimeter experiments are more and more widely run to study pollutant migration in contaminated soils. For the present study, we had hourly and daily data on water flow from a bare field 2 m^3 lysimeter filled with a soil of a former coking plant: pressure heads and water contents measured at 3 depths, cumulative bottom flow and cumulative evaporation. Water flow was represented using one-dimensional (1D) single-porosity model (SPM) by means of the numerical flow code HYDRUS-1D. SPM model involved 5 hydraulic parameters: θ_s, water content at saturation, θ_r, residual water content, K_s, hydraulic conductivity at saturation, α and n, parameters of the van Genuchten-Mualem model. Sensitivity and estimability analyses were performed; simulations were run to calculate values of 248 d. We showed that parameters were mainly sensitive to pressure heads and water contents and that daily data contained more information than hourly data. The decreasing sensitivity order was: θ_s, n, α, K_s and θ_r. Estimability analysis revealed that better results could be obtained by combining pressure heads and water contents in the objective function. In this case, with daily data, we found that all parameters were estimable with the following decreasing order: θ_s, n, K_s, α, θ_r. No correlation was found between parameters. SPM parameters were then optimized in 4 scenarios differing by the values included in the objective function. Eventually, parameter heterogeneity was taken into account by considering 4 soil layers in the lysimeter. Comparable results were obtained with the 4 scenarios but calibration was improved by considering 4 layers.

Keywords: Lysimeter; sensitivity analysis; estimability analysis; parameter optimization; single-porosity model; HYDRUS-1D

[*]Corresponding author . Address : Laboratoire des Sciences du G2nie Chimique, Nancy Université INPL – CNRS, 1 rue Grandville BP20451 F-54001 Nancy Cedex

E-mail addresses : vietdinhph@yahoo.com (V.V. Ngo), latifi@ensic.inpl-nancy.fr (A. Latifi), Marie-Odile.Simonnot@ensic.inpl-nancy.fr (M.O. Simonnot)

1. Introduction

Modelling of water flow and solute transport in the vadose zone requires accurate hydraulic parameters obtained at the relevant scale. From one decade, many authors carried out studies at the lysimeter scale and lysimeter has been considered as an intermediate scale between laboratory and field scales (Hermsmeyer et al., 2002; Ingwersen et al., 2006; Luster et al., 2008; Majdoub et al., 2001; Schoen et al., 1999; Seyfarth and Reth, 2008). Lysimeters are most often equipped by sensors e.g. tensiometers and TDR probes to monitor water contents and pressure heads. Weather data measurement and weighable lysimeters allow an accurate control of fluxes at upper and lower boundaries (Durner, 1994b; Durner et al., 2008; Meissner et al., 2007).

Hydraulic parameters can be directly measured at the bench scale using soil samples. Measurements in the laboratory may be precise and quick but results may be different from what would be obtained at field scale. Therefore, inverse method has been increasingly used to determine those parameters from lysimeter data (Eching and Hopmans, 1993; Kohne et al., 2006a; Mertens et al., 2006; Si and Kachanoski, 2000). Given data reliability for weighable lysimeters, there is now a great predictive potential in coupling flow models and optimization algorithms to determine hydraulic parameters at the lysimeter scale (Olyphant, 2003). However, determination of hydraulic parameters at this scale by inverse simulation has been discussed in few contributions (Abbaspour et al., 1999; Durner et al., 2008; Kelleners et al., 2005; Sonnleitner et al., 2003; Wegehenkel et al., 2008).

Problems of non-uniqueness of such optimized parameters may occur (Simunek et al., 2001; Vrugt et al., 2001). They are assigned to various reasons e.g. low sensitivities of optimised parameters to the investigated criteria (Ines and Droogers, 2002), mutual parameter dependency and high measurement noise (Vrugt et al., 2001) or local algorithm optimization (Kelleners et al., 2005). They were specially met for evaporation experiments performed on bare lysimeters (Schwarzel et al., 2006). This was primarily due to the limited range in the experimental pressure head and water content data. Soil moisture and pressure head variations were too small to produce a well-defined global minimum in the objective function. The non-uniqueness problem can be partly solved if additional and more accurate measurements are included in the objective function (Eching and Hopmans, 1993; Russo et al., 1991a; van Dam et al., 1994). However, data information content appears to be much more important than the amount of data used for model calibration (Gupta et al., 1998); the only focus on subsets where the model is most sensitive to parameters changes can also improve the quality of inverse solution (Vrugt et al., 2001). Therefore, it is necessary to evaluate sensitivities of model parameters, information content of different measurements and correlation between different parameters before parameter calibration.

Recently, an estimability analysis technique has been developed (Yao et al., 2003). This method provides information about model parameter estimability from various output predictions and enables us to account for correlations between parameters. This method is based on the combination of dynamic models and data as well as response variables available at different sampling rates throughout each experimental run (Kou et al., 2005). It has been successfully applied in chemical engineering (Jayasankar et al., 2009; Kou et al., 2005).

In the present contribution, single-porosity model (SPM) was chosen to represent water flow in the bare field lysimeter. This model involved 5 parameters: θ_s, water content at saturation, θ_r, residual water content, K_s, hydraulic conductivity at saturation, α and n, parameters of the van Genuchten-Mualem model. The numerical computer code HYDRUS-1D was used to solve transport equations

and optimize parameters. To begin, parameter sensitivities to different types of data measured at the lysimeter scale were investigated at two time intervals (hour and day). Parameter estimabilities were evaluated as well. Parameters containing sufficient information were optimized in different situations. The model was eventually validated using parameters in different scenarios.

2. Material and methods

2.1. Experimental system

The experimental system was a weighable lysimeter vessel (UGT, Müncheberg, Germany) described in previous contributions (Michel, 2009a; Ngo et al., 2009). This stainless steel vessel (section: 1 m^2, height: 2 m) belonged to a 4-fould lysimeter station implemented in the experimental site of the GISFI (French Scientific Interest Group on Industrial Wastelands, www.gisfi.fr). In February 2008, the lysimeter was filled by a 15 cm layer of sand in the bottom and 3 t of a contaminated soil. This soil had been sampled in the upper horizon of a former coking plant located at Homécourt in the North-East of France (Sirguey et al., 2008). Large amounts had been excavated, homogenized and sieved at 4 cm. Soil volume was thus 1.85 m^3, porosity 0.54 and water content 20 wt %. The total concentration of the 16 PAHs listed by the US EPA was 6.8 g kg^{-1} (Michel, 2009a). Lysimeter surface was bare soil, it was submitted to atmospheric conditions and drainage water was collected at the outlet.

The lysimeter was equipped by 3 sensors (TDR probe, tensiometer, suction probe) at 3 depths (0.5, 1.0 and 1.5 m) and by temperature sensors. All the data (lysimeter weight, volumetric water content, soil hydraulic pressure, bottom flux, soil temperature) were hourly monitored by a data logger. Weather data (air temperature, relative humidity, wind speed and direction) were monitored as well. Hourly evaporation was derived by Penmann-Monteith's method (Allen et al., 1998). If needed, hourly data were averaged to obtain daily data. Evaporation flux was derived from the changes of lysimeter weight. Water percolation and precipitation was also summed for 1 day interval.

2.2. Model description

The model used in this work was the one-dimensional single-porosity model (SPM) and HYDRUS-1D was used for the simulations. In the SPM, variably saturated water flow was described by Richards' equation (Simunek et al., 1998):

$$\frac{\partial \theta(h)}{\partial t} = \frac{\partial}{\partial z}\left(K(\theta)\left(\frac{\partial h}{\partial z} + 1 \right) \right) \qquad (1)$$

where θ is the volumetric water content [$L^3\ L^{-3}$], h the pressure head [L], t is time [T], z the vertical coordinate [L], K the hydraulic conductivity function [$L\ T^{-1}$].

To solve this equation, we used van Genuchten-Mualem's functions to express the relationships between θ, h and K (van Genuchten, 1980b):

$$S_e = \frac{\theta(h) - \theta_r}{\theta_s - \theta_r} = \frac{1}{\left(1 + \alpha h^n\right)^m} \qquad h < 0 \qquad (2)$$

$$S_e = 1 \qquad h \geq 0 \qquad (3)$$

$$m = 1 - 1/n \qquad n > 1 \tag{4}$$

$$K(S_e) = K_S S_e^l \left[1 - \left(1 - S_e^{1/m}\right)\right]^2 \tag{5}$$

where S_e is the effective water content [-], θ_r the residual water content, θ_s the saturated water content, K_S the saturated hydraulic conductivity at saturation [LT^{-1}]; α [L^{-1}], l [-], n [-] and m [-], are empirical parameters.

The pore connectivity parameter *l* (eq. 5) was set to 0.5 (Mualem, 1976a). We have thus 5 parameters: θ_r, θ_s, α, n and K_s.

2.3. Model parameters –initial and boundary conditions

Input parameters are presented in table III-1. Water retention and hydraulic conductivity parameters were estimated by Rosetta software (Schaap et al., 2001) as in many contributions (Hermsmeyer et al., 2002; Kelleners et al., 2005; Ngo et al., 2009; Sander and Gerke, 2009). Preliminary calculations showed that the hydraulic parameters of the sand layer had no significant influence on the results, thus the sand layer was neglected. The initial condition was set at the water content given by the TDR probes at initial time.

$$\theta(z,t) = \theta(z) \quad \text{at t=0} \tag{6}$$

The upper flow boundary condition was specified as the « atmospheric boundary condition with surface run off » with precipitation as the input flux and evaporation from the lysimeter surface as the output flux. The equation of upper boundary condition is given as follows:

$$-K\left(\frac{\partial\theta}{\partial z} - 1\right) = q_T(t) \quad \text{at z = 0} \tag{7}$$

where q_T is the net infiltration rate [$L\ T^{-1}$].

The lower boundary condition was specified as a seepage face (Abdou and Flury, 2004; Kasteel et al., 2007; Sonnleitner et al., 2003):

$$-K\left(\frac{\partial\theta}{\partial z} - 1\right) = q_B(t) \quad \text{at z = L} \tag{8}$$

where q_B is the drainage rate [$L\ T^{-1}$].

Table III-1. Description and initial values of the 5 SPM parameters for soil layer in the lysimeter vessel

Parameter	Unit	Parameter description	Initial value
θ_r	$cm^3\ cm^{-3}$	Residual water content	0.046
θ_s	$cm^3\ cm^{-3}$	Saturated water content	0.41
α	cm^{-1}	Shape factor in the soil water retention curve	0.03
n	-	Hydraulic property shape factor	1.49
K_s	$cm\ d^{-1}$	Saturated hydraulic conductivity	2.89

2.4. Sensitivity analysis

Sensitivity analysis was performed following the method presented in previous contributions (Hamby, 1994; Ngo et al., 2009). Sensitivity coefficients were calculated from the approximations (finite differences) of partial derivative of a function S with respect to a model parameter p:

$$I = \frac{\partial S}{\partial p} = \frac{S^+ - S^-}{2\Delta p} \quad (9)$$

S being a function (e.g. pressure head or water content at a given depth) and p a parameter. S^+ is the value obtained for a p increase of 10 % and S^- for a p decrease of 10 %.

Sensitivity coefficients were then normalized (Hamby, 1994):

$$I_{norm} = \frac{p}{S}\left(\frac{S^+ - S^-}{2\Delta p}\right) \quad (10)$$

Following their absolute values, these coefficients were classified in 4 groups indicating the sensivity of S to p (Lenhart et al., 2002; Ngo et al., 2009).

2.5. Estimability analysis

Estimability analysis must be combined with sensitivity analysis to determine if a set of experimental data contains enough information to estimate model parameters (Jayasankar et al., 2009; Larsbo and Jarvis, 2005; Ngo et al., 2009; Yao et al., 2003). The mathematical method has been described in details (Ngo et al., 2009). A sensitivity coefficient matrix, Z, is built, the term of row i and column j being the normalized sensitivity coefficient I_{norm} (Eq. (10), with the partial derivative of S with respect to parameter p_j at time t_i. This matrix built for SPM parameters had 5 columns and the row number was five time the number of data. Orthogonalization method was then performed (Ngo et al., 2009). A cut-off criterion of 2.4 was taken (Yao et al., 2003). Yao et al. considered that " there would be sufficient information to estimate the parameter if a 10% change in the parameter resulted in at least a 2% change in the response variable".

2.6. Optimization

Optimization procedure was based on the minimization of the differences between experimental and simulated values. The objective function was (Simunek et al., 1998):

$$\phi(b,q,p) = \sum_{j=1}^{m_q} v_j \sum_{i=1}^{n_{qj}} w_{i,j}\left[q_j^*(x,t_i) - q_j(x,t_i,\mathbf{b})\right]^2 + \sum_{j=1}^{m_p} v'_j \sum_{i=1}^{n_{pj}} w'_{i,j}\left[p_j^*(\theta_i) - p_j(\theta_i,\mathbf{b})\right]^2 \quad (11)$$

where the first term on the right hand-side represents the deviations between the measured (q_j^*) and the calculated (q_j) space-time variables (e.g. pressure heads, water contents, cumulative flux across the lysimètre boundary); m_q is the number of sets of measurements; n_{qj} is the number of measurement in a particular measurement set; $q_j^*(x,t_i)$ represents a measurement at time t_i for the *j*th measurement set at location x; $q_j(x,t_i,\mathbf{b})$ are the corresponding model predictions for the vector of optimized parameters $\mathbf{b}(\theta_r, \theta_s, \alpha, n, K_s)$; v_j and $w_{i,j}$ are the weights associated to a particular measurement set or point, respectively. The second term of Eq. (11) represents the differences between independently measured

(p_j^*) and predicted (p_j) soil properties, such as retention or conductivity data at particular pressure heads; m_p, n_{pj}, p_j^*, $p_j(\theta_i,\mathbf{b})$, v_j', w_{ij}' have the similar meanings as for the first term but for soil hydraulic properties.

The weighing coefficient v_j and v_j' that equalize the contribution of the different types of data types to the objective function Φ are given by:

$$v_j = \frac{1}{n_j \sigma_j^2} \tag{12}$$

where σ_j^2 is the measurement variance.

These coefficients allow a normalization of the objective function with respect to the variances of measurement type j.

The error measurements for cumulative outflow, tensiometer and TDR probes were 0.001 cm for the cumulative outflow, 0.5 cm for the pressure heads, and 0.01 cm^3 cm^{-3} for the water contents (Durner et al., 2008). We set $w_{i,j}$ equal to 0.001 for the daily cumulative bottom flux and daily cumulative evaporation, 0.5 for pressure heads, 0.01 for water contents. $w_{i,j}'$ was set equal to 0.001 or 0.1.

The Levenberg-Marquardt optimization algorithm was used to minimize the objective function (Eq. (11) and to calculate confidence intervals for the parameters (Simunek et al., 1998). Compared with global optimization methods (Abbaspour et al., 2001; Durner et al., 2008; Lambot et al., 2002; Mertens et al., 2004), this algorithm provides useful statistical information about the optimized parameters, e.g. their mutual correlation and confidence intervals.

2.7. Model performance analysis

Model performance was evaluated by 3 statistical analysis criteria: the mean absolute error, the root mean square error, the index of agreement. The mean absolute error (MAE) describes the difference between observations (O_i) and simulated values (S_i) as follows:

$$MAE = \frac{1}{N}\sum_{i=1}^{N}\left|O_i - S_i\right| \tag{13}$$

where N is the number of observations.

The root mean square error (RMSE) and the index of agreement (IA) (Willmott, 1981) are given by the following equations:

$$RMSE = \sqrt{\frac{\sum_{i=1}^{N}\left(O_i - S_i\right)^2}{N-1}} \tag{14}$$

$$IA = 1 - \frac{\sum_{i=1}^{N}\left(O_i - S_i\right)^2}{\sum_{i=1}^{N}\left(\left|S_i - \bar{O}\right| + \left|O_i - \bar{O}\right|\right)^2} \tag{15}$$

where $\bar{O}$ is the average of observations.

IA is ranged from 0 to 1.0, the higher IA, the better the agreement between experimental and calculated values.

However, to reduce the effect of square terms, we mainly used the modified index of agreement (MIA) (Willmott et al., 1985):

$$MIA = 1 - \frac{\sum_{i=1}^{N} |O_i - S_i|}{\sum_{i=1}^{N} \left(|S_i - \bar{O}| + |O_i - \bar{O}| \right)} \quad (16)$$

The use of MIA has more interest than IA by eliminating the effect of squares terms. And MIAis a more reliable statistical measure than the determination coefficient R^2 less sensitive to extreme values (Legates and McCabe Jr., 1999).

3. Result and discussions

3.1. Background data

For sensitivity and estimability analysis of model parameters based on daily data, simulations were done for a period of 248 days (February, 15th to October, 19th 2008). Over the entire period of monitoring, the weighing lysimeter registered 21.4 cm of net infiltration and 39.6 cm of net evaporation.

Averaged daily were taken for inverse simulation. Hence, in the reference case, 496 pressure heads values measured at 100 and 150 cm depths and 496 water contents measured at 50 and 150 cm depths were included in the objective function (the tensiometer at 50 cm and the TDR probe at 150 cm were not working). Very small changes were observed in pressure heads (in the range of -1.7 and -25.7 cm at 100 cm depth and -4.1 and -42.3 at 150 cm depth) and water contents (in the range of 0.258–0.295 $cm^3\ cm^{-3}$ at 50 cm depth and 0.276-0.311 $cm^3\ cm^{-3}$ at 100 cm depth).

For model evaluation, prediction was done for a period of 100 days from November, 12th 2008 (from this date, we had the measured water contents at 150 cm depth) to February, 19th 2009.

3.2. Sensitivity and estimability analysis based on hourly data

Sensitivities of the 5 SPM parameters to hourly predictions of pressure head, water content, cumulative bottom flux and cumulative evaporation are presented in table III-2. The results concerning hourly pressure head showed that n was the most sensitive parameter immediately followed by θ_s (very high sensitivity). Sensitivities of α, K_s and θ_r were found to be high, medium and low respectively. The same sensitivity order was found for hourly water contents, with lower values of the coefficients I_{norm}.

The sensitivities of all 5 parameters to hourly cumulative bottom flux and hourly cumulative evaporation were negligible. The reason was that hourly cumulative bottom flux and evaporation remained very low and the parameters did not have a significant influence on their variations. Hence, we would have no chance to estimate these parameters from these measurements.

The results of parameter estimability are given in table III-3. The first row represents the magnitude of each column in the matrix Z corresponding to each parameter, before adjusting the correlations between parameters. From the second to the last row, the magnitudes of each column were listed, the influences of the most estimable parameter on the remaining ones being removed. For each function, estimability decreased from the left to the right.

Table III-2. Sensitivity of the 5 SPM parameters to hourly output predictions

	Pressure head		Water content		Cum. bottom flux		Cum. evaporation	
	I_{norm}	Sensitivity	I_{norm}	Sensitivity	I_{norm}	Sensitivity	I_{norm}	Sensitivity
θ_r	0.04	Low	0.03	Low	0.0005	Negligible	0.0002	Negligible
θ_s	1.07	Very high	0.61	High	0.0005	Negligible	0.0001	Negligible
α	0.51	High	0.15	Medium	0.0004	Negligible	0.0001	Negligible
n	2.13	Very high	0.66	High	0.0007	Negligible	0.0002	Negligible
K_s	0.11	Medium	0.04	Low	0.0005	Negligible	0.0001	Negligible

Regarding hourly pressure head, the estimability order was the same as the sensitivity order. Four out of 5 parameters were estimable, n being the most estimable. Regarding hourly water contents, 3 out of 5 parameters were estimable, which was expected from sensitivity analysis. No parameter was estimable from the other functions. Thus, we can deduce that (i) pressure head data were the most interesting ones for parameter identification and (ii) cumulative bottom flux and evaporation flux were useless.

Parameter estimability is improved by increasing the number of different experimental data (Yao et al., 2003). Previous works had shown that hydraulic parameter estimability increased when pressure heads and water contents were simultaneously included in the objective function (Simunek and van Genuchten, 1997). Thus we combined hourly pressure heads and water contents (table III-4). However, results were not significantly improved; again we found that 4 out 5 parameters were estimable, with the decreasing order: n, θ_s, α, K_s. These results clearly showed that a 1 h time interval was too small regarding the studied process.

Possible correlations between parameters were searched by computing the net influence of the more estimable parameter(s) on the remaining one(s) from the magnitude of each column of Z (Ngo et al., 2009):

$$nI = 100\frac{R_{n+1} - R_n}{R_n} \qquad (17)$$

where R_n, R_{n+1} are the row order in table III-4

If nI=0, there is no correlation, the correlation is negligible between 0 and 5, low between 5 and 20, medium between 20 and 50, high between 50 and 75 and very high above. The influences are listed in table III-5. Parameter n had a very high influence on θ_s, α, θ_r (1st row). Parameter α had a high influence on K_s and θ_r. The existence of these correlations as well the information content of the data (table III-4) clearly showed that an accurate SPM parameter estimation was not possible from hourly data.

Table III-3. Estimability order of the 5 SPM parameters as a function of hourly measurements in the lysimeter: (a) pressure heads at 3 depths, (b) water contents at 3 depths, (c) cumulative bottom flux and (d) cumulative evaporation.

(a) Pressure head at 3 depths					(b) Water contents at 3 depths					(c) Cumulative bottom flux					(d) Cumulative evaporation				
n	θ_s	α	K_s	θ_r	n	θ_s	α	K_s	θ_r	n	θ_r	α	Ks	θ_s	n	θ_r	θ_s	α	K_s
11365	4101	825	39.2	6.06	**1345**	937	66.5	4.28	1.94	0.11	0.04	0.01	0.02	0.02	0.006	0.003	0.003	0.001	0.001
0	**487**	218	26.8	1.60	0	**148**	29.0	0.93	0.09	0	0.02	0.01	0.01	0.01	0	0.001	0.001	0.001	0.001
0	0	**216**	12.0	1.38	0	0	**9.11**	0.93	0.04	0	0	0.01	0.01	0	0	0	0.001	0	0
0	0	0	**3.78**	0.25	0	0	0	0.29	0.02	0	0	0	0.01	0	0	0	0	0	0
0	0	0	0	0.06	0	0	0	0	0.01	0	0	0	0	0	0	0	0	0	0

Table III-4. Estimability order of the 5 SPM parameters when hourly pressure heads and hourly water contents were combined.

n	θ_s	α	K_s	θ_r
12709	5038	891	43.5	8.00
0	**684**	252	36.0	2.05
0	0	**252**	20.1	1.61
0	0	0	**6.84**	0.75
0	0	0	0	0.13

Table III-5. Net influence (%) of the more estimable SPM parameter(s) on the remaining one(s) when hourly pressure heads and water contents were combined.

	n	θ_s	α	K_s	θ_r
n	-	86.4	71.7	17.2	74.4
θ_s		-	0.02	44.1	21.3
α			-	66.0	53.7
K_s				-	82.7
θ_r					-

3.3. Sensitivity and estimability analysis based on daily output predictions

Sensitivities of SPM parameters to daily output predictions are listed in table III-6. Sensitivities were higher than the previous ones (table III-3), hence higher parameter estimability could be expected. With respect to daily pressure heads, sensitivities of θ_s, n and α were very high, as K_s and θ_r sensitivities were respectively high and medium. These results were consistent with those of Kelleners et al. (Kelleners et al., 2005) who concluded that n and θ_s were the most sensitive parameters to daily pressure heads, daily water contents and daily cumulative outflow as θ_r was the least influential parameter. Regarding daily water contents, sensitivity coefficients were lower and the decreasing selectivity order was different: θ_s, n, K_s, θ_r, α. Sensitivities to bottom flux and cumulative evaporation were significantly higher than in the previous case in which they were negligible. Sensitivities of n and K_s to cumulative bottom flux became high and those of n and and θ_s to daily cumulative evaporation became medium. These results clearly showed that the time period of measurements must be high enough to have significant data variations. Daily data contained more information than hourly data for our system.

Among all the measurements, the highest sensitivities were obtained with daily pressure heads. Similar results had been reported by Rocha et al. (Rocha et al., 2006) who investigated the effects of various soil hydraulic properties on subsurface water flow below furrows during two successive irrigation events to analyze the effect of spatial variations in the initial soil water contents within the soil profile.

Estimability analysis results based on daily pressure heads, water contents, cumulative bottom flux and cumulative evaporation are presented in table III-7. As might be expected, with a cut-off criterion of 2.4, the 5 parameters were estimable from daily pressure heads, with the decreasing order: θ_s, n, K_s, α and θ_r. The set of estimable parameters using daily water contents remained 3 out of the 5 parameters, and one parameter, n, could be estimated from daily cumulative bottom flux and evaporation. These latter data still contained poor information for parameter optimization. Others authors found that daily evapotranspiration was better than weekly evapotranspiration for the parameter optimization (Ines and Droogers, 2002). Thus, increasing the time period for this function would not improve the results.

From these results, we decided again to combine daily pressure heads and water contents in the objective function (table III-8). The estimability order was the same as previously: θ_s, n, K_s, α, θ_r.

The influence of the more estimable parameters on the remaining ones is listed in table III-9. This influence remained from low to negligible. Hence, the estimation of the 5 SPM parameters by numerical inversion, using the combination of daily pressure heads and water contents, is expected to be successful.

The conclusions were the same as for sensitivity analysis: daily data contained more information than hourly data. The best situation was obtained by combining daily pressure heads and water contents, but anyway daily pressure heads and water contents were more reliable than daily cumulative bottom flux and evaporation as already observed (Ines and Droogers, 2002; Vrugt et al., 2001).

As noted earlier, the cumulative bottom flux content and cumulative evaporation had very poor information content for parameter optimization. However, Durner et al. (2008) suggested that the last value of cumulative bottom flux and cumulative evaporation should be included in the objective function in order to ensure that the overall mass balance of the system was met.

Table III-6. Sensitivity of the 5 SPM parameters to daily output predictions

	Pressure head		Water content		Cum. bottom flux		Cum. evaporation	
	I_{norm}	Sensitivity	I_{norm}	Sensitivity	I_{norm}	Sensitivity	I_{norm}	Sensitivity
θ_r	0.07	Medium	0.02	Low	0.001	Negligible	0.01	Low
θ_s	2.37	Very high	0.82	High	0.04	Low	0.11	Medium
α	1.00	Very high	0.01	Low	0.01	Low	0.04	Low
n	2.15	Very high	0.51	High	0.31	High	0.13	Medium
K_s	0.57	High	0.06	Medium	0.22	High	0.02	Low

Table III-7. Estimability order of the 5 SPM parameters as a function of daily measurements in the lysimeter: (a) pressure heads at 3 depths, (b) water contents at 3 depths, (c) cumulative bottom flux and (d) cumulative evaporation.

(a) Pressure head at 3 depths					(b) Water contents at 3 depths					(c) Cumulative bottom flux					(d) Cumulative evaporation				
θ_s	n	K_s	α	θ_r	θ_s	n	K_s	α	θ_r	n	K_s	θ_s	α	θ_r	n	θ_s	K_s	θ_r	α
23071	6813	4010	764	8.85	**584**	251	4.39	0.16	0.39	**24.2**	13.0	0.53	0.07	0.01	**4.96**	4.09	0.16	0.07	0.48
0	**6266**	3957	653	8.82	0	**41.6**	2.49	0.16	0.18	0	**1.37**	0.16	0.03	0.01	0	0.64	0.05	0.03	0.07
0	0	**3899**	540	8.53	0	0	**2.41**	0.16	0.04	0	0	0.09	0.01	0.01	0	0	0.03	0.03	0.01
0	0	0	**536**	7.85	0	0	0	0.16	0.01	0	0	0	0.01	0	0	0	0	0.01	0.003
0	0	0	0	6.16	0	0	0	0	0.01	0	0	0	0	0	0	0	0	0	0.003

Table III-8. Estimability order of the 5 SPM parameters when daily pressure heads and water contents at 3 depths in the lysimeter were combined

θ_s	n	Ks	α	θ_r
23655	7065	4014	765	9.23
0	6421	3959	656	9.18
0	0	3903	541	8.79
0	0	0	537	8.11
0	0	0	0	6.40

Table III-9. Net influence (%) of the more estimable parameters on the remaining ones, daily pressure heads and water contents being combined

	θ_s	n	K_s	α	θ_r
θ_s	-	9.12	1.38	14.19	0.61
n		-	1.42	17.59	4.15
K_s			-	0.63	7.82
α				-	20.99
θ_r					-

3.4. Optimization result

In this section, optimization results are presented for 4 scenarios that differed in the way data were included in the objective function:

- the first scenario, SPM1, reference case, used the combination of daily pressure heads at 100 and 150 cm depths and daily water contents at 50 and 100 cm;
- the second scenario, SPM2, used the same data as SPM1 plus the last value of cumulative bottom flux and evaporation;
- the third scenario, SPM3, used the same data as SPM1 plus 10 water retention values, $\theta(h)$, at 100 cm depth: one value corresponded to the highest pressure head value; one to the lowest pressure head value and the 8 other values to 8 first daily data; the weights of these 10 values were supposed to be 0.001;
- the fourth scenario, SPM4, using the same data as SPM3 with the weight of the 10 water retention values equal to 0.1.

The estimated parameters of the 4 scenarios, as well as their confidence intervals, obtained by numerical inversion are summarized in table III-10. The comparison of daily data and simulated values are showed in figures 1(SPM1 and SPM2) and 2 (SPM3 and SPM 4).

In the reference case SPM1, the optimized θ_r value of 0.246 was very close to the lowest water content at 50 cm depth. The narrow confidence interval indicated a successful estimation of this parameter. This good agreement was somewhat surprising since θ_r was the last estimable parameter basing on the combination of daily pressure heads and daily water contents (table III-8).

The optimized θ_s value of 0.377 was much larger than the highest water content at 100 cm depth. Unfortunately, we did not have the measured water contents at 150 cm depth that could be higher than the ones at 100 cm depth. Moreover, the small confidence interval of this parameter reflected the reliable estimation. This overestimation of θ_s, which often occurs in field-scale studies, was probably due to air entrapment and/or irregular flow (Abbasi et al., 2004). In contrast, Ramos et al. (Ramos et al., 2006) estimated the hydraulic parameters from tension disk infiltrometer data and did not find an overestimation of θ_s.

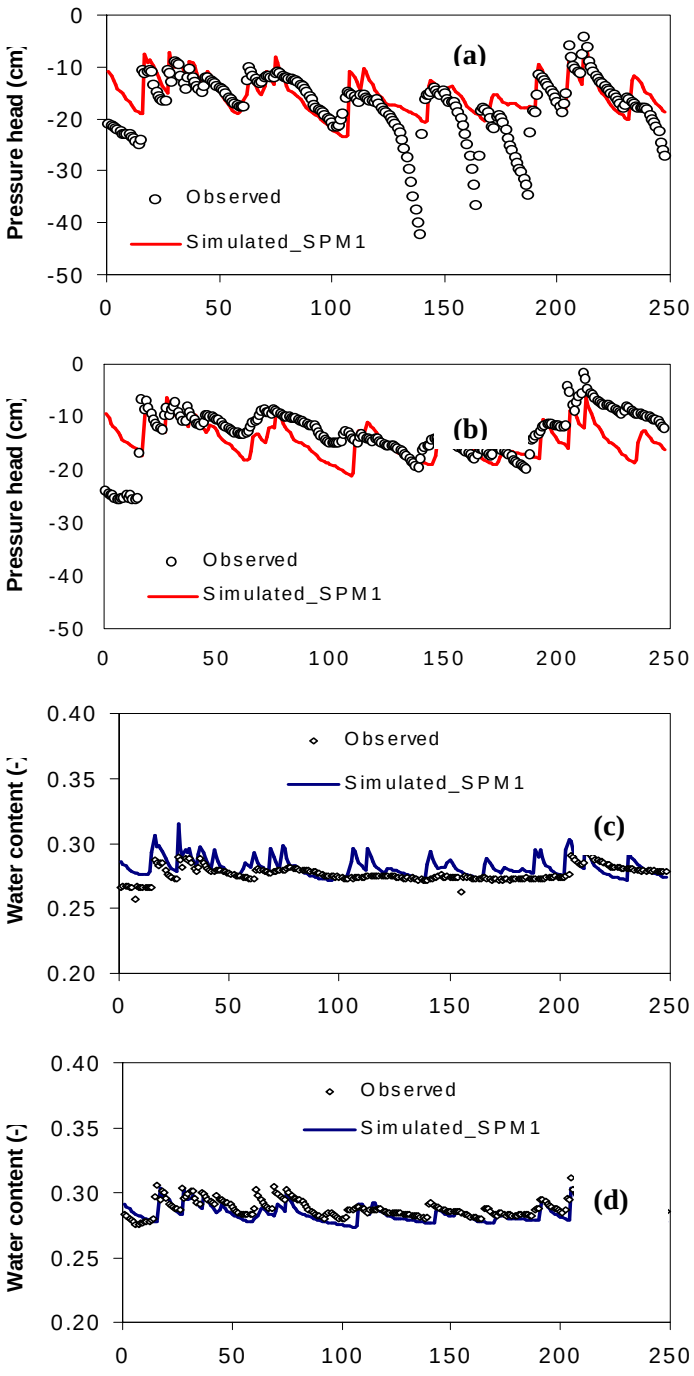

Figure III-1. Daily data and simulated values when daily pressure heads and water contents were simultaneously included in the objective function (SPM1): (a) pressure heads at 100 cm depth, (b) pressure heads at 150 cm depth, (c) water contents at 50 cm depth and (d) water content at 100 cm depth.

Parameter n was successfully estimated as shown by the relatively small confidence interval. The optimized K_s value of 464.09 cm d^{-1} sounded to be very high, with a large confidence interval, revealing a high uncertainty. This poor result was partly explained by the difficulty in K_s optimization because of soil spatial and temporal variability at the field scale (Ramos et al., 2006). A rather high uncertainty was also obtained for α, that was assigned to the narrow range of daily pressure heads and water contents that made it very difficult to accurately determine K_s and α. This result was in good agreement with the conclusions of Schwarzel et al., who found that a bare field lysimeter could give rise to narrow pressure heads and water contents (Schwarzel et al., 2006). Our findings were also consistent with the result obtained by Kelleners et al. (Kelleners et al., 2005) who also determined soil hydraulic parameters at the lysimeter scale by inverse method from different experimental data. To solve this problem, it was suggested that at least one independent measurement of θ(h) at a pressure head sufficiently lower than the lowest h_0 in objective function should be included in the objective function (Schwartz and Evett, 2003). In fact, Ramos et al., 2006 showed that inclusion of two θ(h) at pressure heads of -100 and -15 850 cm allowed an excellent fit of the measured data of tension infiltrometer disk.

Table III-10. Soil hydraulic parameters, with corresponding confidence intervals, estimated from daily data using HYDRUS-1D for the 4 scenarios

	θ_r -	θ_s -	α cm^{-1}	n -	Ks cm d^{-1}	R^2
SPM1	0.2464 ± 0.0029	0.3768 ± 0.0094	0.4191 ± 0.0563	1.68 ± 0.09	464.09 ± 153.98	0.9093
SPM2	0.2459 ± 0.0028	0.3820 ± 0.0109	0.4466 ± 0.0691	1.68 ± 0.08	568.01 ± 238.53	0.9092
SPM3	0.2494 ± 0.0026	0.4164 ± 0.0146	0.5255 ± 0.0823	1.78 ± 0.10	1460.30 ± 513.11	0.9092
SPM4	0.2449 ± 0.0035	0.3873 ± 0.0097	0.5268 ± 0.1013	1.63 ± 0.09	903.55 ± 388.47	0.9088

The statistical result for observed and simulated pressure heads at 100 and 150 cm depths and water contents at 50 and 100 cm depths are shown in table III-11. A better fit was obtained for pressure heads at 150 cm than at 100 cm depth, which was indicated by lower values of MAE and RMSE and higher value of MIA for pressure heads at 150 cm depth. However, RMSE values of 5.23 cm and 4.70 cm for pressure heads at 100 and 150 cm depths, respectively, were relatively larger than the pure measurement error of 0.5 cm. Visual analysis of Figure III-1 showed a large difference between observed and calculated pressure heads at two depths for the 15 first days. That was assigned to uncertainty in pressure head data because of lysimeter instability in the starting period. Hence, during summer period (days from 125 to 190), the model could not predict some pressure heads data at 100 cm depth which decreased suddenly, that may be rather due to data errors and uncertainty than to an incorrect model.

In the same fashion, the agreement between observed and simulated water contents was better at 100 than at 50 cm depth. Hence, the RMSE values of resp. 0.009 and 0.007 cm^3 cm^{-3} for water contents at resp. 50 and 100 cm depths were very low, lower than the pure measurement error (0.01 cm^3 cm^{-3}).

RMSE values for pressure heads were generally much higher than for water contents: since pressure head were measured in small soil volumes, measurement uncertainties were larger than for water content that were measured in larger soil volumes (Jacques et al., 2002). For example, daily soil water contents measured by TDR probes were obtained on a thickness of about 30 cm, and tensiometers determined pressure heads in a spherical volume of ca 5-10 cm around the porous cups (Wegehenkel, 2005).

Previous contributions dealt with the estimation of hydraulic parameters from TDR and tensiometer measurements. Jacques et al. (Jacques et al., 2002) found RMSE values between 0.038 and 0.125 cm^3 cm^{-3} for water contents when optimizing hydraulic parameters from water flow and solute transport at the bench scale. In another study devoted to the validation of a soil water balance model from soil water content and pressure head data at the field scale, RMSE values were between 0.010 and 0.035 cm^3 cm^{-3} (Heidmann et al., 2000) or between 0.03 and 0.130 cm^3 cm^{-3} (Wegehenkel, 2005). Recently, Durner et al. (Durner et al., 2008) also used inverse method to estimate hydraulic parameters from TDR and tensiometer measurements at the lysimeter scale under natural atmospheric conditions, they found the RMSE value for the simulated and measured water contents ranged 0.009-0.20 cm^3 cm^{-3} and the one for simulated and measured pressure heads ranged 0.67-31.82 cm.

Table III-11. Mean absolute error (MAE), root mean square error (RMSE), modified index of agreement (MIA) between observed data and simulated values for 4 scenarios shown in Figures 1 and 2.

	MAE				RMSE				MIA			
	SPM1	SPM2	SPM3	SPM4	SPM1	SPM2	SPM3	SPM4	SPM1	SPM2	SPM3	SPM4
h_{100}	3.71	3.69	3.69	3.71	5.27	5.23	5.26	5.23	0.52	0.52	0.52	0.53
h_{150}	3.48	3.52	3.51	3.52	4.70	4.73	4.70	4.74	0.46	0.46	0.45	0.46
θ_{50}	0.007	0.007	0.007	0.007	0.009	0.009	0.009	0.009	0.36	0.36	0.36	0.36
θ_{100}	0.005	0.005	0.006	0.005	0.007	0.007	0.007	0.007	0.55	0.55	0.54	0.55

Scenario SPM2 gave similar results as SPM1 (tables III-10 and III-11). The addition of the last values of cumulative bottom flux and evaporation into the objective function did not improve optimization quality. Scenario SPM3 gave similar results as SPM1 for θ_r and α, but higher values of θ_s and n and above all of K_S (table III-10). However, the statistical analysis results were not modified (table III-11). Again the addition of the initial values of the hydraulic parameters in the objective function did not increase information content as expected. Similar results were obtained with SPM4.

As a conclusion, it is not necessary to include cumulative outflow (cumulative bottom flux and evaporation) and initial values of hydraulic properties into the objective function. Daily pressure heads and water contents were sufficient to successfully estimate parameters such as θ_r, θ_s and n.

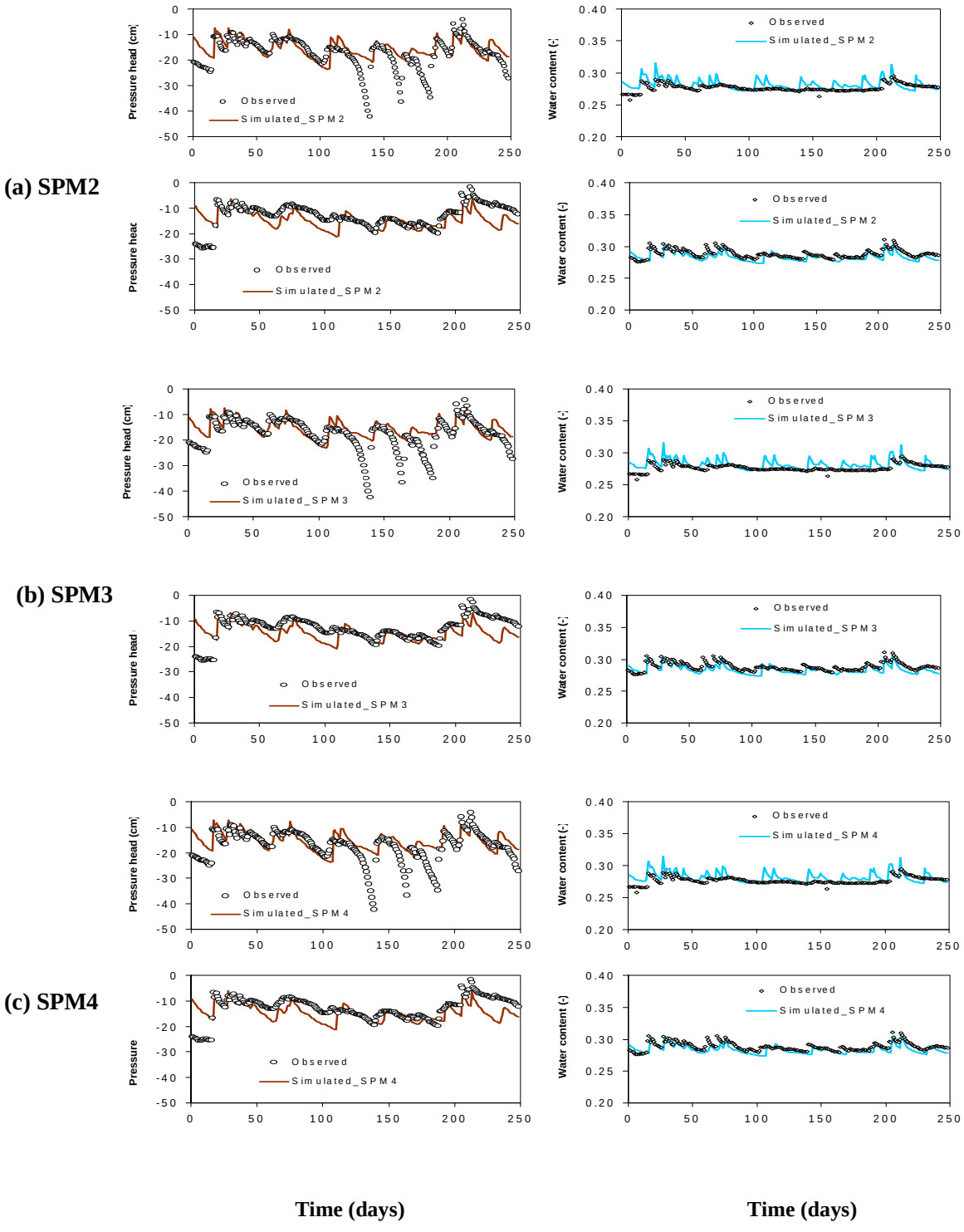

Figure III-2. Daily data and simulated values for 3 scenarios: (a) SPM2 using the data as in SPM1 plus the last value of cumulative bottom flux and evaporation, (b) SPM3 using the data as in SPM1 plus 10 water retention values and their weights were supposed to be 0.001 and (c) SPM4 using the data as in SPM3, the weight of 10 water retention values were supposed to be 0.1.

3.5. Influence of soil heterogeneity on calibration results

In this section, we discuss the influence of soil heterogeneity on optimization results. The lysimeter was divided into 4 layers: layer 1 (10–60 cm) corresponded to the position of the tensiometer and TDR probe at 50 cm depth; layer 2 (60-120cm) to the position of those at 100 cm depth; layer 3 (120-185 cm) to those at 150 cm depth and layer 4 to the sand layer (185-200 cm). All five parameters for the 3 soil layers were optimized simultaneously from the same initial values.

Table III-12. Soil hydraulic parameters, with corresponding confidence intervals, estimated from daily data using HYDRUS-1D for 3 soil layers

	θ_r	θ_s	α	n	K_s	R^2
	-	-	cm^{-1}	-	$cm\ d^{-1}$	
	0.2454	0.2866	0.0327	1.78	0.91	
Layer 1	± 0.0025	± 0.0012	± 0.005	± 0.15	± 0.08	
	0.2671	0.3108	0.0866	1.60	3.68	0.9423
Layer 2	± 0.0027	± 0.0031	± 0.010	± 0.08	± 1.17	
	0.2832	0.3825	0.0666	2.56	0.46	
Layer 3	± 0.0024	± 0.0186	± 0.010	± 0.38	± 0.23	

The optimization results are shown in table III-12. The optimized θ_r values of resp. 0.245 and 0.267 for layers resp. 1 and 2 were found to be very close to the lowest measured water contents in these two layers. In addition, the optimized θ_s values of 0.287 and 0.311, respectively, were very close to the corresponding highest measured water contents at 50 and 100 cm depths. These reliable estimated values were also reflected by their narrow confidence intervals. We did not have water content data at 150 cm depth (layer 3), then we could not compare the measured and calculated values of θ_r and θ_s for layer 3.

Table III-13. Mean absolute error (MAE), root mean square error (RMSE), index of agreement (IA), modified index of agreement (MIA) between observed data and calculated values (figure III-3)

	MAE	RMSE	IA	MIA
h_{100}	3.71	4.81	0.78	0.57
h_{150}	2.30	2.92	0.87	0.63
θ_{50}	0.005	0.006	0.60	0.42
θ_{100}	0.003	0.005	0.82	0.65

By comparison, the optimized values of n for layers 1 and 2 (resp. 1.78 and 1.69) were close to the one of SPM1 (1.68, table III-10). But for layer 3, it was *ca* 1.5 times relatively higher (2.56). The optimized values of α and Ks were found to be very different than for SPM1. For example, the optimized α and K_s values of 0.0327 cm^{-1} and 0.91 cm d^{-1} for layer 1, respectively, were much lower than those for the reference case. Their uncertainties were also represented by large confidence intervals. This meant that considering a multi-layer soil did not improve optimization results of α and K_s that were difficult to estimate in our conditions.

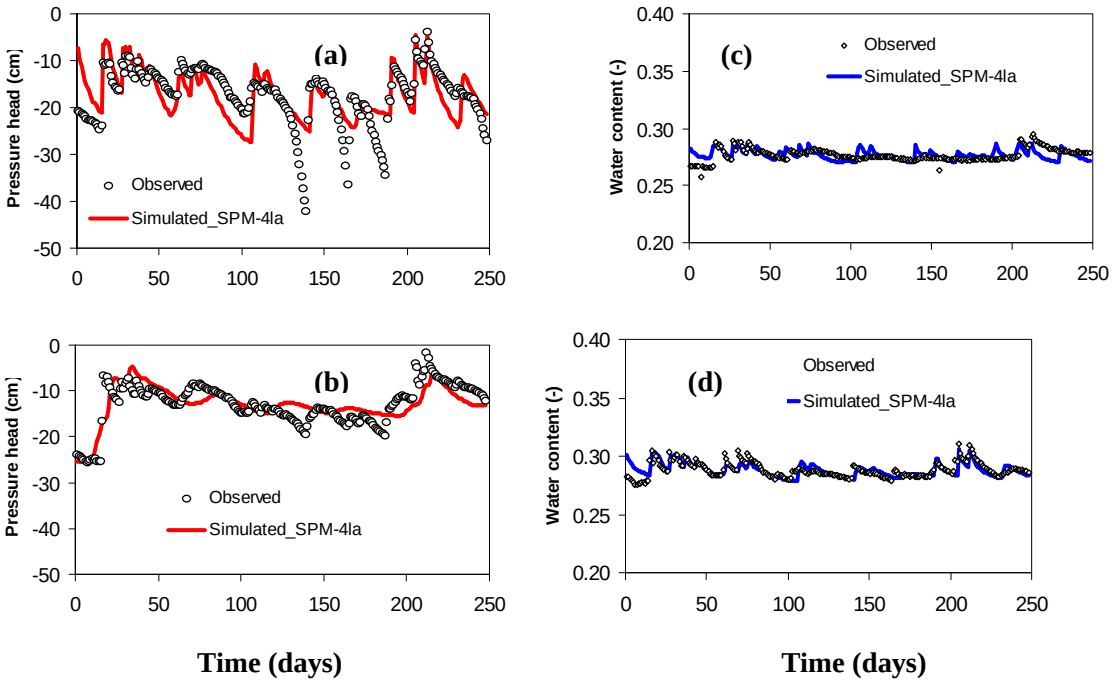

Figure III-3. Daily data and simulated values when lysimeter system was divided into 4 layers (SPM-4la): (a) pressure heads at 100 cm depth, (b) pressure heads at 150 cm depth, (c) water contents at 50 cm depth and (d) water content at 100 cm depth.

Table III-14. Mean absolute error (MAE), root mean square error (RMSE), modified index of agreement (MIA) between the observed data and calculated values (figure III-4)

	MAE		RMSE		MIA	
	SPM_2la	SPM_4la	SPM_2la	SPM_4la	SPM_2la	SPM_4la
h_{100}	16.10	13.46	16.66	14.49	0.17	0.15
h_{150}	8.56	10.37	9.23	11.34	0.00	0.00
θ_{50}	0.007	0.010	0.009	0.011	0.49	0.00
θ_{100}	0.010	0.009	0.012	0.012	0.00	0.53
θ_{150}	0.063	0.009	0.064	0.011	0.00	0.95

The statistical analysis results are given in table III-14. All the MAE and RMSE values for pressure heads and water contents at different depths were lower than for SPM1. For instance, a RMSE value of 2.92 cm for this case was slightly lower than 4.70 cm for SPM1. In addition, the MIA values for pressure heads at 100 and 150 cm depths and water contents at 100 cm depth were higher than the corresponding MIA value for SPM1. Thus, our results showed that considering a multi-layered soil improved the agreement between measured and simulated values. This finding was consistent with previous results, that showed a better fit was achieved when accounting for multi-layered soil profile at the field scale under rainfall conditions (Jacques et al., 2002).

3.6. Model Estimation

To validate the model, we used the optimized parameters for SPM1 and the case which accounted for soil heterogeneity (SPM_4la). The prediction result of pressure heads at 100, 150 cm depths and water contents at 50, 100, 150 cm depths for a period of 100 days were compared with the corresponding measured data and shown in figure III-4. The statistical analysis of validation comparison is listed in table III-14.

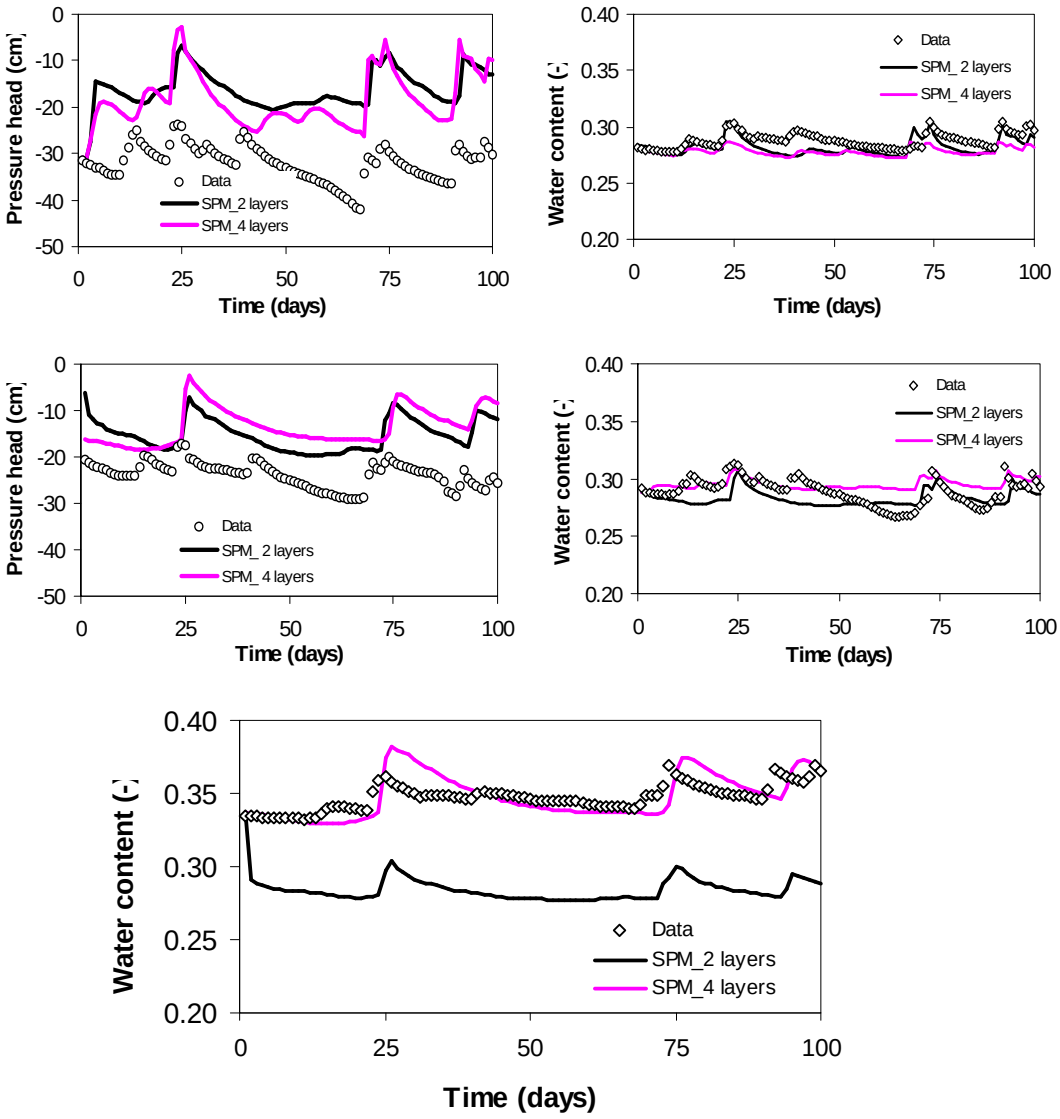

Figure III-4. Comparison of daily data and predicted values for two scenarios SPM_2la and SPM_4la: (a) pressure heads at 100 cm depth, (b) pressure heads at 150 cm depth, (c) water contents at 50 cm depth, (d) water content at 100 cm depth and (e) water contents at 150 cm depth.

For the estimated parameters from the reference case (SPM_2la), the predicted pressure heads just showed “acceptable” agreements with the measured pressure heads at 100, 150 cm depths which were indicated by the RMSE values of 16.66 cm and 9.23 cm, respectively. By comparison, these RMSE values remained within the range of pressure heads errors finding in the literature e.g. (Durner et al., 2008). Similar result about predicted pressure heads were also obtained with SPM_4la.

Altogether, the predicted water contents for SPM_4la corresponded well, and better as compared with SPM_2la, with the measured water contents at 100, 150 cm depths. That was indicated by the smaller RMSE values and higher MIA values for the case SPM_4la. Especially, an excellent agreement between predicted water contents and measured water contents at 150 cm depth was obtained as shown in figure III-4.

4. Conclusions

In this work, we evaluated the effect of hydraulic parameters to different output predictions via sensitivity analysis based on sensitivity coefficient approach. For both hourly and daily output predictions, pressure heads in the lysimeter were more sensitive than water contents, cumulative bottom flux and cumulative evaporation. The sensitivity order of five parameters to hourly pressure heads and water contents was: n, θ_s, α, K_s and θ_r. Specially, the sensitivities of all five parameters to cumulative bottom flux and cumulative evaporation were negligible. According to daily output predictions, the sensitivities of five parameters were almost higher than those obtained with hourly output predictions. For example, sensitivities of parameters n and K_s to daily cumulative bottom flux increased, as indicated by sensitivity coefficients.

Estimability analysis results indicated that for both hourly and daily data, pressure heads contained more information than water contents, cumulative bottom flux and evaporation. If 2.4 was considered as a cut-off criterion for this study, the set of estimable parameters according to hourly measured pressure heads were 4 out of the 5 parameters. And none of five parameters would be estimable from hourly measured cumulative bottom flux and evaporation. The combination between hourly pressure heads and water contents made estimability increase but the set of estimable parameters remained 4. By comparison, it was clear that daily data contained more information content than hourly data for the parameter optimization. For example, the set of estimable parameters became 5 parameters basing only on daily measured pressure heads and 3 out of the 5 parameters basing on daily measured water contents. However, according to daily cumulative bottom flux or evaporation, only parameter n was estimable. Hence, daily measured pressure heads and water contents should be included simultaneously in the objective function since, on the one hand, the combination also made increase estimability parameter and on the other hand no high correlation between different parameters was found due to the combination.

When daily pressure heads and water contents were simultaneously included in the objective function, θ_r, θ_s, n were successfully estimated with narrow confidence intervals. However, uncertainties on optimized α and K_s were high, with large confidence intervals. This could be explained by the fact that the bare field lysimeter produced narrow pressure heads and water contents and that made it difficult to

accurately estimate α and K_s. Including the last values of daily cumulative bottom flux and evaporation or ten values of hydraulic properties $\theta(h)$ did not help to improve the optimization procedure.

Accounting for soil heterogeneity slightly improved simulation quality, as indicated by lower values of MAE and RMSE and higher values of MIA for all pressure heads and water contents. In addition, the prediction of water contents at 150 cm depth was clearly better for the case accounting for soil-layered than those obtained for the case only regarding homogeneity soil.

As shown in this work, estimability is a powerful technique to provide information contents of different types of experimental data. This approach should be generalized to help us to focus on data having highest information contents. It could enable us to improve the design of experimental systems as well.

Acknowledgments

The authors thank the French Scientific Interest Group on Industrial Wastelands (www.gisfi.fr), financially supported by the French government, the "Région Lorraine" and the "Conseil Général de Meurthe et Moselle". They also thank Noële Raoult and Julien Michel for data collection.

Chapitre IV : Analyse d'estimabilité des paramètres du modèle à double porosité

Estimability analysis of Dual-Porosity Model parameters from lysimeter data: Inverse modeling

Van-Viet Ngo, M.A. Latifi, Marie-Odile Simonnot

Laboratoire des Sciences du Génie Chimique, CNRS-ENSIC
1, Rue Grandville, BP20451, 54001 Nancy Cedex, France

Summary

In this study a lysimeter under natural atmospheric conditions were used to investigate the effect of eight hydraulic parameters in dual-porosity model implemented in the HYDRUS software via the sensitivity analysis. Information content of four types of measurements from this field lysimeter (pressure heads, water contents, cumulative bottom water and evaporation) was evaluated by sequentially calculating a sensitivity matrix. Pressure heads contained the most information content for parameter optimization followed by water contents and five out of the eight parameters were estimable from the combination of pressure heads with water contents. Pressure heads and water contents were then included in the objective function to optimize five parameters simultaneously by using the Levenberg-Marquardt optimization. However, saturated water contents in the mobile and immobile regions were impossible to estimate simultaneously due to their high correlations. When water transfer coefficient parameter was included in the optimization procedure, the optimization results became worse due to the low sensitivity of this parameter to pressure heads and water contents. Removing saturated water content in the immobile region and saturated hydraulic conductivity, which had strong correlation more estimable parameters, made improve the optimization results slightly and especially water transfer parameter was also reliably estimated.

1. Introduction

Many observations from the natural soils showed the significant effect of preferential flow (PF) on the accelerating of contaminant transport (e.g., Hagedorn and Bundt, 2002; Jorgensen et al., 2002; Ronkanen and Klove, 2007). Therefore, accounting for the PF in the modelling of water flow and solute transport in the vadose zone hydrology has been received much attention (Simunek et al., 2001). The PF is manifested by physical nonequilibrium which is defied as local differences of flow velocities, pressure heads, water contents, and solute concentration (e.g., Gerke and Van Genuchten, 1993b; Kohne et al., 2004a). The PF is generally characterized by the use of the nonequilibrium models such as dual-porosity and dual-permeability models. However, the application of the dual-permeability model is restricted by their large numbers of model parameters (Simunek et al., 2003; Kohne et al., 2006b). The hydraulic parameters are crucial for the result quality of the water flow and solute transport modelling in the vadose zone, and they can be obtained by the direct measurement (e.g., Jaynes et al., 1995; Logsdon, 2002; Alletto et al., 2006) but they still remained very uncertain due to their dependences on various

porous media characteristics such as flow velocities, soil hydraulic properties and length-scale. Therefore, inverse method is very promising way to determine hydraulic parameters. In the past, several studies have been analysed in detail for evaluation of the region-specific hydraulic parameters related to the preferential flow (e.g., Simunek et al., 2001; Kohne et al., 2004a; Kohne et al., 2006b; Roulier et al., 2008). However, the problem of nonuniqueness and uncertainty of such optimized parameters still exist (Simunek et al., 2001; Kohne et al., 2004a; Kohne et al., 2006b).

The poor results by inverse method may be caused by the insufficient information content of experimental data included in the objective function, the large number of optimized parameters and the high correlations between model parameters that were optimized simultaneously, the local algorithm optimization. For example, both studies done by Simunek et al., 2001 and Kohne et al., 2006b concluded that water flow observations alone may not contain sufficient information content to achieve uniqueness for many estimated parameters required for the dual-permeability model. Additionally, Kohne et al., 2004a reported that saturated water content in the mobile and immobile regions ($\theta_{s,mo}$ and $\theta_{s,im}$) were impossible to estimate simultaneously from water flow and solute transport data at the column scale. According to Hopmans and Simunek, 1999 parameter identifiability may be increased by reducing the number of optimized parameters, or by including appropriate additional experimental information. Therefore, to answer the question whether experimental data of such experimental system are sufficient to identify nonequilibirum model and then to better calibrate model parameters from experimental data as well as to improve the design quality of experimental system; it is necessary to investigate information content of experimental data before using them for the optimization procedure and to evaluate correlations between different parameters.

The overall objectives of this study were to (i) evaluate the sensitivity of hydraulic parameters to different types of measures (pressure heads, water contents, cumulative bottom water and evaporation) in the field lysimeter under natural atmospheric conditions, (ii) investigate the information content of such experimental data, meaning also that parameter estimability from experimental data, and (iii) optimize model parameters from data which have enough information content and also the influence of correlations of model parameters on the optimization results.

2. Material and methods

2.1. Experimental description

This work was carried out in the frame of the French Scientific Interest Group on Industrial Wastelands called GISFI (www.gisfi.prd.fr). The lysimeter was set up in February 2008 and located in the GISFI experimental station grouping 24 lysimeters in Homécourt (North East of France: 49°14'N, 5°59'E). It was a former coking plant site, stopped and torn down in the early 80's, and heavily contaminated with polycyclic aromatic hydrocarbons (4.9 mg kg^{-1}). It was a sandy soil, with a high organic carbon content (139 g kg^{-1}), and a high pH (8.3) due to its anthropogenic activities.

The lysimeter, has a surface of 1 m^2 and a depth of 2 m, was filled with 15 cm of sand (sand is necessary to avoid soil particle entrapment in the pipes and system blockage) and then 185 cm

of undisturbed soil monoliths coming from this site and equipped with 3 kinds of probes at each depth (3 depths: 50, 100, and 150 cm): a TDR probe, a tensiometer and a suction cup. The mean apparent bulk density of the soil monoliths in the lysimeter was 1670 kg m^{-3}.

The lysimeter was placed on the stationary balances which are connected with electronic balances to register the changes of lysimeter weight. The percolation is collected in a 20 L glass bottle at the bottom of the lysimeter. The lysimeter is explored under natural atmospheric conditions; its surface is bare soil (figure IV-1).

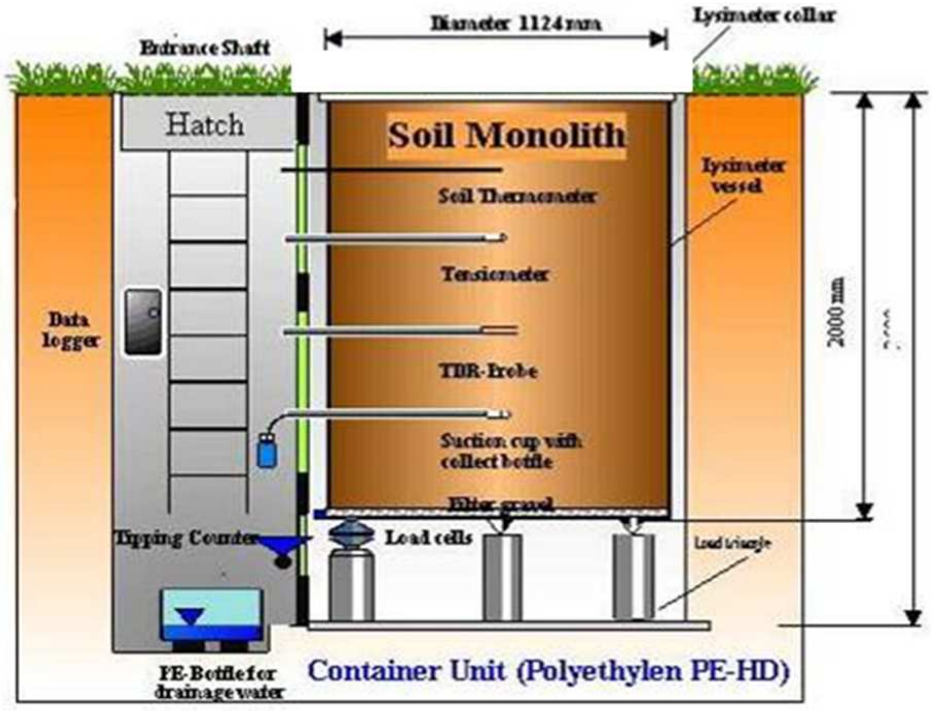

Figure IV-1. Experimental setup of lysimeter, the lysimeter surface is bare soil

A data logger recorded hourly lysimeter weight, volumetric water content, soil hydraulic pressure, and water flux at the bottom of the lysimeter and soil temperature. Hourly data such as pressure heads and water contents were then averaged to obtain daily data. The amount of evaporation was derived from the changes of lysimeter weight. Water percolation and precipitation was also summed for 1 day interval. A weather station near to lysimeter station recorded hourly air temperature, relative humidity, wind speed and direction.

2.2. Model description

The dual-porosity model implemented in the HYDRUS-1D software (Simunek et al., 1998) was chosen for this work. This model requires considerably fewer parameters than the dual-permeability model. HYDRUS-1D software is widely used to simulate water flow and solute transport through the vadose zone (e.g., Haws et al., 2005; Goncalves et al., 2006; Gardenas et al., 2006; Wissmeier and Barry, 2008).

The dual-porosity model concept assumes that water-filled pore space is partitioned into 2 regions: a mobile region, θ_{mo},(interagregate pores or macropores), and an immobile region, θ_{im}, (intraagregate pores or the rock matrix) (van Genuchten and Wierenga, 1976; Simunek et al., 2003; Simunek and van Genuchten, 2008):

$$\theta = \theta_{mo} + \theta_{im} \quad [1]$$

The formulation for dual-porosity water flow can be described by the Richards equation in the mobile region combined with a source/sink term, Γ_w, to account for water exchange with the immobile region (e.g., Simunek et al., 2003). It is expressed as follows:

$$\frac{\partial \theta_{mo}(h_{mo})}{\partial t} = \frac{\partial}{\partial z}\left(K(h_{mo})\frac{\partial h_{mo}}{\partial z} + K(h_{mo}) \right) - \Gamma_w$$
$$\frac{\partial \theta_{im}(h_{im})}{\partial t} = \Gamma_w \quad [2]$$

Where h_{mo} is the pressure head in the mobile region [L], t is the time [T], z is the vertical coordinate [L], K is the hydraulic conductivity [L T^{-1}], Γ_w is the water transfer rate between mobile and immobile regions [T^{-1}].

Two approaches can describe the water transfer rate between two regions: the first one is based on the difference in effective water content of the two regions using the first-order rate equation (Simunek et al., 2001), the second one is based on the difference in pressure heads between the two regions (Gerke and Van Genuchten, 1993b). The advantages and disadvantages of these approaches are discussed in a review by Simunek et al., 2003. In this work, the first approach was used since it needs fewer parameters (Simunek et al., 2003). It is given by:

$$\Gamma_w = \omega_w (S_{e,mo} - S_{e,im}) \quad [3]$$

Where ω_W is the first-order water transfer rate coefficient [T^{-1}], $S_{e,mo}$ et $S_{e,im}$ are effective soil water contents in the mobile and immobile regions, respectively.

The knowledge of unsaturated soil hydraulic functions is required to solve the Richards equation. These functions are made up of the soil water retention curve θ(h) and the unsaturated hydraulic function

K(h), which defines the hydrsulic conductivity as a function of θ and h. The analytical model proposed by van Genuchten, 1980 for θ(h) and K(h) was used here as follows:

$$S_e = \frac{\theta - \theta_r}{\theta_s - \theta_r} = \frac{1}{\left(1 + \alpha h^n\right)^m} \qquad h < 0 \qquad [4a]$$

$$S_e = 1 \qquad h \geq 0 \qquad [4b]$$

$$K(S_e) = K_s S_e^l \left[1 - \left(1 - S_e^{1/m}\right)\right]^2 \qquad [4c]$$

$$m = 1 - 1/n \qquad n > 1 \qquad [4d]$$

The soil hydraulic functions defined in equations 4a and 4c have five unknown parameters: θ_r, θ_s, α, n and K_s. The pore connectivity parameter *l* was set to 0.5 (Mualem, 1976). There are therefore eight parameters in this study: $\theta_{r,mo}$, $\theta_{s,mo}$, α, n, K_s, $\theta_{r,im}$, $\theta_{s,im}$, and ω_w.

2.3. Parameter estimation and initial condition, boundary condition

Input values of five parameters are represented in table IV-1. The initial values of these parameters were estimated by Rosetta software (Schaap et al., 2001) using the grain size composition and the bulk density of the two layers in the lysimeter. The Rosetta software was used in many studies (e.g., Hermsmeyer et al., 2002; Kelleners et al., 2005; Sander and Gerke, 2009). Our preliminary investigations indicated that the hydraulic parameters of sand layer were not important for the results of this work. Therefore, the results concerning sand layer are not showed in this paper.

It appears from published studies that the fraction of immobile water shows a large range of value. For example, Alletto et al., 2006 measured the immobile water fraction for three soil profiles under natural conditions and obtained a range varying from 0.213 to 0.822. Based on this range of values, the following hypothesis were assumed $\theta_{r,mo} = \theta_{r,im} = 0.5\theta_r$ and $\theta_{s,mo} = \theta_{s,im} = 0.5\theta_s$.

Table IV-1. Description and initial value of 8 parameters in dual-porosity model

Parameter	Unit	Parameter description	Value
$\theta_{r,mo}$	$cm^3\ cm^{-3}$	Residual water content in the mobile region	0.023
$\theta_{s,mo}$	$cm^3\ cm^{-3}$	Saturated water content in the mobile region	0.205
α	cm^{-1}	Shape factor in the soil water retention curve in the mobile region	0.03
n	-	Hydraulic property shape factor in the mobile region	1.49
K_s	$cm\ d^{-1}$	Saturated hydraulic conductivity in the mobile region	2.89
$\theta_{r,im}$	$cm^3\ cm^{-3}$	Residual water content in the immobile region	0.023
$\theta_{s,im}$	$cm^3\ cm^{-3}$	Saturated water content in the immobile region	0.205
ω_w	d^{-1}	First-order rate water transfer coefficient	0.1

A very wide range of values was found for the first-order rate water transfer coefficient (ω_w). In this work, the initial value of this parameter was set equal to 0.1 d^{-1} (Kohne et al., 2006c). The preliminary studies indicated that the water retention and saturated hydraulic parameters corresponding to sand layer were not sensitive to the output predictions. Then, the results concerning this layer are not showed in this paper. The values in table IV-1 correspond to soil layer.
The initial condition in this study was set in term of measured water content given by TDR probes at 3 depths (50, 100, and 150 cm):

$$\theta(z,t) = \theta(z) \quad \text{at t=0} \qquad [5]$$

The upper flow boundary condition was specified as the « atmospheric boundary condition with surface run off » with precipitation as the input flux and evaporation from the lysimeter surface as the output flux. The equation of the upper boundary condition is given by:

$$-K\left(\frac{\partial\theta}{\partial z}-1\right) = q_T(t) \quad \text{at z = 0} \qquad [6]$$

where q_T is the net infiltration rate [L T^{-1}].

The lower boundary condition in the lysimeter was specified as a seepage face that was usually used for experiments at the lysimeter scale (Sonnleitner et al., 2003; Abdou and Flury, 2004; Kasteel et al., 2007). It is expressed as follows:

$$-K\left(\frac{\partial\theta}{\partial z}-1\right) = q_B(t) \quad \text{at z = L} \qquad [7]$$

where q_B is the drainage rate [L T^{-1}].

2.4. Sensitivity analysis

Many different methods to investigate sensitivity analysis of model parameters could be found in the literature (Hamby, 1994). In this study, sensitivity analysis was assessed by using sensitivity coefficient which quantifies how model predictions are affected by changes in parameter values. This sensitivity coefficient was taken from approximation by a finite difference of partial derivate describing model prediction dependence as a function of parameter p. The initial parameter value was changed by ± Δp (in this work Δp = 10%) with corresponding variation of model predictions as follows:
$p + \Delta p \rightarrow S^+$
$p - \Delta p \rightarrow S^-$
A sensitivity coefficient was obtained according to below equation:

$$I = \frac{\partial S}{\partial p} = \frac{S^+ - S^-}{2\Delta p} \quad [8]$$

The sensitivity coefficient was then normalized in order to get a dimensionless sensitivity coefficient by removing the effects of units as follows (Hamby, 1994):

$$I_{norm} = \frac{p}{S}\left(\frac{S^+ - S^-}{2\Delta p}\right) \quad [9]$$

The sensitivity coefficients were classified into 4 classes proposed by Lenhart et al., 2002, as shown in table IV-2. Notice that whenever model parameters were significant to model predictions, only the absolute values of I were taken into account.

Table IV-2. Sensitivity classes

Classes	Sensitivity coefficient	Sensitivity
1	$0.00 \leq \lvert I_{norm} \rvert < 0.05$	Low or negligible
2	$0.05 \leq \lvert I_{norm} \rvert < 0.20$	Medium
3	$0.20 \leq \lvert I_{\text{norm}} < 1.00$	High
4	$1.00 \leq \lvert I_{norm} \rvert$	Very high

2.5. Estimability analysis

Sensitivity analysis is necessary but it is not sufficient since parameter correlation may hamper the parameter estimability (Larsbo and Jarvis, 2006). Therefore, it is important to asses estimability analysis to know whether a given data set has enough information content to estimate parameters from it (Jayasankar et al., 2009). Estimability is defined as the ability to compute parameters accurately from a given data set and experimental conditions (Yao et al., 2003; Jayasankar et al., 2009).

Parameter estimability depends not only on model structure and parameter sensitivity but also on correlations between different parameters. The parameter estimability was evaluated and a subset of estimable parameters was established using a method proposed by Yao et al., 2003 which allows quantifying the effect of each model parameter on the various model predictions and accounting for the correlations between the effects of different parameters. This method was successfully applied in the chemical engineering (e.g., Kou et al., 2005; Jayasankar et al., 2009). Estimability analysis method of Yao et al., 2003 compiled dynamic models and dynamic data, as well as response variables available at different sampling rates throughout each experimental run (Kou et al., 2005).

A sensitivity coefficient matrix Z was built, from the individual coefficient as follows:

$$Z = \begin{bmatrix} \frac{p_1}{S}\frac{\partial S}{\partial p_1}\Big|_{t=t_1} & \cdots & \frac{p_m}{S}\frac{\partial S}{\partial p_m}\Big|_{t=t_1} \\ \frac{p_1}{S}\frac{\partial S}{\partial p_1}\Big|_{t=t_2} & \cdots & \frac{p_m}{S}\frac{\partial S}{\partial p_m}\Big|_{t=t_2} \\ \cdots\cdots\cdots\cdots\cdots\cdots & & \\ \frac{p_1}{S}\frac{\partial S}{\partial p_1}\Big|_{t=t_n} & \cdots & \frac{p_m}{S}\frac{\partial S}{\partial p_m}\Big|_{t=t_n} \end{bmatrix}$$

In the Z matrix, the number of columns is equal to the number of model parameters (eight parameters for this study) and each row corresponds to model predictions at a given sampling time.
Elements of the Z matrix were calculated by a module that is programmed by Matlab software. The subset of estimable parameters was identified following 8 steps (Yao et al., 2003):

1. Calculate the magnitude of each column of Z
2. Select the parameter whose column in Z has the largest magnitude (the sum of squares of the elements) as the first parameter. This parameter is considered to have the most effects on model predictions in the soil lysimeter.
3. Mark the corresponding column as X_L (L = 1 for the first iteration)
4. Calculate Z_L, the prediction of the full sensitivity matrix Z, using the subset of columns X_L: $Z_L = X_L \left(X_L{}^T X_L\right)^{-1} X_L{}^T Z$
5. Calculate the residual matrix R_L: $R_L = Z - Z_L$
6. Calculate the sum of squares of the residuals in each column of R_L. The column with the largest magnitude corresponds to the next estimable parameter (among the remaining parameters) which has the largest effects on model predictions and which is not correlated with the effects of already selected parameters.
7. Select the corresponding column in Z, and augment the matrix X_L by including the new column. Denote the augmented matrix as X_{L+1}.
8. Advance the iteration counter one and repeat steps 4 to 7 until the last model parameters.

The algorithm begins with choosing the most estimable parameter which corresponds to the largest magnitude in the Z matrix (steps 1, 2). However, this parameter may have correlation with the remaining model parameters. That is why orthogonalization is required to rank individual parameter influences on the output predictions. That means when the first estimable parameter has been determined, the influences of the most estimable parameter on the remaining parameters must be adjusted for any correlation that exists between each column of Z associated with a remaining parameter and the column of Z associated with the first parameter, so that the “net influence” of each of the remaining parameters can be assessed. This adjustment is made by regressing all of the original columns of the Z matrix on the column associated with the most estimable parameter. It is important to note that this regression results in a matrix of the same dimensions as the original Z matrix, and the column of this residual matrix associated with the most estimable parameter will be a column of zeros (steps 3, 4, 5). The orthogonalization is followed by identifying the largest column in the residual matrix, which enlightens

the parameter having the second strongest "net influence" on the output predictions, after the influence of the most parameter has been delimited (steps 6, 7). The orthogonalization is carried on until the last model parameter.

Yao et al., 2003 used 0.04 as a cut-off criterion for considering whether a model parameter was estimable or not. Their cut-off value means that sufficient information would be contained for estimating a parameter if 10% change in its initial value implied a 2% change in output. The choice of a cut-off criterion is somewhat arbitrary (Yao et al., 2003). However, their approach seems to be reasonable as compared with the sensitivity analysis results in this work. As a consequence, the approach of Yao et al., 2003 was used here to estimate the cut-off value and a value of 2.4 was obtained and considered as a cut-off criterion for this work.

As the number of model parameters was only eight, the calculation procedure of Z matrix was performed until the last parameter because the objective was to show correlation results between all parameters.

2.6. Optimization

The optimization procedure is based on the minimization of the differences between the observations and the simulated values which are described by an objective function as follows (Simunek et al., 1998):

$$\phi(b,q,p)=\sum_{j=1}^{m_q} v_j \sum_{i=1}^{n_{qj}} w_{i,j}\left[q_j^*(x,t_i)-q_j(x,t_i,\boldsymbol{b})\right]^2+\sum_{j=1}^{m_p} v_j' \sum_{i=1}^{n_{pj}} w_{i,j}'\left[p_j^*(\theta_i)-p_j(\theta_i,\boldsymbol{b})\right]^2 \qquad [10]$$

Where the first term on the right hand-side represents deviations between the measured, q_j^*, and calculated, q_j, space-time variables (e.g., pressure heads, water contents, cumulative flux across a boundary of the lysimeter). In this term, m_q is the number of different sets of measurements, n_{qj} is the number of measurement in a particular measurement set, $q_j^*(x,t_i)$ represents specific measurement at time t_i for the jth measurement set at location x, $q_j(x,t_i,\mathbf{b})$ are the corresponding model predictions for the vector of optimized parameters **b**, and v_j and $w_{i,j}$ are weights associated with a particular measurement set or point, respectively. The second term of equation 10 represents differences between independently measured, p_j^*, and predicted, p_j, soil properties, such as retention or conductivity data at particular pressure heads, while the term m_p, n_{pj}, p_j^*, $p_j(\theta_i,\mathbf{b})$, v_j', w_{ij}' have the similar meanings as for the first term but now for the soil hydraulic properties.

The weighting coefficient, v_j and v_j' that equalize the contribution of different data types to the objective function Φ are given by

$$v_j=\frac{1}{n_j\sigma_j^2} \qquad [11]$$

Which normalize the objective function in terms of the variances σ_j^2 of measurement type j.

The error measurements for cumulative flow, tensiometer and TDR methods at the lysimeter scale are found to be 0.001 cm for the cumulative outflow, 0.5 cm for the pressure heads, and 0.01 $cm^3\ cm^{-3}$ for

the water contents (Durner et al., 2008). Then, we assumed that $w_{i,j}$ was set equal to 0.001 for the daily cumulative bottom flux and daily cumulative evaporation, 0.5 for pressure heads, 0.01 for water contents. $w_{i,j}'$ was set equal to 0.001 (Durner et al., 2008).

Simulations were done for a period of 248 days (15 February to 19 October 2008). Over the entire period of monitoring, the weighting lysimeter registered 21.4 cm of net infiltration and 39.6 cm of net evaporation. For the reference case of optimization procedure, 496 values of pressure heads at 100 and 150 cm depths and 496 values of water contents at 50 and 150 cm depths were included in the objective function. Regarding the daily data, we found that only very small changes in pressure heads (in the range of -1.7 and -25.7 cm at 100 cm depth and -4.1 and -42.3 at 150 cm depth) and water contents (in the range of 0.258–0.295 cm^3 cm^{-3} at 50 cm depth and 0.276-0.311 cm^3 cm^{-3} at 100 cm depth).

The Levenberg-Marquardt algorithm was used to minimize the objective function (equation 10) and to calculate confidence intervals for the parameters (Simunek et al., 1998). Compared with global optimization methods (e.g., Abbaspour et al., 2001; Lambot et al., 2002; Mertens et al., 2004; Durner et al., 2008), the Levenberg-Marquardt method provides useful statistical information about the optimized parameters, such as their mutual correlations and confidence intervals.

2.7. Model performance analysis

The model performance analysis was evaluated by 3 statistical analysis criteria: the mean absolute error, the root mean square error, the modified index of agreement.

The mean absolute error (MAE) describes the difference between the observations (O_i) and the simulated values (S_i) as follows:

$$MAE = \frac{1}{N}\sum_{i=1}^{N}\left|O_i - S_i\right| \qquad [12]$$

Where N is the number of observations

The root mean square error (RMSE) is given by:

$$RMSE = \sqrt{\frac{\sum_{i=1}^{N}\left(O_i - S_i\right)^2}{N-1}} \qquad [13]$$

The index of agreement (IA) is given by (Willmott, 1981):

$$IA = 1 - \frac{\sum_{i=1}^{N}(O_i - S_i)^2}{\sum_{i=1}^{N}\left(\left|S_i - \bar{O}\right| + \left|O_i - \bar{O}\right|\right)^2} \quad [14]$$

Where $\bar{O}$ is the average of observations

The IA is ranged from 0 to 1.0, with higher values indicating better agreement between measured data and simulated model.
However, to reduce the effect of square terms, we mainly used the modified index of agreement (MIA) as follows (Willmott et al., 1985):

$$MIA = 1 - \frac{\sum_{i=1}^{N}\left|O_i - S_i\right|}{\sum_{i=1}^{N}\left(\left|S_i - \bar{O}\right| + \left|O_i - \bar{O}\right|\right)} \quad [15]$$

The use of MIA has more interest than IA by eliminating the effect of squares terms. And MIA, as compared with the coefficient of determination (R^2), is a more reliable statistical measure and less sensitive to extreme values (Legates and McCabe Jr., 1999).

3. Result and discussions

3.1. Sensitivity analysis

The sensitivities of 8 parameters to daily output predictions (pressure head, water content, cumulative bottom flux and cumulative evaporation) are represented in table IV-3. Following daily pressure heads, the most sensitive parameter was parameter n (very high). Parameters $\theta_{s,mo}$, $\theta_{s,im}$, α, K_s showed high sensitivity and were less sensitive than parameter n. The sensitivities of parameters ω, $\theta_{r,mo}$, $\theta_{r,im}$ remained low level to daily pressures heads.

Accordingly to daily water contents, the most sensitive parameter was also parameter n followed by parameters $\theta_{s,mo}$, $\theta_{s,im}$ but they remained only at high sensitivity. Especially, the sensitivity coefficients of parameter K_s and α to daily water contents decreased clearly as compared with those to daily pressure heads; their sensitivity degree were medium and low, respectively. One again, the sensitivities of parameters ω, $\theta_{r,mo}$, $\theta_{r,im}$ were low to daily water contents. The sensitivities of all 8 parameters to daily cumulative bottom water and cumulative evaporation decreased clearly; the most sensitive parameter was parameter $\theta_{s,mo}$ but it's sensitivity was only medium. The sensitivities of other parameters were low or negligible. This suggests that we will not have much opportunity to optimize these parameters basing on daily cumulative water and cumulative evaporation. From the sensitivity coefficients of each parameter in function of daily pressure heads, water contents, cumulative bottom water and cumulative

evaporation in table IV-3, we found that daily pressure heads in the soil lysimeter were more sensitive than daily water contents, cumulative bottom water and cumulative evaporation. The similar result was also reported in Rocha et al., 2006.

Table IV-3. Sensitivity coefficients of 8 parameters in dual-porosity model to different daily data

	Pressure head		Water content		Cumulative bottom water		Cumulative Evaporation	
$\theta_{r,mo}$	0.04	Low	0.02	Low	0.002	Negligible	0.007	Negligible
$\theta_{s,mo}$	0.63	High	0.41	High	0.005	Low	0.069	Medium
α	0.46	High	0.03	Low	0.003	Low	0.042	Low
n	1.34	Very high	0.68	High	0.040	Low	0.042	Low
K_s	0.34	High	0.08	Medium	0.025	Low	0.004	Negligible
$\theta_{r,im}$	0.04	Low	0.02	Low	0.001	Negligible	0.005	Negligible
$\theta_{s,im}$	0.61	High	0.27	High	0.003	Negligible	0.027	Low
ω	0.03	Low	0.01	Low	0.001	Negligible	0.014	Low

3.2. Estimability analysis

Tables IV-4a, IV-4b, IV-4c, and IV-4d represent the estimability analysis results of different parameters that separately base on daily pressure heads, water contents, cumulative bottom water, and cumulative evaporation, respectively. From left to right of tables IV-4a, IV-4b, IV-4c, and IV-4d the estimability order of eight parameters decreases. The first row in tables IV-4a, IV-4b, IV-4c, and IV-4d represents the magnitude of each column in Z matrix corresponding to each parameter before adjusting the correlations between different parameters. From the second row to the end of tables IV-4a, IV-4b, IV-4c, and IV-4d list the magnitude of each column in Z matrix after eliminating the influences of more estimable parameter(s) on the remaining model parameter(s).

When 2.4 was chosen as a cut-off criterion for parameter estimability as noted earlier, the set of estimable parameters was five out of the eight parameters following daily pressure heads (table IV-4a). Five estimable parameters were parameters n, $\theta_{s,mo}$, α, $\theta_{s,im}$, and K_s. It is not surprising that parameter n was the most estimable parameter since this was the most sensitive parameter to daily pressure heads.

Following daily water contents, three out of the eight parameters were estimable (n, $\theta_{s,mo}$, $\theta_{s,im}$). It seems to be understandable since parameter sensitivity was less to daily water contents than to daily pressure heads. Especially, basing on daily cumulative bottom water or daily cumulative evaporation, none of eight parameters would be estimable. From these estimability analysis results, we could conclude that daily pressure heads contained the most information content and that daily cumulative bottom water and evaporation had very poor information content for the parameter calibration. Our findings were partly consistent with the result obtained by Ines and Droogers, 2002 and Vrugt et al., 2001, who also concluded that water contents had more information content than cumulative bottom water and evaporation.

Table IV-4. Estimability order of 8 parameters in dual-porosity model in function of daily measurements in the lysimeter: (a) pressure heads, (b) water contents, (c) cumulative water at lower boundary of the lysimeter, (d) evaporation at upper boundary of the lysimeter

(4a)

n	$\theta_{s,mo}$	α	$\theta_{s,im}$	K_s	ω_w	$\theta_{r,mo}$	$\theta_{r,im}$
2834.80	1237.47	702.75	1060	104.56	3.82	2.54	2.04
0	**707.24**	701.87	500.50	78.14	3.82	1.30	1.10
0	0	**536.86**	21.89	69.85	2.48	1.04	1.05
0	0	0	**20.31**	2.69	2.45	0.63	0.52
0	0	0	0	**2.56**	1.06	0.60	0.43
0	0	0	0	0	0.63	0.50	0.42
0	0	0	0	0	0	0.45	0.38
0	0	0	0	0	0	0	0.12

(4b)

n	$\theta_{s,im}$	$\theta_{s,mo}$	α	K_s	$\theta_{r,im}$	$\theta_{r,mo}$	ω_w
433.40	97.44	146.28	1.56	6.18	0.264	0.416	0.0000
0	**46.42**	18.91	1.50	0.54	0.024	0.042	0.0000
0	0	**12.83**	1.20	0.50	0.021	0.031	0.0000
0	0	0	1.18	0.22	0.015	0.012	0.0000
0	0	0	0	0.05	0.0146	0.0117	0.0000
0	0	0	0	0	0.0141	0.0109	0.0000
0	0	0	0	0	0	0.0031	0.0000
0	0	0	0	0	0	0	0.0000

(4c)

n	K_s	$\theta_{r,mo}$	$\theta_{s,mo}$	α	$\theta_{s,im}$	ω_w	$\theta_{r,im}$
0.584	0.217	0.007	0.012	0.005	0.005	0.006	0.002
0	0.085	0.006	0.007	0.005	0.005	0.006	0.002
0	0	0.005	0.005	0.002	0.002	0.005	0.002
0	0	0	0.005	0.002	0.002	0.002	0.001
0	0	0	0	0.002	0.001	0.001	0.001
0	0	0	0	0	0.001	0.001	0.000
0	0	0	0	0	0	0.000	0.000
0	0	0	0	0	0	0	0.000

(4d)

$\theta_{s,mo}$	α	n	$\theta_{s,im}$	K_s	ω_w	$\theta_{r,mo}$	$\theta_{r,im}$
1.734	0.654	0.677	0.279	0.0079	0.0777	0.0202	0.0102
0	0.057	0.046	0.021	0.0028	0.0040	0.0014	0.0011
0	0	0.041	0.016	0.0026	0.0032	0.0012	0.0011
0	0	0	0.011	0.0026	0.0022	0.0011	0.0008
0	0	0	0	0.0025	0.0022	0.0010	0.0008
0	0	0	0	0	0.0014	0.0008	0.0007
0	0	0	0	0	0	0.0008	0.0007
0	0	0	0	0	0	0	0.0005

Table IV-5. Estimability order of 8 parameters in dual-porosity model daily pressure heads and daily water contents at 3 depths in the lysimeter were investigated at the same time

n	$\theta_{s,mo}$	α	$\theta_{s,im}$	K_s	ω_w	$\theta_{r,mo}$	$\theta_{r,im}$
3268.20	1383.75	704.31	1157.45	110.74	3.93	2.95	2.30
0	**730.67**	703.38	550.77	78.80	3.92	1.37	1.13
0	0	**543.10**	67.16	71.41	2.57	1.10	1.09
0	0	0	**64.83**	2.88	2.54	0.70	0.56
0	0	0	0	**2.84**	2.21	0.70	0.50
0	0	0	0	0	**2.04**	0.65	0.48
0	0	0	0	0	0	0.49	0.48
0	0	0	0	0	0	0	0.17

Increasing the number of different experimental data may increase parameter estimability (Yao et al., 2003). Accordingly, Simunek and Van Genuchten, 1997 reported that parameter identifiability was increased when pressure heads and water contents were simultaneously included in the objective function. Therefore, we tried to combine the daily pressure heads and daily water contents and investigate how important it made increase parameter estimability. Table IV-5 showed that when daily pressure heads and water contents were combined together, the magnitudes, corresponding to each model parameter, before and after eliminating the correlations between model parameters increased. However, as compared with a cut-off criterion value of 2.4 the set of estimable parameters still remained five out of the eight parameters as the case that based on daily pressure heads. The estimability order was n, $\theta_{s,mo}$ α, $\theta_{s,im}$, $K_{s.}$

As discussed earlier, it is helpful to evaluate correlations between model parameters before optimizing them. Because it can prevent us the confidence and uncertainty of optimized parameters. We just evaluated the correlations between different parameters in terms of "net influence" of the more estimable parameter(s) on the remaining parameter(s) which was calculated based on the magnitude of each column of the Z matrix as follows:

$$nI = 100\frac{R_{n+1} - R_n}{R_n} \quad [16]$$

Where R_n, R_{n+1} are the row order in table IV-5

Table IV-6 summarizes the influence of more estimable parameter(s) on the remaining parameter(s) when daily pressure heads and water contents were combined. It is important to note that the higher the net influence of more estimable parameter(s) on the remaining parameter(s), the higher the correlation between such parameter couple. Parameter n was found to have considerable influence on other parameters such as $\theta_{s,mo}$, $\theta_{s,im}$, $\theta_{r,mo}$, and $\theta_{r,im}$ (row 1). In addition, parameter $\theta_{s,mo}$ also showed very high influence on parameter $\theta_{s,im}$ (row 2), meaning that parameters $\theta_{s,mo}$ and $\theta_{s,im}$ were highly correlated. And parameter α had very high influence on parameter K_s, meaning also that these two parameters were very strongly correlated. These correlations plus information content obtained in table IV-5 suggest the difficulty in estimating five parameters simultaneously basing on daily pressure heads and water

contents. Recently, Kohne et al., 2004a reported that correlation between parameters $\theta_{s,mo}$ and $\theta_{s,im}$ in dual-permeability model was always high. In addition, Schwarzel et al. (2006 also) concluded the evidence of high correlation between α and K_s.

Table IV-6. Net influence of the more estimable parameter(s) on the remaining model parameter(s) for the dual-porosity model when daily pressure heads and daily water contents were investigated at the same time

	n	$\theta_{s,mo}$	α	$\theta_{s,im}$	K_s	ω_w	$\theta_{r,mo}$	$\theta_{r,im}$
n	-	**47.20**	0.13	**52.42**	28.84	0.25	**53.62**	**50.71**
$\theta_{s,mo}$		-	22.79	**87.81**	9.37	34.59	19.62	3.67
α			-	3.48	**95.97**	1.03	36.21	48.74
$\theta_{s,im}$				-	1.23	13.00	0.04	10.29
K_s					-	7.67	7.20	4.59
ω_w						-	25.52	0.14
$\theta_{r,mo}$							-	63.42
$\theta_{r,im}$								-

3.3. Optimization results

As noted earlier, daily cumulative bottom water and cumulative evaporation had very poor information content for parameter optimization. Therefore, the daily cumulative water outflow and cumulative evaporation were not used for the optimization procedure. However, Durner et al., 2008 suggested that the last value of cumulative bottom water and cumulative evaporation should be included in the objective function in order to ensure that the overall mass balance of the system was met.

In this section, we represent the optimization results for 3 scenarios that differ in the way which data were included in the objective function:

1. the 1st scenario, as a reference case, using the combination of daily pressure heads at 100 and 150 cm depths and daily water contents at 50 and 100 cm depths (called DPM-ref);

2. the 2nd scenario using the same data as in DPM-ref plus the last value of cumulative bottom water and cumulative evaporation (called DPM2);

3. the 3rd scenario using the same data as in DPM-ref plus 10 water retention values, $\theta(h)$, at 100 cm depth in which one value corresponds to the highest value of pressure head and one value corresponds to the lowest value of pressure head and 8 other values correspond to 8 first daily data, their weights were supposed to be 0.001 (called DPM3);

The optimized parameters, as well as their confidence intervals, obtained by the numerical inversion for 3 scenarios are summarized in table IV-7. The comparison of daily data and simulated values are showed in figure IV-2.

Table IV-7. Soil hydraulic parameters of dual-porosity model (DPM), with corresponding confidence intervals, estimated from daily data using HYDRUS-1D for different scenarios

	$\theta_{r,mo}$ -	$\theta_{s,mo}$ -	α cm^{-1}	n -	K_s $cm\ d^{-1}$	$\theta_{r,im}$ -	$\theta_{s,im}$ -	ω_w d^{-1}	R^2
DPM-ref	*	0.100 ± 0.012	0.319 ± 0.018	1.325 ± 0.010	100.5 ± 10.7	*	0.205 ± 0	*	0.89
DPM2	*	0.100 ± 0.012	0.157 ± 0.012	1.461 ± 0.022	20.16 ± 2.87	*	0.205 ± 0	*	0.88
DPM3	*	0.100 ± 0.008	0.383 ± 0.024	1.279 ± 0.008	240.1 ± 24.2	*	0.205 ± 0	*	0.89

* not included in the optimization procedure.

For the reference case (DPM-ref), parameter n was successfully estimated as show by the small confidence interval. The optimized K_s values, varied between 89.8 to 111.3 cm d^{-1}, sounded to be realistic and their confidence interval was relatively small. Again, the optimized α value of 0.319 cm^{-1} has shown a reliable estimate reflected by their small confidence interval. The optimized $\theta_{s,mo}$ value was 0.100 $cm^3\ cm^{-3}$ and their confidence interval was 0.012 $cm^3\ cm^{-3}$. However, this optimized value made us have feeling that in this case the estimation of parameter $\theta_{s,mo}$ was not so reliable because the value of 0.100 $cm^3\ cm^{-3}$ was also a minimal value applied in the optimization procedure and when we did not apply a minimal value the simulation did not always converge. Especially, the optimized $\theta_{s,im}$ value of 0.205 $cm^3\ cm^{-3}$ was exactly the initial value applied for this parameter; hence their confidence interval value of 0 $cm^3\ cm^{-3}$ was unrealistic. The difficulty in estimating parameters $\theta_{s,mo}$ and $\theta_{s,im}$ was explained by the fact that on the one hand these parameters were highly correlated (table IV-6, row 2) and on the other hand these parameters also had a strong correlation with the highest estimable parameter n. This means that parameters $\theta_{s,mo}$ and $\theta_{s,im}$ should not be optimized simultaneously. The similar result was reported in Kohne et al., 2004a when they estimates parameters $\theta_{s,mo}$, $\theta_{s,im}$ and others solute transport parameters from the column experiment.

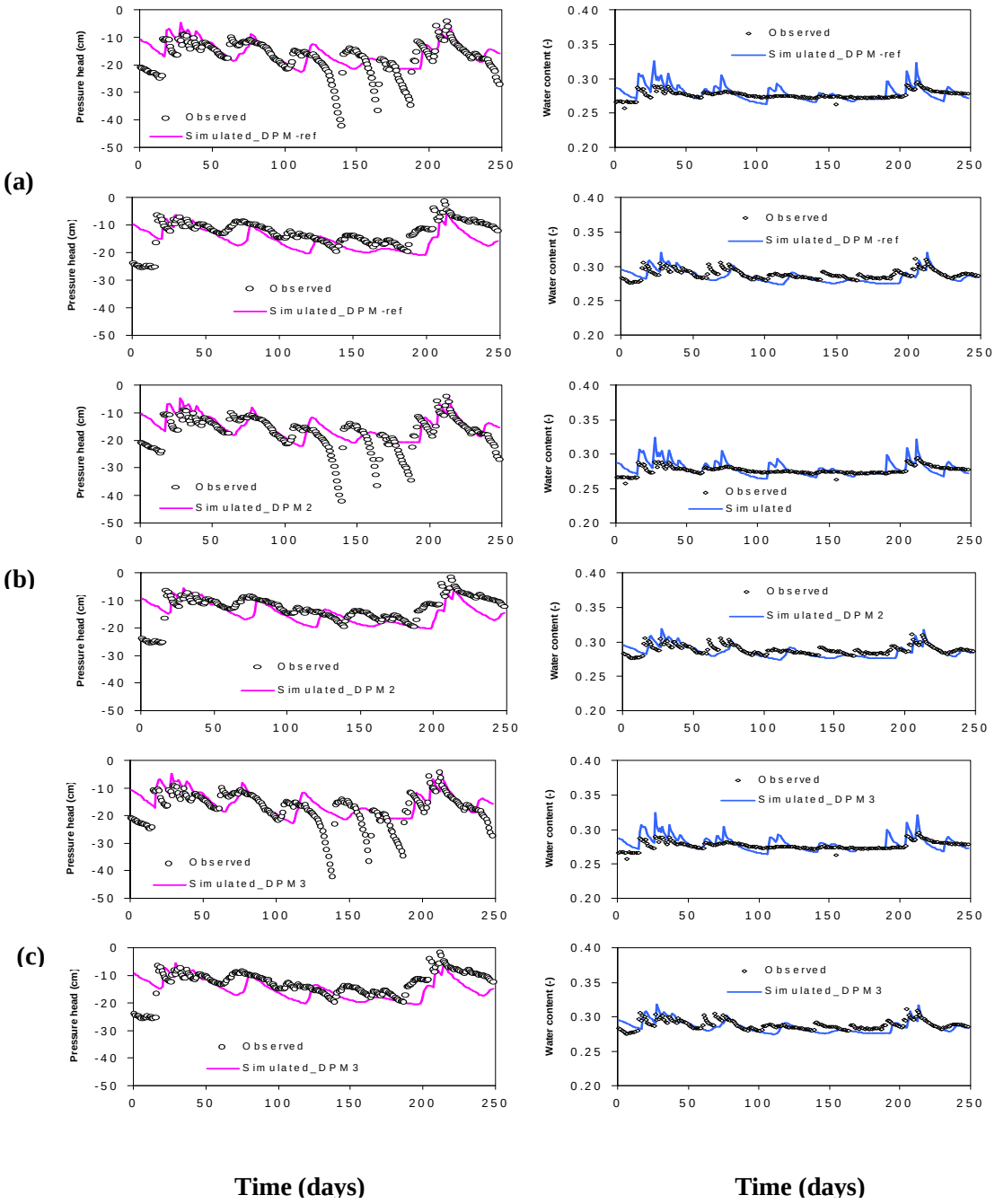

Figure IV-2. Comparison of the observed and simulated values for 3 scenarios: (a) scenario DPM-ref with the use of daily pressure heads and water content in the objective function, (b) scenario DPM2 using the data as in DPM-ref plus the last value of cumulative bottom water and cumulative evaporation, and (c) scenario DPM3 using the data as in DPM-ref plus 10 water retention values.

Table IV-8 presents the statistical analysis results for the observed and calculated pressure heads at 100 and 150 cm depths and the observed and calculated water contents at 50 and 100 cm depths, respectively. The similar fit was obtained for the pressure heads at 100 and 150 cm depths and water contents at 50 and 150 cm depths. That was indicated by the values of MAE, RMSE and MIA criteria. However, the RMSE values of 5.76 cm and 5.41 cm for pressure heads at 100 and 150 cm depths, respectively, are relatively larger than the pure measurement error of 0.5 cm. Visual analysis of figure 2 showed that there was a large difference between the observed and calculated pressure heads at two depths for 15 first days. That was believed by uncertainty pressure heads data because of the lysimeter instability in the starting period. Moreover, during the summer period (days from 125 to 190), model could not predict some pressure heads data at 100 cm depth that decreased suddenly, which may be rather due to data errors and uncertainty than due to an incorrect.

Table IV-8. Mean absolute error (MAE), Root mean square error (RMSE), Modified of index agreement (MIA) comparing observed data and simulated values shows in figure 2

	MAE			RMSE			MIA		
	DPM_ref	**DPM2**	**DPM3**	**DPM_ref**	**DPM2**	**DPM3**	**DPM_ref**	**DPM2**	**DPM3**
$\mathbf{h_{100}}$	4.26	4.34	4.24	5.76	5.88	5.78	0.48	0.48	0.49
$\mathbf{h_{150}}$	4.24	3.90	4.05	5.41	5.17	5.27	0.43	0.45	0.44
$\mathbf{\theta_{50}}$	0.007	0.007	0.007	0.009	0.009	0.009	0.46	0.47	0.47
$\mathbf{\theta_{100}}$	0.007	0.006	0.006	0.009	0.008	0.008	0.49	0.51	0.52

One again, similar agreement between the observed and simulated water contents at 50 and 100 cm depths was also obtained. The RMSE value of 0.009 cm^3 cm^{-3} for water contents at 50 and 100 cm depths was low and a bit smaller than the pure measurement error of 0.01 cm^3 cm^{-3}. It is clear that the RMSE values for pressure heads were much larger than the corresponding RMSE values for water contents; this is reflected by the fact that pressure heads that were measured in smaller soil volumes may be associated with larger uncertainties than water contents that were measured in larger soil volumes (Jacques et al., 2002).

To ensure the water balance of the system, we took into account the final values of cumulative bottom water and cumulative evaporation in the objective function (scenario 2, DPM2). The optimization results were comparable with those in the reference case, which was reflected by the similar results of statistical analysis (table IV-8). In this case, the problem concerning the optimized parameters $\theta_{s,mo}$, $\theta_{s,im}$ was exactly the same for the reference case. This means that taking the last values of cumulative bottom flux and evaporation into the objective function did not improve the optimization quality. Likewise, the optimized α and K_s values were about two times and five times smaller than those obtained in the reference case, respectively.

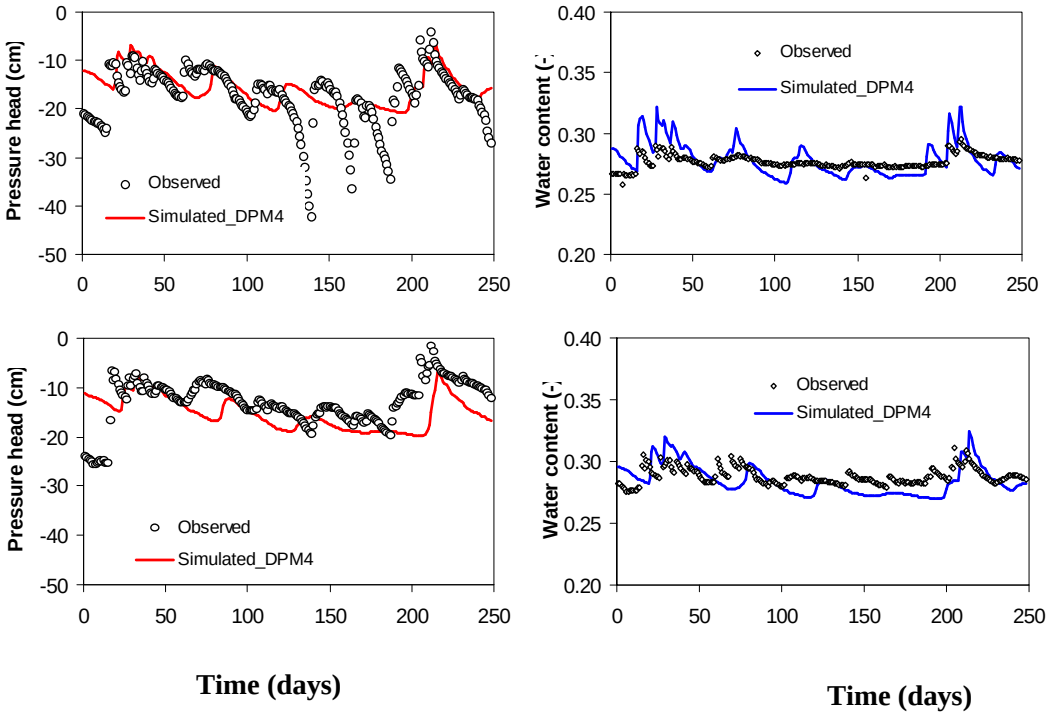

Figure IV-3. Comparison of the observed and simulated values when six parameters were estimated simultaneously (DPM4): (a) pressure heads at 100 cm depth, (b) pressure heads at 150 cm depth, (c) water contents at 50 cm depth and (d) water content at 100 cm depth.

For the third scenario, the optimized K_s value was found to be twice higher than the one obtained in the reference case. The other optimized parameter values were almost similarly compared with those obtained in the reference case. One again, the statistical analysis results remained similarly to the reference case (table IV-8). This means that in this case the additional information such as the initial values of hydraulic properties did not have much information content as expected for the parameter calibration. From the similar results obtained for the second and third scenarios, we could conclude that it was not necessary to account for cumulative outflow (cumulative bottom flux and evaporation) and initial values of hydraulic properties into the objective function. As a conclusion, the optimized K_s values in three scenarios showed distinct differences because this parameter is generally difficult to estimate from the numerical inversion due to spatial and temporal variability of soil in field scale (Ramos et al., 2006).

If the cut-off criterion for parameter estimability was 2.0, parameter ω_w became estimable. From the same data as the reference case (daily pressure heads and water contents were included together in the objective function), this time we tried to estimate six parameters ($\theta_{s,mo}$, α, n, K_s, $\theta_{s,im}$, ω_w) simultaneously (called DPM4). Tables IV-9 and IV-10 summarized the optimization results and statistical analysis results for this case, respectively. Figure IV- 3 compared experimental and simulated pressure heads and water contents. For this case, the similar statistical analysis results were found as compared with those obtained in the reference case. But when we concretely analysed the optimization results, we found that the optimization results showed more uncertainty. The optimized values of 0.377 cm^{-1} and 1.457 for

parameters α and n, respectively, were comparable with the results of the reference case. However, their confidence intervals were much larger. For example, for n the confidence intervals of 0.070 and 0.010 were found for this case and for the reference case, respectively. In addition, the optimized K_s became less reliable as demonstrated by their confidence interval (50% of the optimized value in this case as compared with about 10% of the optimized value in the reference case). Especially, the optimized ω_w value of 6.410^{-7} d^{-1} was not reliable at all as showed by their confidence interval varied from -4.210^{-6} to 5.410^{-6}. Accordingly, the optimized parameters $\theta_{s,mo}$ and $\theta_{s,im}$ were found to have the same values and the same problem as noted in the reference case, meaning that the optimized $\theta_{s,mo}$ was equal to its minimal value and that the optimized $\theta_{s,im}$ was equal to its initial value. This means that taking into account parameter ω_w in the optimization procedure made it more difficult to estimate other model parameters in this study case. There were not enough information to simultaneously estimate six parameters ω_w basing on only pressure heads and water contents. This was simply explained by the fact that parameter showed only low sensitivity degree for both daily pressure heads and water content in the soil lysimeter. Similarly, there was not enough information content from observations water flow alone to obtain the uniqueness of optimized parameters in dual-permeability model (Simunek et al., 2001; Kohne et al., 2006b).

In general, parameter ω_w is very important to characterize preferential flow. Basing on such experimental data, we tried another way to estimate parameter ω_w. As noted earlier, $\theta_{s,im}$ was strongly with more estimable parameters such as $\theta_{s,mo}$ and n (table IV-6, column 5). In addition, parameter K_s correlated with n very strongly with α. Moreover, according to Kohne et al. (2004a) we should not optimize $\theta_{s,mo}$ and $\theta_{s,im}$ simultaneously because of their strong correlation. Then we removed parameters $\theta_{s,im}$ and K_s from the optimization procedure and analysed how optimization results were improved. Four parameters n, $\theta_{s,mo}$, α, and ω_w were estimated simultaneously basing on the combination of daily pressure heads and water contents as the reference case (called DPM5).

Table IV-9. Soil hydraulic parameter in dual-porosity model (DPM), with corresponding confidence intervals, estimated from daily data using HYDRUS-1D for different scenarios

	$\theta_{s,mo}$ -	α cm^{-1}	n -	K_s cm d^{-1}	$\theta_{s,im}$ -	ω_w d^{-1}	R^2
DPM4	0.100 ± 0.004	0.377 ± 0.078	1.457 ± 0.070	185.97 ± 94.60	0.205 ± 0	**6.410^{-7}** (-4.210^{-6} - 5.410^{-6})	0.90
DPM5	**0.130 ± 0.002**	**0.086 ± 0.002**	**2.153 ± 0.072**	*	*	**1.810^{-3}** (**1.210^{-3} - 2.410^{-3}**)	0.93

* not included in the optimization procedure.

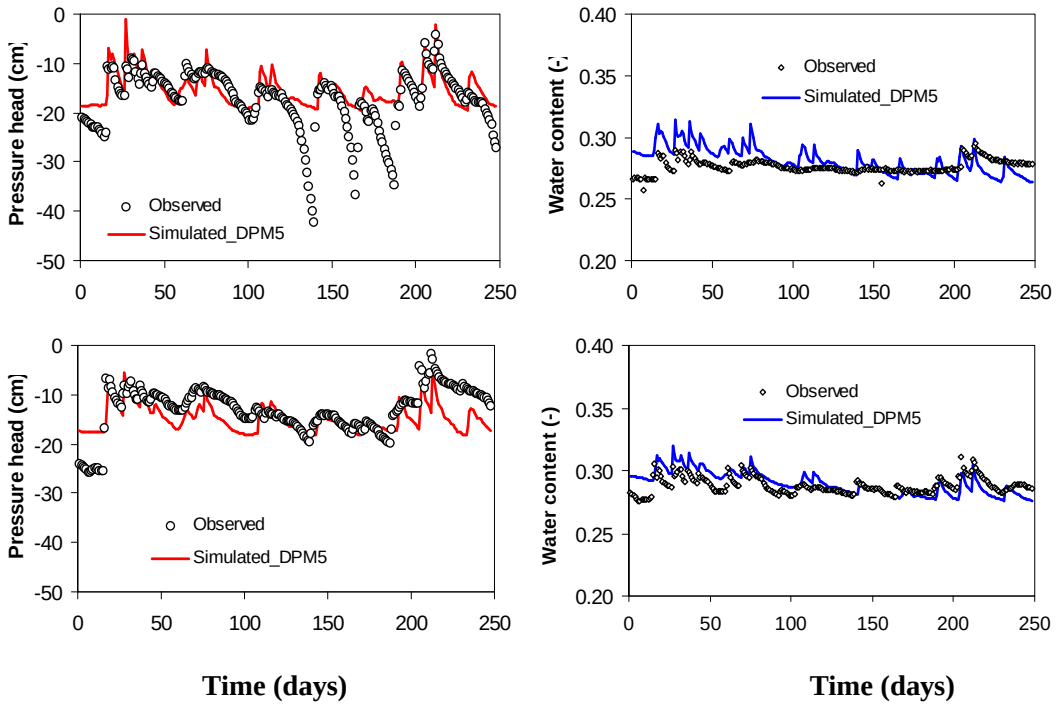

Figure IV-4. Comparison of observed data and simulated values when four parameters were estimated simultaneously (DPM5): (a) pressure heads at 100 cm depth, (b) pressure heads at 150 cm depth, (c) water contents at 50 cm depth and (d) water content at 100 cm depth.

Table IV-10. Mean absolute error (MAE), Root mean square error (RMSE), Modified of index agreement (MIA) comparing the observed data and the simulated values as showed in figures 3 and 4

	MAE		RMSE		MIA	
	DPM4	**DPM5**	**DPM4**	**DPM5**	**DPM4**	**DPM5**
$\mathbf{h_{100}}$	4.43	3.44	5.89	5.01	0.42	0.53
$\mathbf{h_{150}}$	4.04	3.19	5.42	4.16	0.42	0.51
$\mathbf{\theta_{50}}$	0.009	0.010	0.011	0.011	0.41	0.30
$\mathbf{\theta_{100}}$	0.010	0.007	0.012	0.008	0.38	0.46

Optimisation and statistical analysis results were given in tables IV-9 and IV-10. Figure IV-4 showed the comparison of the experimental data with the simulated pressure heads and water contents. The optimization results were found to be slightly better compared with those obtained in the reference case, which was indicated by the lower values of MAE and RMSE criteria and the higher value of MIA criteria. The optimized $\theta_{s,mo}$ of 0.130 cm^3 cm^{-3} was reliable as showed by very small confidence interval of 0.002 cm^3 cm^{-3}. In addition, the small confidence interval of 0.002 cm^{-1} also indicated reliable estimation of the optimized value of 0.086 cm^{-1} for parameter α. Even if the optimized value of 2.153 for parameter n was much higher than this obtained in the reference case, this optimized value was, however, realistic for the mobile region. Especially, ω_w was found to be successfully estimated, which

was indicated by their value within the range of water transfer reported by Haws et al. (2005) and their confidence interval, varied from $1.2 10^{-3}$ to $2.4 10^{-3}$ d^{-1}, seemed very logical. This means that removing model parameters that have strong correlations with other model parameters can improve the optimization results.

From the statistical analysis results, we could conclude that these optimization results were reliable and better than those obtained in various studies also used the TDR method and tensiometer measurements to estimate the hydraulic parameters. Jacques et al., 2002 found the RMSE values within the range of 0.038-0.125 cm^3 cm^{-3} for the measured and fitted water contents. In another study that carried out for the validation of an agro ecosystem model which also used TDR measurements, RMSE values failed in the range of 0.010-0.035 cm^3 cm^{-3} (Heidmann et al., 2000) and in the range of 0.03-0.130 cm^3 cm^{-3} (Wegehenkel, 2005). Recently, Durner et al. (2008) also used inverse method to estimate hydraulic parameters from TDR and tensiometer measurements at the lysimeter scale under natural atmospheric conditions, they found the RMSE values for the simulated and measured water contents ranged 0.009-0.20 cm^3 cm^{-3} and the one for simulated and measured pressure heads ranged 0.67-31.82 cm.

4. Conclusions

The effect of eight hydraulic parameters in dual-porosity model to daily pressure heads, water contents, cumulative bottom water and cumulative evaporation was evaluated via sensitivity analysis in term of sensitivity coefficient. The highest sensitivity degree to daily pressure heads was very high and corresponded to parameter n followed the sensibility order as follows: $\theta_{s,mo}$, $\theta_{s,im}$, α, K_s, $\theta_{r,mo}$, $\theta_{r,im}$, and ω_w. The sensitivity coefficient of eight parameters according to daily water contents decreased clearly. Especially, following daily cumulative bottom water and cumulative evaporation the sensitivity coefficient of each parameter decreased suddenly. As a result of it, the highest sensitivity degree to daily cumulative bottom water and cumulative evaporation remained only medium level and corresponded to parameter $\theta_{s,mo}$. This means that daily pressure heads were more sensitive than daily water contents, daily cumulative bottom water and daily cumulative evaporation.

The estimability analysis results showed that pressure heads contained the most information for the parameter calibration followed by daily water contents, if 2.4 was considered as a cut-off criterion for the parameter estimability. The set of estimable parameters in the dual-porosity model was five out of the eight parameters and three out of the eight parameters basing on only daily pressure heads or daily water contents, respectively. Unfortunately, daily cumulative bottom water and daily cumulative evaporation had very poor information content; as a result of it only parameter $\theta_{s,mo}$ was therefore estimable. Combination of daily pressure heads and water contents made increase parameter estimability. However, the set of estimable parameters still remained five out of eight parameters. Further analysis of influence of more estimable parameter(s) on the remaining model parameter(s) showed that there were very strong correlations between parameters $\theta_{s,mo}$ and $\theta_{s,im}$, and α and K_s. These strong correlations could make difficult to estimate five parameters simultaneously.

The optimization results indicated truly that parameters $\theta_{s,mo}$ and $\theta_{s,im}$ were impossible to estimate simultaneously. In addition, the optimized α and K_s also did not show a very reliable estimation. When a

cut-off criterion decreased and then parameter ω_w was included in the optimization procedure. This made the optimization results badly; meaning that the optimized values of parameters α and K_s were more uncertain as showed by their larger confidence intervals.

Fortunately, when parameters $\theta_{s,mo}$ and K_s were removed in the optimization procedure to remove the very strong correlations between parameters $\theta_{s,mo}$-$\theta_{s,im}$ and α- K_s; the opmization results were improved clearly. Parameters n, $\theta_{s,mo}$ and α were successfully estimated basing on daily pressure heads and water contents. Specially, the low sensitive parameter such as parameter ω_w also showed a reliable estimation.

Acknowledgments

The authors wish to thank the French Scientific Interest Group on Industrial Wastelands, as well as the French Ministry “de l’Enseignement Supérieur et de la Recherche” for his financial support. We thank Noële Raoult and Julien Michel for the collection of data.

Chapitre V : Simulation du transport de traceur (bromure) dans un lysimètre de terrain

Estimability analysis of single and dual-porosity model parameters based on lysimeter tracing

(Article soumis à Vadose Zone J.)

Van-Viet Ngo, Abderazzak Latifi, Julien Michel, Lise Lucas, Marie-Odile Simonnot[2]

Laboratoire des Sciences du Génie Chimique, CNRS-ENSIC

1, Rue Grandville, BP20451, 54001 Nancy Cedex, France

Abstract

Modeling preferential solute transport under transient flow conditions requires many input parameters. Most often, these parameters are not accurately known but estimated thanks to parameter estimation methods. To assess their validity, the effects of model parameters on output predictions should be accurately known. Sensitivity analysis is generally performed, but may not be sufficient. Another method is estimability analysis, applied in the field of chemical engineering. In this paper, the parameter effects of the single-porosity model (SPM) and the dual-porosity model (DPM) on a tracer breakthrough curve (BTC) were investigated. The case study was tracer transport through a soil lysimeter submitted to natural atmospheric conditions. Estimability analysis was based on a sequential calculation algorithm of a sensitivity coefficient matrix to account for possible correlations between parameters. For the SPM, hydraulic property shape factor and saturated water content were the most sensitive parameters; the molecular diffusion coefficient and the residual water content were not significant. Similar results were obtained with the DPM. The mass transfer coefficients, ω_s and ω_w were found to be sensitive to tracer BTC as well. The set of estimable parameters was 5 out of 7 SPM parameters and 7 out of 11 DPM parameters with a cut-off criterion of 0.2. The parameter ω_w was not estimable because of its correlation with the more estimable parameters. Comparison results showed the important role of ω_s and ω_w on the Br^- breakthrough curves. And when ω_s and ω_w are high, DPM predictions become very close to those of SPM.

1. Introduction

There is a growing interest for lysimeter use to study the fate and transport of pollutants in soils under transient flow conditions (*e.g.* Michel, 2009a). Lysimeters are believed to represent an intermediate scale that can bridge the gap between laboratory and field studies *(e.g.* Abdou and Flury, 2004; Kasteel et al., 2007; Michel, 2009a). Studying conservative tracer transport in these systems is often regarded as a prerequisite for understanding reactive solute displacement. Many authors showed

the important role of preferential flow path occurrence in soils by means of tracer studies *(e.g.* Schwartz, 1999; Johnson et al., 2003; Sander and Gerke, 2007; Mahmood-Ul-Hassan, 2008). Water flow and solute transport can be described by models of different degrees of complexity. The simplest one is the conventional uniform or single-porosity model (SPM), which does not allow the accurate description of the preferential flow. Nonequilibrium models include physical and chemical models, depending on the reason of nonequilibrium (Simunek et al., 2003; Gerke, 2006; Kohne et al., 2009b). The present contribution focuses on a physical non equilibrium model called the dual-porosity model (DPM). This model assumes that the water-filled pore space is partitioned into two regions: (i) a mobile region in which water is free to move and solute is moved by convection and dispersion and (ii) an immobile region in which water is stagnant and solute can move into and out by diffusion (van Genuchten and Wierenga, 1976). This model, as well as the dual-permeability one, has been implemented in numerical software like in HYDRUS (Simunek et al., 1998) and are increasingly used to simulate water flow and preferential solute transport through the vadose zone.

Modeling preferential flow and solute transport under transient flow conditions using dual-porosity or dual-permeability models requires many input parameters, some of them cannot be accurately measured (Kohne et al., 2 009a). For instance, Jaynes et al. (1995) proposed a method to measure in situ the fraction of immobile water and the solute rate transfer between the two regions. However, these parameters may vary in a wide range since they depend on various porous media characteristics such as flow velocity, soil hydraulic properties and length-scale (Maraqa, 2001). As a result, many studies showed a large variety of immobile water fractions and solute rate transfer *(e.g.* Jaynes et al., 1995; Vanderborght et al., 1997; Al-Jabri et al., 2002; Haws et al., 2005; Alletto et al., 2006). Solute mass transfer between mobile-immobile regions is considered as a major factor governing preferential solute transport *(e.g.* Fluhler et al., 1996; Kohne et al., 2006b).

Parameter identification methods have been widely used to calibrate unsaturated flow and transport parameters. Before calibrating model parameters, a sensitivity analysis is required to determine the most sensitive parameters for their better estimation (Lenhart et al., 2002). Furthermore, parameter identifiability may be increased by reducing the number of optimized parameters (Hopmans and Simunek, 1999a). But sensitivity analysis may not be sufficient since possible correlations between parameters may hamper calibration (Larsbo and Jarvis, 2006). Recently, Yao et al. (2003) have developed an estimability analysis technique to provide information about estimability of model parameters from various output predictions and to account for correlations between parameters. This estimability analysis method accommodates dynamic models and dynamic data, as well as response variables available at different sampling rates throughout each experimental run (Kou et al., 2005). This technique, successfully applied in the field of chemical engineering *(e.g.* (Kou et al., 2005; Jayasankar et al., 2009), was used in this work.

In this paper, our objective was to investigate parameter estimability for the modeling of inert tracer transport (bromide) through a soil lysimeter submitted to natural atmospheric conditions. We chose single-porosity and dual-porosity models, involving respectively 7 and 11 parameters; bromide breakthrough curves (BTCs) computed with HYDRUS-1D we re the model output. In a first step, the parameter effects of both models were quantified via sensitivity analysis. Estimability analysis was then performed. The models were finally compared in terms of temporal moments by changing two parameters controlling the preferential solute transport.

2. Materials and methods

2.1. System description

The system on which modeling was performed was a lysimeter, located in the experimental site of the French Scientific Interest Group on Industrial Wastelands called GISFI (www.gisfi. fr), in the North East of France (49°14' N, 5°59' E) . This lysimeter vessel was a stainless steel column (1 m^2 x 2 m deep), filled with 3 tons of a contaminated soil sampled from a former coking plant (Benhabib et al., 2009) with a 15 cm sand inferior layer. A sand layer was required to avoid soil particle entrapment in the pipes and system blockage. The mean apparent soil bulk density was 1,670 kg m^{-3}. The lysimeter was submitted to natural atmospheric conditions, its surface was bare soil and drainage water was collected at the vessel bottom. Further details about sensors were given by Michel (Michel, 2009a). Weather data were monitored by a weather station.

A tracing experiment was run by applying 5 L of a 1 M KBr solution at the lysimeter surface in March 2009. Preliminary calculations showed that about 3.5 years were needed to obtain a complete BTC. For the present work, we used weather data taken from June 2006 to October 2008.

2.2. Model description

The equations of the models used in this work are described in the following section.

2.2.1. Single-porosity model

The SPM is based on the Richards equation for variably saturated water flow:

$$\frac{\partial \theta}{\partial t} = \frac{\partial}{\partial z}\left(K(h)\left(\frac{\partial h}{\partial z} + 1\right)\right) - S \qquad [1]$$

where θ is the water content [L^3 L^{-3}], h is the pressure head [L], t is the time [T], z is the vertical coordinate [L], K(h) is the hydraulic conductivity function, S is a sink term [T^{-1}].

Tracer transport is described by the convection-dispersion equation:

$$\frac{\partial \theta C}{\partial t} = \frac{\partial}{\partial z}\left(\theta D \frac{\partial C}{\partial z}\right) - \frac{\partial qC}{\partial z} - S \qquad [2]$$

where C is the solute concentration in the liquid phase [M L^{-3}], D is the dispersion coefficient [L^2 T^{-1}], q is the volumetric fluid flux density [L T^{-1}].

The knowledge of unsaturated soil hydraulic functions is required to solve Eq. [1]. These functions are made up of the soil water retention curve θ(h) and the non saturated hydraulic function K(h) which defines the hydraulic conductivity as a function of θ and h. The analytical model proposed by van Genuchten (van Genuchten, 1980b) for θ(h) and K(h) was used here (Eq. [3] to [6]).

$$S_e(h) = \frac{\theta(h) - \theta_r}{\theta_s - \theta_r} = \frac{1}{\left(1 + \alpha h^n\right)^m} \qquad h < 0 \qquad [3]$$

$$S_e = 1 \qquad h \geq 0 \qquad [4]$$

$$m = 1 - 1/n \qquad n > 1 \qquad [5]$$

$$K(S_e) = K_S S_e^{0.5}\left[1 - \left(1 - S_e^{1/m}\right)\right]^2 \qquad [6]$$

where S_e is the effective water content [-], θ_r the residual water content [-], θ_s the saturated water content [-], α, n and m are empirical parameters.

2.2.2. Dual-porosity model

The DPM concept assumes that water-filled pore space is partitioned into two regions: a mobile one, θ_{mo} (interaggregate pores and macropores) and an immobile one, θ_{im} (intraaggregate pores or the rock matrix) (van Genuchten and Wierenga, 1976; Simunek et al., 2003; Simunek and van Genuchten, 2008) as:

$$\theta = \theta_{mo} + \theta_{im} \qquad [7]$$

The formulation of dual-porosity water flow can be described by the Richards equation in the mobile region combined with a source/sink term, Γ_w, to account for water exchange with the immobile region *(e.g.*(Simunek et al., 2003):

$$\frac{\partial \theta_{mo}(h_{mo})}{\partial t} = \frac{\partial}{\partial z}\left(K(h_{mo})\frac{\partial h_{mo}}{\partial z} + K(h_{mo})\right) - \Gamma_w \qquad [8]$$

$$\frac{\partial \theta_{im}(h_{im})}{\partial t} = \Gamma_w \qquad [9]$$

where h_{mo} is the pressure head in the mobile region [L], t is the time [T], z is the vertical coordinate [L], K is the hydraulic conductivity [L T^{-1}], Γ_w is the water transfer rate between mobile and immobile regions [T^{-1}].

Two approaches can describe the water transfer rate between the two regions: the first one is based on the difference between their effective water contents using the first-order rate equation (Simunek et al., 2001), the second one is based on the difference between their pressure heads (Gerke and van Genuchten, 1993). The advantages and drawbacks of these approaches were discussed in details (Simunek et al., 2003). In this work, the first approach was used since it needs fewer parameters (Simunek et al., 2003). It is expressed as

$$\Gamma_w = \omega_w\left(S_{e,mo} - S_{e,im}\right) \qquad [10]$$

where ω_W is the first-order water transfer rate coefficient [T^{-1}], $S_{e,mo}$ et $S_{e,im}$ are the effective soil water contents in the mobile and immobile regions, respectively.

The formulation of dual-porosity solute transport model is based on the convection-dispersion equation combined with a term describing the solute transfer between two regions:

$$\frac{\partial \theta_{mo} C_{mo}}{\partial t} = \frac{\partial}{\partial z}\left(\theta_{mo} D_{mo}\frac{\partial C_{mo}}{\partial z}\right) - \frac{\partial q_{mo} C_{mo}}{\partial z} - \Gamma_s \qquad [11]$$

$$\frac{\partial \theta_{im} C_{im}}{\partial t} = \Gamma_s \qquad [12]$$

where C_{mo} and C_{im} are the solute concentrations of mobile and immobile regions [M L^{-3}], respectively; D_{mo} is the dispersion coefficient in the mobile region [L^2 T^{-1}]; q_{mo} is the volumetric fluid flux density in the mobile region [L T^{-1}].

The dispersion coefficient in the mobile region is given in Eq.[13] (Kohne et al., 2006a):

$$\theta_{mo} D_{mo} = \theta_{mo} D_o \frac{\theta_{mo}^{7/3}}{\theta_{s,mo}^2} + \lambda_{mo} |q_{mo}| \qquad [13]$$

where D_o is the molecular diffusion of the solute [L^2 T^{-1}], λ_{mo} is the dispersivity in the mobile region [L]; $\theta_{s,mo}$ is the saturated water content in the mobile region.

Solute transfer rate between two regions is described by Eq. [14] (Simunek and van Genuchten, 2008):

$$\Gamma_s = \omega_s (C_{mo} - C_{im}) + \Gamma_w C^* \qquad [14]$$

where ω_s is the first-order rate solute transfer coefficient [T^{-1}] and C^* is equal to C_{mo} for $\Gamma_w > 0$ and C_{im} for $\Gamma_w < 0$.

2.2.3. Initial condition and boundary conditions

The initial condition for water was:

$$\theta(z,t) = \theta(z) \text{ at t=0} \qquad [15]$$

The upper flow boundary condition was specified as the « atmospheric boundary condition with surface run off » with precipitation as the input flux and evaporation from the lysimeter surface as the output flux. The equation of upper boundary condition is given as follows:

$$-K\left(\frac{\partial \theta}{\partial z} - 1\right) = q_T(t) \quad \text{at z = 0} \qquad [16]$$

where q_T is the net infiltration rate [L T^{-1}], meaning that the difference between the input and output fluxes.

The lower boundary condition in the lysimeter was specified as a seepage face, usually used for experiments at the lysimeter scale (Sonnleitner et al., 2003; Abdou and Flury, 2004; Kasteel et al., 2007):

$$-K\left(\frac{\partial \theta}{\partial z} - 1\right) = q_B(t) \quad \text{at z = L} \qquad [17]$$

where q_B is the drainage rate [L T^{-1}].

Concerning solute transport, the initial Br^- concentration was assumed to be equal to zero since Br^- is not a soil natural component (Kohne and Gerke, 2005) and a bromide solution was applied as a flux-type boundary condition for a one day period to the soil surface of the lysimeter.

$$C(z,t) = 0 \quad \text{at t = 0} \qquad [18]$$

The upper boundary condition is given as:

$$-\theta D\frac{\partial C}{\partial z} + qC = \begin{cases} q_T C_0(t) & 0 < t \le 1\ d \\ 0 & t > 1\ d \end{cases} \quad \text{at z = 0} \qquad [19]$$

And the lower boundary condition is expressed as:

$$-\theta D\frac{\partial C}{\partial z} = 0 \quad \text{at z = L} \qquad [20]$$

2.3. Data used

The data used in this work are presented in table V-1. Water retention parameters and hydraulic conductivity parameters were estimated by Rosetta software (Schaap et al., 2001) that has been used in different studies *(e.g.* Hermsmeyer et al., 2002; Sander and Gerke, 2009). Rosetta software input parameters were the grain size composition and the bulk density of the sand and soil layers.

The molecular diffusion coefficient was set to 1.72 cm^2 d^{-1} according to previously published data *(e.g.* Kohne et al., 2006a; Gerke and Kohne, 2004) and dispersivity to 20 cm (Schoen et al., 1999; Ventrella et al., 2000). The immobile water fraction may vary in a wide range, *e.g.*, for three soil profiles measured under natural conditions, this fraction was between 0.213 and 0.822 (Alletto et al., 2006). Based on this range of values, we assumed that $\theta_{r,mo} = \theta_{r,im} = 0.5\theta_r$ and $\theta_{s,mo} = \theta_{s,im} = 0.5\theta_s$.

A very wide range was found as well for the first-order rate solute transfer coefficient ω_s and the first-order rate water transfer coefficient ω_w. For example, ω_s varied for top and subsoil layers within the range of 0.001 to 1 d^{-1} (Jaynes et al., 1995; Kohne et al., 2006b). In this work, the initial values of these parameters were set equal to 0.1 d^{-1}.

2.4. Sensitivity analysis

A sensitivity analysis is necessary before parameter estimation. Our objective was to determine whether parameter estimation made sense. As a matter of fact, if the variation of a parameter has a very small effect on the result, the estimation of this parameter has little sense. This analysis was applied to the parameters corresponding to the contaminated soil layer, since preliminary calculations had shown that hydraulic parameters corresponding to the sand layer were not sensitive to Br^- breakthrough (not presented here). Many different methods to investigate sensitivity analysis of model parameters have been found in literature (Hamby, 1994). In the present contribution, two approaches were selected,

differing in the way the evaluation of the response variation was defined while a 10 % change was applied to the initial value of one model parameter and the others were fixed.

The first approach (approach #1) was based on Br^- concentration variation (%) in the leaching solution, called *vpc* (Eq. [21]):

$$vpc = 100\frac{\Delta C}{\Delta p} \qquad [21]$$

Table V-1. Definition and initial values of the SPM and DPM parameters.

Model	Parameter	Unit	Parameter description	Value
SPM	θ_r	$cm^3\ cm^{-3}$	Residual water content	0.046
	θ_s	$cm^3\ cm^{-3}$	Saturated water content	0.41
	α	cm^{-1}	Shape factor of the soil water retention curve	0.03
	n	-	Hydraulic property shape factor	1.49
	K_s	$cm\ d^{-1}$	Saturated hydraulic conductivity	2.89
	λ	cm	Dispersivity	20
	D_o	$cm^2\ d^{-1}$	Molecular diffusion coefficient	1.72
DPM	$\theta_{r,mo}$	$cm^3\ cm^{-3}$	Residual water content in the mobile region	0.023
	$\theta_{s,mo}$	$cm^3\ cm^{-3}$	Saturated water content in the mobile region	0.205
	α	cm^{-1}	Shape factor in the soil water retention curve in the mobile region	0.03
	n	-	Hydraulic property shape factor in the mobile region	1.49
	K_s	$cm\ d^{-1}$	Saturated hydraulic conductivity in the mobile region	2.89
	$\theta_{r,im}$	$cm^3\ cm^{-3}$	Residual water content in the immobile region	0.023
	$\theta_{s,im}$	$cm^3\ cm^{-3}$	Saturated water content in the immobile region	0.205
	ω_w	d^{-1}	First-order rate water transfer coefficient	0.1
	ω_s	d^{-1}	First-order rate solute transfer coefficient	0.1
	λ	cm	Dispersivity	20
	D_o	$cm^2\ d^{-1}$	Molecular diffusion	1.72

The second approach (approach #2) was based on the sensitivity coefficient I_{norm} which quantified how model predictions were affected by changes in parameters values (Hamby, 1994); (Lenhart et al., 2002). The coefficient I_{norm} was obtained from the approximation by a finite difference of a partial derivative describing Br^- concentration dependence as a function of parameters p (Eq. [22]). The initial parameter value p_0 was changed by ± Δp (in this work Δp = 10 %). The response to $p_0 + \Delta p$ was called C^+ and the response to $p_0 - \Delta p$ was C^-. The sensitivity function of C with respect to p was given by:

$$I = \frac{\partial C}{\partial p} \approx \frac{C^+ - C^-}{2\Delta p} \qquad [22]$$

This function was normalized to get a dimensionless sensitivity coefficient by removing the effects of units (Hamby, 1994), as:

$$I_{norm} = \frac{p}{C}\left(\frac{C^{+} - C^{-}}{2\Delta p}\right) \qquad [23]$$

Table V-2. Sensitivity classes based on vpc and on I_{norm}.

Method	Classes	Limits	Sensitivity
Based on vpc	1	|vpc| < 2	Low or negligible
	2	2 ≤ |vpc| <10	Medium
	3	10 ≤ |vpc| < 20	High
	4	20 < |vpc|	Very high
Based on I_{norm}	1	0.00 ≤ $\|I_{norm}\|$ <0.05	Low or negligible
	2	0.05 ≤ $\|I_{norm}\|$ <0.20	Medium
	3	0.20 ≤ $\|I_{norm}\|$ <1.00	High
	4	1.00 ≤ $\|I_{norm}\|$	Very high

Sensitivity coefficients were grouped into 4 classes (Lenhart et al., 2002) (table V-2). It is important to note that for significant model parameters; only the absolute values of *vpc* and I_{norm} were used to discuss the results.

2.5. Estimability analysis

Sensitivity analysis is necessary but not sufficient since parameter correlation may hamper parameter estimability (Larsbo and Jarvis, 2006) and have an effect on the non uniqueness of optimized parameters. Therefore, it is important to investigate estimability analysis which is a measure of whether a given data set contains enough information to estimate parameters from it (Jayasankar et al., 2009). Estimability is defined as the ability to compute parameters accurately from a given data set and experimental conditions (Yao et al., 2003; Jayasankar et al., 2009).

Parameter estimability depends not only on model structure and parameter sensitivity but also on correlations between different parameters. Estimability was evaluated and a subset of estimable parameters of the two models was established following the method proposed by Yao et al. (2003) which allows to quantify the effect of each model parameter on model predictions and to account for the correlations between the effects of different parameters. This method was successfully applied in chemical engineering *(e.g.* Kou et al., 2005; Jayasankar et al., 2009). The estimability analysis method of Yao et al. (2003) compiled dynamic models and dynamic data, as well as response variables available at different sampling rates throughout each experimental run (Kou et al., 2005).

A sensitivity coefficient matrix Z was built, from the individual coefficient as follows:

$$Z = \begin{bmatrix} \left.\frac{p_1}{C}\frac{\partial C}{\partial p_1}\right|_{t=t_1} & \cdots & \left.\frac{p_m}{C}\frac{\partial C}{\partial p_m}\right|_{t=t_1} \\ \left.\frac{p_1}{C}\frac{\partial C}{\partial p_1}\right|_{t=t_2} & \cdots & \left.\frac{p_m}{C}\frac{\partial C}{\partial p_m}\right|_{t=t_2} \\ \cdots\cdots\cdots\cdots\cdots & & \\ \left.\frac{p_1}{C}\frac{\partial C}{\partial p_1}\right|_{t=t_n} & \cdots & \left.\frac{p_m}{C}\frac{\partial C}{\partial p_m}\right|_{t=t_n} \end{bmatrix} \quad [24]$$

The number of columns was equal to the number of model parameters *(e.g.* 7 for the SPM and 11 for the DPM) and each row corresponded to Br^- concentration at a given sampling time. The Z matrix elements were calculated by means of centered finite differences method. The subset of estimable parameters was identified following 8 steps (Yao et al., 2003):

1. The magnitude of each column was calculated. It was defined as the quadratic sum of the elements.
2. The parameter whose column in Z had the highest magnitude was selected as the first parameter. This parameter was considered to have the highest effects on Br^- breakthrough in the soil lysimeter.
3. The corresponding column was marked as X_L (L = 1 for the first iteration).
4. Z_L, prediction of the full sensitivity matrix Z, was calculated using the subset of columns X_L as:
$$Z_L = X_L \left({X_L}^T X_L \right)^{-1} {X_L}^T Z \quad [25]$$
5. The residual matrix R_L was built as:
$$R_L = Z - Z_L \quad [26]$$
6. The quadratic sum of the residuals was calculated in each column of R_L. The column with the highest magnitude corresponded to the next estimable parameter (among the remaining ones) having the largest effects on Br^- breakthrough and not correlated with the effects of the already selected parameters.
7. The corresponding column in Z was selected and included into X_L. The new matrix was called X_{L+1}.
8. The iteration counter was incremented and steps 4 to 7 were repeated until the last parameter was treated.

The algorithm began by choosing the most estimable parameter p_1 (steps 1, 2). But p_1 may be correlated with the other ones. Orthogonalization was required to rank individual parameter influences on Br^- breakthrough: the influence of p_1 on the other parameters had to be adjusted for any possible correlation between the column of p_1 in Z and the other ones, so that the "net influence" of each of the remaining parameters could be assessed. This adjustment was done by regressing all of the original columns of the Z matrix on the column associated with p_1. This regression resulted in a matrix of the same dimensions as Z, and the column of this residual matrix associated with p_1 was a column of zeros (steps 3- 5). Orthogonalization was followed by identifying the largest column in the residual matrix in order to find the parameter p_2 having the second strongest "net influence" on Br^- breakthrough, after the

influence of p_1 had been delimited (steps 6, 7). Orthogonalization was carried on until the last model parameter was treated.

Yao et al. (2003) used 0.04 as a cut-off criterion for considering whether a model parameter was estimable or not. They considered thus that information was sufficient to estimate a parameter if a 10 % change in its value implied a 2 % change in output. Despite the arbitrary character of the choice of a cut-off criterion, we followed their method and obtained 0.2 as a cut-off threshold in the present work.

2.6. Temporal moments of the residence time distribution

BTCs were analyzed by means of the residence time distribution (RTD) approach. This method, conventionally used in chemical engineering had been often applied to analyze tracer BTCs *(e.g.* Sardin et al., 1991a; Villermaux, 1993). The residence time of a molecule is the time this molecule has spent in the system. The residence time distribution or RTD is determined experimentally by injecting a tracer into the system and measuring the evolution of its concentration at the system outlet. The response to pulse input is represented by the RTD function E(t):

$$E(t) = \frac{C(t)}{\int_0^\infty C(t)dt} \qquad [27]$$

where C(t) is the tracer concentration at the system outlet (mol L^{-1}) at time t (s).
The normalized moments μ_n of the distribution are given by:

$$\mu_n = \int_0^\infty t^n E(t)dt \qquad [28]$$

The central normalized moments μ_n' are defined as:

$$\mu_n' = \int_0^\infty (t-\mu_1)^n E(t)dt \qquad [29]$$

The first-order normalized moment μ_1 is the mean residence time of the tracer. The second-order normalized moment gives the RTD variance.

3. Results and discussion

3.1. Sensitivity analysis

The results of the sensitivity analysis of the 7 SPM parameters obtained with both approaches are given in table V-3. Following approach #1, Br^- concentrations were most sensitive to saturated water content, $\theta_{s,}$ followed by the shape factor, n. The sensitivity to θ_s was consistent with previous results about tracer transport (Boateng and Cawlfield, 1999). The sensitivities of saturated hydraulic conductivity, K_s, dispersivity, λ, and shape factor α were medium to low. The sensitivities of the residual water content θ_r and the molecular diffusion coefficient D_o were negligible. These results were consistent with those of Piggott and Cawfield, who found that D_o was insignificant for the nonreactive and reactive contaminant transport through the soil column (Piggott and Cawlfield, 1996).

Following approach #2, the parameter sensitivity classification for the SPM was: n, θ_s, K_s, λ, α. D_o and θ_r were not sensitive. The sensitivity of Br^- BTCs to the four most sensitive parameters following approach #2 (n, θ_s, K_s, λ) in the SPM was represented in figure V-1. Given that λ was found to vary in a wide range in the literature *(e.g.* (Vanderborght and Vereecken, 2007), it was changed 50 % to better show the effect of this parameter on the Br^- BTCs. Figure V-1 showed that the Br^- breakthroughs and the maximum concentrations were almost the same when parameters n and K_s varied 10 %. However, the maximum concentrations were slightly different when parameters θ_s, λ varied 10 % and 50 %, respectively.

Table V-3. Results of the SPM and DPM parameter sensitivity analysis.

Model		Approach #1		Approach #2	
		|vpc|	Sensitivity	$\|I_{norm}\|$	Sensitivity
SPM	θ_r ($cm^3\ cm^{-3}$)	0.17	Negligible	0.02	Negligible
	θ_s ($cm^3\ cm^{-3}$)	26.22	Very high	2.76	Very high
	α (cm^{-1})	1.86	Low	0.21	High
	n (-)	15.31	High	4.11	Very high
	K_s ($cm\ d^{-1}$)	5.80	Medium	0.70	High
	λ (cm)	3.07	Medium	0.36	High
	D_o ($cm^2\ d^{-1}$)	0.26	Negligible	0.03	Negligible
DPM	$\theta_{r,mo}$ ($cm^3\ cm^{-3}$)	1.32	Negligible	0.08	Medium
	$\theta_{s,mo}$ ($cm^3\ cm^{-3}$)	14.91	High	1.48	Very high
	α (cm^{-1})	2.38	Medium	0.29	Medium
	n (-)	13.93	High	1.58	Very high
	K_s ($cm\ d^{-1}$)	5.24	Medium	0.71	High
	$\theta_{r,im}$ ($cm^3\ cm^{-3}$)	0.34	Negligible	0.02	Negligible
	$\theta_{s,im}$ ($cm^3\ cm^{-3}$)	14.84	High	1.49	Very high
	ω_w (d^{-1})	1.99	Low	0.17	Medium
	ω_s (d^{-1})	2.20	Medium	0.23	High
	λ (cm)	3.16	Medium	0.38	High
	D_o ($cm^2\ d^{-1}$)	0.03	Negligible	0.003	Negligible

The sensitivity analysis results for the 11 DPM parameters are also presented in table V-3. According to approach #1, a high sensitivity was found for saturated water content in both mobile and immobile regions, $\theta_{s,mo}$ and $\theta_{s,im}$, as well as for the shape factor n. The sensitivities of the saturated hydraulic conductivity, K_s, the dispersivity, λ, the shape factor, α, and the first-order rate solute transfer coefficient ω_s were medium. The first-order rate water transfer coefficient ω_w was less significant. Once again, the sensitivity of the residual water contents $\theta_{r,mo}$, $\theta_{r,im}$ and of the molecular diffusion coefficient D_o were negligible.

The sensitivity analysis results using approach #2 showed that the most sensitive parameters for the dual-porosity model were n, $\theta_{s,mo}$, $\theta_{s,im}$, the sensitivities of ω_s, ω_w were also high and medium, respectively as the sensitivity of D_o was negligible. The sensitivity of Br^- BTCs to the four sensitive parameters ($\theta_{s,mo}$, $\theta_{s,im}$, λ, ω_s) in the dual-porosity model was represented in figure V-2. Figure V-2 showed that the simulated maximum concentrations were different when parameters λ and for ω_s varied 50 %.

Altogether, sensitivity analysis results given by the two approaches did not show a significant difference. There was little difference in parameter sensitivity classification, but this was mostly due to the differences of the class boundaries.

These sensitivity analysis approaches are just local approach, the sensitivity degree of model parameters may depend on the temporal and spatial variability. In addition, the sensitivity of model parameters may also depend on its initial parameter values. However, some authors concluded that their sensitivity analysis results just showed a little difference when they applied different initial values for the parameters in the hydrological model (Lenhart et al., 2002). Therefore, the influences of initial parameter value on sensitivity analysis were not investigated in this work.

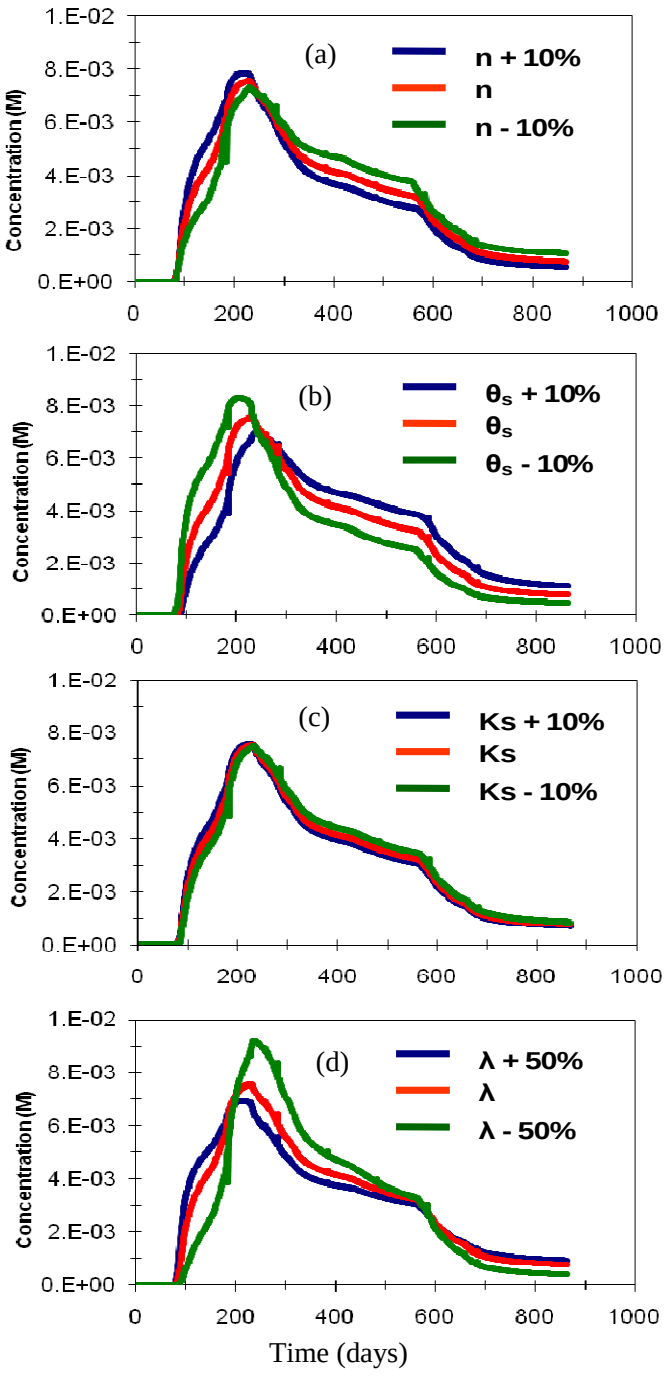

Figure V-1. Sensitivity of Br^- BTCs to (a) the hydraulic property shape factor n, (b) the saturated water content θ_s, (c) the saturated hydraulic conductivity Ks and (d) the dispersivity λ for the SPM.

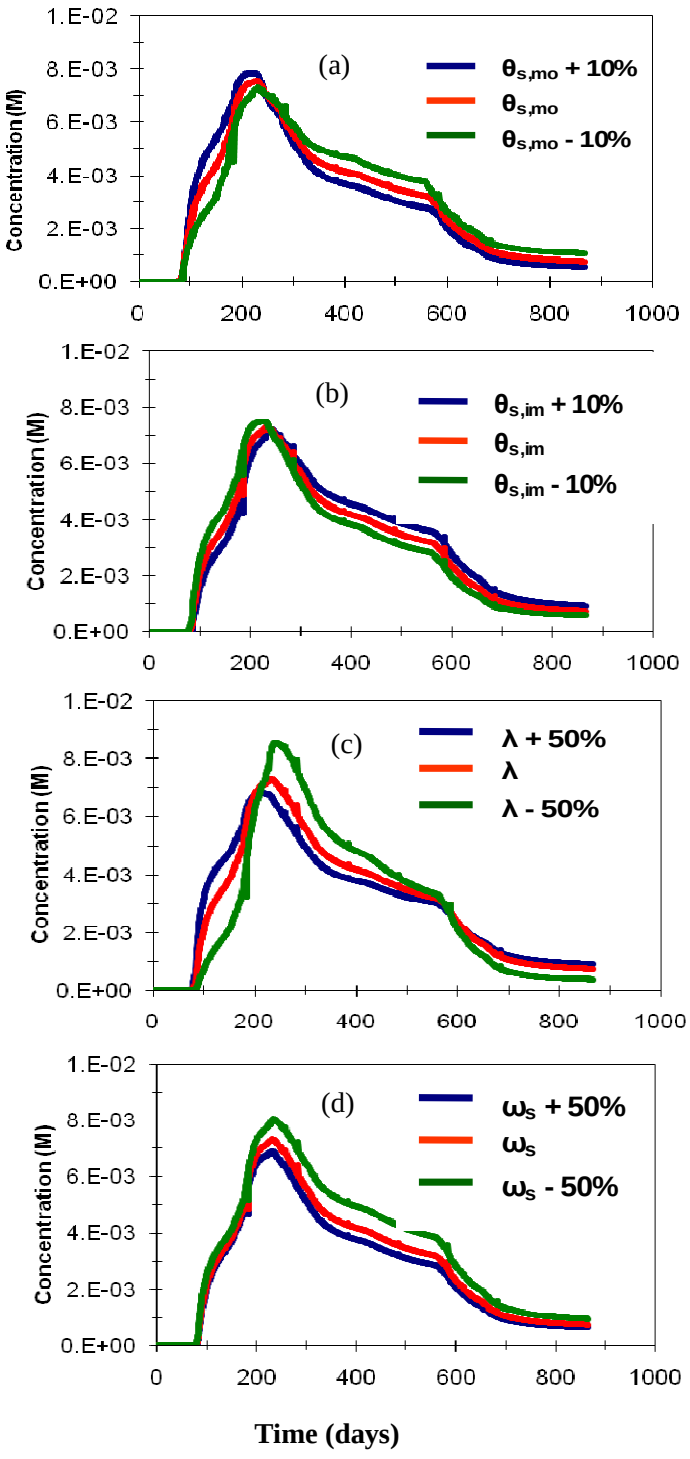

Figure V-2. Sensitivity of Br^- BTCs to (a) the saturated water content in the mobile region $\theta_{s,mo}$, (b) the saturated water content in the immobile region $\theta_{s,im}$, (c) the dispersivity λ and (d) the first-order rate solute transfer coefficient ω_s for the DPM.

3.2. Parameter estimability

The estimability results of SPM and DPM parameters are given in tables V-4 and V-5, respectively. In these tables, estimability decreased from the left to the right. The first rows represent the magnitude of each column in Z matrix corresponding to each parameter before adjusting the correlations between different parameters. The following rows give the magnitude of each column in Z matrix after eliminating the influence of more estimable parameter(s) on the remaining parameter(s).

Thus, with a cut-off criterion of 0.2, the set of estimable parameters was 5 out of the 7 SPM parameters and 7 out of the 11 DPM parameters. As expected, n was the most estimable one since it was the most sensitive parameter for both models. The parameter estimability classification differed from the parameter sensitivity classification: the order of estimability of SPM parameters was n, θ_s, λ, K_s, α whereas the sensitivity order was n, θ_s, K_s, λ, α according to approach #2. The estimability order of DPM parameters was n, λ, $\theta_{s,im}$, ω_s, K_s, $\theta_{s,\,mo}$, α while the order of sensitivity was n, $\theta_{s,im}$, $\theta_{s,mo}$, K_s, λ, α, ω_s. Sensitivity was higher for K_s than for λ according to both sensitivity analysis approaches; but estimability was lower for K_s than for λ because the influence of two more estimable parameters (n and θ_s) was much higher on K_s than on λ. Thus, estimability analysis provided more information for parameter identification than sensitivity analysis, since it accounted for correlations between parameters (Yao et al., 2003). However, it should be noted that this estimability analysis method is a local approach, the estimability order of model parameters may also depend on temporal and spatial variability.

Table V-4. Estimability order of the 7 SPM parameters based on Br^- BTCs

n	θ_s	λ	K_s	α	θ_r	D_o
(-)	($cm^3\ cm^{-3}$)	(cm)	($cm\ d^{-1}$)	(cm^{-1})	($cm^3\ cm^{-3}$)	($cm^2\ d^{-1}$)
14602.56	6634.73	115.18	430.01	38.06	0.34	0.62
0	1799.69	85.69	149.51	7.29	0.20	0.57
0	0	53.73	9.04	2.01	0.19	0.35
0	0	0	2.86	1.68	0.15	0.06
0	0	0	0	0.95	0.15	0.05
0	0	0	0	0	0.13	0.04
0	0	0	0	0	0	0.03

The results presented in table V-4 showed that SPM parameters θ_r, D_o may not be estimated only from Br^- BTC, because they had a too small influence on this curve. Their effects were highly correlated with the effects of other parameters. Thus, further experiments would be required to estimate therm.

Table V-5. Estimability order of the DPM 11 parameters based on Br- BTCs †

n	λ	$\theta_{s,im}$	ω_s	K_s	$\theta_{s,mo}$	α	ω_w	$\theta_{r,mo}$	$\theta_{r,im}$	D_o
2154.60	125.19	1935.37	48.23	433.36	1900.36	72.35	25.64	5.44	0.56	0.01
0	118.53	61.53	15.29	27.65	57.63	3.77	10.11	2.83	0.05	0.0099
0	0	59.11	14.08	10.55	56.48	3.42	9.26	2.64	0.05	0.0013
0	0	0	14.08	0.94	2.25	3.40	9.26	2.53	0.02	0.0010
0	0	0	0	0.89	0.45	0.35	0.05	0.02	0.02	0.0007
0	0	0	0	0	0.45	0.29	0.05	0.02	0.01	0.0007
0	0	0	0	0	0	0.20	0.02	0.02	0.0099	0.0006
0	0	0	0	0	0	0	0.02	0.02	0.0097	0.0003
0	0	0	0	0	0	0	0	0.01	0.0084	0.0003
0	0	0	0	0	0	0	0	0	0.0084	0.0003
0	0	0	0	0	0	0	0	0	0	0.0002
0	0	0	0	0	0	0	0	0	0	0.0002

† unit of 11 parameters are showed in the table V-1

Concerning the DPM, λ was not expected to be the second estimable parameter while λ was much less sensitive than other parameters like $\theta_{s,mo}$, $\theta_{s,im}$. This result showed that λ could be successfully estimated from the BTCs. The parameter ω_s was found to be estimable from the BTC. However, the parameter ω_w was unestimable meaning that ω_w and the other parameters may be highly correlated. The correlations of ω_s or ω_w with other parameters will be discussed in the following section. Again, the molecular diffusion coefficient D_0 and the residual water content θ_r in both regions were not estimable. They were insignificant for the BTCs. As a consequence, they could be set as constants while simulating Br^- transport through the vadose zone.

It is useful to know correlations between different parameters before optimizing model parameters. We represented these correlations by defining the net influence nI of more estimable parameter(s) on the remaining one(s) calculated from the magnitude of each column of the Z matrix as follows:

$$nI = 100\frac{R_{n+1} - R_n}{R_n} \qquad [30]$$

where R_n, R_{n+1} are the row order in tables V-7, V-8.

Table V-6. Correlation classes

Net influence (%)	Correlation
nI = 0	Null
0< nI ≤ 5	Negligible
5< nI ≤ 20	Low
20 < nI ≤ 50	Medium
50 < nI ≤ 75	High
75 < nI	Very High

The higher the "net influence", the higher the correlation between two parameters. Correlation was divided into different classes (table V-6). Table V-7 represents the net influence of the more estimable parameters(s) on the remaining parameter(s) for the SPM. Parameter n was found to be highly correlated with θ_s, K_s and very highly correlated with α (row 1, table V-7). This conclusion was consistent with other results (Simunek and Van Genuchten, 1996); (Simunek et al., 1998a). Parameter λ was found to be highly correlated with only two less sensitive parameters K_s and D_o (row 3, table V-7), that could explain its high estimability. No correlation was found between K_s and θ_r.

Table V-7. Net influence of the more estimable parameter(s) on the remaining one(s) for the SPM †

	n	θ_s	λ	K_s	α	θ_r	D_o
n	-	72.87	25.60	65.23	80.85	41.18	8.06
θ_s		-	37.30	93.95	72.43	5.00	38.60
λ			-	68.36	16.42	21.05	82.86
K_s				-	43.45	0	16.67
α					-	13.33	20.00
θ_r						-	25.00
D_o							-

† unit of 7 parameters are showed in the table V-1

Table V-8. Net influence of the more estimable parameter(s) on the remaining one(s) for the DPM †

	n	λ	$\theta_{s,im}$	ω_s	K_s	$\theta_{s,mo}$	α	ω_w	$\theta_{r,mo}$	$\theta_{r,im}$	D_o
n	-	5.32	96.82	68.30	93.62	96.97	94.79	60.57	47.98	91.07	1.00
λ		-	3.93	7.91	61.84	2.00	9.28	8.41	6.71	0.00	86.87
$\theta_{s,im}$			-	0	91.09	96.02	0.58	0	4.17	60.00	23.08
ω_s				-	5.32	80.00	89.71	99.46	99.21	0	30.00
K_s					-	0	17.14	0	0	50.00	0
$\theta_{s,mo}$						-	31.03	60.00	0	1.00	14.29
α							-	0	0	2.02	50.00
ω_w								-	50.00	13.40	0
$\theta_{r,mo}$									-	0	0
$\theta_{r,im}$										-	33.33
D_o											-

† unit of 11 parameters are showed in the table V-1

The net influences of the more estimable parameter(s) on the remaining one(s) for the DPM are listed in table V-8. Parameter n was highly correlated with the hydraulic property parameters: $\theta_{s,im}$, $\theta_{s,mo}$, $\theta_{r,im}$, K_s, α. In addition, it was very surprising that there were no correlations between $\theta_{s,im}$ with ω_s and ω_w. However, very high correlations were found between ω_s and $\theta_{s,mo}$, $\theta_{r,mo}$, α (table V-8). More specifically,

ω_s was strongly correlated with ω_w. This means that it was difficult to simultaneously calibrate ω_s and ω_w only from the Br^- BTCs. This conclusion was in accordance with other results about the failure of simultaneous calibration of ω_s and ω_w in the DPM (Kohne et al., 2006b). To increase the estimability of parameters such as ω_s and ω_w, we probably need more information such as Br^- concentrations over time in the soil solution and solid phase. This means that in our study, we may also need the observed data at different levels of the lysimeter. Estimability analysis technique being a local technique, initial parameter values may affect sensitivity coefficients and the estimability analysis of model parameters. However, it has been shown that estimability analysis may be considered independent on the initial parameter value because the magnitude in the Z matrix corresponding to the unestimable parameters remained close to the bottom of rank of the estimability analysis (Kou et al., 2005). For this reason, the influence of the input parameter values on the estimability analysis was not investigated here.

3.3. Comparison of the SPM and DPM

As shown in the section devoted to sensitivity analysis, ω_w and ω_s of DPM were sensitive to Br^- BTCs, but they cannot be accurately measured. In this work, the influences of ω_w and ω_s on Br^- BTCs were investigated more concretely by means of the temporal moment method. To study the influence of ω_s, ω_w value was set to 0.1 d^{-1}, and ω_s values were ranged between 0.1 and 0.001 d^{-1}. The same procedure was carried out to study the influence of ω_w. The reference case corresponds to ω_s and ω_w values which were equal to 0.1 d^{-1} (figure V-3).

Table V-9. Effect of ω_w and ω_s on the residence time distribution

Models	**SPM**	**DPM1** $\omega_s = 0.1$ $\omega_w = 0.1$	**DPM2** $\omega_s = 0.01$ $\omega_w = 0.1$	**DPM3** $\omega_s = 0.001$ $\omega_w = 0.1$	**DPM4** $\omega_s = 0.1$ $\omega_w = 0.01$	**DPM5** $\omega_s = 0.1$ $\omega_w = 0.001$
Mean residence time (d)	395	397	445	470	367	346
σ^2 (x 10^4 d^2)	4.8	4.6	5.8	8.4	4.1	3.9

To apply the temporal moment method, Br^- BTCs were extrapolated to reach the abscissa axis by adding the additional weather data in the simulation. The moments were calculated by integrating the curves (Eq.[28]) using the trapezoidal method. The mean residence times and variances are given in table V-9.

The mean residence time was in accordance for both models. This result was exactly what was expected given the model parameters. When ω_w and ω_s were high (table V-9, DPM1), water exchanges and solute transfer between two regions were fast, thus no differences could be seen between the two regions. DPM results were close to SPM ones. In addition, the mean residence times and the time needed to completely achieve BTCs for each model were in the same order of magnitude with what could be calculated from the literature for field tracer experiments (Butters, 1989).

Then, the residence time increased as ω_s decreased. Again, this could be easily explained by the physical significance of this parameter. On the one hand, it has been suggested that solute release from immobile to mobile regions was very slow compared to solute transfer in the opposite direction (Kohne et al., 2006b). On the other hand, solute would have been less accessible for transport in the soil matrix (Fortin et al., 2002). When ω_s decreased, transfers became slower, meaning that the tracer would need more time to leave the lysimeter. This conclusion was consistent with previous results *(e.g.* (Jaynes et al., 2001); (Fortin et al., 2002) suggesting that mobile-immobile transfer may considerably reduce leaching losses. In addition, slower exchange rates could explain variance and thus dispersion increase. In contrast, when ω_w decreased, the residence time decreased as well: exchanges between mobile and immobile water were of less importance; consequently the tracer could be transported faster through the soil lysimeter, and the dispersion would be minimized, which was observed in terms of lower variance.

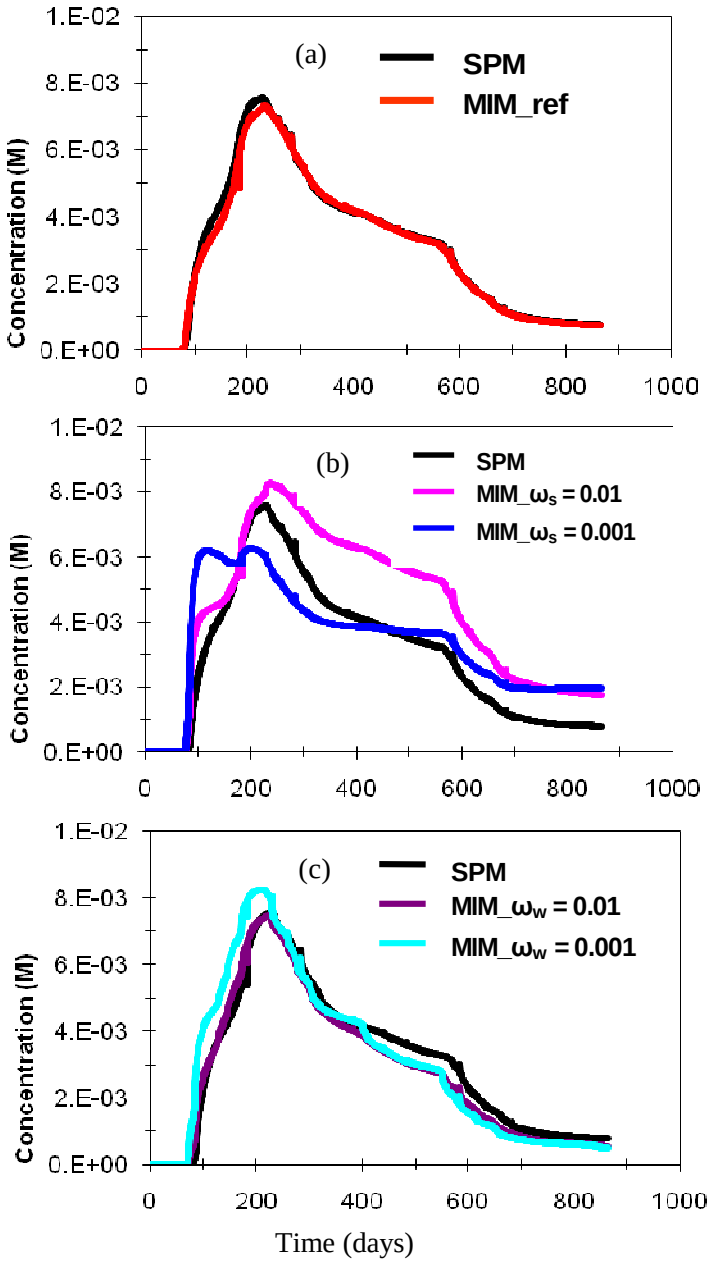

Figure V-3. Illustration of the effects of the first-order rate solute transfer coefficient ω_s and the first-order rate water transfer coefficient ω_w on the Br^- BTCs for the DPM: (a) SPM and reference case of the DPM, (b) ω_s is decreased 10 and 100 times and ω_w is fixed, (c) ω_w is decreased 10 and 100 times and ω_s is fixed.

4. Conclusions

The effects of SPM and DPM parameters were quantified via sensitivity analysis. For the SPM, the most sensitive ones were the hydraulic property shape factor n and the saturated water content θ_S whereas the molecular diffusion coefficient D_0 and the residual water content θ_r were insignificant to Br^- breakthrough. Sensitivity analysis results were similar for the DPM, meaning that the sensitivity of hydraulic property shape factor and saturated water content in both regions was the highest but the sensitivity of molecular and residual water content in both regions was negligible. Accordingly, first-order rate solute transfer coefficient and first-order rate water transfer coefficient were found to be sensitive to the Br^- breakthrough.

An estimability analysis was also performed. The cut-off criterion corresponded to a 2 % Br^- concentration variation in response to a 10 % change in the parameter value. We found that 5 out of the 7 SPM parameters and 7 out of the 11 DPM parameters were estimable. For both models, the molecular diffusion coefficient and the residual water contents were not estimable because of their small influence on Br^- BTC. The first-order rate water transfer coefficient was not estimable from BTCs since this parameter is highly correlated with the others, especially with the first-order rate solute transfer coefficient. The estimability analysis method applied (Yao et al., 2003) contained more information than the general sensibility analysis as it also provided the correlations between model parameters.

The comparison between two models was assessed by the temporal moment method and the results showed that when first-order rate solute transfer coefficient and first-order rate water transfer coefficient were high, the DPM became very close to the SPM.

Acknowledgments

The authors wish to thank the French Scientific Interest Group on Industrial Wastelands (GISFI), as well as the French Ministry “de l’Enseignement Supérieur et de la Recherche” for his financial support.

Chapitre VI : Simulation du transport des HAP dans les colonnes de sol

Simulation of Polycyclic aromatic hydrocarbons leaching through the contaminated soil column using the two-site model

Van Viet Ngo, Julien Michel, Valérie Gusijaite, Marie-Odile Simonnot, M.A. Latifi

Laboratoire des Sciences du Génie Chimique, CNRS-ENSIC
1, Ru Grandville, BP20451, 54001 Nancy Cedex, France

Abstract

The soil and groundwater at former industrial sites polluted by polycyclic aromatic hydrocarbons (PAHs) produce a very challenging environmental issue. The description of PAHs transport by means of mathematical models is therefore needed to risk assessment and remediation strategies at these sites. Despite the complexity of PAHs release kinetics and transport behavior in aged contaminated soils, their transport is firstly evaluated at the laboratory column. Solute transport parameters were then estimated from the experimental data using the inverse method. To better assess the uncertainty and nonquniqueness of the optimized parameters, we used the estimability analysis method of Yao et al. (2003) to firstly investigate the information content of experimental data and the correlations between four solute transport parameters in the two-site sorption model implemented within the HYDRUS-1D software, based on the leaching of Acenaphthylene (ACE), Fluoranthene (FLA), and Pyrene (PYR) of the contaminated soil column under the saturated and nonsaturated flow conditions. For the saturated column, the observed concentrations of FLA and PYR leaching contained less information content than those of ACE leaching due to their higher degree of chemical nonequilibrium transport. Contrary to the ACE, the FLA and PYR concentrations in the leaching solution of the nonsaturated column had more information content than those of the saturated column. For all three compounds, the fraction of sites with instantaneous sorption, f, was found to be highly correlated to the adsorption distribution coefficient, K_d. The chosen "estimable" parameters were then optimized by using the Levenbert-Marquard method. For both saturated and nonsaturated columns, the first-order rate coefficient, ω, was not successfully estimated based on the ACE leaching and the long-term simulation and deeper soil profile was needed to better estimate this parameter. The low optimized f value for the FLA and PYR transport in the nonsaturated column further indicated their high degree of chemical nonequilibrium transport as suggested by the estimability analysis results.

Key-words: Polycyclic aromatic hydrocarbons, estimability analysis, inverse method, HYDRUS-1D

1. Introduction

The polycyclic aromatic hydrocarbons (PAHs) caused the pollution of soil and groundwater at many former industrial sites and made a remarkable environmental issue (Totsche et al., 2007). The understanding of the PAHs release kinetic and transport behavior in contaminated soil is therefore required to risk assessment and remediation strategies at the contaminated PAHs sites (Totsche et al., 2006; Totsche et al., 2007). Despite the complexity of PAHs release kinetics and transport behavior, especially for the aged contaminated soil, the evaluation of PAHs transport is generally performed by means of laboratory column (e.g., Wehrer andTotsche, 2003; Wehrer and Totsche, 2005; Totsche et al., 2006).

Mathematical models are critical tools to understand and optimally quantify the solute transport processes. At our knowledge, very few modeling works have been, however, conducted to study the transport of PAHs in aged contaminated soil. The interaction between organic contaminants and the solid phase might be nonlinear (e.g. Wehrer and Totsche, 2005) and the release of contaminant is often limited by mass transfer kinetic (e.g. Brusseau et Rao, 1989; Seuntjens et al., 2001; Culver et al., 2000), which is indicated by diffusion and/or sorption kinetic. Depending on the physical or chemical factors, nonequilibrium transport is then represented by physical or chemical nonequilibrium models (Simunek and van Genuchten, 2008), respectively.

The application of nonequilibrium models needs to accurately know model parameters at the appropriate scale, especially for the solute parameters that play an important role in the fate of contaminant such as distribution coefficient, mass transfer rate coefficient etc. In reality, many studies reported the existence of a significant difference between solute transport parameters measured through batch experiments and those obtained in the column or field experiments by the inverse method (e.g., Seuntjens et al., 2001; Pot et al., 2005; Moradi et al., 2005; Dontsova et al., 2006).

Therefore, the inverse parameter estimation is a promising way to estimate the solute transport parameters required at the studied scale. The inverse method is widely used in the literature and showed many progress but the problem concerning the uncertainty and nonuniqueness of estimated parameters still exist (e.g., Simunek et al., 2001; Kohne et al., 2004a; Kohne et al., 2006b). The nonuniqueness may be due to the low sensitivity of optimized parameters to the criteria being investigated (Ines et Droogers, 2002), the strong correlations between different parameters (Vrugt et al., 2001), the low information content included in the objective function (Simunek et al., 2001; Kohne et al., 2006b), the local optimization algorithm (Kelleners et al., 2005). Therefore, it is necessary to evaluate the information content and the correlations between different parameters before calibrating the model parameters since it could better calibrate the model parameters and improve the experimental design.

The overall objective of this paper is to evaluate the solute parameter estimability and the correlations between different parameters based on the ACE, FLA, and PYR leaching of the contaminated soil columns under saturated and nonsaturated flow conditions by using the estimability analysis method of Yao et al. (2003). After choosing the set of estimable parameters, these parameters would be estimated by the inverse method.

2. Material and methods

2.1. Experimental description

Soil sample

The polluted soil used for this study was sampled at a former coking plant site, located in the north eastern of France, in the Lorraine district. This production site was stopped and torn down in the early 80's. The soil was sampled in the upper horizon and large amounts of soil were excavated and homogenized by quartering. Subsamples were collected, air-dried at 25 °C and sieved between 50 µm and 2 mm. It was analysed for its physical and chemical properties (Sirguey et al., 2008). This sample showed a quite high PAH concentration (6.8 g kg^{-1}), with mainly 4 and 5 rings of PAHs (respectively 45 and 35%). The soil exhibited high organic carbon content (122 g kg^{-1}) and a high pH (8.3), because of high limestone content.

Experimental set up

The experimental set up used here (**Erreur ! Source du renvoi introuvable.**) allowed us to carry out experiments with soil columns at the laboratory scale, under saturated or nonsaturated flow conditions and a permanent flow regime (e.g., Totsche and Scheibke, 1999). It was composed of a peristaltic pump (Ismatec), a stainless steel soil column (inside diameter = 9.4 cm, height = 21 cm) and a fraction collector (Spectra/Chrom), allowing us to collect soil solution samples for further analysis. The controller unit was driven by a computer.

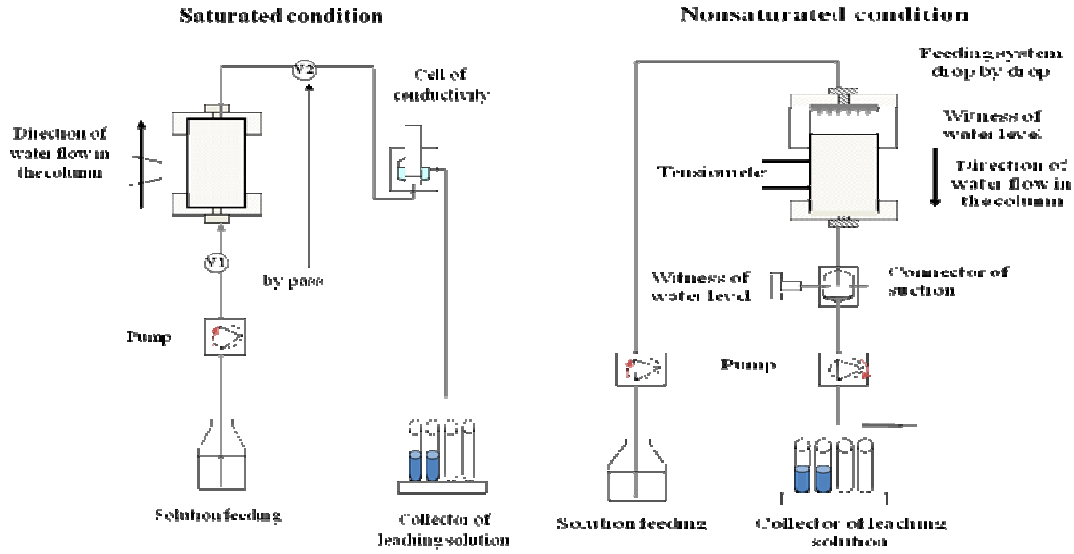

Figure VI-1. Experimental set up

Soil columns were filled manually and shaken to obtain a reproducible filling. Before any experiments, the soil columns were fully saturated from bottom to top with a 2 mM $Ca(NO_3)_2$ solution, at a flow rate of 0.2 mL min^{-1}, then q=0.185 cm h^{-1}. This low flow rate was chosen to avoid preferential flow and air entrapment between soil aggregates. Solutions were prepared with deionized and degassed water. A 0.5 µm stainless steel filter was mounted at the end of the column. During leaching experiments, columns were continuously fed with a 2 mM $Ca(NO_3)_2$ solution.

Under saturated flow conditions, the leaching experiment was started right after the end of the saturation process, at a constant flow rate (3.1 mL min^{-1}) and the flow direction was from top to bottom. Under nonsaturated flow conditions, the flow direction was set downward right after the completion of the saturation process (2.9 mL min^{-1}). Succion was set thanks to a vacuum pump (KNF), leading to a constant depression in a 5 L tank located under the column. This constant depression was applied at the bottom of the column, *via* a specific cell. In this case, the soil column was fed with a sprinkler unit placed on top of it. Experimental conditions are presented in Table VI-1**.** Experimental conditions

. V_p is the soil column pore volume, and corresponds to its void volume. V_0 is the water volume of the soil column; it is equal to V_p under saturated flow conditions and lower than V_p under nonsaturated flow conditions.

Table VI-1. Experimental conditions

Flow condition	Q (mL min^{-1})	V_p (mL)	V_0 (mL)	m_{soil} (g)	ρ (g cm^{-3})
Saturated	3.1 ± 0.1	724	724	1 832	1.26
Nonsaturated	2.9 ± 0.1	759	690	1 834	1.26

2.2. Model description

Pot et al. (2005) reported that the chemical nonequilibrium transport of herbicides in the laboratory column was found at all rainfall intensities. Moreover, Dontsova et al. (2006) also observed the chemical nonequilibrium transport of TNT, TDX at the saturated column. More recently, Suarez et al., 2007 reported that the two-site sorption model was observed to best represent the pesticides data of the miscible displacement experiments in laboratory soil columns. That explained why the two-site sorption model implemented in the HYDRUS-1D software (Simunek et al., 2005b) was chosen in this study.

The concept of two-site sorption (van Genuchten et Wagenet, 1989) that permits consideration of nonequilibrium adsorption-desorption reactions was used to describe the transport of Acenaphthylene (ACE), Fluoranthene (FLA), and Pyrene (PYR). It assumes that the sorption sites can be divided into two fractions:

$$s = s^e + s^k \qquad [1]$$

Sorption s^e [M M^{-1}], on one fraction of the sites (type-1 sites) is assumed to be instantaneous, while sorption s^k [M M^{-1}], on the remaining sites (type-2) is considered to be a first-order kinetic rate process. The first-order kinetic equation for the type-2 sites without the presence of degradation is given by:

$$\frac{\partial s^k}{\partial t} = \omega\left[(1-f)K_d c - s^k\right] \quad [2]$$

Where t is the time [T], c is the solute concentration [M L^{-3}], f (-) is the fraction of exchange sites assumed to be in equilibrium with the liquid phase, ω is a first-order rate constant [T^{-1}], K_d is the linear distribution coefficient [L^3 M^{-1}]. Degradation of ACE, FLA, and PYR was neglected given the short time scale of the experiment. A linear distribution coefficient was used (Michel, 2009a) The governing transport equations describing the two-site model is given by:

$$\frac{\partial(\theta c)}{\partial t} + \rho\frac{\partial s^e}{\partial t} + \rho\frac{\partial s^k}{\partial t} = \frac{\partial}{\partial z}\left(\theta D\frac{\partial c}{\partial z}\right) - \frac{\partial(qc)}{\partial z} \quad [3]$$

$$s^e = fK_d c \quad [4]$$

$$D = \lambda\frac{q}{\theta} \quad [5]$$

Where θ is the water content [L^3 L^{-3}], z is the spatial coordinate [L], ρ is the bulk density [M L^{-3}], D is the dispersion coefficient [L^2 T^{-1}] assumed to be the product of the longitudinal dispersivity, λ [L], and the convective flux, q [L T^{-1}], divided by θ (Eq. 5). In this study, four solute transport parameters were chosen to be investigated are parameters f, ω, λ, and K_d.

2.3. Estimability analysis

Parameter estimability is defined as the ability to compute parameters accurately from a given data set and experimental conditions (Yao et al., 2003; Jayasankar et al., 2009). Parameter estimability depends not only on model structure and parameter sensitivity but also on correlations between different parameters. Parameter estimability was evaluated and then a subset of estimable parameters established following the method proposed by Yao et al. (2003) which allows to quantify the effects of the four chosen solute parameters on ACE, FLA, and PYR leaching and to account for the correlations between the effects of different parameters. This method was successfully applied in the chemical engineering (e.g., Kou et al., 2005; Jayasankar et al., 2009). The estimability analysis method of Yao et al. (2003) compiled dynamic models and dynamic data, as well as response variables available at different sampling rates throughout each experimental run (Kou et al., 2005).

A sensitivity coefficient matrix Z was independently built for each PAH, from the individual coefficient as follows:

$$Z = \begin{bmatrix} \left.\frac{p_1}{C}\frac{\partial C}{\partial p_1}\right|_{t=t_1} & \cdots & \left.\frac{p_m}{C}\frac{\partial C}{\partial p_m}\right|_{t=t_1} \\ \left.\frac{p_1}{C}\frac{\partial C}{\partial p_1}\right|_{t=t_2} & \cdots & \left.\frac{p_m}{C}\frac{\partial C}{\partial p_m}\right|_{t=t_2} \\ \cdots\cdots\cdots\cdots\cdots\cdots\cdots & & \\ \left.\frac{p_1}{C}\frac{\partial C}{\partial p_1}\right|_{t=t_n} & \cdots & \left.\frac{p_m}{C}\frac{\partial C}{\partial p_m}\right|_{t=t_n} \end{bmatrix} \quad [6]$$

The number of columns was equal to 4 corresponding to four solute transport parameters and each row corresponded to PAH concentration at a given sampling time.

The Z matrix elements were calculated by means of centered finite differences method which is of second order accuracy. The subset of estimable parameters was identified following 8 steps (Yao et al., 2003):

1. The magnitude of each column was calculated. It was defined as the quadratic sum of the elements.
2. The parameter whose column in Z had the highest magnitude was selected as the first parameter. This parameter was considered to have the highest effects on PAHs leaching.
3. The corresponding column was marked as X_L (L = 1 for the first iteration).
4. Z_L, prediction of the full sensitivity matrix Z, was calculated using the subset of columns X_L as:

$$Z_L = X_L \left({X_L}^T X_L \right)^{-1} {X_L}^T Z \quad [7]$$

5. The residual matrix R_L was built as:

$$R_L = Z - Z_L \quad [8]$$

6. The quadratic sum of the residuals was calculated in each column of R_L. The column with the highest magnitude corresponded to the next estimable parameter (among the remaining ones) having the largest effects on PAHs leaching and not correlated with the effects of the already selected parameters.
7. The corresponding column in Z was selected and included into X_L. The new matrix was called X_{L+1}.
8. The iteration counter was incremented and steps 4 to 7 were repeated until the last parameter was treated.

The algorithm began by choosing the most estimable parameter p_1 (steps 1, 2). But p_1 may be correlated with the other ones. Orthogonalization was required to rank individual parameter influences on PAHs leaching: the influence of p_1 on the other parameters had to be adjusted for any possible correlation between the column of p_1 in Z matrix and the other ones, so that the “net influence” of each of the remaining parameters could be assessed. This adjustment was done by regressing all of the original columns of the Z matrix on the column associated with p_1. This regression resulted in a matrix of the same dimensions as Z, and the column of this residual matrix associated with p_1 was a column of zeros (steps 3- 5). Orthogonalization was followed by identifying the largest column in the residual matrix in

order to find the parameter p_2 having the second strongest "net influence" on PAHs leaching, after the influence of p_1 had been delimited (steps 6, 7). Orthogonalization was carried on until the last model parameter was treated.

2.4. Initial input parameters and parameter optimization

In this work, the experimental data of three polycyclic aromatic hydrocarbons such as ACE, FLA and PYR were chosen. The numerical analysis of experimental data was carried out as follows. First, the soil hydraulic parameters, θ_r, θ_s, α, n, and K_s, were measured for the same contaminated soil and parameter λ was estimated from the tracer data obtained from the same column and flow conditions. The initial value of parameter K_d for each PAH was calculated from the linear sorption $s = K_d c$, which is equal to the PAH concentration in the solid phase and c is equal to the PAH concentration in the leaching solution at the first sampling time. Parameters f and ω were set to 0.5 and 0.1, respectively, for all three PAHs. Table 2 summarizes the description, unit and initial value of four solute transport parameters f, ω, λ, K_d.

Table VI-2. Definition and initial values of four solute transport parameters in the two-site sorption model (2SM)

Model	Parameter	Unit	Parameter description	Value
	f	-	Fraction of sites with instantaneous sorption	0.5
2SM	ω	h^{-1}	First-order rate contant	0.1
	λ	cm	Dispersivity	1.7
	K_d^{ACE}	$cm^3\ mg^{-1}$	Linear adsorption distribution coefficient of ACE	2.12
	K_d^{FLA}	$cm^3\ mg^{-1}$	Linear adsorption distribution coefficient of FLA	21.42
	K_d^{PYR}	$cm^3\ mg^{-1}$	Linear adsorption distribution coefficient of PYR	26.02

The estimability analysis of four solute parameters for each PAH was performed by using the method of Yao et al. (2003) for each PAH. We chose the number of estimable parameters following two criterias as discussed in the result section.

After choosing the set of estimable parameters for each PAH, the parameter identification was performed by using the Levenberg-Marquardt (Marquardt, 1963) that is based on the minimization of the objective function ϕ given by (Simunek et al., 2005b):

$$\phi(\boldsymbol{b}) = \sum_{j=1}^{m_q} v_j \sum_{i=1}^{n_{qj}} w_{i,j} \left[O_j(z,t_i) - S_j(z,t_i,\boldsymbol{b}) \right]^2 \qquad [9]$$

Where m represents the number of different measurement sets (m = 1 in this work), n is the number of observations in a particular measurement set, $O_j(z,t_i)$ are observations at time t_i at loctaion *z*, $S_j(z,t_i,\boldsymbol{b})$ are the corresponding simulated space-time variables for the vector **b** of optimized

parameters, and v_j and $w_{i,j}$ are weighting factors associated with a particular measurement set or point, respectively. In this work, v_j and $w_{i,j}$ were set equal to 1.

Model performance analysis was then evaluated using the index of agreement (IA) given by (Willmott, 1981):

$$IA = 1 - \frac{\sum_{i=1}^{n}(O_i - S_i)^2}{\sum_{i=1}^{n}\left(\left|S_i - \bar{O}\right| + \left|O_i - \bar{O}\right|\right)^2} \qquad [10]$$

where $\bar{O}$ is the average of observations.

The IA is ranged from 0 to 1, with higher values of IA show better agreement between measured data and simulated values.

However, to reduce the effect of square terms, we mainly used the modified index of agreement (MIA) as follows (Willmott et al., 1985):

$$MIA = 1 - \frac{\sum_{i=1}^{n}\left|O_i - S_i\right|}{\sum_{i=1}^{n}\left(\left|S_i - \bar{O}\right| + \left|O_i - \bar{O}\right|\right)} \qquad [11]$$

3. Results and discussion

3.1. Parameter estimability

3.1.1. Saturated column

Tables 3a, 3b, and 3c represent the estimability analysis results of four parameters: the fraction of sites with instantaneous adsorption f, the adsorption distribution coefficient K_d, the dispersivity λ, and the first-order rate coefficient for two-site nonequilibrium adsorption ω for ACE, FLA, and PYR, respectively, based on their concentrations in the leaching solution of the saturated column. From left to right of tables VI-3a, VI-3b and VI-3c the estimability order of four parameters decreases. The first row in tables VI-3a, VI-3b and VI-3c represents the magnitude of each column in Z matrix corresponding to each parameter before adjusting the correlations between different parameters. From the second to the fourth rows of tables VI-3a, VI-3b and VI-3c, the magnitude of each column in Z matrix after

eliminating the influences of the more estimable parameter(s) on the remaining model parameter(s) is reported. The fifth row in tables VI-3a, VI-3b and VI-3c represents the average changes in PAH concentration in the leaching solution when a 10% in parameter value changed.

Yao et al. (2003) used 0.04 as a cut-off criterion for considering whether a model parameter was estimable or not. They considered thus that information was sufficient to estimate a parameter if a 10% change in its value implied a 2% in output predictions. However, the choice of cut-off criteria value is somewhat arbitrary (Yao et al., 2003). Ngo et al., (to be submitted) applied this estimability analysis technique as well as this approach for choosing the cut-off criteria value to make a set of estimable parameters following different measurements at a field lysimeter. By analyzing the uncertainty and nonuniqueness of optimized parameters, Ngo et al., (to be submitted) found that the highly correlated parameters should not be simultaneously optimized because the correlations between different parameters may hamper the optimization results. This suggested that the choice of a number of model parameters to be simultaneously estimated should take into account the correlations between different parameters. Furthermore, Kohne et al. (2004) reported that saturated water content in the mobile and immobile regions, $\theta_{s,mo}$ and $\theta_{s,im}$, were impossible to be simultaneously estimated from water flow and solute transport data at the column scale because of their high correlation. Therefore, in this work a parameter is considered "estimable" only when this parameter satisfies the two following criteria:

1. first of all, a 10% change in its value had to imply at least a 2% change in solute concentration,
2. and this parameter did not show high correlations with other one(s).

We evaluated the correlations between the parameters in terms of "net influence" of the more estimable parameter(s) on the remaining parameter(s) which was calculated based on the magnitude of each column in the Z matrix as follows:

$$nI = 100\frac{R_{n+1} - R_n}{R_n} \qquad [12]$$

Where R_n, R_{n+1} are the row order in tables VI-4a, VI-4c and VI-4e. The higher the net influence, the higher the correlation between two parameters.

Following these two criteria, we found that for the ACE transport in the saturated column, parameter f was the most estimable since the magnitude in the Z matrix corresponding to this parameter was the highest and a 10% change in this parameter implied a 11.7% change. Parameter ω was the second estimable parameter. Parameter λ was not estimable. Table VI-3a shows that a 10% change in initial value of K_d implied a 11.5% change in ACE concentration in the leaching solution. This means that the sensitivity degree of parameter f and K_d was almost similar, the magnitudes in the Z matrix are thus 125.3 and 122.6, respectively. However, after eliminating the influence of f on K_d, the magnitude in the Z matrix corresponding to parameter K_d became very small, $1.8\ 10^{-5}$, meaning that f and K_d were highly correlated (not shown). Then these two parameters are impossible to be simultaneously optimized. Based on ACE concentration in the leaching solution, only two parameters f and ω are considered to be

estimable simultaneously. From the discussion above, K_d was also expected to be simultaneously estimable with parameter ω.

Table VI-3. Estimability order of four solute transport parameters based on ACE, FLA, and PYR leaching in the saturated column, respectively

(3a) **ACE**

f	ω	λ	Kd
125.31	22.81	2.99	122.58
0	**14.39**	0.72	2.5×10^{-5}
0	0	0.57	2.1×10^{-5}
0	0	0	1.8×10^{-5}
11.66%	**4.08%**	**1.59%**	**11.54%**

(3b) **FLA**

f	λ	Kd	ω
11.24	0.80	7.06	0.27
0	0.06	0.01	0.002
0	0	0.006	0.002
0	0	0	7.5×10^{-5}
2.74%	**0.83%**	**2.12%**	**0.48%**

(3c) **PYR**

f	λ	Kd	ω
7.00	0.71	3.73	0.21
0	0.03	0.02	0.003
0	0	0.01	0.003
0	0	0	2.6×10^{-5}
2.07%	**0.76%**	**1.02%**	**0.46%**

For FLA transport, only f was considered estimable based on the FLA concentration in the leaching solution since this parameter satisfied the two criteria above. Parameter K_d satisfied the first criteria, as shown by the fact that a 10% change in its value implied a 2.12% in FLA concentration but it was highly correlated with the most estimable parameter, f (not shown). Therefore, K_d was not simultaneously estimable with f. In addition, λ and ω were not estimable. It was unexpected that ω showed a very little sensitivity degree for FLA leaching, reflected by the fact that a 10% change in value of parameter ω only implied a 0.48% change in FLA concentration in the leaching solution.

For PYR transport, estimability analysis results were similar to those obtained for FLA transport, meaning that only parameter f was estimable and three other ones were not estimable.

For the saturated column, estimability analysis results showed that the solute transport parameters were much more sensitive to ACE leaching than to FLA and PYR leaching. This implied that parameter estimability based on ACE concentrations might be higher than the one based on FLA, PYR concentrations in the leaching solution. This may be explained as follows. The calculation of K_d from the linear sorption $s = K_d c$ leads to values of 2.12, 21.42, and 26.02 cm^{-3} mg^{-1} for ACE, FLA, and PYR, respectively. This result suggests that FLA and PYR had much more affinity with the solid phase than ACE. Therefore, desorption of FLA and PYR compounds may need much more time and so the degree of chemical nonequilibrium transport of FLA and PYR is higher than the one of ACE. As a result, for the saturated column, the effect of water velocity on the FLA and PYR nonequilibrium transport is smaller.

3.1.2. Nonsaturated column

For ACE transport in nonsaturated column, the estimability order of four parameters and the correlations between four parameters are showed in tables VI-4a and VI-4b, respectively. Following the two criteria above, f and ω were simultaneously estimable. On the other hand, λ and K_d were found to be highly correlated with the most estimable parameter f (row 1 in table VI-4b). Parameters λ and K_d were therefore impossible to estimate together with parameters f and ω. In addition, since K_d showed the same sensitivity degree as parameter f (row 1 and 5 in table VI-4a), K_d and ω were expected to be simultaneously estimable. Parameter f was found to be not correlated to ω but highly correlated with λ. This result further suggested that the degree of chemical nonequilibrium transport of ACE was low. In comparison with the estimability analysis results obtained in the saturated column, we found that the parameter estimability in the nonsaturated column was lower, shown by the smaller value of the corresponding magnitude in the Z matrix and the smaller sensitivity degree. This gave us the feeling that when a solute transport has low degree of chemical nonequilibrium, the saturated condition may contain more information for optimization of model parameters. The uncertainty of optimized parameter(s) in the next section would further show this suggestion.

Tables VI-4c and VI-4d represent the estimability analysis results and the correlations between four parameters for FLA transport in nonsaturated column. Parameters f and λ were found to be simultaneously estimable. Parameter ω showed a high sensitivity to the leaching of FLA, as indicated by a 3.92% change in its concentration in the leaching solution when a 10% change in initial value of this parameter was introduced. However, parameter ω was highly correlated with parameter f, indicated by the fact that parameter f had the net influence of 89.7% on parameter ω. That is why in this case parameter ω may not be simultaneously estimated with parameter f. In addition, K_d also showed a very high sensitivity degree to FLA leaching. Parameters K_d and λ were expected to be simultaneously estimable.

Once again, estimability analysis results and correlations between four parameters (tables VI- 4e and VI-4f) for PYR transport in the nonsaturated column were very similar to those obtained in the case of FLA transport, meaning that f and λ or K_d and λ were expected to be simultaneously estimable and parameter ω was not estimable only based on the PYR concentration in the leaching solution.

As a conclusion, unlike with the ACE transport; parameter f was not correlated with parameter λ and was highly correlated with parameter ω for both FLA and PYR. This further indicated the high degree of chemical nonequilibrium transport of FLA and PYR. In addition, the magnitude in the Z matrix corresponding to each solute parameter for both FLA and PYR transport in the nonsaturated column was much higher than the one obtained in the saturated column. The solute concentration in the nonsaturated column may contain much more information than in the case of the saturated column (contrary to the ACE transport). For all three compounds, parameter f was found to be highly correlated with parameter K_d, further meaning that these two parameters should not be simultaneously optimized.

Table VI-4. Estimability order and correlations of four solute transport parameters based on ACE, FLA, and PYR leaching in the nonsaturated column, respectively

ACE

(4a)

f	ω	λ	K_d
88.77	71.91	11.84	88.38
0	**67.20**	0.94	2.0×10^{-4}
0	0	0.93	2.0×10^{-4}
0	0	0	2.0×10^{-4}
5.44%	**4.72%**	**1.78%**	**5.44%**

(4b)

	f	ω	λ	K_d
f	-	6.55	**92.05**	**100**
ω		-	0.95	0.04
λ			-	2.29
Kd				-

FLA

(4c)

f	λ	ω	K_d
89.65	5.49	5.02	73.70
0	**4.16**	0.52	0.01
0	0	0.45	2.3×10^{-3}
0	0	0	2.2×10^{-3}
8.42%	**2.88%**	**3.92%**	**7.63%**

(4d)

	f	λ	ω	K_d
f	-	24.18	**89.74**	**99.99**
λ		-	12.88	77.51
ω			-	5.65
Kd				-

PYR

(4e)

f	λ	ω	K_d
70.65	4.53	3.62	54.98
0	**4.31**	0.27	0.02
0	0	0.24	$4.8\ 10^{-3}$
0	0	0	$4.0\ 10^{-3}$
7.46%	**2.66%**	**3.22%**	**6.59%**

(4f)

	f	λ	ω	K_d
f	-	4.97	**92.40**	**99.97**
λ		-	12.50	74.58
ω			-	17.10
Kd				-

3.2. Parameter optimization

3.2.1. Saturated column

In this section, we will present the optimization results of estimable parameter(s) deduced from the estimability analysis. As noted earlier, for the ACE transport in the saturated column, only two couples of parameters f and ω or K_d and ω were expected to be simultaneously optimized. The optimized parameter values for these two cases, as well as the statistical analysis results are shown in table VI-5. The comparison of measured ACE concentrations and simulated values are showed in figure VI-2.

When f and ω were simultaneously optimized, the optimized f value of 0.70 showed an acceptable estimation reflected by its relatively large confidence interval from 0.31 to 1. Unfortunately, ω was not successfully estimated, as indicated by its very large confidence interval. The modified index of agreement showed an acceptable optimization quality in this case. The optimized f value of 0.70 showed a low degree of chemical nonequilibrium transport of ACE as suggested in the estimability analysis results.

When K_d and ω were simultaneously optimized, the optimized K_d value varied from 7.02 to 11.92, thus showing a good estimation. However, it is similar to the previous case: the optimized value of ω was very uncertain since its confidence interval was also too large. A little improvement in estimation for this case was shown by a higher MIA value and the better shape of the leaching curve. A possible explanation for the uncertainty of optimized ω value in both cases could be due to the sorption kinetic that was much lower compared to other transport processes. This means that the study of the first-order rate coefficient, ω, requires the long-term simulations and deeper soil profile than it is for short-term experiment carried out on short column as in this study. This is in agreement with the review by Kohne et al. (2009) who reported that the laboratory column is not suitable for studying the mass transfer coefficient of pesticides using the two regions concept model.

Table VI-5. Solute transport parameters in the two-site sorption model, with the corresponding confidence intervals, estimated from measured ACE concentrations in the leaching solution of the saturated column using HYDRUS-1D and the modified index of agreement (MIA)

	Optimized parameter	MIA	Optimized parameter	MIA
f	**0.70** (0.31-1)		*	
ω	**0.031** (-0.017 - 0.079)	**0.60**	**0.051** (-0.024 - 0.126)	**0.74**
Kd	*		**7.97** (7.02 - 11.92)	

Table VI-6. Fraction of sites with instantaneous sorption in the two-site sorption model, as well as its confidence interval, estimated from measured FLA and PYR concentrations, respectively, in the leaching solution of the saturated column using HYDRUS-1D and the modified index of agreement (MIA)

	FLA		PYR	
	Optimized parameter	MIA	Optimized parameter	MIA
f	**0.25** (-14.85 - 15.34)	**0.38**	**0.01** (-910.54 - 910.56)	**0.47**

The optimization of parameter f based on the FLA and PYR concentrations in the leaching solution of the saturated column, as well as their confidence interval, is summarized in table VI-6. The comparison of the measured FLA and PYR concentrations with calculated values are shown in figure VI-3. For FLA transport, the optimized f value was highly uncertain, indicated by its confidence interval ranged from -14.85 to 15.34. The MIA value of 0.38 and the shape of leaching curve also showed the bad optimization result. For PYR transport, the optimized f value was still much smaller and more uncertain than the one obtained for the FLA transport. The confidence interval was much larger than the one obtained in the case of FLA transport. The high uncertainty of optimized parameter f when this parameter was optimized alone was also reported in latter studies (e.g., Roulier andJarvis, 2003; Kohne et al., 2006a). Despite the high uncertainty of optimization results for parameter f, we found that the optimized f value decreased for ACE, FLA, and PYR. This further indicated the higher degree of chemical nonequilibrium transport for FLA and PYR than for ACE as suggested by the estimability analysis results.

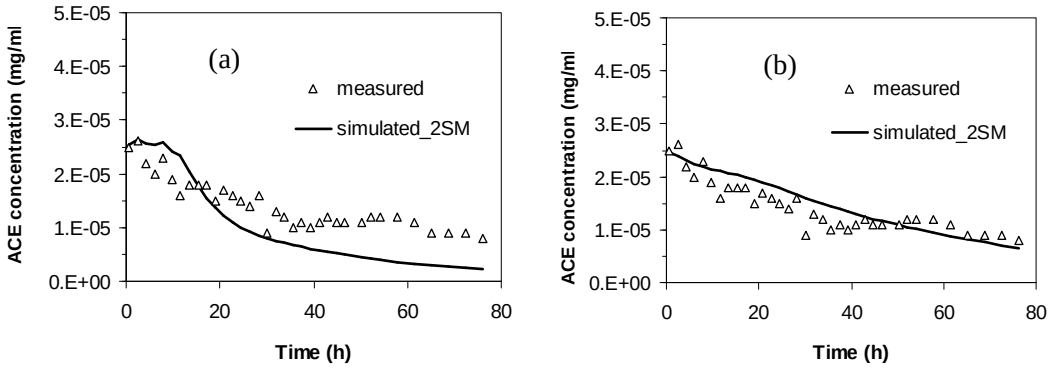

Figure VI-2. Comparison of the measured and simulated ACE concentrations in the leaching solution of the saturated column: (a) when parameters f and ω were simultaneously optimized, (b) when parameters K_d and ω were simultaneously optimized

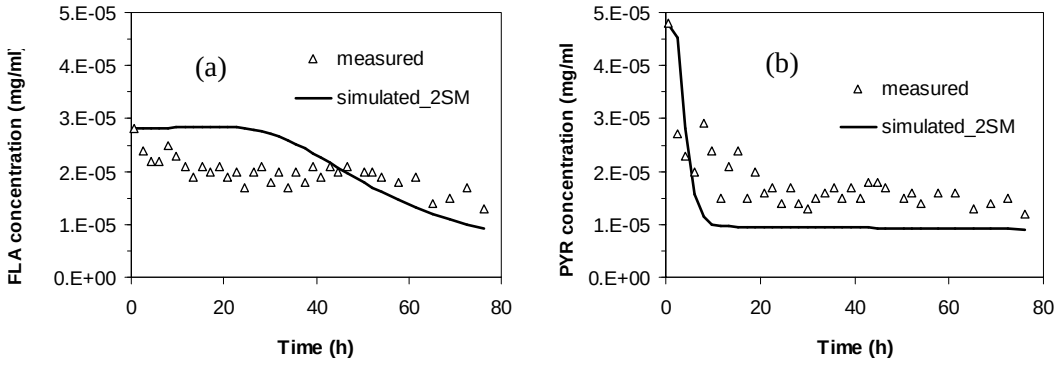

Figure VI-3. Comparison of the measured and simulated FLA and PYR concentrations in the leaching solution of the saturated column: (a) when parameter f optimized based on the observed FLA concentrations, (b) when parameter f optimized based on the observed PYR concentrations

3.2.2. Nonsaturated column

For the ACE transport in the nonsaturated column, estimability analysis results showed that f and ω or K_d and ω were simultaneously estimable. However, to see how the simultaneous optimization of four parameters could hamper the optimization results, we tried to optimize four parameters based on the same data as when two couples of parameters f and ω or K_d and ω were simultaneously optimized. The optimization results, the associated confidence intervals and statistical analysis results were represented in table VI-7. Figure VI-4 shows the comparison between the observed and simulated ACE concentrations.

When f and ω were simultaneously optimized, the optimized f value of 0.76 sounded realistic but not certain as shown by its very large confidence interval from -0.29 to 1.81. The uncertainty in the optimized ω value of 0.003 was also demonstrated by its large confidence interval. By analyzing the shape of the ACE leaching curve, there was only little deviation between the measured and simulated ACE concentrations as indicated by the high MIA value of 0.86.

When K_d and ω were simultaneously optimized, the similar problem was found in term of uncertainty of the optimization results, meaning that both optimized K_d and ω values were realistic but their confidence intervals were large despite the good agreement of comparison between the observed ACE concentrations and simulated ACE concentrations.

When we optimized four parameters simultaneously, the optimization results were found to become worse. First of all, the optimized f value of 1.41 was physically impossible and its confidence interval varied from -1876 to 1879 was very large. The optimized K_d value of 6.23 was realistic but its confidence interval was much larger than this obtained when only two parameters K_d and ω were simultaneously estimated. In contrast, the optimized ω value was 0.000 5 but its confidence interval of ±0 was not realistic at all. In addition, the optimized λ value of 41.8 cm was very much higher than the

one obtained by the tracer data for the same column displacement experiment. As a conclusion, the correlations between parameters f and K_d and/or f and λ increased the uncertainty of optimized parameters. But it is a bit surprising since the comparison between the measured and simulated ACE concentrations was also good, indicated by the same value obtained for the MIA criteria. In the past, Seuntjens et al. (2001) also observed the good description of the ^{111}Cd breakthrough curve when all four parameters, k_F and n in the Freundlich model plus f and ω, were simultaneously optimized but the optimization results were not reliable.

Altogether, the optimization results for the ACE transport in the nonsaturated column were very uncertain, especially when four solute transport parameters were simultaneously optimized. This may be explained partly by the fact that there were only five measured ACE concentrations in the leaching solution that were positive and the other ones were, lower than the detection limit, zero (figure 4)

Table VI-7. Solute transport parameters in the two-site sorption model, with the corresponding confidence intervals, estimated from measured ACE concentrations in the leaching solution of the nonsaturated column using HYDRUS-1D and also the modified index of agreement (MIA)

	Optimized parameter	MIA	Optimized parameter	MIA	Optimized parameter	MIA
f	**0.76** (-0.29 - 1.81)		*		**1.41** (-1875.9 - 1878.8)	
ω	**0.003**(-0.027 - 0.034)	**0.86**	**0.0005** (-0.022 - 0.024)	**0.86**	**0.0005** (±0)	**0.86**
Kd	*		**3.39** (-0.73 - 7.50)		**6.23** (-8265.1 - 8277.5)	
λ	*		*		**41.8** (32.4 - 51.3)	

As noted earlier, for FLA and PYR transport in the nonsaturated column, only two couple of parameters f and λ or K_d and λ were expected to be simultaneously estimated. The optimization results, as well as their confidence intervals, and the statistical analysis results are summarized in table VI-8. Fitted concentrations and observed concentrations for two compounds are showed together in figure VI-5.

When parameters f and λ are simultaneously optimized based on the FLA concentrations in the leaching solution, parameter f was successfully estimated since the optimized f value of 0.31 had a relatively narrow confidence interval ranged from 0.26 to 0.40. However, the optimized λ value of 20.1 cm was quite uncertain as show by its relatively large confidence interval ranged from 12.6 to 27.5 cm and was much higher than the one estimated by tracer data for the same column experiment. When parameters K_d and λ were simultaneously estimated, parameter K_d was also found to be successfully estimated as shown by the relatively narrow confidence interval. Similarly as for the above case, the optimized λ value was almost the same in term of fitted value and confidence interval. The comparison between observed and simulated FLA concentrations showed a noticeable difference.

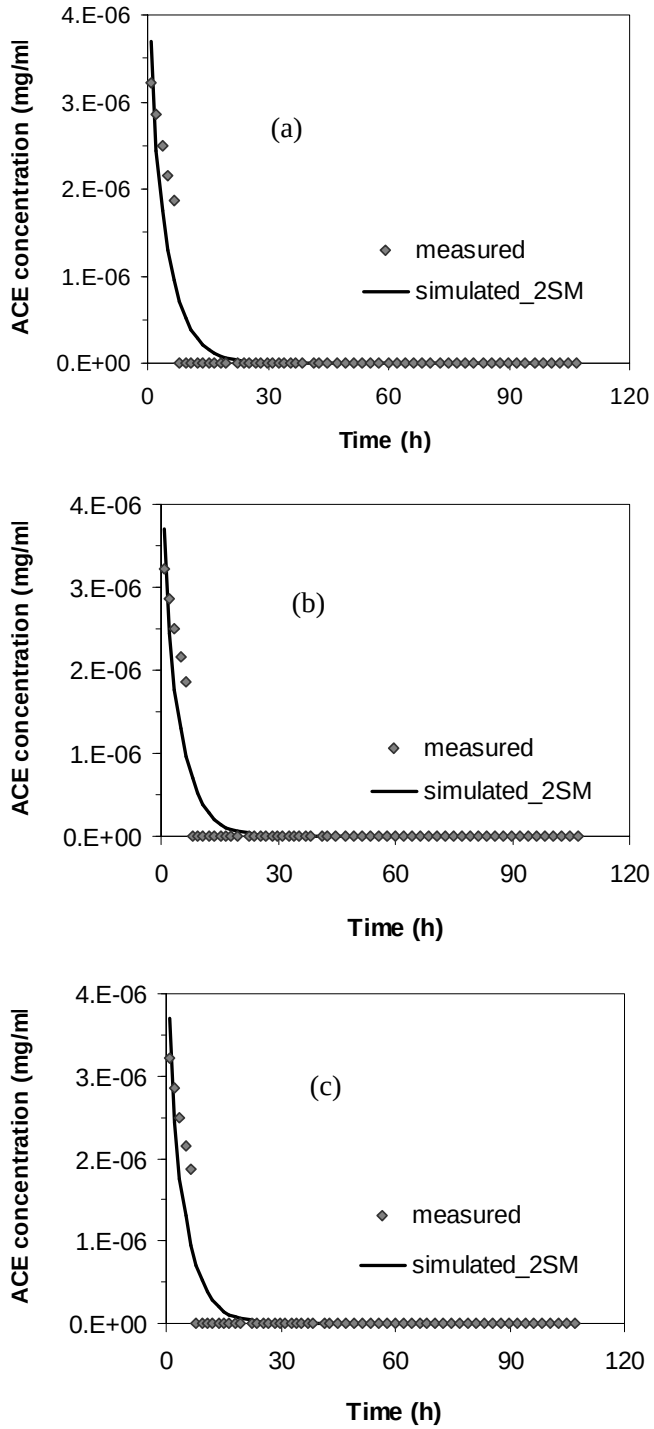

Figure VI-4. Comparison of the measured and simulated ACE concentrations in the leaching solution of the nonsaturated column: (a) f and ω were simultaneously optimized, (b) K_d and ω were simultaneously optimized, and (c) f, ω, λ, and K_d were simultaneously optimized

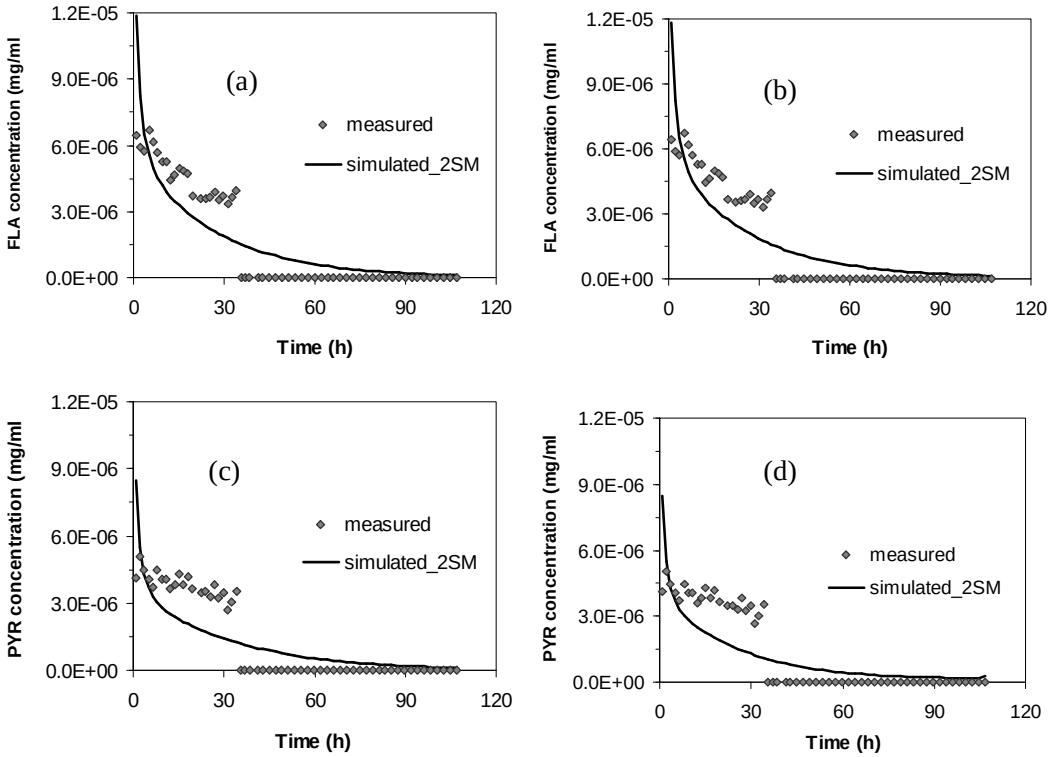

Figure VI-5. Comparison of the measured and simulated FLA and PYR concentrations in the leaching solution of the nonsaturated column: (a) f and λ were simultaneously optimized based on the observed FLA concentrations, (b) K_d and λ were simultaneously optimized based on the observed FLA concentrations, (c) f and λ were simultaneously optimized based on the observed PYR concentrations, and (d) K_d and λ were simultaneously optimized based on the observed PYR concentrations

For the PYR transport, the optimized λ values and their confidence intervals were similar with those obtained for the FLA transport when parameters f and λ or K_d and λ were simultaneously optimized. The optimized f value was 0.05 but its confidence interval of ±0 was, however, somewhat surprising. The estimation of parameter K_d seems to be accurate, indicated by its very narrow confidence interval ranged from 24.68 to 24.88.

In comparison with the optimization results in the saturated column, we found that the optimized f values for the FLA and PYR transport in the nonsaturated column were higher and also more accurate than those obtained in the saturated column. This result is explained by the effect of water velocity on the chemical nonequilibrium transport, meaning that when water flow is slower, there are more sites seem to be relative equilibrium with the soil solution. Recently, Pot et al. (2005) studied the effect of water velocity on the nonequilibrium transport of two pesticides at the column displacement experiment and reported that the fraction of sites with instantaneous sorption, f, is usually increased when water velocity decreased.

Figure VI-5 shows the significant differences between the measured concentrations and simulated concentrations for both FLA and PYR. Note that we did not account for the PAHs dissolution during the simulation; this may partly explain this deviation. Another possible explanation could be due to the additional process that also controls the release of PAHs contained in the droplets of non-aqueous liquid phases in which their major constituents are PAHs (Pumphrey et Chrysikopoulos, 2004; Totsche et al., 2006).

Table VI-8. Solute transport parameters in the two-site sorption model, as well as its confidence interval, estimated from measured FLA and PYR concentrations, respectively, in the leaching solution of the nonsaturated column using HYDRUS-1D and also the modified index of agreement (MIA)

FLA				
	Optimized parameter	MIA	Optimized parameter	MIA
f	**0.31** (0.26 - 0.40)		*	
Kd	*	**0.74**	**14.1** (10.7 - 17.5)	**0.74**
λ	**20.1** (12.6 - 27.5)		**20.0** (12.4 - 27.7)	
PYR				
f	**0.05** (±0)		*	
Kd	*	**0.69**	**24.78** (24.68 - 24.88)	**0.69**
λ	**18.8** (11.8 - 25.9)		**20.8** (13.1- 28.5)	

4. Conclusions

The estimability analysis of four solute transport parameters, f, ω, λ, and K_d, based on the ACE, FLA, and PYR concentrations in the leaching solution of the contaminated soil column under the saturated and nonsaturated flow conditions were investigated.

For the saturated column, only parameters f and ω or K_d and ω were considered to be simultaneously estimable based on the ACE leaching; only parameter f was estimable based on their FLA leaching or PYR leaching. Parameter estimability was smaller for FLA and PYR transport than for ACE transport because of their lower sensitivity to solute parameters under saturated flow condition. This may be caused by the higher degree of chemical nonequilibrium transport of FLA and PYR.

For the ACE transport in the nonsaturated column, parameters f and ω or K_d and ω were expected to be simultaneously optimized. Parameter f was found to be highly correlated to parameters λ and K_d. Similar

estimability analysis results obtained for the FLA and PYR transport in the nonsaturated column, show that parameters f and λ or K_d and λ were simultaneously estimable and parameter f had the very strong correlations with parameters ω and K_d. The FLA and PYR leaching in the nonsaturated column contained more information than those in the saturated column due to the higher sensitivity to solute parameters under the nonsaturated flow condition.

After choosing the set of estimable parameters, these parameters were optimized by numerical inversion. Parameters f and K_d were quite successfully estimated based on the ACE concentrations in the leaching solution of the saturated column but the optimized ω value was very uncertain. The more long-term simulation and deeper soil profiles may be needed to better optimize parameter ω. Parameter f was not successfully estimated alone based on the FLA or PYR concentrations in the leaching solution of the saturated column. The low optimized f values for FLA and PYR transport further confirmed their high degree of chemical nonequilibrium transport.

The optimization results for the ACE transport in the nonsaturated column were very uncertain, especially when four solute transport parameters were simultaneously optimized since the correlations between parameters f and K_d and/or f and λ increased the uncertainty of optimized parameters. Based on the FLA and PYR concentrations in the leaching of the nonsaturated column, parameters f and K_d were found to be successfully optimized but the optimized λ value was, however, still uncertain. Compared to the optimization results in the saturated column, the optimized f values for the FLA and PYR transport in the nonsaturated column were found to be higher and also more certain than those obtained in the saturated column. This is due to the effect of water velocity on the chemical nonequilibrium transport, meaning that when water flow is slower, there are more sites seem to be relative equilibrium with the soil solution.

Conclusion générale

Les activités industrielles passées ont donné lieu à la pollution des sols et des eaux souterraines, notamment par des HAP et des métaux. Le présent travail se situe dans le cadre de l'étude de la migration des polluants dans ces sols mené dans le cadre du GISFI. Or cette la modélisation de la migration des polluants passe nécessairement par la modélisation de l'écoulement dans la zone non saturée du sol, incluant l'écoulement préférentiel et le transport hors équilibre. Nos principaux objectifs scientifiques étaient :

- étudier l'écoulement préférentiel et le transport hors équilibre à différentes échelles sous différentes conditions d'écoulement en utilisant différents types de modèles,
- étudier la sensibilité et l'estimabilité des paramètres ainsi que leurs corrélations existantes,
- optimiser les paramètres à partir des différents types de mesures expérimentales.

Pour atteindre ces objectifs, nous avons choisi d'utiliser le logiciel HYDRUS couramment appliqué dans la littérature, comprenant différents modèles permettant de décrire l'écoulement préférentiel, le transport hors équilibre physique et chimique, le transport facilité par les colloïdes ainsi qu'une méthode d'optimisation. De plus, nous avons utilisé la méthode d'analyse d'estimabilité de Yao et al. (2003) qui permet de quantifier les effets des paramètres sur les différents types de prédictions et de rendre compte des corrélations entre les différents paramètres.

Les mesures de hauteur d'eau percolée dans les bacs de rétention de trois types de parcelles (terre nue, végétation spontanée, luzerne) sur la station expérimentale de GISFI ont été choisies afin de tester le logiciel HYDRUS-1D. Le logiciel HYDRUS-1D a montré sa validation par l'accord entre les hauteurs d'eau mesurées et simulées dans les bacs de rétention correspondant aux parcelles de terre nue pour tous les périodes de percolation et aux parcelles de végétation spontanée et de luzerne pour les périodes de percolation en hiver. Le grand écart entre les hauteurs d'eau mesurées et simulées pour les parcelles de végétation spontanée et de luzerne pendant les périodes de percolation en été est l'origine de la mal-connaissance de la couverture des plantes et la distribution des racines. Ceci nous renforce sur la nécessité de mieux suivre le développement des plantes sur les parcelles, de mesurer les hauteurs d'eau dans les bacs de rétention plus souvent et d'avoir besoin des dispositifs qui permettent de mesurer les teneurs en eau à différents profondeurs des parcelles.

Après avoir montré la validité du logiciel HYDRUS pour notre approche, ce logiciel a été retenu pour tous nos travaux de modélisation. Les principales contributions de ce travail sont d'améliorer les connaissances concernant non seulement la sensibilité, l'estimabilité des paramètres des modèles en fonction de données expérimentales et aussi les corrélations des paramètres. De plus, les résultats de l'optimisation et les analyses de la non-unicité et de l'incertitude des paramètres estimés (sauf pour les études concernant le traceur) sont présentés en détails :

Dans un premier temps, les données horaires et quotidiennes de pression et de teneur en eau à trois profondeurs, d'eau percolée cumulative et d'évaporation cumulative dans un lysimètre de terrain ont été utilisées (i) pour étudier la sensibilité et l'estimabilité de cinq paramètres hydrodynamiques (θ_r, θ_s, α, n, K_s) et (ii) pour optimiser les paramètres estimables paramètres. Pour tous les deux types de données horaires et quotidiennes, on a montré que les pressions contenaient le plus d'information, suivies par les teneurs en eau et puis l'eau percolée cumulative et l'évaporation cumulative. Les données quotidiennes contiennent plus d'information que les données horaires. De plus, la combinaison des pressions et des teneurs en eau a permis d'augmenter l'estimabilité des paramètres. Ainsi, les cinq paramètres se sont avérés estimables, et surtout aucune forte corrélation des paramètres n'a été trouvée. Trois paramètres θ_r, θ_s, n ont été estimés avec succès mais l'estimation de deux paramètres α, K_s était encore incertaine. Ceci a été expliqué par la faible amplitude de la variation des pressions et des teneurs en eau du lysimètre dans la période considérée. La prise en compte de l'hétérogénéité du sol a fait augmenter nettement la qualité de l'optimisation des paramètres ainsi que la validation du modèle.

Ensuite, les mêmes données ont été utilisées pour étudier la sensibilité et l'estimabilité de 8 paramètres ($\theta_{r,mo}$, $\theta_{r,im}$, $\theta_{s,mo}$, $\theta_{s,im}$, α, K_s, et ω_w) du modèle à double porosité et estimer les paramètres. En se basant sur la combinaison des pressions et des teneurs en eau, seulement cinq paramètres ($\theta_{s,mo}$, $\theta_{s,im}$, α, K_s) ont été considérés estimables. Cependant, deux couples de paramètres $\theta_{s,mo}$- $\theta_{s,im}$ et α-K_s ont présenté de fortes corrélations. Les résultats de l'optimisation ont montré que deux paramètres $\theta_{s,mo}$ et $\theta_{s,im}$ ne pouvaient pas être optimisés simultanément. Le seuil d'estimabilité a été diminué pour que paramètre ω_w soit considéré estimable mais le fait d'ajouter ω_w dans la procédure d'optimisation a perturbé nettement les résultats de l'optimisation. Quand on a retiré les deux paramètres $\theta_{s,im}$ et K_s dans la procédure d'optimisation pour éliminer les fortes corrélation, les résultats de l'optimisation ont été clairement améliorés. Trois paramètres n, $\theta_{s,mo}$ et α ont pu être estimés avec succès.

L'étude de sensibilité et d'estimabilité des paramètres du modèle de transport uniforme (SPM) et du modèle à double porosité (DPM) a été réalisée en se basant sur la percé du traceur de bromure sur le lysimètre. Les résultats d'étude de sensibilité ont montré que pour le modèle SPM, les paramètres n et θ_s étaient les plus sensibles tandis que D_o et θ_r n'étaient pas sensibles. De même pour le modèle DPM, les paramètres n, $\theta_{s,mo}$ et $\theta_{s,im}$ étaient les plus sensibles tandis que D_o, $\theta_{r,mo}$, $\theta_{r,im}$ n'étaient pas sensibles. En outre, deux paramètres ω_s, ω_w étaient sensibles à la percé de traceur bromure. Pour l'estimabilité des paramètres, seulement 5 sur 7 paramètres du modèle SPM et 7 sur 11 paramètres du modèle DPM ont pu être considérés comme estimables. Pour ces deux modèles, le coefficient de diffusion moléculaire et la teneur en eau résiduelle n'étaient pas estimables. Particulièrement, le coefficient de transfert d'eau (ω_w) n'était pas estimable en se basant seulement sur les concentrations de bromure dans les solutions de percolation. Afin d'augmenter l'estimabilité de ce paramètre, nous avons besoin probablement des mesures de concentration de traceur bromure dans la phase liquide ainsi que dans la phase solide.

Et puis, l'estimabilité et l'optimisation de quatre paramètres de transport (f, ω, λ, et K_d) du modèle à deux sites de sorption ont été étudiées en se basant sur les concentration de trois HAP (ACE, FLA, PYR) dans les solution de percolation d'une colonne de laboratoire sous les conditions saturée ou non saturée.

Pour la colonne saturée, seulement deux couples de paramètres f-ω et K_d-ω étaient estimables en se basant sur les concentrations d'ACE dans les solutions de percolation tandis que seul f était estimable en se basant sur les concentrations de FLA ou de PYR. L'estimabilité des paramètres de transport est plus faible pour le transport de FLA ou de PYR que celui pour le transport d'ACE à cause de leurs degrés de sensibilité plus faibles. Ceci a suggéré le degré plus élevé de transport hors équilibre chimique de FLA et de PYR.

Pour la colonne non saturée, en se basant sur la courbe de percée d'ACE, seulement deux couples de paramètres f-ω et K_d-ω étaient estimables simultanément et f était fortement corrélé avec deux paramètres λ et K_d. Pour le transport de FLA et de PYR, seulement deux couples de paramètres f-λ et K_d-λ ont été considérés comme estimables simultanément mais cette fois f était fortement corrélé à ω et K_d. De plus, le transport de FLA et PYR dans la colonne non saturée contenait plus d'information que ceux dans la colonne saturée en raison de leur degré de sensibilité plus élevé.

Après avoir choisi les paramètres estimables, ces paramètres ont été optimisés. Les paramètres f et Kd ont été estimés avec succès en se basant sur les concentrations d'ACE dans les solutions de lixiviation de la colonne saturée mais la valeur optimisée était entachée d'une forte incertitude. Une échelle de simulation plus longue et des profils de sol plus profonds peuvent être nécessaires pour mieux optimiser ces paramètres. Les faibles valeurs du paramètre f optimisées pour le transport de FLA et de PYR ont confirmé leur niveau important de transport hors équilibre chimique.

Les résultats de l'optimisation pour le transport d'ACE dans la colonne non saturée sont très incertains surtout quand quatre paramètres sont optimisés simultanément car les corrélations entres paramètres f-K_d et/ou f-λ ont fait augmenter les incertitudes. Par contre, les résultats de l'optimisation de paramètres f et K_d pour le transport de FLA et de PYR dans la colonne non saturée sont plus élevés et beaucoup plus fiables que ceux pour le transport de FLA et de PYR dans la colonne saturée. On peut penser que ceux-ci sont dus à l'effet de la vitesse de l'eau sur le transport hors équilibre chimique de FLA et de PYR, c'est-à-dire quand le flux d'eau est plus lent, il y a plus de sites qui sont à équilibre avec la phase liquide.

Ainsi, ce travail a permis d'étudier en détail la sensibilité, l'estimabilité et l'optimisation de paramètres dans différentes situations. Cette approche pourrait et devrait être appliquée avant toute recherche de paramètres par méthode inverse.

En perspective à ce travail, je proposerais les points suivants :

- Tout d'abord, pour augmenter la fiabilité de la modélisation, il faudrait en premier lieu multiplier les mesures pour obtenir les données les plus précises possibles. Par exemple les calculs concernant les parcelles auraient pu être notablement améliorés si on avait pu disposer de davantage de mesures et choisir une réponse plus fiable que la simple hauteur d'eau dans les bacs. Ceci démontre sans ambiguïté la nécessité de prendre en compte la modélisation dès le départ du travail expérimental afin de ne pas oublier de mesurer des grandeurs qui seront importantes pour la modélisation.
- Une autre perspective serait de collecter des données et établir des bases car beaucoup de données ne peuvent pas être trouvées dans la bibliographie. Par exemple, en ce qui concerne

l'influence des plantes, on trouve dans la bibliographie des données sur des plantes très étudiées (maïs, luzerne etc.) mais pas forcément sur les plantes qui ont été utilisées dans les parcelles.

- En ce qui concerne le transport des HAP en zone non saturée, la modélisation pourrait être améliorée si on avait une meilleure connaissance des processus qui le gouvernent. En particulier on aimerait pouvoir décrire de manière plus précise et quantifier le transfert des HAP de la phase solide vers la phase aqueuse. Il serait bon également de pouvoir prendre en compte le transport colloïdal.
- Enfin, la modélisation devrait progresser grâce au couplage de codes décrivant le transport de l'eau et les processus physico-chimiques assez simples (comme Hydrus) avec des codes de spéciation. L'utilisation d'algorithmes d'optimisation globaux constituerait aussi une avancée par rapport à celui de Levenberg-Marquart.

Ainsi ce travail de thèse n'est pas une fin en soi mais ouvre la voie vers d'autres recherches qui permettraient d'encore mieux décrire et prévoir le transport de l'eau et des HAP dans les sols de friches industrielles.

Références

Abbasi, F., Feyen, J. and van Genuchten, M.T., 2004. Two-dimensional simulation of water flow and solute transport below furrows: Model calibration and validation. J. Hydrol., 290(1-2): 63-79.

Abbasi, F., Simunek, J., Feyen, J., van Genuchten, M.T. and Shouse, P.J., 2003. Simultaneous Inverse Estimation of Soil Hydraulic and Solute Transport Parameters from Transient Field Experiments: Homogeneous Soil. Transactions of the American Society of Agricultural Engineers, 46(4): 1085-1095.

Abbaspour, K.C., Schulin, R. and Van Genuchten, M.T., 2001. Estimating unsaturated soil hydraulic parameters using ant colony optimization. Adv. Water Resour., 24(8): 827-841.

Abbaspour, K.C., Sonnleitner, M.A. and Schulin, R., 1999. Uncertainty in estimation of soil hydraulic parameters by inverse modeling: Example lysimeter experiments. Soil Sci. Soc. Am. J., 63(3): 501-509.

Abdou, H.M. and Flury, M., 2004. Simulation of water flow and solute transport in free-drainage lysimeters and field soils with heterogeneous structures. Eur. J. Soil Sci., 55(2): 229-241.

Al-Jabri, S.A., Horton, R. and Jaynes, D.B., 2002. A point-source method for rapid simultaneous estimation of soil hydraulic and chemical transport properties. Soil Sci. Soc. Am. J., 66(1): 12-18.

Allen, R.K., Pereira, L.S., Raes, D. and M. Smith. 1998. Crop evapotranspiration. Guideline for computing crop water requirements. FAO Irrigation and Drainage Paper No. 56. United Nations Food and Agricultural Organization, Rome.

Alletto, L., Coquet, Y., Vachier, P. and Labat, C., 2006. Hydraulic conductivity, immobile water content, and exchange coefficient in three soil profiles. Soil Sci. Soc. Am. J., 70(4): 1272-1280.

Anderson, M.P., 1984. Movement of contaminants in groundwater: Groundwater transport-advection and dispersion. In: N.A. Press (Editor), In Groundwater Contamination, Studies in Geophysics, Washington, D.C., pp. pp. 37-45.

Bache, B.W. and Williams, E.G., 1971. A phosphate sorption index for soils. Eur. J. Soil Sci., 22(3): 289-296.

Bard, Y., 1974. Nonlinear parameter estimation, Academic Press, New York.

Benhabib, K., Faure, P., Sardin, M. and Simonnot, M.-O., 2010. Characteristics of a solid coal tar sampled from a contaminated soil and of the organics transferred into water. Fuel, 89 (2), pp. 352-359.

Blaney, H.F. and Criddle, W.D., 1950. Determining water requirements in irrigation areas from climatological and irrigation data., USDA, SCS-TP96.

Boateng, S. and Cawlfield, J.D., 1999. Two-dimensional sensitivity analysis of contaminant transport in the unsaturated zone. Ground Water, 37(2): 185-193.

Boivin, A., Simunek, J., Schiavon, M. and Van Genuchten, M.T., 2006. Comparison of pesticide transport processes in three tile-drained field soils using HYDRUS-2D. Vadose Zone J., 5(3): 838-849.

Brooks, R.H. and Corey, A., 1964. Hydraulic properties of porous media, Hydrology Paper 3, Colorado State University., Fort Collins, CO.

Butters, G.L., W.A. Jury and F.F. Ernst, 1989. Field scale transport of bromide in an unsaturated soil 1. Experimental methodology and results. Water Resour. Res., 25: 1575-1581.

Campbell, G.S., 1974. A method for determining unsatured conductivity moisture retention data. Soil Sci., 117(6): 311-314.

Cey, E.E., Rudolph, D.L. and Passmore, J., 2009. Influence of macroporosity on preferential solute and colloid transport in unsaturated field soils. J. Contam. Hydrol., 107(1-2): 45-57.

Clapp, R.B. and Hornberger, G.M., 1978. Empirical equations for some soil hydraulic properties. Water Resour. Res., 14(4): 601-604.

Contardi, J.S., Turner, D.R. and Ahn, T.M., 2001. Modeling colloid transport for performance assessment. J. Contam. Hydrol., 47(2-4): 323-333.

DeNovio, N.M., saiers, J.E. and Ryan, J.N., 2004. Colloid Movement in Unsaturated Porous Media. Recent Advances and Future Directions. Vadose Zone J., 3: 338-351.

Dong, H. et al., 2002. Simultaneous transport of two bacterial strains in intact cores from Oyster, Virginia: Biological effects and numerical modeling. Appl. Environ. Microbiol., 68(5): 2120-2132.

Durner, W., 1994. Hydraulic conductivity estimation for soils with heterogeneous pore structure. Water Resour. Res., 30(2): 211-223.

Durner, W., Jansen, U. and Iden, S.C., 2008. Effective hydraulic properties of layered soils at the lysimeter scale determined by inverse modelling. Eur. J. Soil Sci., 59(1): 114-124.

Eching, S.O. and Hopmans, J.W., 1993. Optimization of hydraulic functions from transient outflow and soil water pressure data. Soil Sci. Soc. Am. J., 57(5): 1167-1175.
Evett, S.R., Towell, T.A., Todd, R.W., Schneider A.D., and Tolk, J.A., 2000. Alfalfa reference et measurement and prediction. Proceedings on the 4th Decennial National Irrigation Sym., Nov. 14-16, 2000, Phoenix, AZ.: 266-272.
Fitter, A.H. and Sutton, S.D., 1975. The use of the freundlich isotherm for soil phosphate sorption data. Eur. J. Soil Sci., 26(3): 241-246.
Flerchinger, G.N., Hanson, C.L. and Wight, J.R., 1996. Modeling evapotranspiration and surface energy budgets across a watershed. Water Resour. Res., 32(8): 2539-2548.
Fluhler, H., Durner, W. and Flury, M., 1996. Lateral solute mixing processes - A key for understanding field-scale transport of water and solutes. Geoderma, 70(2-4): 165-183.
Flury, M. and Qiu, H., 2008. Modeling colloid-facilitated contaminant transport in the vadose zone. Vadose Zone J., 7(2): 682-697.
Fortin, J., Gagnon-Bertrand, E., Vezina, L. and Rompre, M., 2002. Organic compounds in the environment: Preferential bromide and pesticide movement to tile drains under different cropping practices. J. Environ. Qual., 31(6): 1940-1952.
Freundlich, H., 1909. *Kapillarchemie; eine Darstellung der Chemie der Kolloide und verwandter Gebiete*., Akademische Verlagsgellschaft, Leipzig, Germany.
Gardenas, A.I., Simunek, J., Jarvis, N. and van Genuchten, M.T., 2006. Two-dimensional modelling of preferential water flow and pesticide transport from a tile-drained field. J. Hydrol., 329(3-4): 647-660.
Gerke, H.H., 2006. Preferential flow descriptions for structured soils. J. Plant Nutr. Soil Sci., 169(3): 382-400.
Gerke, H.H. and Kohne, J.M., 2004. Dual-permeability modeling of preferential bromide leaching from a tile-drained glacial till agricultural field. J. Hydrol., 289(1-4): 239-257.
Gerke, H.H. and van Genuchten, M.T., 1993. A dual-porosity model for simulating the preferential movement of water and solutes in structured porous media. Water Resour. Res., 29(2): 305-319.
Gerke, H.H. and van Genuchten, M.T., 1996. Macroscopic representation of structural geometry for simulating water and solute movement in dual-porosity media. Adv. Water Resour., 19(6): 343-357.
Geyer, T., Birk, S., Licha, T., Liedl, R. and Sauter, M., 2007. Multitracer test approach to characterize reactive transport in karst aquifers. Ground Water, 45(1): 36-45.
Goppert, N. and Goldscheider, N., 2008. Solute and colloid transport in karst conduits under low- and high-flow conditions. Ground Water, 46(1): 61-68.
Grolimund, D., Borkovec, M., Barmettler, K. and Sticher, H., 1996. Colloid-facilitated transport of strongly sorbing contaminants in natural porous media: A laboratory column study. Environ. Sci. and Technol., 30(10): 3118-3123.
Gujisaite, V., 2008. Transport réactif en milieux poreux non saturés, Thèse, Institut National Polytechnique de Lorraine, Nancy, 231 p pp.
Gunary, D., 1970. A new adsorption isotherm for phosphate in soil. Eur. J. Soil Sci., 21(1): 72-77.
Gupta, H.V., Sorooshian, S. and Yapo, P.O., 1998. Toward improved calibration of hydrologic models: Multiple and noncommensurable measures of information. Water Resour. Res., 34(4): 751-763.
Hamby, D.M., 1994. A review of techniques for parameter sensitivity analysis of environmental models. Environ. Monit. Assess., 32(2): 135-154.
Hansen, S., Jensen, H.E., Nielsen, N.E. and Sveden, H., 1990. DAISY: Soil Plant Atmosphere System Model. NPO Report No. A 10, The National Agency for Environmental Protection, Copenhagen.
Haws, N.W., Rao, P.S.C., Simunek, J. and Poyer, I.C., 2005. Single-porosity and dual-porosity modeling of water flow and solute transport in subsurface-drained fields using effective field-scale parameters. J. Hydrol., 313(3-4): 257-273.
Heidmann, T., Thomsen, A. and Schelde, K., 2000. Modelling soil water dynamics in winter wheat using different estimates of canopy development. Ecol. Model., 129(2-3): 229-243.
Hendrickx, J.M.H. and Flury, M., 2001. Uniform and preferential flow mechanisms in the vadose zone. p. 149-187. In: N.A. Press (Editor), *In* Conceptual models of flow and transport in the fractured vadose zone., Washington, DC.
Hermsmeyer, D., Ilsemann, J., Bachmann, J., Van Der Ploeg, R.R. and Horton, R., 2002. Model calculations of water dynamics in lysimeters filled with granular industrial wastes. J. Plant Nutr. Soil Sci., 165(3): 339-346.
Hopmans, J.W. and Simunek, J., 1999a. Review of inverse estimation of soil hydraulic properties. In: L. M.Th. van Genuchten, F.J., Wu, L. (Editor), Proceedings of the International Workshop, Characterization and measurement of the hydraulic properties of unsaturated porous media., University of California, Riverside, CA, pp. 643-659.

Hopmans, J.W. and Simunek, J., 1999b. Review of inverse estimation of soil hydraulic properties. p. 643-659. *In* M.Th. van Genuchten et al. (ed.) Characterization and measurement of the hydraulic properties of unsaturated porous media, University of California, Riverside.

Ines, A.V.M. and Droogers, P., 2002. Inverse modelling in estimating soil hydraulic functions: A Genetic Algorithm approach. Hydrol. Earth Syst. Sci., 6(1): 49-65.

Ingwersen, J., Bucherl, B., Neumann, G. and Streck, T., 2006. Cadmium leaching from micro-lysimeters planted with the hyperaccumulator *Thlaspi caerulescens*: Experimental findings and modeling. J. Environ. Qual., 35(6): 2055-2065.

Jacques, D. and Simunek, J., 2005. User manual of the multicomponent variably-saturated flow and transport model HP1: Description, verification and examples. Version 1.0, BLG-998 Rep.SCK-CEN, Mol, Belgium.

Jacques, D., Simunek, J., Timmerman, A. and Feyen, J., 2002. Calibration of Richards' and convection-dispersion equations to field-scale water flow and solute transport under rainfall conditions. J. Hydrol., 259(1-4): 15-31.

Jansson, P.E. and Karlberg, L., 2001. Coupled heat and mass transfer model for soil-plant-atmosphere systems. Royal Institute of Technology, Dept of Civil and Environmental Engineering, Stockholm.

Jarvis, N.J., 1994. The MACRO model (Version 3.1), Technical description and sample simulations. Reports and Dissertations 19, Dept. Soil Sci., Swedish Univ. Agric. Sci., Uppsala, Sweden, 51 pp pp.

Javaux, M., Kasteel, R., Vanderborght, J. and Vanclooster, M., 2006a. Interpretation of dye transport in a macroscopically heterogeneous, unsaturated subsoil with a one-dimensional model. Vadose Zone J., 5(2): 529-538.

Jayasankar, B.R., Ben-Zvi, A. and Huang, B., 2009. Identifiability and estimability study for a dynamic solid oxide fuel cell model. Comput. Chem. Eng., 33(2): 484-492.

Jaynes, D.B., Ahmed, S.I., Kung, K.-J.S. and Kanwar, R.S., 2001. Temporal dynamics of preferential flow to a subsurface drain. Soil Sci. Soc. Am. J., 65(5): 1368-1376.

Jaynes, D.B., Logsdon, S.D. and Horton, R., 1995. Field method for measuring mobile/immobile water content and solute transfer rate coefficient. Soil Sci. Soc. Am. J., 59(2): 352-356.

Johnson, A. et al., 2003. High-resolution laboratory lysimeter for automated sampling of tracers through a 0.5 m soil block. J. Autom. Methods Manage. Chem., 25(2): 43-49.

Jorgensen, P.R., Helstrup, T., Urup, J. and Seifert, D., 2004. Modeling of non-reactive solute transport in fractured clayey till during variable flow rate and time. J. Contam. Hydrol., 68(3-4): 193-216.

Jouannin, F., 2004. Etudes de la mobilité des hydrocarbures aromatiques polycycliques (HAP) contenu dans un sol industriel pollués, Thèse, Institut National des Sciences Appliqués de Lyon, Lyon, 165 p pp.

Kan, A.T. and Tomson, M.B., 1990. Ground water transport of hydrophobic organic compounds in the presence of dissolved organic matter. Environ. Toxicol. Chem., 9(3): 253-263.

Karathanasis, A.D., 1999. Subsurface Migration of Copper and Zinc Mediated by Soil Colloids. Soil Sci. Soc. Am. J., 63: 830-838.

Kasteel, R., Putz, T. and Vereecken, H., 2007. An experimental and numerical study on flow and transport in a field soil using zero-tension lysimeters and suction plates. Eur. J. Soil Sci., 58(3): 632-645.

Kelleners, T.J., Soppe, R.W.O., Ayars, J.E., Simunek, J. and Skaggs, T.H., 2005. Inverse analysis of upward water flow in a groundwater table lysimeter. Vadose Zone J.(4): 558-572.

Kodesova, R., Kozak, J., Simunek, J. and Vacek, O., 2005. Single and dual-permeability models of chlorotoluron transport in the soil profile. Plant Soil Environ., 51(7): 310-315.

Kohne, J.M. and Gerke, H.H., 2005. Spatial and Temporal Dynamics of Preferential Bromide Movement towards a Tile Drain. Vadose Zone J., 4: 79-88.

Kohne, J.M., Kohne, S., Mohanty, B.P. and Simunek, J., 2004. Inverse Mobile–Immobile Modeling of Transport During Transient Flow: Effects of Between-Domain Transfer and Initial Water Content. Vadose Zone J., 3: 1309-1321.

Kohne, J.M., Kohne, S. and Simunek, J., 2006. Multi-process herbicide transport in structured soil columns: Experiments and model analysis. J. Contam. Hydrol., 85(1-2): 1-32.

Kohne, J.M., Kohne, S. and Simunek, J., 2009. A review of model applications for structured soils: a) Water flow and tracer transport. J. Contam. Hydrol., 104(1-4): 4-35.

Kohne, J.M., Kohne, S. and Simunek, J., 2009b. A review of model applications for structured soils: b) Pesticide transport. J. Contam. Hydrol., 104(1-4): 36-60.

Kohne, J.M. and Mohanty, B.P., 2005. Water flow processes in a soil column with a cylindrical macropore: Experiment and hierarchical modeling. Water Resour. Res., 41(3): 1-17.

Kohne, J.M., Mohanty, B.P. and Simunek, J., 2006. Inverse dual-permeability modeling of preferential water flow in a soil column and implications for field-scale solute transport. Vadose Zone J., 5(1): 59-76.

Kohne, J.M., Mohanty, B.P., Simunek, J. and Gerke, H.H., 2004. Numerical evaluation of a second-order water transfer term for variably saturated dual-permeability models. Water Resour. Res., 40(7): W074091-W0740914.

Kohne, S., Lennartz, B., Kohne, J.M. and Simunek, J., 2006. Bromide transport at a tile-drained field site: experiment, and one- and two-dimensional equilibrium and non-equilibrium numerical modeling. J. Hydrol., 321(1-4): 390-408.

Komnitsas, K., Bartzas, G. and Paspaliaris, I., 2006. Inorganic contaminant fate assessment in zero-valent iron treatment walls. Environmental Forensics, 7(3): 207-217.

Kool, J.B., Parker, J.C. and van Genuchten, M.T., 1987. Parameter estimation for unsaturated flow and transport models - A review. J. Hydrol., 91(3-4): 255-293.

Kosugi, K., 1996. Lognormal distribution model for unsaturated soil hydraulic properties. Water Resour. Res., 32(9): 2697-2703.

Kou, B., McAuley, K.B., Hsu, C.C., Bacon, D.W. and Yao, K.Z., 2005. Mathematical model and parameter estimation for gas-phase ethylene homopolymerization with supported metallocene catalyst. Ind. Eng. Chem. Res., 44(8): 2428-2442.

Lambot, S., Javaux, M., Hupet, F. and Vanclooster, M., 2002. A global multilevel coordinate search procedure for estimating the unsaturated soil hydraulic properties. Water Resour. Res., 38(11): 61-615.

Langmuir, I., 1918. The adsorption of gases on plane surfaces of glass, mica and platinum. J. Am. Chem. Soc., 40(9): 1361-1403.

Larsbo, M. and Jarvis, N., 2005. Simulating solute transport in a structured field soil: Uncertainty in parameter identification and predictions. J. Environ. Qual., 34(2): 621-634.

Larsbo, M. and Jarvis, N., 2006. Information content of measurements from tracer microlysimeter experiments designed for parameter identification in dual-permeability models. J. Hydrol., 325(1-4): 273-287.

Legates, D.R. and McCabe Jr., G.J., 1999. Evaluating the use of 'goodness-of-fit' measures in hydrologic and hydroclimatic model validation. Water Resour. Res., 35(1): 233-241.

Leij, F.J. and Bradford, S.A., 1994. 3DADE: A computer program for evaluating three-dimensional equilibrium solute transport in porous media. *Research Report No.* 134, U.S. Salinity Laboratory, USDA, ARS, Riverside, CA.

Leij, F.J. and Toride, N., 1997. N3DADE:A computer program for evaluating nonequilibrium three-dimensional equilibrium solute transport in porous media. *Research Report No.* 143, U.S. Salinity Laboratory, USDA, ARS, Riverside, CA.

Lenhart, T., Eckhardt, K., Fohrer, N. and Frede, H.-G., 2002. Comparison of two different approaches of sensitivity analysis. Phys. Chem. Earth., 27(9-10): 645-654.

Lindqvist, R. and Enfield, C.G., 1992. Biosorption of dichlorodiphenyltrichloroethane and hexachlorobenzene in groundwater and its implications for facilitated transport. Appl. Environ. Microbiol., 58(7): 2211-2218.

Lindstrom, F.T., Haque, R., Freed, V.H. and Boersma, L., 1967. Theory on the movement of some herbicides in soils linear diffusion and convection of chemicals in soils. Environ. Sci. and Technol., 1(7): 561-565.

Luster, J. et al., 2008. Initial changes in refilled lysimeters built with metal polluted topsoil and acidic or calcareous subsoils as indicated by changes in drainage water composition. Water, Air, and Soil Pollution: Focus, 8(2): 163-176.

Magee, B.R., Lion, L.W. and Lemley, A.T., 1991. Transport of dissolved organic macromolecules and their effect on the transport of phenanthrene in porous media. Environ. Sci. and Technol., 25(2): 323-331.

Mahmood-Ul-Hassan, M., Akhtar, M.S. and Nabi, G., 2008. Boron and Zinc Transport Through Intact Columns of Calcareous Soils. Pedosphere, 18(4): 524-532.

Majdoub, R., Gallichand, J. and Caron, J., 2001. Simulation of bromide leaching in pan lysimeters using the numerical method of lines. Revue des Sciences de l'Eau, 14(4): 465-488.

Mansfeldt, T., Leyer, H., Barmettler, K. and Kretzschmar, R., 2004. Cyanide leaching from soil developed from coking plant purifier waste as influenced by citrate. Vadose Zone J., 3: 471-479.

Maraqa, M.A., 2001. Prediction of mass-transfer coefficient for solute transport in porous media. J. Contam. Hydrol., 50(1-2): 1-19.

McCarthy, J.F. and McKay, L.D., 2004. Colloid Transport in the Subsurface: Past, Present, and Future Challenges. Vadose Zone J., 3: 326-337.

Meissner, R., Seeger, J., Rupp, H., Seyfarth, M. and Borg, H., 2007. Measurement of dew, fog, and rime with a high-precision gravitation lysimeter. J. Plant Nutr. Soil Sci., 170(3): 335-344.

Mertens, J., Madsen, H., Feyen, L., Jacques, D. and Feyen, J., 2004. Including prior information in the estimation of effective soil parameters in unsaturated zone modelling. J. Hydrol., 294(4): 251-269.

Mertens, J., Stenger, R. and Barkle, G.F., 2006. Multiobjective inverse modeling for soil parameter estimation and model verification. Vadose Zone J., 5(3): 917-933.
Michel, J., 2009. Transport d'hydrocarbures aromatiques polycycliques et de métaux dans les sols non saturés. PhD. Thesis, Nancy Université INPL, Nancy, 252 p pp.
Millington, R.J. and Quirk, J.M., 1961. Permeability of porous solids. Transactions of the Faraday Society, 57: 1200-1207.
Monteith, J.L., 1965. Evaporation and environment. Symp. Soc. Exp. Biol., 19: 205-234.
Mualem, Y., 1976. New model for predicting the hydraulic conductivity of unsaturated porous media. Water Resour. Res., 12(3): 513-522.
Nghi, V. V., Dung, D.D., Lam, D.T., 2008. Potential evapotranspiration estimation and its effect on hydrological model response at the Nong Son Basin. VNU Journal of Science, Earth Sciences, 24:213-228.
Ngo, V.V., Latifi, A., Michel, J., Lucas, L. and Simonnot, M.O., 2009. Estimability analysis of single and dual-porosity model parameters based on lysimeter tracing Vadose Zone J., submitted.
Noell, A.L., Thompson, J.L., Corapcioglu, M.Y. and Triay, I.R., 1998. The role of silica colloids on facilitated cesium transport through glass bead columns and modeling. J. Contam. Hydrol., 31(1-2): 23-56.
Olyphant, G.A., 2003. Temporal and spatial (down profile) variability of unsaturated soil hydraulic properties determined from a combination of repeated field experiments and inverse modeling. J. Hydrol., 281(1-2): 23-35.
Pang, L. and Simunek, J., 2006. Evaluation of bacteria-facilitated cadmium transport in gravel columns using the HYDRUS colloid-facilitated solute transport model. Water Resour. Res., 42(12).
Parker, J.C. and van Genuchten, M.T., 1984. Determining transport parameters from laboratory and field tracer experiments. *Bull*. 84-3, Va Agric. Exp. St., Blacksburg,VA.
Penman, H.L., 1948. Natural evaporation from open water, bare soil, and grass. Proceedings the Royal of Society London A, 193: 120-146.
Piggott, J.H. and Cawlfield, J.D., 1996. Probabilistic sensitivity analysis for one-dimensional contaminant transport in the vadose zone. J. Contam. Hydrol., 24(2): 97-115.
Pot, V. et al., 2005. Impact of rainfall intensity on the transport of two herbicides in undisturbed grassed filter strip soil cores. J. Contam. Hydrol., 81(1-4): 63-88.
Ramos, T.B., Goncalves, M.C., Martins, J.C., van Genuchten, M.T. and Pires, F.P., 2006. Estimation of soil hydraulic properties from numerical inversion of tension disk infiltrometer data. Vadose Zone J., 5(2): 684-696.
Rasse, D.P., Smucker, A.J.M. and Santos, D., 2000. Alfalfa root and shoot mulching effects on soil hydraulic properties and aggregation. Soil Sci. Soc. Am. J., 64(2): 725-731.
Rocha, D., Abbasi, F. and Feyen, J., 2006. Sensitivity analysis of soil hydraulic properties on subsurface water flow in furrows. J. Irrig. Drain. E., 132(4): 418-424.
Russo, D., Bresler, E., Shani, U. and Parker, J.C., 1991a. Analyses of infiltration events in relation to determining soil hydraulic properties by inverse problem methodology. Water Resour. Res., 27(6): 1361-1373.
Russo, D., Bresler, E., Shani, U. and Parker, J.C., 1991b. Analysis of infiltration events in relation to determining soil hydraulic properties by inverse problem methodology. Water Resour. Res., 27(6): 1361-1373.
Ryan, J.N. and Elimelech, M., 1996. Colloid mobilization and transport in groundwater. Colloids and Surfaces A: Physicochemical and Engineering Aspects, 107: 1-56.
Sander, T. and Gerke, H.H., 2007. Preferential flow patterns in paddy fields using a dye tracer. Vadose Zone J., 6(1): 105-115.
Sander, T. and Gerke, H.H., 2009. Modelling field-data of preferential flow in paddy soil induced by earthworm burrows. J. Contam. Hydrol., 104(1-4): 126-136.
Sardin, M., Schweich, D., Leij, F.J. and Van Genuchten, M.T., 1991a. Modeling the nonequilibrium transport of linearly interacting solutes in porous media: a review. Water Resour. Res., 27(9): 2287-2307.
Schaap, M.G., Leij, F.J. and Van Genuchten, M.T., 2001. Rosetta: A computer program for estimating soil hydraulic parameters with hierarchical pedotransfer functions. J. Hydrol., 251(3-4): 163-176.
Schoen, R., Gaudet, J.P. and Bariac, T., 1999. Preferential flow and solute transport in a large lysimeter, under controlled boundary conditions. J. Hydrol., 215(1-4): 70-81.
Schwartz, R.C. and Evett, S.R., 2003. Conjunctive use of tension infiltrometry and time-domain reflectometry for inverse estimation of soil hydraulic properties. Vadose Zone J., 2: 530-538.
Schwartz, R.C., K.J. McInnes, A.S.R. Juo, and C.E. Cervantes, 1999. The vertical distribution of a dye tracer in a layered soil. Soil Sci., 164: 561-573.
Schwartz, R.C., McInnes, K.J., Juo, A.S.R. and Cervantes, C.E., 1999. The vertical distribution of a dye tracer in a layered soil. Soil Sci., 164(8): 561-573.

Schwarzel, K., Simunek, J., Stoffregen, H., Wessolek, G. and Van Genuchten, M.T., 2006. Estimation of the unsaturated hydraulic conductivity of peat soils: Laboratory versus field data. Vadose Zone J., 5(2): 628-640.
Sen, T.K. and Khilar, K.C., 2006. Review on subsurface colloids and colloid-associated contaminant transport in saturated porous media.Adv. Colloid. Interface. Sci., 119(2-3): 71-96.
Sen, T.K., Nalwaya, N. and Khilar, K.C., 2002. Colloid-associated contaminant transport in porous media: 2. Mathematical modeling. AIChE Journal, 48(10): 2375-2385.
Seyfarth, M. and Reth, S., 2008. Lysimeter Soil Retriever (LSR)-an application of a new technique for retrieving soils from lysimeters. Water, Air, and Soil Pollution: Focus, 8(2): 227-231.
Shapiro, R.E. and Fried, M., 1959. Relative release and retentiveness of soil phosphates. Soil Sci. Soc. Am. J., 23: 195-198.
Si, B.C. and Kachanoski, R.G., 2000. Estimating soil hydraulic properties during constant flux infiltration: Inverse procedures. Soil Sci. Soc. Am. J., 64(2): 439-449.
Sibbesen, E., 1981. Some new equations to describe phosphate sorption by soils. Eur. J. Soil Sci., 32(1): 67-74.
Simunek, J., Angulo-Jaramillo, R., Schaap, M.G., Vandervaere, J.-P. and Van Genuchten, M.T., 1998a. Using an inverse method to estimate the hydraulic properties of crusted soils from tension-disc infiltrometer data. Geoderma, 86(1-2): 61-81.
Simunek, J., He, C., Pang, L. and Bradford, S.A., 2006a. Colloid-facilitated solute transport in variably saturated porous media: Numerical model and experimental verification. Vadose Zone J., 5(3): 1035-1047.
Simunek, J., Jarvis, N.J., Van Genuchten, M.T. and Gardenas, A., 2003. Review and comparison of models for describing non-equilibrium and preferential flow and transport in the vadose zone. J. Hydrol., 272(1-4): 14-35.
Simunek, J., Sejna, M. and Van Genuchten, M.T., 1998. The HYDRUS-1D software package for simulating the one-dimensional movement of water, heat, and multiple solutes in variably-saturated media. Version 2.0. IGWMC-TPS-70., International Ground Water Modeling Center, Colorado School of Mines, Golden.
Simunek, J. and van Genuchten, M.T., 1996. Estimating unsaturated soil hydraulic properties from tension disc infiltrometer data by numerical inversion. Water Resour. Res., 32(9): 2683-2696.
Simunek, J. and van Genuchten, M.T., 1997. Estimating unsaturated soil hydraulic properties from multiple tension disc infiltrometer data. Soil Sci., 162(6): 383-398.
Simunek, J. and van Genuchten, M.T., 2006. Contaminant transport in the unsaturated zone: theory and modeling. In: J.W. Delleur (Editor), The handbook of groundwater engineering, New York, pp. 988 p.
Simunek, J. and van Genuchten, M.T., 2008. Modeling nonequilibrium flow and transport processes using HYDRUS. Vadose Zone J., 7(2): 782-797.
Simunek, J., Van Genuchten, M.T. and Sejna, M., 2005b. The HYDRUS-1D software package for simulating the one-dimensional movement of water, heat, and multiple solutes in variably-saturated media. Version 3.0, HYDRUS Software Series 1,, Department of Environmental Sciences, University of California Riverside, Riverside, CA, 270pp pp.
Simunek, J., van Genuchten, M.T., Sejna, M., Toride, N. and Leij, F.J., 1999. The STANMODcomputer software for evaluating solute transport in porous media using analytical solutions of convection-dispersion equation. Versions 1.0 and 2.0, IGWMC-TPS-71., International Ground Water Modeling Center, Colorado School of Mines, Golden, Colorado, 32 pp pp.
Simunek, J., Wendroth, O., Wypler, N. and Van T, M., 2001. Non-equilibrium water flow characterized by means of upward infiltration experiments. Eur. J. Soil Sci., 52(1): 13-24.
Sirguey, C., Tereza de Souza e Silva, P., Schwartz, C. and Simonnot, M.-O., 2008. Impact of chemical oxidation on soil quality. Chemosphere, 72(2): 282-289.
Sonnleitner, M.A., Abbaspour, K.C. and Schulin, R., 2003. Hydraulic and transport properties of the plant-soil system estimated by inverse modelling. Eur. J. Soil Sci., 54(1): 127-138.
Sprague, L.A., Herman, J.S., Hornberger, G.M. and Mills, A.L., 2000. Atrazine adsorption and colloid-facilitated transport through the unsaturated zone. J. Environ. Qual., 29(5): 1632-1641.
Thiele-Bruhn, S., 2003. Pharmaceutical antibiotic compounds in soils - A review. J. Plant Nutr. Soil Sci., 166(2): 145-167.
Tilahun, K., Botha, J.F. and Bennie, A.T.P., 2005. Transport of bromide in the Bainsvlei soil: Field experiment and deterministic/stochastic model simulation. II. Intermittent water application. Aust. J. Soil Res., 43(1): 81-85.
Tolls, J., 2001. Sorption of veterinary pharmaceuticals in soils: A review. Environ. Sci. and Technol., 35(17): 3397-3406.
Toride, N., Leij, F.J. and Van Genuchten, M.T., 1993. A comprehensive set of analytical solutions for nonequilibrium solute transport with first-order decay and zero-order production. Water Resour. Res., 29(7): 2167-2182.

Toride, N., Leij, F.J. and van Genuchten, M.T., 1995. The CXTFIT code for estimating transport parameters from laboratory or field tracer experiments. Version 2.0, *Research Report No.* 137, U. S. Salinity Laboratory, USDA, ARS, Riverside, CA.

Totsche, K.U., Jann, S. and Kogel-Knabner, I., 2007. Single event-driven export of polycyclic aromatic hydrocarbons and suspended matter from coal tar-contaminated soil. Vadose Zone J., 6(2): 233-243.

Tufenkji, N., 2007. Modeling microbial transport in porous media: Traditional approaches and recent developments. Adv. Water Resour., 30(6-7): 1455-1469.

Twarakavi, N.K.C., Å imÅ¯nek, J. and Schaap, M.G., 2009. Development of pedotransfer functions for estimation of soil hydraulic parameters using support vector machines. Soil Sci. Soc. Am. J., 73(5): 1443-1452.

van Dam, J.C. et al., 1997. Theory of SWAP, version 2.0. simulation of water flow, solute transport and plant growth in the soil-water-atmosphere-plant environment., Dep. of Water Resour. Rep. 71. Tech. Doc. 45. DLO Winand Staring centre, Wageningen, the Netherlands.

van Dam, J.C., Stricker, J.N.M. and Droogers, P., 1994. Inverse method to determine soil hydraulic functions from multistep outflow experiments. Soil Sci. Soc. Am. J., 58(3): 647-652.

van Genuchten, M.T., 1980. A closed-form equation for predicting the hydraulic conductivity of unsaturated soils. Soil Sci. Soc. Am. J., 44(5): 892-898.

van Genuchten, M.T., 1981. Non-equilibrium transport parameters from miscible displacement experiments. Research Report No. 119, U.S. Salinity Laboratory, USDA, ARS, Riverside, CA.

van Genuchten, M.T., Leij, F.J. and Yates, M.V., 1991. The RETC code for quantifying the hydraulic functions of unsaturated soils, Version 1.0., Salinity Laboratory, Departement of Agriculture, Agricultural Research Service, Riverside, California, U.S.

van Genuchten, M.T. and Wierenga, P.J., 1976. Mass transfer studies in sorbing porous media - 1. Analytical solutions. Soil Sci. Soc. Am. J., 40(4): 473-480.

Vanderborght, J., Mallants, D., Vanclooster, M. and Feyen, J., 1997. Parameter uncertainty in the mobile-immobile solute transport model. J. Hydrol., 190(1-2): 75-101.

Vanderborght, J. and Vereecken, H., 2007. Review of dispersivities for transport modeling in soils. Vadose Zone J., 6(1): 29-52.

Ventrella, D., Mohanty, B.P., Simunek, J., Losavio, N. and Van Genuchten, M.T., 2000. Water and chloride transport in a fine-textured soil: Field experiments and modeling. Soil Sci., 165(8): 624-631.

Villermaux, J., 1993. Génie de la réaction chimique (conception et fonctionnement des réacteurs). Lavoisier.

Vinten, A.J.A., Yaron, B. and Nye, P.H., 1983. Vertical transport of pesticides into soil when adsorbed on suspended particles. J. Agric. Food Chem., 31(3): 662-664.

Vogel, T., Gerke, H.H., Zhang, R. and Van Genuchten, M.T., 2000a. Modeling flow and transport in a two-dimensional dual-permeability system with spatially variable hydraulic properties. J. Hydrol., 238(1-2): 78-89.

Vogel, T., Van Genuchten, M.T. and Cislerova, M., 2000b. Effect of the shape of the soil hydraulic functions near saturation on variably-saturated flow predictions. Adv. Water Resour., 24(2): 133-144.

van Gunten, H.R., Waber, U.E. and Krahenbuhl, U., 1988. The reactor accident at Chernobyl: A possibility to test colloid-controlled transport of radionuclides in a shallow aquifer. J. Contam. Hydrol., 2(3): 237-247.

Vrugt, J.A., Bouten, W. and Weerts, A.H., 2001. Information content of data for identifying soil hydraulic parameters from outflow experiments. Soil Sci. Soc. Am. J., 65(1): 19-27.

Walter, E., 1982. Identifiability of state space models with applications to transformation systems. New York, USA: Springer-Verlag.

Wang, T., Zlotnik, V.A., Simunek, J. and Schaap, M.G., 2009. Using pedotransfer functions in vadose zone models for estimating groundwater recharge in semiarid regions. Water Resour. Res., 45(4).

Wegehenkel, M., 2005. Validation of a soil water balance model using soil water content and pressure head data. Hydrol. Process., 19(6): 1139-1164.

Wegehenkel, M., Zhang, Y., Zenker, T. and Diestel, H., 2008. The use of lysimeter data for the test of two soil-water balance models: A case study. J. Plant Nutr. Soil Sci., 171(5): 762-776.

Willmott, C.J., 1981. On the validation of models. Phys. Geogr., 2: 184-194.

Willmott, C.J. et al., 1985. Statistics for the evaluation and comparison of models. J. Geophys. Res, 90: 8995-9005.

Yao, Z.K., Shaw., B.M., Kou., B., Mcauley., K.B. and Bacon., D.W., 2003. Modeling Ethelene/Buten Copolymerization with Multi-site Catalysts: Parameter estimability and Experimental Design. Polym. React. Eng., 11(3): 563-588.

Zhang, P., Simunek, J. and Bowman, R.S., 2004. Nonideal transport of solute and colloidal tracers through reactive zeolite/iron pellets. Water Resour. Res., 40(4): W042071-W0420711.

Annexes

Annexe A:

Procédure de calcul de la matrice Z quand quatre paramètres sont étudiés

```
% ********************************************************************
% We have to read into Matlab the Z sensitivity matrix

Z = xlsread('2SM_Z.xls');
[stk,p]= size(Z);
% stk = s*tk

% ********************************************************************
% STEP 1: Calculate the magnitude of each column in the Z matrix
for j = 1:p
   sum(j) = 0;
    for i = 1:stk
       sum(j) = sum(j)+Z(i,j).^2;
    end;
end;

% ********************************************************************
% STEP 2: Look for the most sensitive parameter
sumI = [sum(1),sum(2),sum(3),sum(4)]; % to add if there are more parameters
P1=max(sumI);

%*********************************************************************
% STEP 3: Mark the corresponding column as XL
[i1,j1]= find(sumI==P1);
XL = Z(1:stk,j1);

%*********************************************************************
% STEP 4 +5: Calculate ZL, from the full sensitivity matrix Z, using the
%           subset of columns XL
ZL = XL*inv(XL'*XL)*XL'*Z;
RL = Z-ZL;

%*********************************************************************
% STEP 6: Calculate the magnitude of each column in the RL matrix and
%         look for the second sensitive parameter
[m,n]=size(RL);
for j = 1:n
  sum(j) = 0;
```

```
   for i = 1:m
      sum(j) = sum(j)+RL(i,j).^2;
   end;
end;
sumII = [sum(1),sum(2),sum(3),sum(4)];
P2= max(sumII);

%*********************************************************************
% Repeat until at the end

% *********************************************************************
[i2,j2]= find(sumII==P2);
XL2 = Z(1:stk,j2);
XLII = [XL XL2];
ZL2 = XLII*inv(XLII'*XLII)*XLII'*Z;
RL2 = Z-ZL2;
[d,v]=size(RL2);
for j = 1:v
  sum(j) = 0;
   for i = 1:d
      sum(j) = sum(j)+RL2(i,j).^2;
   end;
end;
sumIII = [sum(1),sum(2),sum(3),sum(4)];
P3= max(sumIII);

% *********************************************************************

[i3,j3]= find(sumIII==P3);
XL3 = Z(1:stk, j3);
XLIII = [XLII XL3];
ZL3 = XLIII*inv(XLIII'*XLIII)*XLIII'*Z;
RL3 = Z-ZL3;
[q,t]=size(RL3);
for j = 1:t
  sum(j) = 0;
   for i = 1:q
      sum(j) = sum(j)+RL3(i,j).^2;
   end;
end;
sumIV = [sum(1),sum(2),sum(3),sum(4)];
P4= max(sumIV);
 [i4,j4]= find(sumIV==P4);
```

```
%*********************************************************************
C= [j1,j2,j3,j4]
A= [sumI; sumII; sumIII; sumIV];

%*********************************************************************
 B =[C;A]
rep=input(' Do you want to save the calculated data? (y/n)','s');
 if rep=='y'
   filename=input('file name:','s');
     save(filename,'B','-ascii');
 end
```

Annexe B :

Modelling of polycyclic aromatic hydrocarbons leaching through the soil column using MIM model

B.1. Estimability analysis

Table B1. Estimability order (1a, 1c, 1e) and correlations (1b, 1d, 1f) of four solute transport parameters in MIM model based on ACE, FLA, and PYR leaching in the nonsaturated column, respectively

1.

ACE (1a)

f	ω	λ	K_d
167,49	71,11	22,79	166,38
0	68,08	1,28	0,67
0	0	1,24	0,56
0	0	0	0,45
8,42%	**7,13%**	**1,85%**	**7,94%**

(1b)

	f	ω	λ	K_d
f	-	4,26	94,39	99,60
ω		-	3,06	16,67
λ			-	19,68
K_d				-

FLA (1c)

f	λ	ω	K_d
132,77	8,85	1,88	130,26
0	4,85	0,14	0,03
0	0	0,06	0,03
0	0	0	0,03
10,13%	**2,48%**	**1,17%**	**9,93%**

(1d)

	f	λ	ω	K_d
f	-	45,23	92,48	99,98
λ		-	56,46	7,25
ω			-	0,19
K_d				-

PYR (1e)

f	λ	K_d	ω
96,63	6,24	95,33	1,39
0	4,98	0,03	0,09
0	0	0,03	0,03
0	0	0	0,03
8,57%	**2,08%**	**8,44%**	**1,05%**

(1f)

	f	λ	K_d	ω
f	-	20,14	99,96	93,86
λ		-	6,57	67,90
K_d			-	0,02
ω				-

B.2. Parameter optimization

Table B2. Solute transport parameters in the MIM model, with corresponding confidence interval, estimated from measured ACE concentrations in the leaching solution of the nonsaturated column using HYDRUS-1D and also the modified index of agreement (MIA) of the estimation

ACE

	Optimized parameter	MIA	Optimized parameter	MIA	Optimized parameter	MIA
λ	*		*		43.65 (22.25-65.05)	
ω	1.2 E-05 (-1.1 E-02_1.1 E-02)	0.85	2.6 E-03 (-8.9 E-02_9.4 E -02)	0.85	4.8 E -05 (-4.1 E-02_4.1 E-02)	0.85
f	5.11 (3.78-6.45)		*		1.67 (1.67-1.67)	
K_d	*		21.55 (15.12-27.98)		6.59 (6.59-6.59)	

Table B3. Solute transport parameters in the MIM model, as well as its confidence interval, estimated from measured FLA and PYR concentrations, respectively, in the leaching solution of the nonsaturated column using HYDRUS-1D and also the modified index of agreement (MIA) of the estimation

FLA

	Optimized parameter	MIA	Optimized parameter	MIA
λ	19.03 (10.77-27.29)		18.86 (10.7-27.04)	
f	0.33 (0.24-0.42)	0.73	*	0.73
K_d	*		14.18 (10.37-17.99)	

PYR

λ	17.33 (9.73-24.94)		16.84 (8.98-24.70)	
f	0.09 (0.02-0.12)	0.67	*	0.66
K_d	*		26.54 (17.92-35.15)	

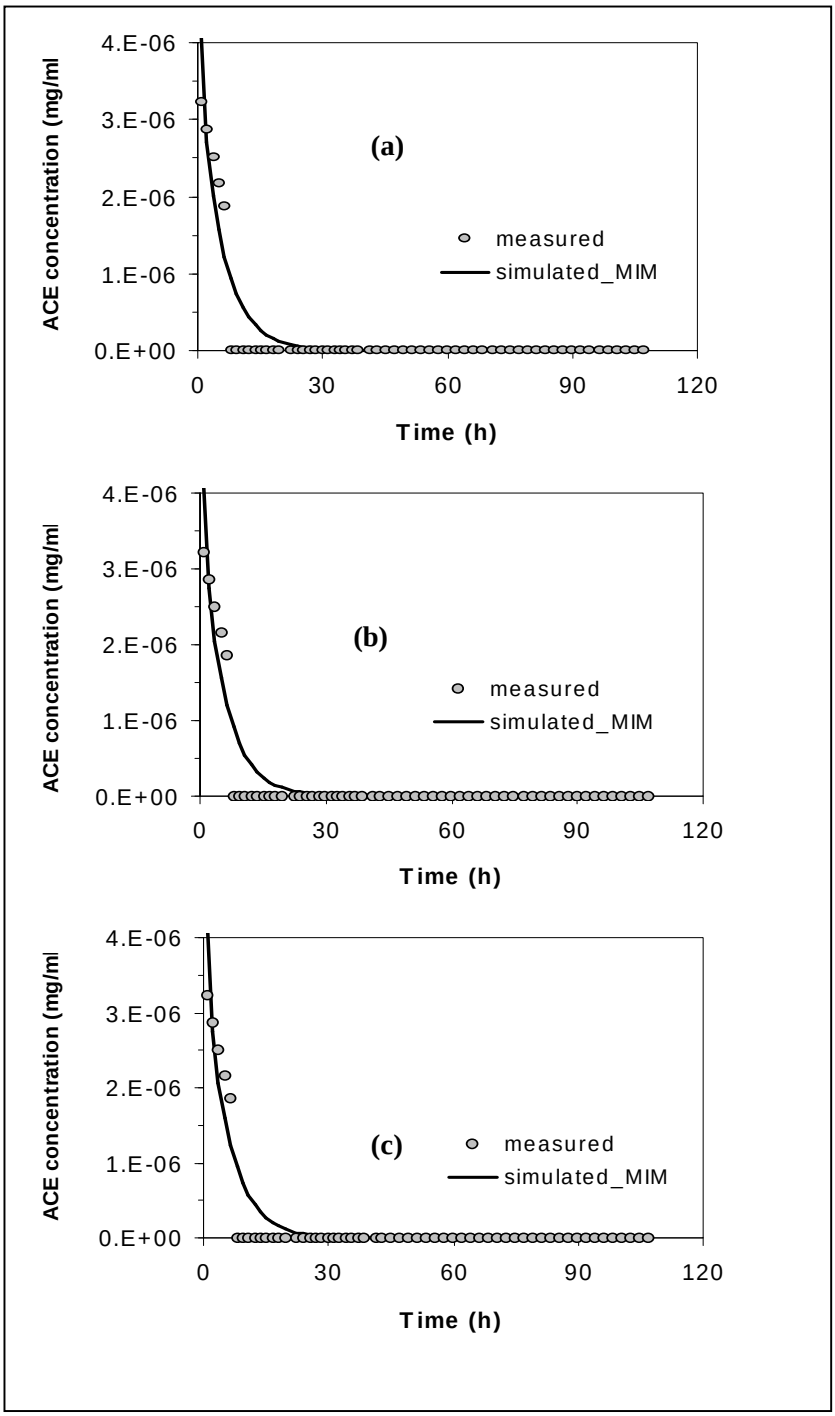

Figure B1. Comparison of the measured and simulated ACE concentrations in the leaching solution of the nonsaturated column: (a) when parameters f and ω were simultaneously optimized, (b) when parameters K_d and ω were simultaneously optimized, and (c) when four parameters f, ω, λ, and K_d were simultaneously op K_d timized

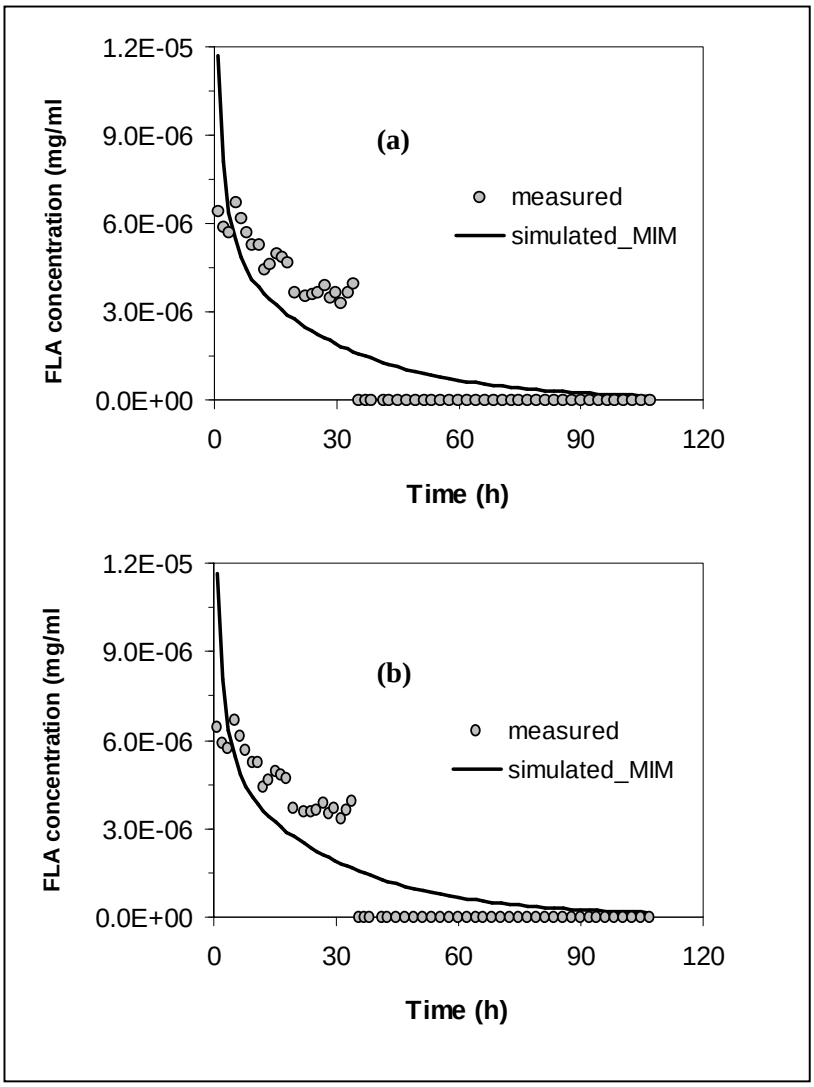

Figure B2. Comparison of the measured and simulated FLA concentrations in the leaching solution of the nonsaturated column: (a) when parameters f and λ were simultaneously optimized based on the observed FLA concentrations; (b) when parameters K_d and λ were simultaneously optimized based on the observed FLA concentrations.

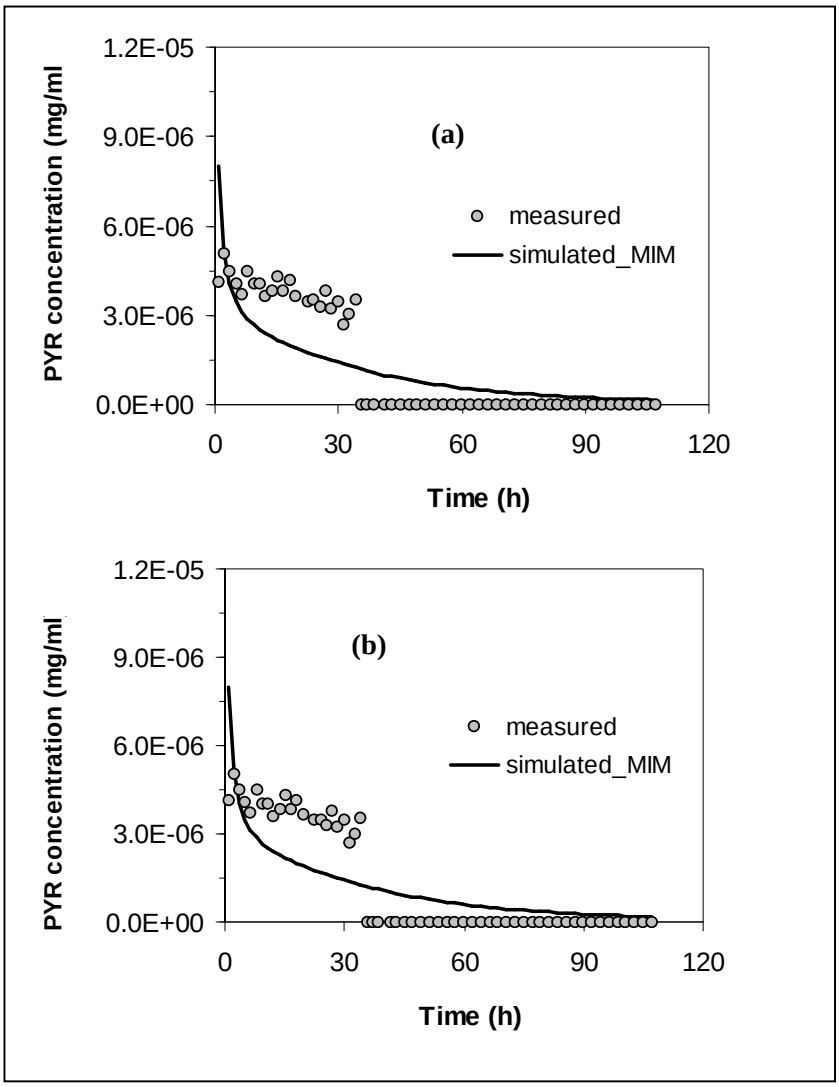

Figure B3. Comparison of the measured and simulated PYR concentrations in the leaching solution of the nonsaturated column: (a) when parameters f and λ were simultaneously optimized based on the observed PYR concentrations; (b) when parameters K_d and λ were simultaneously optimized based on the observed PYR concentrations.

INSTITUT NATIONAL
POLYTECHNIQUE
DE LORRAINE

AUTORISATION DE SOUTENANCE DE THESE
DU DOCTORAT DE L'INSTITUT NATIONAL
POLYTECHNIQUE DE LORRAINE

o0o

VU LES RAPPORTS ETABLIS PAR :
Monsieur Jean-Paul GAUDET, Ingénieur de Recherche, INPG, Grenoble

Monsieur Michel LEGRET, Directeur de Recherche, LCPC, Bougenais Cedex

Le Président de l'Institut National Polytechnique de Lorraine, autorise :

Monsieur NGO Van Viet

à soutenir devant un jury de l'INSTITUT NATIONAL POLYTECHNIQUE DE LORRAINE, une thèse intitulée :

« Modélisation du transport de l'eau et de polluants dans les sols contaminés des friches industrielles »

en vue de l'obtention du titre de :

DOCTEUR DE L'INSTITUT NATIONAL POLYTECHNIQUE DE LORRAINE

Spécialité : « **Génie des procédés et des produits** »

Fait à Vandoeuvre, le 01 décembre 2009

Le Président de l'I.N.P.L.,

F. LAURENT

NANCY BRABOIS
2, AVENUE DE LA
FORET-DE-HAYE
BOITE POSTALE 3
F - 54501
VANDŒUVRE CEDEX

TEL. 33/03.83.59.59.59
FAX 33/03.83.59.59.55

Modélisation du transport de l'eau et des polluants dans les sols contaminés des friches industrielles

Résumé : Les objectifs de la thèse sont de (i) modéliser le transport de l'eau, d'un traceur et des polluants dans les sols contaminés, (ii) étudier l'estimabilité des paramètres et les corrélations entre les paramètres, (iii) optimiser les paramètres. Les différents modèles implantés dans le logiciel HYDRUS qui permettent de rendre compte ou pas de l'écoulement préférentiel et du transport hors équilibre physique et chimique sont choisis. Les études concernant le transport d'eau dans un lysimètre de terrain ont montré que les données quotidiennes de pressions et de teneurs en eau volumique contiennent plus d'information que les données horaires, que les pressions ont plus d'information que les teneurs en eau volumique, et que les corrélations des paramètres ont fait perturber les résultats de l'optimisation. Sur le même lysimètre, l'étude d'estimabilité des paramètres caractéristiques pour le transport du traceur (bromure) a montré que les concentrations dans les solutions de percolation ne sont pas suffisantes pour estimer le paramètre de transfert de l'eau entre les zones mobile et immobile car ce paramètre est fortement corrélé avec le paramètre de transfert de soluté. Pour le transport des hydrocarbures aromatiques polycycliques (HAP) dans les colonnes de laboratoire sous différentes conditions de saturation en eau, quand le degré de transport hors équilibre chimique des HAP est élevé, les concentrations en HAP dans les solutions de percolation de la colonne non saturée contiennent plus d'information que celles dans la colonne saturée.

Mot-clés: Sols contaminés, friches industrielles, HAP, écoulement préférentiel, transport hors équilibre, lysimètre, analyse d'estimabilité, optimisation, HYDRUS

Modeling of water flow and contaminant transport in the contaminated soils from the former industrial sites

Abstract: Preferential flow and nonequilibrium transport are probably the most frustrating in terms of hampering accurate predictions of contaminant transport through the vadose zone. The mathematical description of preferential flow and nonequilibrium transport needs many parameters that are not measurable. Therefore, the inverse method is a promising way to estimate model parameters. The main objectives of this work are to (i) study the water flow using the uniform flow and dual-porosity models, tracer and contaminant transport using the uniform transport model and/or physical and chemical nonequilibrium transport models, (ii) investigate parameter estimability and correlations between different parameters, and (iii) optimize the hydraulic properties and solute transport parameters. The results concerning the water flow in the bare field lysimeter show that daily data contained much more information than hourly data, daily pressure heads contained more information than daily water contents; the correlations between different parameters hamper the optimization results strongly. Basing on the tracer concentrations in the leaching solution of the lysimeter, the first-order rate water transfer coefficient was not estimable since this parameter was highly correlated with the solute transfer coefficient. PAH concentrations in the leaching solution of the contaminated soil column under saturated and nonsaturated flow conditions show that when the degree of chemical nonequilibirum transport is high, the solute leaching of the nonsaturated column contained more information than those of the saturated column. In addition, the fraction of sites with instantaneous sorption and the linear adsorption distribution coefficient always showed a very strong correlation, they were impossible to optimize simultaneously.

Key-words: contaminated soils, PAH, heavy metals, preferential flow, nonequilibrium transport, lysimeter, column, estimability analysis, optimization, HYDRUS